STUDY OF GOLD-BASED ALLOY

PHASE DIAGRAMS

Submitted For The Degree Of Doctor Of Philosophy

BY

M. TAQI ZAHID BUTT

Department of Materials Technology,
Brunel, The University of West London, U.K.
July 1990.

ACKNOWLEDGEMENTS

All praise to Allah, almighty, sustainer of the world, the merciful and kind who enabled me to complete this work. Blessing and peace be upon Moses, Jesus and the last prophet Muhammad whom God sent for guidance to mankind to manifest His extreme mercy.

I should like to express my deep appreciation and gratitude to my supervisor Prof. C. Bodsworth for his guidance, constructive criticism and his great patience throughout this project. Also, I acknowledge the unforgettable guidance and invaluable assistance of Prof. A. Prince in the course of this work.

I would like to thank Dr. D. Talbot and all office and technical staff who have helped me in this work over the last few years.

I am thankful to Prof. B. Ralph, Head of the Department of Materials Technology, for the provision of the laboratory facilities. I, also, wish to thank Englehard Limited for the loan of Gold.

Finally, I gratefully acknowledge the Ministry of Science and Technology, **Government of Pakistan** for the **S & T** scholarship award and Punjab University, Lahore for the grant of leave for this period of research.

DEDICATED TO ALL MY FAMILY MEMBERS

ESPECIALLY MY PARENTS

ABSTRACT

The partial constitutions of the Au-Ge-X and Au-Pb-X ternary alloys have been investigated, where X is a metallic element, selected from the sub-groups period IIB and IIIB of the periodic table (In, Ga, Zn, or Cd), which forms one or more stable compounds with gold, but which forms no stable compound with Ge and Pb. The Smith Thermal Analysis Method, supplemented by metallographic and X-ray techniques, was used to determine the constitutions of the ternary systems. Eutectiferous, pseudobinary systems were found between Ge and the stable congruent intermediate compounds, AuIn, $AuIn_2$, AuGa, $AuGa_2$, AuZn and AuCd. The solubility of Ge in the AuX compounds was not determined directly. However, it was 1.3 at.% Ge for Zn and Cd containing alloys and less than 1.0 at.% Ge for In and Ga containing alloys at the eutectic temperatures, which is in accordance with the Hume-Rothery rule. Ternary eutectic points were also determined in the AuIn-$AuIn_2$-Ge, $AuIn_2$-In-Ge and AuGa-$AuGa_2$-Ge partial ternary systems. No evidence of liquid immiscibility was found in any of these ternary systems. The experimental results obtained were in good agreement with computed features of the diagrams. However, pseudobinary systems were not found between Pb and the stable congruent melting intermediate compounds, AuGa, $AuGa_2$, AuZn and AuCd (the AuIn-Pb and $AuIn_2$-Pb sections had already been investigated). The evidence of an extensive liquid immiscibility was found in each of these systems. The miscibility in the liquid state was found to decrease progressively down group IV when the elements of this group react with AuX compounds, which can be attributed to the progressive increase of the atomic size and decrease in electronegativities and solubility parameters of the elements, down this group.

Two rules were derived to relate the liquid immiscibility/miscibility of ternary systems. One of the rules based upon the atomic sizes and melting points of the constituent elements showed a fair agreement with many systems. However, the other rule based upon the solubility parameter and electronegativities of the constituent elements showed good agreement with immiscible systems, but gave a poor predictability for miscible systems.

The lower temperature equilibria of the Au-rich portion of the Au-Sn binary phase diagram are not well defined. So, long term heat treatment of samples at appropriate temperatures and compositions was carried out. Optical microscopy and SEM/EDAX techniques were employed and hence the low temperature equilibria of the Au-Sn binary system have been amended.

CONTENTS

CHAPTER 1

(1) INTRODUCTION

(1.1) EQUILIBRIUM PHASE DIAGRAMS

One of the most important sources of information regarding a material system is the phase diagram, in which phase composition and phase stability are displayed as a function of temperature, composition and pressure (in metallic alloy systems the pressure is usually regarded as constant and ignored). These diagrams are usually plotted with temperature in degrees Centigrade, as the ordinate and alloy composition in atomic percent (or weight percent) as the abscissa. Ideally the phase diagram will show the relationship under equilibrium conditions. Equilibrium conditions can be achieved by extremely slow heating and cooling, so that if a phase change does occur, sufficient time is allowed. The change of phase depends upon the rate at which the alloy is heated or cooled. Basically the task of a phase diagram is to summarize all phase changes which take place, at equilibrium, in the system as temperature changes. However, a phase diagram will not provide any information on the reaction rate, and also it does not give any information on the possible existence of non-equilibrium phases, such as martensite in iron alloys and some other alloys. Thermodynamically, a phase diagram may be regarded as a

manifestation of the thermodynamic state of the system.

(1.1.1) Advantages of Phase Diagrams:

The use of phase diagrams for recording phase changes in alloys offers three advantages.

(i) The conditions under which phase changes occur can be recorded simply and clearly for a large number of alloy compositions in a relatively small space.

(ii) The existence of certain rules of construction greatly reduces the number of experimental observations necessary to determine the phase relationships that exist in a whole series of alloys.

(iii) The recognition of quasi relationships between the constitution of alloys and their structure and properties makes the phase diagram an invaluable guide in the control of metallurgical processes.

(1.2) HISTORICAL BACKGROUND

(1.2.1) Empirical Determination:

A complete and comprehensive historical background of phase diagrams is presented by Haughton (1). In the late nineteeth and early twentieth centuries, the pioneer work in the determination of phase diagrams was made by Heycock and Neville, who determined the liquidus curves for some binary alloys systems. Also the work on ternary phase diagrams was started more or less in the same era, and the first 14 ternary diagrams were developed by C. A. R.

Wright from 1888 to 1898. He developed his first ternary diagram of Pb-Sb-Sn in 1888. Early workers, in particular Heycock and Neville, determined phase diagrams which have proved to be surprisingly accurate in view of the lack of technology and development in apparatus at that time.

A lot of diagrams were produced in the first decade of the twentieth century. In the years 1905-1915 equilibrium phase diagrams for many alloy systems were published by the workers of the German school associated with the name of Tammann. In this period an average of 30 diagrams per annum were produced, but from 1916 to 1918 only four binary and two ternary diagrams were produced due to the interruption of work by the First World War. After the First World War, the general standard of equilibrium phase diagram work was raised largely in the British National Physical Laboratory, which was working under the guidance of Rosenhain, and produced diagrams associated with the names of Gayler, Haughton and Hanson. In 1922 again the output reached the pre-war level, and from 1925 it again increased rapidly until shortly after the outbreak of the Second World War.

In the past four decades, the extensive collection of phase diagrams of metal systems which is now available to us is the product of painstaking labour of a large number of skillful investigators working in all parts of world. Presently, everywhere in the world a lot of binary, ternary and multicomponent systems are being

studied in different research institutions. Now almost all binary systems are well known and the accuracy of many systems has been confirmed by a combination of thermodynamic and experimental techniques.

In the early days, the pyrometer was the only instrument used for practical measurements. The alloys were usually prepared in fire-clay pots by using a coke or gas fired furnace, which usually caused contamination; cooling runs were performed by cutting off the power to the furnace. Earlier, the physical properties were the basis of plotting equilibrium phase diagrams for the alloy systems, but later on thermal and microscopical analysis were used. X-rays were first used as a metallograpical tool by Heycock and Neville in the study of the Cu-Sn alloy system, but at that time it was not considered to be a popular technique. Twenty years later the X-ray spectrometer began to play an important role in the study of the constitution of alloys. With the advancement of science and technology, more instruments and methods have been devised for the determination of phase diagrams, the details of which are given in the later part of the thesis.

(1.2.2) Thermodynamical Approach:

The whole foundation of thermodynamics was laid before the middle of the nineteeth century. The work of different scientists established the basic principle of the theory of energy. The next task was to build up from these principles a great body of

thermodynamic theorems. This was the work of many great scientists. Amoung those was J. Willard Gibbs who, in 1876, gave a thermodynamical approach to phase equilibria. According to this approach, the basic features of construction of all phase diagrams are dictated by a single natural law, the phase rule, which relates the physical state of a mixture with the number of substances of which it is composed and with the environmental conditions imposed on it. The third and modern stage of thermodynamic development is characterized by the design of more specific thermodynamic methods and their application to particular chemical processes together with a systematic accumulation and utilization of thermodynamic data.

As described earlier, the thermodynamic principles of phase equilibria were well established by the work of Gibbs. At present they are being put into extensive use for evaluating and calculating phase equilibrium diagrams. At first, most of the metallurgists/scientists were reluctant to use the thermodynamic approach for the determination of phase equilibria due to the awkward and time consuming mathematics involved. Prior to moderately powerful computers becoming available, the calculation of phase diagrams using thermodynamic data was generally restricted to simple binary systems (2-6). With the advancement of computer techniques, calculation has become more and more easy. A large number of thermodynamic calculations have now been made for various systems from the thermochemical data that is available in the literature (7-9) and from data which has been

critically assessed by groups around the world such as CALPHAD (10) and SGTE (11). The first book on phase diagram calculation was written by Kaufman and Bernstein (12) in 1970. Then in 1971 the CALPHAD group was established at a conference held at NPL and Brunel university, U.K. This approach has, subsequently, developed rapidly and there is now extensive cooperation between groups of workers in Europe, the U.S.A and Canada on the critical assessment of thermochemical data and on the calculation and assessment of phase diagrams.

(1.3) RANGE OF INTEREST

The alloying behaviour of gold is not only of academic interest for the technological applications of gold alloys are dependent upon the knowledge of their constitution. The industrial use of gold for interconnection and surface coating in microelectronics inevitably demands interaction data for device processing and a constitutional approach is a key element in the provision of these data. In electrical and electronic industries or in semiconductor industries, bonds are frequently made to Au-coated surfaces with other metallic solders. A number of problems are often encountered when combinations of other materials are used on the Au-coated surface. These include poor mechanical properties like brittleness and high solubility of Au in solder (scavenging), ageing, wetting etc. The problems encountered, their understanding and their solutions are

described in detail in references (13-19).

(1.3.1) Uses of Gold and Its Alloys:

Gold is used extensively in the form of film, circuit board, electronic board, solder or wire etc, in the electrical and electronic industries. It is used, also, as a material for electrical make-and-break contacts operating with light pressures and controlling small current. Gold, often lightly alloyed and applied as an electrodeposit, is extensively used in semiconductor assemblies and to form conducting paths, solderable surfaces and contacting fingers in printed circuits. There are many other applications of gold and its alloys such as in solder for high-temperature operations and as reflective films for infra-red radiation, in thermocouples (20). In many electrical and electronic industries, the solders are either of eutectic or near eutectic composition due to their unique and lowest possible melting point in a particular system. Basically there are three main types of electronic components in which gold is used (21).

(i) Separable connectors.

(ii) Bonded interconnections.

(iii) Soldered interconnections.

(1.3.2) Characteristics of Gold and Its Alloys:

Gold is used in industry, because it exhibits the following excellent characteristics (20,21)

(i) Good wetting properties.

(ii) High oxidation and corrosion resistance.

(iii) Excellent conductor of heat and electricity.

(iv) Low electrical contact resistance.

(v) Ready deposition onto a wide range of substrates and surfaces.

(vi) Good mechanical properties.

(vii) Gold and its alloys exhibit selective reflectivity of radiation (which results in their colour).

(viii) Gold has the advantage that it is free from high-resistance oxide and sulphide films and also that it does not, like platinum, catalyse the break down of organic vapour to form black deposits on the contact surface.

(1.3.3) Characteristics of a Solder:

High integrity electronic devices are often constructed with gold plated circuit boards (components are fixed to the board by soldering). The solder used on these boards must have particular characteristics, such as low melting point, easy wettability, inertness and thermal and expansion match to the substrate.

In the present investigation Au-Ge-X systems are discussed in detail. Germanium has proved to be a useful component of solders according to the properties explained above, in particular, Ge expands on solidification and compensates for the volume contraction of the other constituent metal(s) in the solders, thus reducing the stresses developed at the interface between the solder and the substrate and reducing the risk of failure of the joint.

(1.4) PRESENT WORK

The phase diagrams for alloys containing gold as one of the constituents are dealt with in this thesis. The high cost and limited use of the precious metal and their alloys has mitigated against the extensive study of their characteristics. In the past few years, however, research into the constituents of gold alloy systems has been expanded. The present work was originated with G.E.C Hirst Research Centre, Wembly, U.K., but gold alloys were also being studied, for example, at Grenoble University, Paris and University of Provence in France.

(1.4.1) Gold-Alloy Systems:

The present work can be divided into two groups. The major activity was a study of ternary systems containing gold as one of the constituents. A subsidiary study was made also of the gold-rich portion of the Au-Sn binary system.

(1.4.1.1) Gold-ternary alloy systems:- Equilibrium has been investigated in ternary alloys containing Au and Ge together with a third element X selected from the B-subgroup of the IInd and IIIrd period of the periodic table, which form one or more stable compounds with Au. When a quasi-binary system is formed between one of the pure components and a stable compound formed between the other two components of a ternary system, then the ternary can be regarded as two sub-ternary systems which coincide along the quasi-binary join. This investigation was

designed, therefore, primarily to determine whether or not quasi-binary systems were formed between Ge and Au-X compounds formed between Au and the X element selected from the B-subgroups. Having developed some experimental data on Au-Ge-X systems, some additional work was done on similar systems, i.e Au-Sn-X and Au-Pb-X, to ascertain if there are any common rules which could be used for the prediction of phase equilibria or there exists any periodicity among these systems.

(1.4.1.2) Gold-tin binary system:- The Au-Sn binary phase diagram is not well defined in the gold rich portion of the diagram. There are two published versions of the diagram. One version is given by H. Okamoto and T. B. Massalski. Doubts on the validity of this version were raised by Legendre, Prince and co-workers etc., who proposed the presence of two peritectic reactions in the Au-rich alloys. Thus, the low temperature equilibria are uncertain. To assist in the selection of the correct version a series of alloys, covering the appropriate range of compositions, have been equilibrated isothermally at four selected temperatures in the appropriate temperature range. Two temperatures were studied in UMIST by Dr. F. H. Hayes and co-worker, while the study of the other two temperatures (220°C and 300°C) is presented in this thesis.

(1.4.2) Experimental Techniques Available and Techniques Used:
There are many techniques available for the determination of phase equilibrium diagrams. However, Differential Thermal Analysis

(DTA) has been used extensively in the study of phase equilibria. It has the ability to detect very small thermal effects. When a phase transformation occurs, the temperature gradient between the furnace and the specimen will increase, and this will increase the rate of heat transfer. Hence the reaction will become vigorous and develop the heterogeneity in the specimen which causes spurious thermal arrest(s) if very slow rates of heating and cooling are not employed. In 1940 Smith proposed a modified method of thermal analysis, usually known as the Smith Thermal Analysis (STA) technique, which is particularly suited for the determination of phase diagrams. In this technique a constant temperature difference can be established between the specimen and the furnace during and after a phase change; homogeneity can be maintained in the specimen and spurious thermal effects can be avoided. In addition the STA is also suitable for the determination of heats of reactions and specific heats with fair accuracy.

The techniques available for determining the phase diagrams, their advantages and disadvantages, the principles of DTA and STA and their merit and demerits have been discussed in detail in a later part of the thesis. However, STA is one of the most inexpensive, quick, accurate and reliable techniques for thermal analysis for the determination of phase diagrams and has been used in this study. Also metallographic, X-ray and SEM techniques were used to determine the constitution of the equilibrium diagrams.

(1.4.3) Thermodynamic Approach and Computer Calculations:

Thermodynamic calculations have proved to be a valuable tool in the investigation of phase equilibria. The development of computer techniques made these calculations easy and now a less skilled person can calculate phase diagrams easily on a computer by feeding in the appropriate thermochemical values. The power of computer calculation lies more in ternary and higher order systems where hand calculation becomes prohibitive.

In general, however, computer calculation of phase boundaries or indeed the whole phase diagram, should not be regarded as a substitute or alternative to experimental determination of the phase diagram. They are complementary approaches. So no phase diagram can be considered to be final or reliable when it is calculated on the thermodynamic basis alone. An experimental determination is also required. Determination of the thermodynamic properties of ternary or multicomponent phases are often expensive and time consuming, so most of the ternary and multicomponent phase diagrams are calculated on the basis of thermodynamic properties of the binary systems involved.

The majority of previous workers on phase equilibria have not dealt with the thermodynamic approach. The work of O. Kubaschewski and other investigators have demonstrated that the application of thermodynamics to phase equilibria can provide a useful check on experimental data and allow its extension to the regions which are difficult to determine experimentally. Therefore the secondary aim

of this work was to compute the phase diagrams on a thermodynamical basis and compare them with the experimentally derived phase diagrams.

CHAPTER 2

(2) FUNDAMENTALS OF PHASE EQUILIBRIA

(2.1) SYMBOLS AND UNITS

In the past confusion has arisen over the use of different symbols and units for the same physical properties or units. To rectify this unsatisfactory state of affairs, the International Union of Pure and Applied Chemistry (IUPAC) has recommended the use of the following symbols and units all of which are compatible with the SI system (22). They are used throughout this thesis.

Name of the Quantity	Symbols	SI Units
Temperature	T----θ	K (^oC)
Mass	m	kg
Pressure	P----p	kg $m^{-1}s^{-2}$ = Pa
Volume	V	m^3
Gibb's Free Energy	G	J
Enthalpy	H	J
Entropy	S	J K^{-1}
Heat Capacity		
(i) at constant volume	C_v	J K^{-1}
(ii) at constant pressure	C_p	J K^{-1}
Internal Energy	U	J
Quantity of Heat	q	J

Time	t	s
Universal Gas Constant	R	$J\ K^{-1}mole^{-1}$
Boltzmann's Constant	k	$J\ K^{-1}$
Mole Fraction	X	Dimensionless

(2.2) BASIC ASPECTS OF THERMODYNAMICS

In dealing with phase equilibria, a number of terms are frequently encountered. Therefore, it is important that these terms be well defined before undertaking the detailed treatment of phase equilibria.

(2.2.1) Equilibrium:

Phase transformations occur in order to lower the energy of a system to achieve equilibrium. So a system is said to be in equilibrium when it is most stable and shows no desire to change, and possesses the lowest possible energy.

(2.2.2) Internal Energy and First Law of Thermodynamics:

The internal energy of a system is the sum of the kinetic and potential energies of all parts of the system. For a closed system the internal energy of the system would remain constant. If the system is allowed to react with its surroundings its internal energy will change. If the system is subject to change from one state to an other state, it is accompanied by an increase in internal energy (dU). This

change is brought about by the extraction of heat (δq) from the surroundings, and simultaneous performance of work (δW) by the system on the surroundings The First Law of Thermodynamics (energy can neither be created nor destroyed) states that the increase in internal energy, dU, is:

$dU = \delta q - \delta W$ ----------(2.1)

The symbol 'd' is used for a change in a state quantity or exact differential while the symbol 'δ' is used for a non-state change or inexact differential.

At constant pressure, the First Law becomes

$dU = \delta q - PdV$ ----------(2.2)

and at constant volume

$dU = \delta q$ ----------(2.3)

(2.2.3) Heat Content or Enthalpy:-

The heat content or enthalpy is the total internal and external energy of the system. The heat content or enthalpy of a system is related to its internal energy and is a state property, given by the equation:

$H = U + PV$ ----------(2.4)

$dH = dU + PdV + VdP$

From equation (2.2) $\delta q = dU + PdV$, so,

$dH = \delta q + VdP$ ----------(2.5)

at constant pressure, $VdP = 0$ so equation (2.5) gives:

$dH = \delta q$ ----------(2.6)

and, at constant volume equation (2.4) reduces to:

$dH = dU$ ----------(2.7)

(2.2.4) Heat Capacity (C):

The heat capacity of a substance is the heat required to raise the temperature, T, of unit mass by one degree, K, and is given by

$$C = \frac{\delta q}{dT}$$

at constant volume

$$C = C_V = \left(\frac{\delta q}{dT}\right)_V = \frac{dU}{dT}$$ (since from eq. 2.3 $\delta q = dU$, at constant volume)

at constant pressure

$$C = C_P = \left(\frac{\delta q}{dT}\right)_P = \frac{dH}{dT} \qquad \text{----------(2.8)}$$

(since from eq. 2.6 $\delta q = dH$, at constant pressure). Therefore

$$dH = C_p dT \qquad \text{----------(2.9)}$$

and the variation of enthalpy with temperature is given by:

$$\int_{T_1}^{T_2} dH = \int_{T_1}^{T_2} C_P dT \qquad \text{----------(2.10)}$$

$$H_{T_2} = H_{T_1} + \int_{T_1}^{T_2} C_P dT \qquad \text{----------(2.11)}$$

Conventionally, the enthalpy of a pure substance in its standard state (i.e most stable state) is defined to be zero at 298.16 K. So equation (2.11) can be written as:

$$H_T = \int_{298}^{T} C_P dT \qquad \text{----------(2.12)}$$

$$H_T = \int_{298}^{T} \left(a + bT + cT^2 \right) dT$$

$$H_T = \int_{298}^{T} \left[\sum C_{P;Products} - \sum C_{P;Reactants} \right] dT$$

and where a phase change occurs in the temperature range of interest:

$$H_{T_2} = H_{T_1} + \int_{T_1}^{T'} C_P' \, dT + H_t + \int_{T'}^{T_2} C_P'' \, dT$$

Where C_P' and C_P'' are the heat capacities before and after transformation respectively.

H_{T_1} = Enthalpy at standard temperature.

H_{T_2} = Enthalpy at high temperature in question.

T' = Transformation temperature.

H_t = Enthalpy change at transformation.

The variation of enthalpy and heat capacity with temperature is shown in Fig 2.1 and 2.2.

(2.2.5) Entropy and Second Law of Thermodynamics:

Entropy can be considered from two points of view. One is an atomistic mechanical approach in which it is the measure of the randomness of a system. The other is a thermodynamical approach according to which entropy arises from a consideration of the conditions under which heat can be converted into work (e.g Carnot cycle). Mathematically entropy (S) is given by

$$dS = \frac{\delta q}{T} \qquad \text{----------(2.13)}$$

$$dS = \frac{dH}{T} \qquad \text{(at constant pressure)}$$

and for a reversible change of state

$$S_{T_2} - S_{T_1} = \Delta S = \int_{T_1}^{T_2} \frac{\delta q}{T} \qquad \text{----------(2.14)}$$

To give a fixed reference point the entropy of a pure substance at 0 K is taken to be zero (Third Law of Thermodynamics). So the entropy at T K is given by:

$$S = \int_{0}^{T} \frac{\delta q}{T}$$

since at constant pressure $\delta q = dH = C_P dT$. So,

$$S = \int_{0}^{T} \frac{C_P}{T} dT \qquad \text{----------(2.15)}$$

The consideration of an isolated system leads to an important conclusion. The entropy of such a system either remains constant (dS=0) or increases (dS>0). The entropy remains constant when the system is in an equilibrium state. If it is not, the entropy increases until equilibrium is reached. This is an expression of the Second Law of Thermodynamics, that the entropy in an isolated system tends to a maximum to gain stability (equilibrium).

So when $dS = 0$ reaction is in equilibrium.

$dS > 0$ reaction will occur spontaneously.

$dS < 0$ reaction is impossible.

The variation of entropy with temperature is shown in Fig 2.3.

(2.2.6) Gibbs Free Energy:

Under isobaric conditions, any system undergoes a change to stabilize itself, and the stability of a system is defined by its Gibbs Free Energy given as:

$G = H - TS$ ----------(2.16)

where H = Enthalpy; T = temperature; S = Entropy and

$\Delta G = \Delta H - T\Delta S$ ----------(2.17)

At constant temperature and pressure, a closed system (i.e fixed mass and composition) will be in equilibrium if it has the lowest possible value of Gibbs free energy (dG=0). When a change occurs in a system it is an attempt to minimize the overall energy of the system to attain stability. Equation (2.16) shows that the lowest possible value of G (highest stability) is only possible with a lower value of enthalpy (internal energy) and a higher value of entropy. The necessary criteration for any transformation is:

$\Delta G = G_2 - G_1 < o$

where G_1 is initial and G_2 is a final stage. Equation (2.16) can be written in differential form as:

$dG = dH - TdS$ ----------(2.18)

Now (i) If $\Delta G = 0$ (i.e $dH - TdS = 0$) the system is in equilibrium and there will be no phase change. Since $dH = C_P dT$, so at equilibrium:

$C_P dT - TdS = 0$ or $C_P dT = TdS$

(ii) If $\Delta G < 0$, then change will occur.

(iii) If $\Delta G > 0$, the process is impossible.

(2.2.7) Helmholtz Free Energy:

The stability of any system at constant volume is defined by the Helmholtz free energy. As conditions of constant volume are not dealt with, it will not be described in detail here.

(2.2.8) Mathematical Manipulation of Different Equations:

By the mathematical manipulation of different equations, useful results can be obtained as follow

From equation (2.16) $G = H - TS$

also from equation (2.4) $H = U + PV$ so:

$G = U + PV - TS$ and by differentiating

$$dG = dU + VdP + PdV - TdS - SdT \quad \text{----------(2.19)}$$

From the first law of thermodynamics i.e equation (2.2)

$$dU = \delta q - PdV \quad \text{----------(2.2)}$$

Also from the definition of Entropy, $dS = \frac{\delta q}{T}$ or $\delta q = TdS$

So equation (2.2) becomes:

$$dU = TdS - PdV \quad \text{----------(2.20)}$$

Inserting this value of equation (2.20) in equation (2.19):

$$dG = VdP - SdT \quad \text{----------(2.21)}$$

This is the combined form of the first and second laws of thermodynamics. And at constant pressure $dP = 0$ so,

$dG = -SdT$

This means that G decreases with increasing T at a rate given by $-S$ as shown in Fig 2.4.

Again by differentiating equation (2.4) i.e $H = U + PV$

$dH = dU + PdV + VdP$ Substituting for dU from equation (2.20),

$dH = TdS + VdP$ ----------(2.22)

(2.2.9) The Kinetics of Phase Equilibria:-

The thermodynamic functions only describe whether a reaction will occur or not. So it can therefore be used to calculate the driving force for transformation (i.e $\Delta G = G_2 - G_1 < 0$), but it will not tell how fast this transformation will proceed. This belongs to the science of kinetics.

(2.3) BINARY PHASE DIAGRAMS

(2.3.1) Free Energy of a Binary System:-

Consider A and B atoms, having the same crystal structure in their pure state which can be mixed in any proportions to make a solid solution with the same crystal structure. Consider X_A and X_B are the mole fraction of A and B respectively, taking part so that:

$X_A + X_B = 1$; then the total free energy before mixing is given by

$G_1 = X_A G_A + X_B G_B$ ----------(2.23)

Which is shown schematically in Fig 2.5, where G_A and G_B are the molar free energies of A and B respectively. And after mixing the free energy of the solution is:

$G_2 = G_1 + \Delta G_{mix}$ ----------(2.24)

where

$$\Delta G_{mix} = \Delta H_{mix} - T\Delta S_{mix} \qquad \text{----------(2.25)}$$

where ΔH_{mix} is the heat of the solution (absorbed or evolved) and represents the difference in internal energy before and after mixing. Also ΔS_{mix} is the difference of the entropy between the mixed and unmixed state. The equation (2.24) becomes:

$$G_2 = G_{alloy} = X_A G_A + X_B G_B + \Delta G_{mix} \qquad \text{----------(2.26)}$$

(2.3.2) Phase Diagrams and Free Energy Curves:

The free energy-composition curves give the composition of co-existing phases under equilibrium conditions of the solution and phase mixture. By plotting a series of these curves at different temperatures, one can establish the manner in which the phase compositions change with temperatures. In other words, phase boundaries as a function of temperature can be determined. A phase diagram is nothing more than a presentation of data on the position of the phase boundaries as a function of temperature.

(2.3.3) Phase Rule:

If a system contains C components distributed between P phases, the composition of each phase is completely defined by C–1 concentration terms. Therefore in order to define the composition of the P phases completely, it becomes necessary to have P(C–1) concentration terms; i.e the total number of concentration variables is equal to P(C–1). Further, in the temperature and pressure of the system, which are the same for all the phases at equilibrium, there are two variables to be considered in addition to the concentration

terms. In the absence of the other external variables, at equilibrium:

Total number of variables = P (C – 1) + 2 ----------(2.27)

Also, in general, there will be C independent equations, one for each component. Thus for a system containing P phases and C components there will be a total C (P – 1) independent equations. In this manner it can be written:

Number of variables automatically fixed = C (P – 1)-------(2.28)

So in order to define a system, the number of independent variables is equal to the total number of variables minus, those variables which are automatically fixed i.e:

$$F = [P(C-1)+2] - [C(P-1)]$$

$$P + F = C + 2 \qquad \text{----------(2.29)}$$

Equation (2.29) is the Gibbs phase rule. In equation (2.29) F is called the variances or degrees of freedom.

In metallic systems, the vapour pressures of liquid and solid phases are usually negligible as compared to atmospheric pressure (i.e pressure is considered to be constant). So the Phase Rule reduces to:

$$\mathbf{P + F = C + 1} \qquad \text{----------(2.30)}$$

Throughout this thesis, conditions are considered to be isobaric i.e at constant pressure.

(2.3.4) A Simple Phase Diagram:

The simplest case of a binary system is that where component A and B are soluble in all proportions in both liquid and solid state. This occurs when A and B atoms have similar radii, the same valency and crystal structure (23). In this system A and B form an ideal solution (the details of ideal solution are given in chapter 3) in both liquid and solid states i.e the forces between the similar atoms are equal to the forces between the dissimilar atoms. To obtain this type of phase diagram, the position of two curves (free energy/composition) for liquid and solid at various temperatures have to be studied. This is shown schematically in Fig 2.6. The equilibrium melting temperature of the pure components occurs when $G_S = G_l$, i.e at melting point of A and B. A series of free energy curves such as Fig 2.6(b,c,d) allow the co-existing liquid and solid phases to be plotted. The temperature-composition diagram so obtained is given in Fig 2.6(f). On the assumption that both the solid and liquid solutions are ideal, it is possible to calculate the compositions of the liquid and solid phases in equilibrium at each temperature between T_A and T_B and thus derive the diagram shown in Fig 2.6(f). This has been done for the Ge-Si system (3), as shown in Fig 2.7.

(2.3.5) System Exhibiting Miscibility Gap in Solid State:

2.3.5.1) Minimum in liquidus:- This type of system is shown in Fig 2.8 where the free energy curves apply for a system in which the liquid phase is approximately ideal, but for the solid phase $\Delta H_{mix} > 0$ i.e dissimilar atoms A and B "dislike" each other. Therefore, at

lower temperature, T_3, the free energy curves for the solid assumes a negative curvature in the middle, in Fig 2.8(c) and the solid solution is most stable as a mixture of two phases and with composition (e) and (f). At higher temperature, T_c, critical temperature, when $-T\Delta S_{mix}$ becomes larger (e) and (f) approach each other and eventually disappears as shown in the phase diagram, Fig 2.8(d). The α_1 and α_2 region is known as a miscibility gap. This is called a positive deviation from ideality.

(2.3.5.2) Maximum in liquidus:- Fig 2.9 shows the free energy curve for a system, just the opposite to that explained above, which arises when $\Delta H_{mix} < 0$. In these systems melting will occur above the melting point of the constituents and so a maximum may appear in this system as shown in Fig 2.9. With $\Delta H_{mix} < 0$ there is a greater attractive force between dissimilar atoms than between similar atoms and with $\Delta H^{\alpha}_{mix} < \Delta H^{l}_{mix} < 0$ the attractive force would be greater for the solid solution than the liquid. This is a negative departure from ideality.

(2.3.6) Eutectic System:

If ΔH^{s}_{mix} is much larger than zero the miscibility gap in Fig 2.8(d) can be extended into the liquid phase. In this case a simple eutectic phase diagram results as shown in Fig 2.10. A similar phase diagram can result when constituents A and B have different crystal structures as illustrated in Fig 2.11. These Figures show how the eutectic phase diagram can be derived from free energy curves.

(2.3.7) System Containing Intermediate Phases:

When the ΔH_{mix} is negative with ΔH^{β}_{mix} much more negative than ΔH^{l}_{mix}, the phase diagram of the type shown in Fig 2.9 shows the formation of an intermediate phase as shown in Fig 2.12(f). Here the forces of attraction between the dissimilar atoms are much greater than between the similar atoms. Fig 2.12 shows how a phase diagram containing the intermediate phase can be derived from free energy curves.

(2.3.8) Other Systems:

There are other systems, like the peritectic and monotectic systems shown in Fig 2.13 and 2.14 respectively, which are derived from free energy curves. Other systems are not important with respect to this thesis, so will not be discussed here.

(2.3.9) Tie-Lines in Binary System and Lever Rule:

The horizontal line which joins the composition points of the conjugate phases that co-exist at a designated temperature in equilibrium, is called a tie-line. This is used for the determination of the actual composition of the phases of an alloy and the relative amount of each phase in equilibrium, in a two-phase region at a particular temperature. This can be accomplished by the so-called Lever Rule, which states that the length of the line from the composition of interest to the phase boundary is inversely

proportional to the amount of the phase present. In Fig 2.15, for an alloy 'x' according to the Lever rule:

%age of liquid = mx/mn x 100

%age of solid = nx/mn x 100

while the compositions of solid and liquid can be read directly i.e at point (a) and (b) respectively in the Fig 2.15.

(2.3.10) Rules for the Construction of Binary Phase Diagrams:

Phase diagrams can be quite complicated and difficult to construct if limited experimental data are available. So there are some rules which can help in constructing the phase diagram to avoid error. These are as follows:

(a) The Phase Rule: No construction in a diagram may violate the phase rule given as: $P + F = C + 2$

(b) The boundary rule:- Any P-phase region can be bounded only by the regions containing $P \pm 1$ phases, where P represents the number of phases.

(c) The boundary curvature rule:- Boundaries of one-phase regions must meet with the curvatures such that the boundaries extrapolate into the adjacent two phase region.

(d) The solubility rule:- All components are soluble to some degree in all phases.

(2.4) TERNARY PHASE DIAGRAMS

A three dimensional model, commonly known as a space model, is

used to represent completely the phase equilibria of a ternary system, at constant pressure. An equilateral triangle is usually used, with temperature represented on the normal axis and with the base of the prism as composition. Two dimensional sections are more convenient than the space model, so their use is preferred. A two-dimensional section through this space model may be taken horizontally (isothermally) at various temperatures level or vertically. Like the binary system, it is possible to draw Gibbs free energy curves for each phase, stable at the lowest value, and compositions of these phases in equilibrium must be given by points connected by a common tangential plane in the Gibbs triangle.

(2.4.1) Two Phase Equilibria:

In this system three components are completely soluble in one an other both in the liquid and solid states. Above the liquidus, all alloys are fully molten, below the solidus all are completely solid. However, two-phase areas consist of bundle of tie-lines of varying direction. The tie-lines will be explained in the next part.

(2.4.2) Three Phase Equilibria:

A three phase equilibrium can be produced by the coalescence of two two-phase regions as shown in Fig 2.16. Here the temperature falls until, at T_2, contact is made at point k. At a temperature immediately below T_2 a three-phase equilibrium involving phases of compositions a, b and c is formed at T_3.

(2.4.3) Four Phase Equilibria:

A maximum of four phases may co-exist in a ternary system. So an invariant reaction in a ternary system occurs, when four phases co-exist in equilibrium. Two forms of reaction can occur during solidification, each involving a liquid and three solid phases. One is the ternary eutectic and other is the peritectic reaction.

(2.4.4) Tie-Lines and Tie-Triangles in Ternary Systems:

As in a binary system, the two-phase region is composed of tie lines joining conjugate liquid and solid phases. In a ternary system, however, tie-lines do not constitute a two dimensional area but occur as a bundle of tie-lines of varying directions filling the three-dimensional two-phase space. Unlike the binary system, the orientations of tie-lines in a ternary system have to be determined experimentally. However, there are some general rules, based on the theoretical conditions, which are helpful in drawing the tie-lines correctly.

(i) The direction of the tie-lines vary gradually from that of one boundary line to that of the other without crossing each other.
(ii) They must run between two one-phase regions.
(iii) Except for the two binary tie-lines, they are not necessarily pointed towards the corner of the compositional triangle.

A tie-triangle is a triangle, the corner of which, defines the compositions of the conjugate phases that co-exist in equilibrium at

a particular temperature. In Fig 2.17 $\alpha\beta$, $\beta\gamma$ and $\alpha\gamma$ are the tie lines, while $\alpha\beta\gamma$ represents the tie-triangle. For a ternary alloy 'x' in Fig 2.17, the composition of three phases can be calculated by applying the Lever Rule in the same way as described in the binary system.

Tie-triangles occur in a ternary system when three phases co-exist. But if a phase occurs at a point within the triangle, such as point 'x' in Fig 2.17 as a liquid phase in equilibrium with other phases, then the tie-triangle may be applied also where the four phases co-exist in equilibrium i.e liquid,α,β and γ.

(2.4.5) Projected Sections of Ternary Diagrams:

(2.4.5.1) Horizontal (Isothermal) sections:- One of the most widely used ways of presenting a ternary system is to cut a horizontal section of the ternary space diagram at a specified temperature. The visualization of tie lines and explanation for the sequence of the freezing of an alloy system is more easy in these isothermal sections. Fig 2.18 shows the isotherms of the ternary isomorphous phase diagram, as derived from Fig 2.19. The tie-lines are shown by dotted lines. The exact paths of the phase boundaries can only be determined experimentally. Fig 2.20 shows the isotherms and phases formed during the freezing of an alloy at different temperatures of a ternary eutectic system as shown in Fig 2.21.

(2.2.5.2) Vertical sections:- The other way of revealing the internal structure of the ternary phase diagram is to cut the ternary space diagram into vertical sections (perpendicular to the composition

triangle). These sections are also called isopleths as they resemble binary diagrams. Two types of vertical sections are used.

(i) Representing the constant composition ratio of two components i.e passing through one vertex of the composition triangle.

(ii) Representing the constant composition of one component i.e parallel to the one side of the composition triangle.

Fig 2.22 and 2.23 show vertical sections through a ternary eutectic system which is shown in Fig 2.21.

(2.4.6) Rules for the Construction of Ternary Phase Diagrams:

The formation of phases formed in the higher order system is similar to that in a binary system. However, there are a number of rules governing the disposition of the adjoining phase regions while constructing the isotherms of a ternary phase diagram.

(a) When two equilibrium curves intersect then their meta-stable extensions in the neighbourhood of the point of intersection lie either inside or outside the three phase triangle as shown in Fig 2.24.

(b) The maximum number of phases that can be at equilibrium in a ternary isothermal section is four, as dictated by phase rule.

(c) Two-phase regions are enclosed by four boundaries, of which two opposite boundaries are straight lines and the other two opposite boundaries lie between the two-phase region and its two neighbouring one-phase regions.

(d) The three-phase regions are triangles bounded by two phase regions on three sides and are in contact with one-phase regions at

the corners.

(2.5) THE LAW OF ADJOINING PHASE REGIONS

A most useful rule on the association of phase regions in phase diagrams was derived by Palatink and Landau (24). It is known as the Law of the Adjoining Phase Regions and is given by

$R_1 = R - D^- - D^+ \geq 0$

where R_1 is the dimension of the boundary between neighboring phase regions.R is the dimension of the phase diagram or section of the phase diagram (vertical or isothermal) and D^- and D^+ are the number of phases that disappear and the number that appear in a transition from one phase field to an other respectively.

From this law the junctions of various phase regions in binary phase diagrams or two dimensional sections of ternary phase diagrams can be summarized as follows:

(i) A one-phase region with a two-phase region along a line.

(ii) A one-phase region with a three-phase region at a point.

(iii) A two-phase region with a three-phase region along a tie-line.

(iv) A two-phase region meeting another two-phase region at a point.

(v) A one-phase region meeting another one-phase region at a point.

(2.6) QUASIBINARY OR PSEUDOBINARY SYSTEMS

When a congruent-melting intermediate compound AB occurs in one of the edge binary phase diagrams, A-B, in a ternary system of components A, B and C, it some times happens that the phase AB forms a binary eutectic type phase diagram when reacted with component C. All the tie-lines connecting the phases in equilibrium lie in the plane of the section from AB to C. The system AB-C is then said to be a quasibinary or pseudobinary system.

(2.7) FURTHER READING ON PHASE EQUILIBRIA

The field of phase equilibria is so vast that it cannot be explained comprehensively in a condensed way in a few pages. There are several books (25-31) which are recommended for further detailed reading. Most of the details in this chapter are taken from these books.

CHAPTER 3

(3) THERMODYNAMICS OF PHASE EQUILIBRIA

(3.1) INTRODUCTION

Thermodynamic calculation can be done by:

(i) Minimizing the free energy.

(ii) Equating the chemical potentials.

(iii) Equating the activities.

From the thermodynamic point of view all these three are equivalent and simply represent different ways of saying the same thing. However, for computer calculation they use different equations and numerical analysis techniques etc. The basic principle involved in computing a phase diagram is that, at equilibrium, (i.e when the phases are in equilibrium at a certain temperature) the composition is given by the common tangent construction, corresponding to the minimum Gibbs free energy. That is to say, the phases or mixture of phases having the lowest Gibbs energy of formation, for any particular composition, is the most stable.

The free energy concept, in turn, for a binary or ternary system can be calculated by the formulation of:

(i) Thermodynamic properties of each pure component vs

temperature.

(ii) Thermodynamic properties of formation of each phase vs temperature.

(iii) Thermodynamic properties of formation of each phase vs mole fraction.

The principles of the calculation of phase diagrams from thermodynamic data have been described clearly by Kaufman and Bernstein (12) and Prince (26). Binary systems have been described by Kubaschewski and Chart (32), and ternary systems by Kaufman and Nesor (33) and Chart et al (34-36). The method normally used relies on the calculation of tie-lines and tie-triangles. The Gibbs energies of the various phases present are represente d mathematically as a function of composition and temperature, and phase boundaries are computed using minimization of Gibbs energy techniques. A comprehensive review of the different methods for thermodynamical calculation of binary and ternary phase diagrams is given by Ansara (37).

(3.2) IMPORTANCE OF CALCULATIONS

In many cases calculation can provide valuable information which is not easily obtainable by experiments i.e Thermal Analysis and X-rays etc. For example in the case of equilibria involving metastable phases or for phase equilibria at a temperature which is

inaccessible to conventional techniques, especially where the phase boundaries are difficult to determine due to a kinetic effect, some time solid solution reaction at low temperature due to the slow nucleation or high temperature difficulties and toxicity etc, calculation may be the only way in which the required information can be established conveniently or within a reasonable time scale. See for example, the Cr-Mo and Fe-Cr phase diagrams, where Kubaschewski and Chart (32) extended the phase diagrams of these systems to lower temperature by calculation. Calculation can also provide information for metastable boundaries. Further, calculation may provide a useful check on the experimentally derived phase diagrams. However, it should not be regarded as a substitute for experimental determination of phase diagrams. Another important aspect is to optimize the thermodynamic description of binary systems i.e to obtain sets of excess free energy of mixing coefficients which give the best overall agreement with phase boundaries and thermodynamical experimental data points. This optimization has been principally developed by Lukas and co-workers (38). The method basically is to develop a best set of coefficients for a system by using the combination of calculated phase diagrams from all sources plus all the best experimental measurements of that phase diagram. This optimization, for example, has been used by Dorner (39), Murray (40) and Niemela (41) for the Al-Si, Cu-Ag and Cu-Pb binary phase diagrams respectively. Such binary optimizations are required prior to the ternary calculations being carried out.

(3.3) CALCULATION OF PHASE EQUILIBRIA

(3.3.1) Calculation of Binary Phase Diagrams:

The procedure for calculating an equilibrium phase diagram is to find out the Gibbs energy/composition curve for all possible phases and select the phases of highest stability (i.e the phases having the lowest possible Gibbs energy). Two phase equilibrium can occur only when either the Gibbs energy/composition curves of two stable phases intersect, as shown in Fig 3.1, or when the Gibbs energy/composition curve of a single phase has two minima, as shown in Fig 3.2. The compositions of phases co-existing at any temperature are given by the common tangent construction corresponding to the stable equilibria of minimum Gibbs energy, and can be calculated directly. For the derivation of a complete binary diagram, this type of stable equilibria has to be calculated at a series of temperatures. However, if several phases are potentially present over a small range of composition, then the situation will be more complicated and the most stable combination of two-phase equilibria has to be considered as shown in Fig 3.3. Kaufman and Bernstein (12), Ansara (37) and Jansson (42) developed their own techniques to cope with this situation. All methods have different techniques to identify the most stable equilibria. To economize on computer time, the temperature intervals for computation are usually set as far apart as possible consistent with the accuracy required for the calculated diagram. Generally, temperature intervals decrease as the curvature of the phase boundaries

increase or vice versa.

For the calculation of a binary phase diagram a knowledge of the thermodynamic stability (i.e Gibbs energy of formation of each phase) as a function of both temperature and composition is required. However, it is possible, in some cases, to calculate phase diagrams where the thermodynamic data is not complete. The early work is described by Kaufman and Bernstein (12). They used the regular solution model to describe the excess Gibbs free energy of mixing, together with a lattice stability parameter for the pure components. They also considered that for solid phases, regular solution interaction parameters can be derived from the enthalpy difference between two different states of the pure components and for the liquid phase interaction parameters are derived from the enthalpy of vaporization of the pure components. These calculations were carried out for alloy systems for which no thermochemical measurements of the mixing properties had been carried out. The resulting calculated diagram in many cases showed only fair agreement with the observed phase diagram.

(3.3.2) Calculation of Ternary Phase Diagrams:

For the calculation of ternary or multiphase equilibria, the same technique is used as that used for binary systems. Here again the most stable phase combination is the one which has the lowest Gibbs free energy. This is represented by a common tangent plane to Gibbs energy/composition surfaces. For ternary phase equilibria

two types of situation are recognized:

(i) In the most common situation, very little or no knowledge of either the binary constitutions or thermochemical properties of the ternary system exists. The thermochemical properties of multicomponent alloys are often unavailable and are expensive and time consuming to determine due to the large number of alloys required for investigation, so it is necessary to estimate the ternary phase diagram from the data for the constituent binary systems involved. Such diagrams are tentative and require experimental verification.

(ii) The other situation, which is rare, is where extensive measured ternary thermodynamic data are available in the literature. In this case the ternary system can be optimized by the combination of this available ternary data with the thermodynamic data for all three edge binary systems. This can generate a set of best-fit thermodynamic coefficients for the entire ternary system. This is called an "optimized ternary calculation" and is considered to be the best description of a ternary system.

(3.3.2.1) Extrapolation of binary data into ternary (or multicomponent) systems:- When the appropriate binary systems can be described adequately in term of thermochemical properties, the extension into ternary (or higher order) systems can be done by empirical equations and models. Several approaches to this extrapolation, in terms of geometrical models, have been described by Ansara (37,43), which relates the ternary properties to those of

the constituents of the binary systems. The most widely used geometrical models are due to Bonnier et al (44), Toop (45), Kohler (46), Colinet (47) and Muggianu et al (48), for the description of ternary excess Gibbs free energies. The comparison of the equations involved in these models is given in (37,43). These geometrical models used the interaction parameters to produce complex descriptions of the ternary equilibria and an additional source of error if an incorrect choice is made. From the theoretical point of view none of the models can be considered to be anything more than an approximation. Different models are suitable under different situations and there is no overriding reason why one model should be chosen in preference to another. However, the most sophisticated way of describing the excess Gibbs energy of solution phases was described by Lukas et al (49).

The comprehensive approach for computer calculation in the ternary systems was basically designed by Lukas and co-workers (38), [the same approach has been used in the present study (50)]. This Lukas method for the calculation of a ternary phase diagram is divided into the following steps:

(i) Optimization of the binary systems to get the adequate base for.

(ii) Extrapolation (of the optimized thermodynamic functions) of the binary phases into ternary as a first approximation.

(iii) Optimization of the correction function using a few ternary data only.

This Lukas technique of optimization has applied by Hayes and co-workers (51) recently for the Cu-Ag-Pb system. A combination of

re-optimized sets of best-fit binary coefficients of edge binaries involved, plus existing boundary points and the lattice stabilities of the pure components were used in the ternary optimization of this system.

(3.4) MODEL APPROACH TO PHASE EQUILIBRIA

As the calculation of phase equilibria on the thermodynamic basis is also included in this thesis, the thermodynamic principles underlying the models used to calculate the equilibria are presented here. There are a number of models (37,52) used for the calculation of phase equilibria. Only very simple models, (ideal and regular solution models), which are very common and have been applied to a number of alloy systems, will be discussed here to describe the mixing energy (ΔG_{mix}) of the solution.

(3.4.1) Ideal Solution Model:

Ideal Solution:- An ideal solution is one in which:

(i) No heat is absorbed or evolved during mixing ($\Delta H_{mix}=0$).

(ii) No volume change occurs during mixing ($\Delta V=0$).

(iii) The activity is equal to the mole fraction of the constituents.

(iv) The activity coefficient is unity.

(v) The forces of attraction between dissimilar atoms are equal to the forces between similar atoms.

(vi) Atoms are surrounded by the same number of nearest

neighbour atoms.

(vii) The entropy of an ideal solution is a definite positive quantity.

Consider the liquid phase in a system of two metals A and B, forming an ideal solution which is characterized by a random distribution of the atoms on a lattice with an interchange energy of zero. So ΔG_{mix} is only influenced by the temperature and entropy of mixing.i.e;

$\Delta G_{mix} = \Delta H_{mix} - T\Delta S_{mix}$ ----------(3.1)

when the solution is ideal $\Delta H_{mix} = 0$ So,

$\Delta G_{mix} = - T\Delta S_{mix}$ ----------(3.2)

In statistical thermodynamics entropy is related to the randomness according to the Boltzmann's equation

$S = k\ln\omega$ ----------(3.3)

Where k is Boltzmann's constant and ω is the number of ways of arranging the system or measure of the randomness. There are two contributions to the entropy. One is a thermal contribution, S_1, which will be zero for an ideal solution, and the other is the configurational contribution, S_2. All configurations of A and B atoms are equally probable. Therefore the number of distinguishable ways of arranging the atom sites is:

$$\omega = \frac{(N_A + N_B)!}{N_A! + N_B!}$$

Where N_A and N_B are the number of A and B atoms respectively. So equation (3.3) becomes:

$$\Delta S_{mix} = S_2 - S_1 = k\ln\left[\frac{(N_A + N_B)!}{N_A! + N_B!}\right]$$

Applying the Stirling's approximation, $\ln m! \cong m \ln m - m$

$$\Delta S_{mix} = -k\left[N_A \ln\left(\frac{N_A}{N_A + N_B}\right) + N_B \ln\left(\frac{N_B}{N_A + N_B}\right)\right]$$

But $N_A = X_A N$ and $N_B = X_B N$ (where X_A and X_B are the mole fractions of A and B respectively and N is Avogadro's number). Therefore,

$$\Delta S_{mix} = -kN\left[X_A \ln X_A + X_B \ln X_B\right] \qquad \text{----------(3.4)}$$

But kN = R (Universal gas constant) Hence,

$$\Delta S_{mix} = -R\left[X_A \ln X_A + X_B \ln X_B\right] \qquad \text{----------(3.5)}$$

which is the entropy of formation of an ideal binary solution, independent of the temperature of the solution. Fig 3.4 shows the variation of ΔS_{mix} with composition in an ideal binary A–B solution. The free energy of mixing, ΔG_{mix}, for an ideal solution is obtained from equation (3.5) and (3.2):

$$\Delta G_{mix} = RT\,(X_A \ln X_A + X_B \ln X_B) \qquad \text{----------(3.6)}$$

Fig 3.5 shows ΔG_{mix} as a function of composition and temperature. Suppose now that the reference phases for pure A and B are not the liquid phase. In this case it is necessary to consider the free energy of transformation of the pure metals from the reference phases to the liquid phase which can be labeled by G_A and G_B respectively. The contribution from these terms to the Gibbs energy of formation will be: $X_A G_A + X_B G_B$ (as described previously).

Therefore, the general expression for the Gibbs energy of formation for such an ideal solution is given by: [i.e from equation (2.26) and

(3.6)].

$$G_{Alloy} = X_A G_A + X_B G_B + RT\,(X_A \ln X_A + X_B \ln X_B) \text{ ----------(3.7)}$$

This expression could equally apply to the transformation to another phase (such as f.c.c & b.c.c). Therefore, for some materials a simple ideal solution model is able to represent known thermodynamic and phase diagram data adequately. For a ternary alloy system of components A, B and C the equation can be written as:

$$G_{Alloy} = X_A G_A + X_B G_B + X_C G_C + RT\,(X_A \ln X_A + X_B \ln X_B + X_C \ln X_C) \text{---(3.8)}$$

It can easily be extended to any number of components in the solution to give the general equation:

$$\Delta G = \sum_{i=1}^{n} X_i G_i + RT \sum_{i=1}^{n} X_i \ln X_i$$

where n is the number of components and X_i their concentrations, G_1 is the Gibbs energy of transformation from the pure component i in its reference state to the phase in question at temperature T_i.

(3.4.2) Regular Solution Model:

Solutions which exhibit ideal behavior are rare. In practice mixing is usually either exothermic or endothermic as the bond energies between like and unlike atom species are not identical. If it is assumed that the mixed atoms are symmetrically arranged in the lattice (i.e substitutional solution in which every atom is surrounded by z nearest neighbours, z being the same whatever central atom is considered and for which the mean composition is similar to the rest of the solution) and that ΔH_{mix} is only a consequence of the

bond energies between adjacent atoms, then the resultant solution is said to be "regular" i.e $\Delta H_{mix} \neq o$ and entropy is positive and equal to that for an ideal solution, as no ordering is assumed in the solution. For this assumption to be valid it is necessary that the volumes of pure A and B are equal and do not change during mixing, so that the interatomic distances and bond energies are independent of the composition.

The deviation of a solution from its ideal behavior gives rise to a concept which is known as the excess Gibbs free energy, G_{EX}, which is the most important feature of interest. This subject has been reviewed by a number of authors, particularly by Oriani and Alcock (53), Ansara (37,43) and Kapoor (54). The regular solution model has been widely used as a first approximation to estimating thermodynamical properties of binary alloys and for computing phase diagrams in ternary systems. This theory of regular solution was developed by Hildebrand (55-57).

Consider a mole of binary solution of A and B elements making a regular solution in which enthalpy changes on mixing arise from a net interaction between the elements. Now there will be three interaction energy terms present:

(i) The energy of A–A pair of atoms, E_{AA}.

(ii) The energy of B–B pair of atoms, E_{BB}.

(iii) The energy of A–B pair of atoms, E_{AB}.

The total lattice energy of a solution having a composition in mole

fraction terms (X_A and X_B) can be written as:

$$E = n_{AA}E_{AA} + n_{BB}E_{BB} + n_{AB}E_{AB} \qquad \text{----------(3.9)}$$

where n_{AA}, n_{BB} and n_{AB} are the number of bonds types A–A , B–B and A–B respectively. Similarly the enthalpy of a homogeneous solution can be represented as:

$$H = n_{AA}H_{AA} + n_{BB}H_{BB} + n_{AB}H_{AB} \qquad \text{----------(3.10)}$$

where H is introduced to represent the enthalpies of the bonds. If the solution has a coordination number 'z' then the total number of bonds will be 1/2 zN (N is the number of atoms per mole).

Hence number of A–A bonds = Total number of bonds x Probability of A–A bonds. i.e,

$n_{AA} = 1/2\ zNX_A^2$ Similarly,

$n_{BB} = 1/2\ zNX_B^2$

$n_{AB} = zNX_AX_B$

So equation (3.10) becomes:

$$H = H_1 = \frac{zN}{2}\left[X_A^2H_{AA} + X_B^2H_{BB} + 2X_AX_BH_{AB} \right] \qquad \text{----------(3.11)}$$

The enthalpy of pure A and pure B in the unmixed state can be obtained from equation (3.11) by substituting the value $X_A = 1$ and $X_A = 0$ (when $X_B = 1$) respectively,

For pure A $$H_A = \frac{zNH_{AA}}{2}$$

and for pure B $$H_B = \frac{zNH_{BB}}{2}$$

So the enthalpy of the solution in the unmixed state is given by:

$$H_{Unmixed} = H_2 = X_AH_A + X_BH_B = \frac{zN}{2}\left[X_AH_{AA} + X_BH_{BB} \right] \qquad \text{----(3.12)}$$

The enthalpy of mixing ΔH_{mix} on forming the non-ideal solution is given by; $\Delta H_{mix} = H_1 - H_2$ [i.e eq. (3.11) – eq. (3.12)]

$$\Delta H_{mix} = \frac{zN}{2}\left[X_A H_{AA} (X_A - 1) + X_B H_{BB} (X_B - 1) + 2X_A X_B H_{AB} \right]$$

$$\Delta H_{mix} = \frac{zN}{2} X_A X_B \left[2H_{AB} - H_{AA} - H_{AB} \right] \qquad \text{----------(3.13)}$$

or $\Delta H_{mix} = NX_A X_B \omega$ Where $\omega = z/2\ (2H_A H_B - H_{AA} - H_{BB})$

$$\Delta H_{mix} = X_A X_B \Omega_{AB} \qquad \text{----------(3.14)}$$

where $\Omega_{AB} = N\omega$; In equation (3.14) ΔH_{mix} is the enthalpy of mixing and therefore the excess Gibbs free energy is given by:

$$\Delta G_{EX} = X_A X_B \Omega_{AB}$$

For a ternary system of components A, B and C, the excess free energy is given by:

$$\Delta G_{EX} = X_A X_B \Omega_{AB} + X_A X_C \Omega_{AC} + X_B X_C \Omega_{BC}$$

The expression for the excess Gibbs free energy term can be generalized for a multicomponent system through the same procedure outlined above to give:

$$\Delta G_{EX} = \sum_{i=1}^{n-1} \sum_{j=i+1}^{n} X_i X_j \Omega_{ij}$$

Fig 3.6 shows the curve for Gibbs energy of formation with different values of the interaction parameter of 'Ω' i.e factor $[H_{AB} - 1/2\ (H_{AA} + H_{BB})]$. When $\Omega = 0$, $[H_{AB} = 1/2\ (H_{AA} + H_{BB})]$ the bonding forces are equal between similar and dissimilar atoms and the solution is ideal, as in curve (a). If Ω is negative, $[H_{AB} < 1/2\ (H_{AA} + H_{BB})]$, ΔH_{mix} will be negative. Also the force of attraction between dissimilar atoms is greater than the similar atoms. This implies that there is a tendency towards the formation of a superlattice or compound. This

is shown by curve (b) in the Figure, showing the negative enthalpy of formation. If Ω is positive the ideal entropy term and enthalpy of formation term oppose each other and at a certain temperature will result in a curve such as (c) with two minima leading to the region where two phases of the same structure are immiscible. For a regular solution a positive interaction term will always lead to a miscibility gap for the temperature less than $\Omega/2R$ providing the phase itself is stable.

The free energy on mixing of a binary, A-B, regular solution is given, from equation (3.1), (3.5) and (3.14) as:

$$\Delta G_{mix} = X_A X_B \Omega_{AB} + RT(X_A \ln X_A + X_B \ln X_B) \qquad \text{----------(3.15)}$$

and by analogy for a ternary, A-B-C, regular solution the equation (3.15) can be written as:

$$\Delta G_{mix} = X_A X_B \Omega_{AB} + X_A X_C \Omega_{AC} + X_B X_C \Omega_{BC} + RT(X_A \ln X_A + X_B \ln X_B + X_C \ln X_C)$$

Also from equation (2.26) and (3.15), for a binary system:

$$G_{Alloy} = X_A G_A + X_B G_B + X_A X_B \Omega_{AB} + RT(X_A \ln X_A + X_B \ln X_B).$$

CHAPTER 4

(4) DETERMINATION OF PHASE EQUILIBRIA

(4.1) INTRODUCTION TO METHODS FOR THE DETERMINATION OF PHASE EQUILIBRIA

The two classical methods for the determination of phase diagrams are thermal analysis and microscopic examination, and many diagrams have been determined by these means alone. X-ray diffraction, however, supplements these older techniques in many useful ways. In addition it provides the means for determining the crystal structure of the various phases involved. Most of the phase diagrams today are therefore determined by the combination of all these three techniques. However, physical properties are also used to plot phase diagrams.

In general, the various experimental techniques differ in sensitivity, and therefore in usefulness, from one portion of a phase diagram to another. Thus, thermal analysis is the best method for the determination of solidus and liquidus, including eutectic and peritectic reactions, but it may fail to reveal the existence of

eutectoid and peritectoid reactions, because of the sluggishness of some solid-state reactions or the small heat effect involved. Such features of the diagram are best determined by microscopic examination or X-ray diffraction, and the same applies to the determination of solvus (solid solubility) curves. So it should be noted, any way, that no phase diagram can be considered fully reliable until corroborating observations have been made by at least two independent methods. Even so, the diagram cannot be accepted if its construction violates the phase rule or any other rules of construction that have been derived by thermodynamical reasoning.

There are two types of methods, involved for the determination of phase equilibria i.e the static and the dynamic method.

(4.1.1) Static Methods:

Static methods are those in which the temperature of the sample is held constant until equilibrium is attained (i.e determination occurs at fixed temperature). The most widely used of these is the quenching method. As its name implies, upon achieving equilibrium, the specimen is quenched to ambient temperature, which generally involves rapid cooling in a bath of water, mercury or heavy oil. Its success depends upon the preservation of the phase assemblage present at equilibrium upon cooling to room temperature. Metallographic and X-ray techniques are usually employed to analyse the phase assemblage of specimens because of their high

sensitivity of detection of second phase particles. The principle advantage of static methods is that they allow conclusive identification of the phases present. These methods, although time consuming, have the virtue of experimental simplicity and straight forward interpretation. Static methods are ideal for determining the vertical and near vertical phase boundaries.

(4.1.2) Dynamic Methods:

Dynamic methods are those in which phase equilibrium determination occurs over a temperature range. This method involves monitoring of some property as a function of temperature and recording the changes which occur. Generally the method consists of expressing the relationship between the "degree of change" and time. This approach possesses two advantages over the static method. Since quenching is not involved, it is possible to explore the limit of phase stability quickly and the danger of a change in phase assemblage occurring during quenching is avoided.

Dynamic methods include thermal analysis, electrical conductivity (resistivity) measurements, thermal gravimetric analysis, vapour pressure measurements and dilatometric method etc. Techniques such as dilatometry and electrical resistivity are suitable for solid state transformations, while thermal analysis is more applicable to phase changes which involve a liquid component.

As described earlier the static method is preferred for

determination of vertical and near vertical phase boundaries, while dynamic methods are ideal for isothermal phase boundaries. Hence, a combination of the two methods is usually used for the determination of phase equilibria.

(4.2) THERMAL ANALYSIS

Thermal analysis is a general term covering a group of related techniques whereby the dependence of the parameters of any physical properties of a substance on temperature is measured. Changes in thermal properties are commonly employed for detecting phase change/structural change. When a transformation takes place at constant temperature, there will occur an evolution or absorption of a latent heat of transformation. In other cases, changes will occur in the specific heat of the material. Therefore, if a specimen is heated or cooled under uniform conditions a structural change will be indicated by the discontinuities or abnormal curvatures in the time/temperature curves. Under suitable experimental conditions the determination of time/temperature curves, or other curves derived from these, may enable one to deduce the temperature or temperature range associated with certain transformations. The determination and interpretation of such curves is known as thermal analysis. The principle techniques of thermal analysis are shown in Fig 4.1 as a "family tree" (58). Several reviews and books are available on this general subject. A general review on thermal analysis is provided by McLaughlin (59)

and Antonin Blazek (60). Thermal analysis is extensively described by Hume-Rothery et al (31) and Raynor (61). Several methods of thermal analysis are also described in detail by Mackenzie (58). The most commonly used thermal analysis techniques are as follow:

(4.2.1) Techniques Dependent on Weight Changes (Thermogravimetery, TG):

A technique whereby the weight of a substance in an environment heated or cooled at a controlled rate, is recorded as a function of temperature or time. This type of technique is used where an increase or decrease of mass occurs like thermal decomposition, sublimation, dehydration, oxidation and reduction etc.

(4.2.2) Techniques Dependent on Dimensional Changes (Dilatometry):

A technique whereby changes in dimension(s) of a substance are measured as a function of temperature. This method utilizes the change in volume associated with nearly all phase changes. It measures the change in length of a specimen heated or cooled at a given rate. Curves of length against time and temperature against time are obtained simultaneously, and these may be combined (in many instruments automatically) to give length-temperature curves. The dilatometric curves are simpler in interpretation to ordinary heating and cooling curves, and the temperature of a transition is indicated by a change in direction of the curve. In comparison with other methods of thermal analysis, this technique

has the advantage that the heating and cooling rate may be as slow as desired, and temperature may be held at any value for a time sufficient to enable equilibrium to be attained. The method, basically, is suitable only for the determination of solid state reactions. For many alloy systems, however, it is impossible to prepare specimens sufficiently uniform and homogeneous and of suitable dimensions to apply the method accurately. This technique is especially useful for ceramics and glasses.

(4.2.3) Techniques Associated With Evolved Volatiles (Evolved gas detection EGD and Evolved gas analysis EGA):-

The EGD term covers any technique of detection whether or not a volatile product is formed during the thermal analysis. EGA is a technique for determine the nature and/or amount of volatile product or products formed during thermal analysis.

(4.2.4) Techniques Associated with Energy Changes:-

Every method has its own advantages and disadvantages. For the study of conventional phase diagrams, the energy changes in the form of heat are used in preference to those changes as described above. These are mainly of three types.

(a) Differential Thermal Analysis (DTA).

(b) Smith Thermal Analysis (STA).

(c) Differential Scanning Calorimetry (DSC).

(a) Differential Thermal Analysis (DTA):- Differential thermal

analysis is a technique for recording the difference in temperature between the substance and a reference material against either time or temperature as the two specimens are subjected to an identical temperature regime in an environment heated or cooled at a controlled rate. The curve so obtained is called a DTA curve. The detail and principle of this method are given in detail in the next section.

(b) Smith Thermal Analysis (STA):- DTA has been used extensively in the study of phase equilibria. It has the ability to detect very small thermal effects. In this technique when any transformation occurs, the temperature gradient between the furnace and the specimen increases or decreases. This causes the rate of heat transfer to increase or decrease. Thus the specimen is forced through the reaction relatively quickly, increasing the possibilities of developing heterogeneity and thus the spurious thermal effects. These spurious thermal effects can be avoided by the adoption of the Smith Thermal Analysis (STA) technique whereby a constant temperature difference can be sustained between the specimen and the furnace, ensuring that the rate of the heat transfer is fixed at a steady value, resulting in homogeneity being maintained both during and after each phase change. So, due to a significant improvement over DTA, the STA technique can be used quite safely for thermal analysis for the determination of phase diagrams. With calibration, STA apparatus can also provide the quantitative information on the heat capacity and the enthalpy of any transformation encountered in the specimen. The detail and principle of STA are given in the next section.

(c) Differential Scanning Calorimetry (DSC):- This technique is based on the original principle of DTA. DSC is a technique of recording the energy necessary to establish zero temperature difference between a substance and a reference material against either time or temperature as the two specimens are subjected to an identical temperature regime in an environment heated or cooled at a controlled rate, and the record is called a DSC curve which represents the heat supplied per unit time against either time or temperature. This technique might also be called inverse DTA. In this method the sample is submitted to linear heating, and the rate of heat flow in the sample, proportional to the instantaneous specific heat, is measured continuously. This method involves a continuously increasing or decreasing temperature environment. However extra heat is added to the sample or to the reference sample as necessary to maintain the two at identical temperature. This amount of heat is recorded as a function of time or temperature. Hence what is measured is not the temperature difference as in classical DTA, but the electrical heat input necessary for the maintance of isothermal conditions. The DSC is being used more often mainly because of the experimental simplicity and availability of the apparatus. The DSC not only gives the information about the temperature at which the melting or transformation occurs, but it can also give information for specific heats, quantitative measurements of enthalpies of fusion and transformation etc. This has been applied, for example, by Plato and Glasgow (62).

The disadvantage of the DSC availabe in the department is that it can be used only up to 700°C. The use of the method at higher temperature would be advantageous as the determination of specific heat and heat of reaction is relatively simple and direct.

(4.3) PRINCIPLES OF DIFFERENTIAL THERMAL ANALYSIS

In DTA, thermal arrests are detected as a result of heat absorbed or evolved by the sample, causing a difference in temperature between the sample (under investigation) and a reference material. The reference material used should not be exhibit any phase transformation over the temperature range to be studied in the experiment. Two thermocouple junctions are used. One is close to the sample under investigation and the other is close to the reference material. The junctions are connected in series and are wired in opposition to each other so that when both samples are at the same temperature the net differential e.m.f is zero. Fig 4.2 shows a schematic diagram of this arrangement, where T_S and T_R are the temperatures of the sample and the reference material respectively. One more thermocouple is also placed in the furnace, which determines the furnace temperature. Any temperature difference ΔT between the two specimens is recorded as a differential e.m.f. The cooling and the heating rate of the furnace is

normally preset to some fixed value. Thus, the temperature of the furnace is completely independent of the temperature of both the sample and reference material. So the temperature of the furnace is not influenced by any changes or thermal events that occur in the sample during experiment. This is shown schematically in Fig 4.3. When a change in the sample occurs with absorption or evolution of heat, a temperature difference (ΔT) arises between the sample and the reference material. The differential e.m.f will have a zero value in the absence of any change of state. The phase changes or reactions are detected as peaks in the differential e.m.f vs time curve during heating or cooling. If the temperature of the sample falls below that of the reference material, the ΔT will be negative and the peak will be an endothermic peak (i.e in case of cooling). If the temperature of the sample rises above that of the reference material, ΔT will be positive and the peak will be an exothermic peak (i.e in case of heating).

(4.4) PRINCIPLES OF SMITH THERMAL ANALYSIS

The STA technique was proposed by Smith (63). The original Smith technique provided a quantitative measurement of specific heat and latent heat. However, this method is also very useful for the measurement of the phase boundary temperatures. The apparatus requires two thermocouple junctions, Fig 4.4. One of these is placed in the centre of the sample and serves as measuring thermocouple,

while the other is in contact with the furnace wall and lies in the same horizontal plane as the junction in the sample. In this technique it is the millivolts difference between the two junctions which is maintained at some preset value by the controlled circuitry. This will maintain a constant temperature difference between the sample and the furnace wall which results in a constant rate of heat transfer between the furnace and the sample over small ranges of temperature. Alternatively a differential thermocouple with its junction inside and outside the container wall, can be used to regulate the temperature difference as shown in Fig 4.5.

For a cooling run the differential e.m.f will be negative and heat will transfer from the sample to the furnace, and for a heating run the differential e.m.f will be positive and heat will transfer from the furnace to the specimen. At constant heat transfer rate, the rate at which the temperature of the sample changes is governed by the mass and the heat capacity of the sample. When the sample arrives at a curved phase boundary on heating or cooling a new phase will appear or disappear. At this point the rate at which the enthalpy of the system changes with temperature shows a discontinuity. Thus, if the sample is gaining or losing heat at constant rate, one will observe a change in the rate at which the temperature changes with time at this point. For an isothermal phase reaction, this rate falls to zero. Fig 4.6 shows a schematic temperature-time curve on heating. It can be seen that the temperature of the furnace at any point is governed by events occurring in the sample. To respond quickly to

these changes, the thermal inertia of the Smith furnace is deliberately kept low. In this situation, when a sudden change within the sample such as liquid to solid transformation happens, the furnace will respond to the change very quickly and a sharp thermal arrest will be detected.

It should be noted that the e.m.f/temperature-difference relation of the differential thermocouple is not quite independent of temperature. Also the thermal conductivity of any refractory material is not exactly constant as the temperature changes. Consequently the heat flow varies slightly with temperature. However, a given container can be calibrated over a range of temperature by using a mass of known specific heat and will give reproducible quantitative results.

In addition to examining the temperature of any phase transformation, the STA has the ability to supply further data on thermal properties of the alloy like heat capacity and latent heat (63). To obtain this information the apparatus must be calibrated by using a thermally inert specimen of known mass whose thermal properties are known over a wide range of temperature. Copper is a suitable standard (63) since it undergoes no transformation and its specific heat is known fairly accurately over a wide range of temperature. Three compatible sets of measurements are required to derive the thermal data, i.e, the time/temperature curves for the specimen, the standard specimen and the empty container alone. In

all these experiments the value of the temperature difference across the walls of container must have the same constant value.

The heat generated by the furnace serves to supply the heat capacity of the specimen and the thermal barrier (container) and the enthalpy of any transformation i.e:

Heat Generated = Heat to Raise the Temperature of the Specimen + Heat used to Raise the Temperature of the Container + Transformation Heat

$q\Delta t_1 = m_1 C_1 \Delta T_1 + m_c C_c \Delta T_1 + L_1 m_1$

Where q = Heat flow per unit time.

C_1 & C_c = Heat capacities of unknown specimen and container respectively.

m_1 & m_c = Masses of specimen and container (effective part of the container).

ΔT_1 = Temperature change in time Δt_1.

L_1 = Latent heat of transformation.

The heat capacity of the unknown specimen, then, is given by (63)

$$C_1 = \frac{m_1}{m_2} C_2 \cdot \frac{\frac{\Delta t_2}{\Delta T_2} - \frac{\Delta t_c}{\Delta T_c}}{\frac{\Delta t_1}{\Delta T_1} - \frac{\Delta t_c}{\Delta T_c}}$$

where '2' stand for the standard specimen and $\frac{\Delta t}{\Delta T}$ is the slope of the time-temperature curve or the figure obtained directly for an inverse rate in the usual way.

Also the Latent heat of transformation is given by

$$L_1 = \frac{m_2}{m_1} \cdot C_2 \cdot \frac{t}{\frac{\Delta t_2}{\Delta T_2} - \frac{\Delta t_c}{\Delta T_c}}$$

Where 't' is the arrest time during which $\Delta T = 0$

The heat of transformation of the pearlite/austenite transformation has been determined in this way by Hagel, Pound and Mehl (64). If the transformation occurs over a range of temperatures, the enthalpy of the reaction for the unknown specimen will appear as an apparent heat capacity and can be obtained by the graphical integration using the standard formula:

$$H_1 = \int_{298}^{T} C_1 \, dT$$

Where C_1 is the heat capacity of the unknown specimen.

(4.5) COMPARISON OF DTA AND STA

The two methods have been discussed in detail in the previous sections. Both these methods are used for the determination of phase diagrams. But STA has some significant advantages over the DTA.

One of the major advantages of STA is that it provides the facility to maintain the furnace temperature at a constant amount above or below that of the specimen transformation temperature. It remains constant during a horizontal arrest and rises or falls only when the specimen heats or cools, as in this process the furnace is controlled by the specimen as shown in Fig 4.6. Temperature gradients within the specimen are reduced. All these factors are in favour of homogeneity of the specimen, leading to the formation of sharp arrests and the reduction of spurious thermal effects. Consequently the interpretation of the curves is very easy.

In the conventional DTA method, the heating or cooling rate of the furnace is preset and is independent of the specimen temperature as shown in Fig 4.3. So when a transformation occurs within a specimen the temperature gradient between the specimen and the furnace will increase, thereby causing the rate of heat transfer to increase. Consequently the specimen is forced through the reaction relatively quickly, increasing the possibility of developing heterogeneity and thus spurious thermal effects. Hence interpretation of these results in relation to the phase equilibria becomes more difficult.

The other major advantage is that STA makes possible the detection of any small heat effect at a temperature only a few degrees below that at which a major effect has occurred, while with the

conventional DTA method sufficient stabilization after a large heat effect for the detection of a small one may not occur until the specimen has reached a temperature of as much as 30°C to 50°C from that at which the large effect occurred.

One more advantage of the Smith equipment is the design which allows a liquid specimen to be stirred with the sheath of the measurement thermocouple. However, commercial DTA equipment in general is not fitted with a stirrer unless it is especially modified.

In addition to these advantages, Smith's method is able to determine the quantitative heat measurements, specific heats and latent heat, as described earlier. Moreover it is accurate, inexpensive and quick in response, even if the the change is very small.

(4.6) REASONS FOR USING STA FOR PRESENT STUDY

From the above discussion it can be deduced that the Smith technique of thermal analysis provides the specimen under examination with thermal conditions which offer a significant improvement over DTA for the determination of metallurgical equilibrium diagrams. On this basis the STA technique was selected for the determination of phase boundaries in the present study. It is probable that this method provides the best compromise between accuracy and simplicity for routine determination. It has been used

successfully by several investigators (50,65-73)

(4.7) STA APPARATUS

The STA apparatus is shown in Fig 4.7. The design of the furnace used is as shown in Fig 4.4, taken from the original paper by the Smith (63). The sectioning view of the furnace is shown in Fig 4.8. All explanations are given with the Figures.

CHAPTER 5

(5) EXPERIMENTAL METHODS

(5.1) MATERIALS

The alloys used for thermal analysis and for isothermal transformation studies were prepared from high purity metals supplied by different sources. The details are given as follows:

Metal	Source	Purity
Gold	Englehard Limited	99.9999%
Germanium	GEC Hirst Research. Centre Wembley. and BDH Limited.	99.9999%
Indium	GEC Hirst Research Centre Wembley.	99.9999%
Gallium	GEC Hirst Research Centre Wembley.	99.99%
Zinc	Johnson Matthey.	99.9999%
Cadmium	Aldrich Chemical Co.	99.9998%
Lead	BDH Limited.	99.9999%
Tin	International Tin Research Institute	99.9999%

(5.2) SAMPLE PREPARATION FOR THERMAL ANALYSIS

Different methods have been used for the sample preparation of alloys according to the nature of the metals used.

(5.2.1) Alloys in the AuZn-Pb, AuGa-Pb and $AuGa_2$-Pb Systems:

The weighed amount of each sample was between 2–3g for the thermal analysis. Each alloy was melted in a silica crucible, 9 mm o.d and 1 mm wall thickness, under a shield of burning hydrogen to avoid oxidation. Once the alloy had attained a temperature 30–50 ^{o}C above the estimated liquidus temperature, the melt was stirred vigorously for a while with the help of the silica thermocouple sheath to ensure homogenization. Then, keeping the silica thermocouple sheath right in the centre of the molten specimen, the silica crucible was immersed into cold water, resulting in a fine-grain structure. This is the same procedure as reported by Humpston and Evans (65). The assembly comprising the alloy in the silica crucible, with the embedded thermocouple sheath, was then carefully transferred into the thermal analysis furnace.

(5.2.2) Alloys in the AuIn-Ge and $AuIn_2$-Ge Systems:

The procedure for preparing samples for thermal analysis for these systems was similar to that described above [5.2.1 section] with the exception that the molten alloys were quenched into boiling water as described in (74), to counter the tendency of the silica crucibles to crack when quenched into cold water. Cracking is associated with

the expansion of Ge on solidification. The assembly was then transferred into the thermal analysis furnace as described above.

(5.2.3) Alloys in the AuZn-Ge, AuGa-Ge and $AuGa_2$-Ge Systems:

Even when quenched into boiling water, these alloys were prone to crack the silica crucibles. So conventional alloying techniques were used as described in (75-77), where the weighed amounts of the constituent elements between 2–4 g were placed into a silica crucible, (of the same size as described in previous section) and the silica thermocouple sheath was inserted into the silica crucible. This assembly was placed carefully into the thermal analysis rig. The constituents were then, allowed to melt in the STA furnace under an atmosphere of dry 15 vol.%H_2 and 85 vol.%N_2 gas. Melts were maintained above the estimated liquidus temperature for 1–2 hour with stirring from time to time to ensure homogeneity. The thermal analysis followed immediately after melting and homogenization, without an intermediate quench.

(5.2.4) Alloys in the AuCd-Ge System:

The procedures for alloy preparation described in the above section [section 5.2.3] were further modified for the AuCd-Ge alloy system. Now not only the cracking of the silica crucible, on the solidification of Ge, but the high vapour pressure of the Cd at elevated temperature necessitated further modification of the technique. Two types of samples were prepared for thermal analysis for this alloy system as follows, which have been described in (78).

(i) The weighed (2–4 g) quantities of Au, Cd and Ge were placed in the silica crucible. The remainder of the crucible was filled with charcoal and a lid was placed on the top with a central hole through which the silica thermocouple sheath was inserted. The assembly was placed carefully into the thermal analysis furnace and constituents were allowed to melt. The melt was held above the estimated liquidus temperature for 15 to 20 minutes, whilst it was stirred continuously with the silica thermocouple sheath to ensure homogeneity. Thermal analysis of the alloy was then started.

(ii) In the alternative procedure, the weighed amount of the constituent elements were sealed in an evacuated silica crucible, (of the same dimensions as used in the other systems), keeping the silica thermocouple sheath in the centre of the constituent elements. This assembly was then placed into the thermal analysis rig and the alloy was allowed to melt and to attain a temperature above the estimated liquidus temperature.

(5.2.5) Alloys in the AuCd-Pb System:

Again due to the high vapour pressure of Cd at elevated temperature, two types of samples were prepared for thermal analysis.

(i) The procedure to prepare alloys was similar to that described in section [5.2.4(i)] with the exception that instead of melting the constituents in the furnace, they were melted and quenched into cold water, before placing in the thermal analysis furnace, as the absence of Ge allowed quenching without the risk of cracking the silica crucible.

(ii) The second procedure was again the same as described in section [5.2.4 (ii)] with one modification that the alloy was melted and quenched in cold water before placing in the rig for thermal analysis, as again absence of Ge allowed quenching without the risk of cracking the silica crucible.

(5.3) THERMAL ANALYSIS (EXPERIMENTAL PROCEDURE)

The thermal analysis was carried out, basically, using the Smith (63) techniques as described by Humpston and Evans (65). After the quenched alloy had been prepared in the manner described in section [5.2.1], [5.2.2] and [5.2.5], it was placed inside the Smith Thermal Analysis furnace. Then the calibrated thermocouple was lowered in to the specimen through the silica thermocouple sheath. Now the furnace was allowed to heat up and held at a temperature 20–30 ^{o}C below the lowest estimated arrest temperature for 30–40 min to establish thermal equilibrium. The lowest arrest temperature was determined by heating the alloy through the reaction at a rate 2-3^{o}C-min^{-1}. When this heating run was completed the alloy was again held 20–30 ^{o}C above this lowest arrest point for 30-40 min, and then allowed to cool down at a cooling rate of 2–3^{o}C-min^{-1} through the reaction. These heating and cooling cycles were repeated at least two times for each alloy to establish the lowest arrest temperature.

The effectiveness of quenching the alloy followed by this thermal cycling technique to avoid a spurious thermal effect is described by Evans and Prince (69). After one reaction had been well established at the solidus point, the sample was reheated until melting was completed at the estimated liquidus point. The alloy was again held 20–30°C above this estimated liquidus temperature for 30–40 min. and allowed to cool down through the liquidus arrest temperature, at a rate of 2-3°C-min^{-1}. This liquidus arrest temperature with cooling run was determined at least twice for each alloy composition.

The alloys described in section [5.2.3] and [5.2.4] were prepared by the conventional method and were melted in the STA furnace. So the thermal analysis was started from the liquidus arrest for these alloys as described by (75-78). Melts were maintained above the liquidus temperature for 1–2 hr (but only 15–20 min for Cd and Ge containing alloys) with frequent stirring to ensure homogeneity. Thermal analysis during solidification was carried out at a cooling rate of 2–3°C-min^{-1}. The alloy was then held for 1 hour below the lower arrest temperature before a heating run was made at a heating rate of 2–3°C-min^{-1} to determine the solidus temperature. These cooling and heating cycles for solidus and liquidus arrest temperatures were repeated two or three times for each alloy composition.

The alloys were stirred continuously during cooling to determine

the liquidus temperature. Stirring of liquid alloy reduces the extent of undercooling during the cooling run. Hence the accuracy of the liquidus temperatures determination increased. The arrest temperatures for the solidus line were obtained from both heating and cooling curves, while the arrest temperatures for the liquidus were taken only from the cooling curves.

All thermal analysis was performed under the dry atmosphere of 15 vol.%H_2 and 85 vol.%N_2 to avoid oxidation. Thermal analysis of all alloys which were contained in sealed evacuated silica crucibles were dealt with in a similar fashion as described above with the omission of the stirring option, as the silica thermocouple sheath was fixed with the sealed crucible.

(5.3.1) Print Out of STA Curve:

The print-outs of the thermal analysis curves for a cooling and heating run with pure Indium are shown in Figs 5.1 and 5.2 respectively. The first column represents the actual temperature of the specimen expressed in millivolts. The second column shows the millivolts difference between the actual reading and values obtained by the extrapolation of the previous 20 readings. The last column shows the heating or cooling rate of the specimen in $^{o}C/min$. A negative sign in this column identifies the cooling rate as in Fig 5.1, while there is no sign for heating rate, as shown in Fig 5.2. The computer programme was written to give readings for all three columns at intervals of 18 seconds. The curve with "Δ" symbol (i.e dotted line curve 'U') shows the time versus second column reading.

The curve with "+" symbol (i.e bold line curve 'V') shows the heating or cooling rate of the specimen (i.e the reading of the third column) versus time. At the start of a reaction, there is a sudden change in heating or cooling rate, which appears as a change of slope on the curve. In Fig 5.1 there is a change in the cooling rate, and change in slope at point (1) on the curve, while the reaction is completed at point (2). So the melting point of Indium will be the maximum millivolts between the points (a) and (b), corresponding to the points (1) and (2) on the curve as shown in Fig 5.1. Hence the melting point (i.e 156.78 ^{o}C) of indium will be equal to 5.0862 millivolts. Also in Fig 5.2 for the heating run the melting point of indium (i.e 156.78 ^{o}C) will be equivalent to the minimum millivolts, 5.1202, between points (a) and (b) corresponding to the points (1) and (2) on the curve.

(5.3.2) Calibration of the Equipment:

The temperature measuring thermocouples of the thermal analysis apparatus (chromel-alumel) were regularly calibrated against the melting points of pure In, Sn, Pb, Zn and Sb from time to time during the course of the experiments. The temperature measurements are considered to be accurate within $\pm$ 1^{o}C, so far as thermocouple calibration behaviour is concerned. Periodically, a dummy run using a standard specimen was used to check the consistency of the apparatus.

(5.3.3) Composition:

The weight of each alloy was calculated in such a way that the sample, after melting, produced a roughly spherical shape within the silica crucible. This reduces thermal gradients and diffusion anisotropy. If no loss of a component occurred during thermal analysis it was diluted to form the next composition in the series. Alloys were usually started with 1 at.% of the constituent element other than the congruently melting compounds (i.e Ge and Pb) and diluted to 3 at.% and 5 at.% to provide STA data for three compositions. A second master alloy with 2 at.% of the same constituents was prepared and diluted to 4 at.% and 6 at.%. If consistent results were obtained for the six alloy compositions, the dilution procedure was used with confidence. At the end no variance was detected by reweighing and by SEM results, so the alloy compositions quoted are the nominal compositions based on the initial weights of the components. However, for Cd-containing alloys a new specimen was prepared for each experiment to avoid any weight loss risk due to the volatilization of Cd. All compositions were expressed as atomic percent.

(5.4) METALLOGRAPHY (OPTICAL)

Optical metallography was carried out to find out the eutectic points of the Au-Ge-X phase diagrams developed experimentally. For a particular system a number of specimens, with varying amounts of Ge around the estimated eutectic composition, were prepared.

Samples of alloys for metallographic examination were prepared by melting the constituents of a particular alloy in a silica crucible under the shield of a hydrogen flame (or under the charcoal atmosphere for Cd-containing alloys) to avoid oxidation. The alloys were stirred to homogenize, then held for a while in the liquid state before cooling in air to room temperature. The samples were sectioned longitudinally, mounted, ground and polished using standard techniques. In some phase diagram systems one phase present was softer as compared to the other and, hence, it was very difficult to obtained a good polished surface without scratches. The samples were, then, etched in suitable reagents specified in Appendix (1), and examined under the microscope.

(5.5) MICROHARDNESS

To give additional information about the hardness for all the pure congruent melting compounds, the microhardnesses have been measured. This was done using the Vicker pyramidal diamond indenter and suitable load.

(5.6) SCANNING ELECTRON MICROSCOPY (SEM)

The Scanning Electron Microscope (SEM) was used to identify the phases present in the specimens and for the counter check of the

compositions of the specimens. It was also used for photographic purposes.

(5.7) Au-Sn BINARY SYSTEM

(5.7.1) Long Time Annealing:

The constitution of the Au-Sn binary phase diagram is uncertain in the gold rich portion at lower temperatures. To rectify this uncertainty a series of Au-rich alloys covering the appropriate composition range were allowed to equilibrate isothermally at two selected temperatures (220°C and 300°C) with two sets of specimens for each temperature. One set of specimens at 300°C was withdrawn for examination after 4464 hrs (≅ 6 months), while the other set was withdrawn after 12864 hrs (≅ 18 months). Similarly the first batch of specimens at 220°C was withdrawn for examination after 13488 hrs (≅ 19 months), while the second set of specimens was withdrawn after 17000 hrs (≅ 24 months). Special techniques were adopted to prepare these specimens prior to placing in the furnaces, which are described below:

(5.7.2) Sample Preparation:

To reduce the diffusion paths and hence reduce the time to reach equilibrium, a number of techniques were tried for the preparation of the samples. Initially, after melting the constituents, the alloys were quenched in cold water. An attempt was made to cold work these samples by hammering, but due to the brittle nature of these

samples, hammering was not feasible. Rolling and pressing were tried, but again failed to produce thin specimens (in which the diffusion path can be reduced) due to the brittleness. Finally a special technique was applied to prepare the samples. This involved rapid quenching from the melt, where the constituent elements, weighing between 3–4 g for each alloy composition, were placed in a silica crucible and melted under a hydrogen flame, stirring well to homogenize. The molten alloy was held well above the liquidus temperature for a while, before pouring suddenly onto a well-cleaned, mild steel flat plate dipped into liquid nitrogen. The resulting sample was like a thin button/sheet. The button type specimens were then sealed in an evacuated silica tube. All specimens for each composition and temperature were prepared in the same manner.

After the heat treatment, the specimens were quenched suddenly into cold icy water. The samples for each composition were then mounted, ground and polished. A number of etchants were tried, but only a very dilute KI solution used as an etchant during polishing on gamma alumina proved to be suitable to identify the phases. These samples were examined by optical microscopy. The samples were also examined by SEM using Electron Microprobe Analysis techniques. During the long heat treatment many holes/pores/cavities were produced, which caused difficulties during microscopy and SEM examination.

(5.7.3) Heat Treatment/Temperature Control:

First the most stable zone of each furnace, one at 220°C and the other at 300°C, were checked by noting the temperature of different zones at different time intervals for four weeks. The temperatures were checked using a cylindrical 4 gm copper specimen in which a hole had been drilled to accommodate an alumel-chromel thermocouple, using an efficient furnace temperature controller. Then the specimens were placed into the uniform temperature zone of the furnace. An additional thermocouple was also placed near the specimens to counter check the temperature variation, if any. The maximum variation was not more than ± 4°C during the whole heat treatment period of time.

(5.7.4) Optical Microscopy:

After annealing had been completed the specimens were quenched into cooled icy water, sectioned through the centre and mounted in cold-setting polymer resin, so that the microstructure of the specimens would not be affected by the operating temperature of hot mounting. These specimens were ground, polished, etched and examined with an optical microscope at different magnifications.

(5.7.5) Electron Micro-Probe (X-Ray/SEM) Analysis:

Electron Micro-probe Analysis technique was employed to identify the phase or phases present in each sample. Both etched and unetched samples were used for this purpose.

CHAPTER 6

(6) RESULTS

(6.1) TERNARY PHASE DIAGRAMS

(Thermal Analysis Results)

The partial constitutions of Au-Ge-X and Au-Pb-X ternary alloys have been investigated, where X is one of the B sub-group metallic elements In, Ga, Zn, or Cd, of the periodic table which form one or more stable compounds with gold. The Smith Thermal Analysis Method, supplemented by metallographic and X-ray techniques, was used to determine the constitutions of the ternary systems.

(6.1.1) Au-Ge-X SYSTEMS

Prior to this investigation, the only published work on the phase relationships in Au-Ge-X ternary systems was an examination of the Au-rich corner of the Au-Ge-In system (79).

Eutectiferrous, quasibinary systems were found between Ge and the stable compounds AuX (AuIn, $AuIn_2$ AuGa, $AuGa_2$ AuZn, AuCd). The liquidus and solidus curves in all the systems were experimentally

determined only up to 50 or 60 at.%Ge, because expansion on solidification shattered the silica crucibles at higher Ge concentration. Both liquidus and solidus curves were extrapolated, therefore, from 50 (or 60 at.% Ge) to the pure germanium axis at the melting point of 938.5°C for Ge (80) and according to the eutectic temperatures of the relevant systems respectively.

Calculations of the liquidus curves for most of the AuX-Ge alloys using the equation:

$$\ln(1-X_{Ge}) = \frac{\left[\frac{1}{T_{AuX}} - \frac{1}{T_{Eu}}\right] H^{F}_{AuX}}{R} \qquad \text{----------(6.1)}$$

and a value from the literature (81,82) for the enthalpy of fusion for AuX, predicted eutectic compositions which were in good agreement with the experimental values.

The solubility of Ge in the AuX compounds was not determined directly. However, it was 1.3 at.% Ge for Cd and Zn containing alloys and less than 1.0 at.% Ge for In and Ga containing alloys at the eutectic temperatures. All alloys having more than this limited concentration of Ge, showed one liquidus and one solidus arrest at the eutectic temperature. All Au-Ge-X systems show complete miscibility in the liquid state for all compositions. The eutectic temperatures, eutectic compositions and solubilities of the various

systems which were examined are summarized in Figs 6.1 to 6.6 and in Table 1. The details are given as follow:

(6.1.1.1) Au-Ge-In SYSTEM:

The Au-Ge binary system shows a single eutectic reaction which was determined experimentally (83) to occur at 28 at.% Ge and 361°C. This is in good agreement with a recent computed version of the diagram (84). The Ge-In binary system also shows a single eutectic reaction at 99.9927 at.% In and at 156.29°C (85). The Au-In binary phase diagram is complex, showing the existence of two congruent melting-point line compounds, AuIn and $AuIn_2$. The most recent evaluation of this system was considered (86). All three binary phase diagrams involved in this ternary system are shown in Fig 6.7. The phase relationships which were found to occur in various portions of the Au-Ge-In ternary system are given below:

(a) AuIn-Ge Section:- The melting point of the stable compound AuIn has been given as, 506°C (87,88), 509.6°C (89) and 511°C (86). The value determined in the present work is 506±1°C in good agreement with references (87) and (88). The thermal analysis results are given in Appendix (2) and the phase diagram produced is shown in Fig 6.1. The AuIn-Ge section is a pseudobinary eutectic system with a eutectic at 2.0 at.% Ge and 488°C.

(b) $AuIn_2$-Ge Section:- The melting point of the $AuIn_2$ was taken as 540°C (86). The $AuIn_2$-Ge section is also a pseudobinary eutectic system with a eutectic at 4.1 at.% Ge and 522°C. The STA results are

given in Appendix (3) and the resultant phase diagram is illustrated in Fig 6.2.

(c) AuIn-Ge-$AuIn_2$ Partial Ternary Section (Isopleth of $Au_{41.5}In_{58.5}$⇒Ge Section):- Since the AuIn-Ge and $AuIn_2$-Ge joins were found to be eutectic systems and AuIn and $AuIn_2$ also form a eutectic system (86,89), it was assumed that the AuIn-Ge-$AuIn_2$ partial section would contain a ternary eutectic. To determine the ternary eutectic composition and temperature, STA was performed on the isopleth of $Au_{41.5}In_{58.5}$ to Ge. The thermal analysis results on this isopleth gave the phase diagram shown in Fig 6.8(a); Appendix (4). A magnified portion of this isopleth for alloys containing less than 8 at.% Ge is shown in Fig 6.8(b). The monovariant curve from the $AuIn_2$-Ge eutectic e_3 to the ternary eutectic E, Fig 6.8(c) is intersected at 4.0 at.%Ge at 488°C. The tie line between the ternary eutectic E and $AuIn_2$ is intersected at 2.75 at.% Ge at 471°C. The ternary eutectic composition, corresponding to the reaction $L_E \Leftrightarrow AuIn_2 + AuIn + Ge$, is estimated to be 3.5 at.% Ge, 43.25 at.% Au at 471°C.

(d) $AuIn_2$-Ge-In Partial Ternary Section (Isopleth of $Au_{20}In_{80}$⇒Ge Section):- A ternary eutectic was also anticipated in this section, so a $Au_{20}In_{80}$ to Ge isopleth was determined by thermal analysis. The phase diagram so produced is shown in Fig 6.9(a), from the STA results given in the Appendix (5). The magnified portion of this diagram with Ge contents less than 7 at.% Ge is given in Fig 6.9(b).

The presence of a degenerate ternary eutectic is indicated, located very close to the In corner and at a temperature of 156°C.

(6.1.1.2) Au-Ge-Ga SYSTEM:

The Ga-Ge binary system shows a single eutectic reaction at 99.994 at.% Ge and 29.77°C (90). The Au-Ga binary phase diagram, which was experimentally determined by Cooke and Hume-Rothery (91), shows two intermediate line compounds, AuGa and $AuGa_2$ exhibiting congruent melting points. The binary phase diagrams forming the boundaries of the Au-Ge-Ga system are shown in Fig 6.10. The details of the various sections which were determined are given below:

(a) AuGa-Ge Section:- According to reference (91), the AuGa compound melts congruently at 461.3°C. The present investigation indicated a melting point of 461±1°C. The AuGa-Ge section was found to be a pseudobinary eutectic system with the eutectic at 5.5 at.% Ge and 446°C, as shown in Fig 6.3. All STA results for this diagram are tabulated in Appendix (6).

(b) $AuGa_2$-Ge Section:- The congruent melting point of $AuGa_2$ was reported to be 492°C by Hansen (92) and 491.3°C according to Cooke and Hume-Rothery (91) at 66.6667 at.% Ga. The value determined in the present work is 492±1°C for this compound. The $AuGa_2$-Ge section is a pseudobinary eutectic system with a eutectic at 5.0 at.% Ge and 476°C. The STA results are presented in Appendix

(7) and the corresponding derived phase diagram is illustrated in Fig 6.4.

(c) AuGa-Ge-$AuGa_2$ Partial Ternary Section (Isopleth of $Au_{40}Ga_{60}$→Ge Section):- The AuGa-Ge and $AuGa_2$-Ge joins were found to be eutectic experimentally, while AuGa and $AuGa_2$ also form a eutectic system with each other (91). So it was assumed that the AuGa-Ge-$AuGa_2$ partial section would contain a ternary eutectic. To determine the ternary eutectic composition and temperature, STA was performed on the isopleth of $Au_{40}Ga_{60}$ to Ge. The resulting phase diagram is shown in Fig 6.11(a); Appendix (8). The magnified portion of this diagram for alloys containing less than 8 at.% Ge is shown in Fig 6.11(b). The monovariant curve from the $AuGa_2$-Ge eutectic e_3 to the ternary eutectic E, Fig 6.11(c) is intersected at 3.9 at.%Ge at 466°C. The tie line between the ternary eutectic E and $AuGa_2$ is intersected at 2.25 at.% Ge at 438°C. The ternary eutectic composition, corresponding to the reaction $L_E \Leftrightarrow AuGa_2 + AuGa + Ge$, is estimated to be 3.2 at.% Ge, 41.8 at.% Au at 438°C.

(6.1.1.3) Au-Ge-Zn SYSTEM:

AuZn-Ge Section:- The Zn-Ge binary system shows a single eutectic at 94.7 at.% Zn and 394°C (93). The Au-Zn binary phase diagram has been determined by various investigators. The most recent evaluation (94) has been considered here. All the edge binaries involved in this ternary system are shown in Fig 6.12(a,b,c). The congruent melting point of the binary compound AuZn has been variously reported as 725°C at 50 at.% Zn (92), 753°C at 48.5 at.% Zn

(95), 751°C at 50 at.% Zn (94) and 758°C at 48.5 at.% Zn (96). The present investigation indicated that the melting point of a 50 at.% Zn alloy is 759±1°C. The thermal analysis results for the AuZn-Ge section are tabulated in Appendix (9) and the phase diagram so derived, forming a pseudobinary eutectic system having a eutectic composition of 12.2 at.% Ge at 673°C is illustrated in Fig 6.5. The microstructure of the eutectic alloy is given in Fig 6.13.

(6.1.1.4) Au-Ge-Cd SYSTEM

AuCd-Ge Section:- The Ge-Cd binary system shows a single eutectic at 99.77 at.% Cd and 320°C (97). The Au-Cd binary system is a complex system which has been assessed recently (98). The binary phase diagrams forming the boundaries of the ternary Au-Ge-Cd system are shown in Fig 6.14(a,b,c). The liquidus of the Au-Cd binary system shows only a slow change with the temperature in the vicinity of the equiatomic composition. The maximum temperature of the liquidus, corresponding to the melting point of the congruent compound AuCd has been reported as 629°C at 47.0 at.% Cd (98).

In the present investigation the AuCd melting point was determined to be 630±1°C by taking 48.0 at.% Cd as the concentration of the AuCd compound. In the study of the AuCd-Ge section, discolouration of alloys was observed, owning to the high vapour pressure of Cd which caused the volatilization at elevated temperature. This discolouration was more pronounced as the liquidus temperature

increased with the increase of Ge contents, and a marked difference of reproducibility was observed. So a charcoal atmosphere was used as described in the experimental chapter. Even so, a slight discoloration of Cd volatilization was observed, but good reproducibility of the arrest temperatures on repeated heating and cooling indicated that only very minor changes in the composition had occurred. However, a new alloy was made for each composition to avoid any error due to the possibility of cumulative Cd volatilization.

To counter check these results, the thermal analyses were also performed in an evacuated silica crucible. No discolouration was found with the evacuated silica crucibles. The first thermal cycle with the open crucible arrangement (under charcoal) agreed within ± 5°C with those obtained with the evacuated crucibles.

The AuCd-Ge section was found to be a pseudobinary eutectic system with a eutectic at 10.0 at.% Ge and 555°C, as shown in Fig 6.6; Appendix (10). The microstructure of the eutectic alloy is also shown in Fig 6.15.

(6.1.2) Au-Pb-X SYSTEMS

The partial constitutions of Au-Pb-X ternary alloys have also been investigated, where X stands for the elements as described

previously (i.e In, Ga, Zn or Cd). Again a combination of quantitative Thermal Analysis and metallographic techniques, were used. The most recent evaluation of the Au-Pb binary phase diagram is considered here (99), Fig 6.16. The selected Au-X binary phase diagrams were described in the previous section, while the rest of the relevant binaries were taken from reference (100). The investigation of AuX-Pb sections in Au-Pb-X ternary systems, showed extensive liquid immiscibility over a wide range of compositions; immiscibility was easily seen on metallographic sections (by naked eye). The details of previous work and the present study in the various sections of the Au-Pb-X systems are given below:

(6.1.2.1) Au-Pb-In SYSTEM:

Prior to the present study the AuIn-Pb and $AuIn_2$-Pb sections of the Au-Pb-In system had already been investigated. Both sections were reported to be pseudobinary eutectic systems by Karnowsky and Yost (16). The AuIn-Pb section contains a monotectic reaction and a eutectic reaction. The $AuIn_2$-Pb section was reported to be a simple eutectic system. However, recent examination by Prince (101) showed that the $AuIn_2$-Pb section is a pseudobinary but not the AuIn-Pb section.

(6.1.2.2) Au-Pb-Ga SYSTEM:

Prior to the current investigation, no published data were available on the phase relationships in the Au-Pb-Ga ternary system. The Ga-Pb binary system forms a monotectic reaction at 313°C (100). Fig

6.17. The liquid immiscibility ranges from 2.4 at.% Pb to 94.5 at.% Pb. The maximum temperature of this liquid-liquid immiscibility gap is 606°C. The AuGa-Pb and $AuGa_2$-Pb sections were studied and the results are given below:

(a) AuGa-Pb Section:- This section does not form a pseudobinary eutectic system between the congruently melting compound, AuGa, and Pb. However, it shows extensive liquid immiscibility at 438°C between alloys having composition 5.0 at.% Pb and 80 at.% Pb. Liquid immiscibility can be seen easily macrographically; Fig 6.18. The upper temperature limit of the liquid immiscibility gap was not determined. In this section two further arrests were observed. One isothermal reaction occurred at 317°C and other at about 202°C; Fig 6.19; Appendix (11).

(b) $AuGa_2$-Pb Section:- The $AuGa_2$-Pb section also does not have the characteristics of a pseudobinary system between the congruently melting compound $AuGa_2$ and Pb and shows extensive liquid immiscibility. Liquid immiscibility was detected at 481°C, extending at least over the range from 5.0 at.% Pb to 80 at.% Pb. The upper temperature limit of the liquid-liquid immiscibility gap was not determined. The immiscibility of alloys lying on this section can also be seen macrographically as shown in Fig 6.20. Two further isothermal arrests were observed at 325°C and 317°C, for each composition. All STA results are illustrated in Appendix (12) and Fig 6.21.

(6.1.2.3) Au-Pb-Zn SYSTEM:

AuZn-Pb Section:- The Zn-Pb binary system shows tremendous liquid immiscibility from 0.3 at.% Pb to 94 at.% Pb with a monotectic reaction at 417.8°C (100); Fig 6.22. The maximum temperature limit of the miscibility gap is 798°C at 28 at.% Pb.

The only data on the phase relationships in the Au-Pb-Zn ternary system was reported by Pehlke and Okajima (102) and was restricted to the lead-rich corner. In the present study it was found that the AuZn-Pb section does not have the characteristics of a pseudobinary system. However, liquid immiscibility was detected at 750°C in the Au-rich portion but this temperature decreased with increasing Pb contents to 712°C at 90 at.% Pb. The upper temperature limit of the miscibility gap was not determined. The liquid immiscibility for alloys on this section can be visualized by the naked eye; Fig 6.23. An isothermal reaction at 211°C occurs throughout the section and one additional arrest was found varying from 322°C at 95 at.% Pb to 281°C at 10 at.% Pb. The thermal analysis results are illustrated in Fig 6.24 and Appendix (13).

(6.1.2.4) Au-Pb-Cd SYSTEM:

AuCd-Pb Section:- The Cd-Pb binary phase diagram consists of a eutectic at 71.9 at.% Pb at a temperature of 248°C (100); Fig 6.25. The liquidus for Cd-rich alloys shows an inflection followed by a slow rate of change with composition, suggesting an unmixing

tendency in the liquid state.

Prior to the present investigation, the only published work on the Au-Pb-Cd system was an examination of Pb-rich alloys. This was reported by Heycock and Neville (103), who measured the depression of the freezing point of a 4.66 at.% Cd, 95.34 at.% Pb alloy on addition of Au up to 6.09 at.% Au, and similar measurements for a 3.85 at.% Au, 96.5 at.% Pb alloy on addition of Cd up to 8.68 at.% Cd. The present investigation showed that the AuCd-Pb section is complex and certainly not a pseudobinary section. However, an extensive liquid immiscibility was found for alloys containing up to 70 at.% Pb associated with temperatures varying from 595°C to 584°C. This variation was not due to the Cd volatilization, as all results were confirmed with the evacuated silica crucibles technique. The upper temperature limit of the immiscibility was not determined and, like the other AuX-Pb sections, the liquid immiscibility for alloys on this section can be visualized macrographically; Fig 6.26. A number of arrests occurred at temperatures below the melting point of Pb for each alloy composition. The thermal analysis results are illustrated in Fig 6.27; Appendix (14).

(6.2) THERMODYNAMIC CALCULATION OF TERNARY PHASE DIAGRAMS

Of the ternary systems studied experimentally, optimized

thermodynamic data were available for the relevant binary systems only for the Au-Ge-In system. The computed thermocalculations of various sections in the phase equilibria of the Au-Ge-In system described in part [6.1.1.1 (a), (b) and (c)] i.e AuIn-Ge, $AuIn_2$-Ge and $Au_{41.5}In_{58.5}$-Ge sections, are shown in Figs 6.28-6.31.

The isotherms on the liquidus surface were also computed at various temperature intervals for the AuIn-Ge-In sub-ternary system which are shown in Figs 6.32(a) and 6.32(b).

(6.3) Au-Sn BINARY PHASE DIAGRAM

The first set of samples for determination of the Au-rich portion of the Au-Sn binary phase diagram, which was allowed to equilibrate at 300°C with compositions 7.5, 10.5, 12.0, 14.5 and 16.0 at.% Sn was withdrawn from the furnace after 4464 hrs (≅ 6 months), while the second set of specimens with the same compositions was withdrawn after 12864 hrs (≅ 18 months). These samples were studied under the optical microscope. The SEM/X-ray by using Electron Microprobe Analysis techniques was also employed to identify the phase/phases present in these samples. The samples which were withdrawn after 6 months did not show equilibrium structures and pieces of pure gold were observed, which were so prominent in some samples that it can be visualized with naked eye. However, the samples withdrawn after 18 months showed complete equilibrium structure. The micrographs of these samples

are shown in Figs 6.33-6.37.

Similarly both batches of the samples at 220°C with compositions 7.5, 12.0, 14.5, 16.0, 17.5 and 20.0 at.% Sn were withdrawn subsequently after 13488 hrs (≅ 19 months) and 17000 hrs (≅ 24 months). These samples were treated in similar way to those which were equilibrated at 300°C. These samples showed the equilibrium structures for both sets of specimens. A lot of holes/cavities were observed in all samples due to the long term heat treatment. The micrographs of these samples are shown in Figs 6.38-6.43.

The heat treatment time, temperatures, compositions and resultant phase or phases formed in each of the alloys are given in Table 2. The lower-temperature region of this portion of the diagram obtained from these results is illustrated in Fig 6.44 (thick lines).

(6.4) MICROHARDNESS

The microhardnesses of single phase congruent melting compounds of AuIn, $AuIn_2$, AuGa, $AuGa_2$ and AuZn were determined and are given in Table 3.

CHAPTER 7

(7) DISCUSSION

(7.1) LIQUID MISCIBILITY AND IMMISCIBILITY IN TERNARY SYSTEMS

The AuX-Ge and AuX-Pb sections of the Au-Ge-X and Au-Pb-X ternary systems respectively, have been studied. AuX-Ge sections were found to have pseudobinary characteristics. However, the AuX-Pb sections of the Au-Pb-X ternary system do not show pseudobinary characteristics, except the AuIn-Pb section which had already been determined as a pseudobinary system prior to the present study.

The examination of the AuIn-$AuIn_2$-Ge partial ternary system in the Au-Ge-In ternary system showed the presence of a ternary eutectic with a composition 3.5 at.% Ge, 43.25 at.% Au and 53.25 at.% In at 471°C. Also the presence of a degenerate ternary eutectic located very close to the In corner at a temperature of 156°C was detected in the $AuIn_2$-Ge-In partial ternary system.

The study of the AuGa-Ge-$AuGa_2$ partial system in the Au-Ge-Ga system also showed the presence of a ternary eutectic with a

composition 3.2 at.% Ge, 41.8 at.% Au and 55.0 at.% Ga at 438°C. The reaction schemes for the above systems are shown in Table 4. All these ternary systems showed complete miscibility in the liquid state at all compositions.

The AuX-Pb sections in the Au-Pb-X ternary system did not show pseudobinary characteristics (the AuIn-Pb and $AuIn_2$-Pb sections had already been determined; the former shows pseudobinary characteristics but not the latter). The possible interpretation for these sections with the data obtained in the present investigation will be discussed in the later part of the thesis. However, extensive immiscibility was detected over a wide range of compositions in each of the sections studied in the Au-Pb-X ternary systems. This liquid immiscibility could be visualized by naked eye for all alloys slowly cooled from above the liquidus to ambient temperature.

The object of the present study was to establish the requirements for complete liquid miscibility/liquid immiscibility for a system of three metallic elements.

When the heat of mixing is sufficiently great, separation into two phases occurs and the two liquids are only partially miscible. Thermodynamically, a liquid "unmixes", or exhibits a miscibility gap, when the sum of the Gibbs free energies of the two separated phases is less than the Gibbs free energy of a homogeneous solution of the components. In general it requires that:

(i) The enthalpy of forming the homogeneous solution from its individual constituent molecules be greater than the sum of the enthalpies of forming the separate phases and
(ii) The solution enthalpy differs sufficiently over some temperature and composition range (the area of the miscibility gap) that it can not be overcome by the contribution of the entropy of mixing to the Gibbs free energy.

Considering models to predict ternary liquid behaviour, it is necessary to define liquid immiscibility and liquid miscibility.

Liquid immiscibility: There are four types of liquid immiscibility which could be encountered in a ternary metallic system A, B and C.
CASE I:- Where the liquid immiscibility occurs in a ternary system A, B and C, of which none of the binary systems involved show liquid immiscibility, but the liquid immiscibility occurs on the section between some composition, A_xB_y, and pure element C as shown in Fig 7.1(a).
CASE II:- Where one (or more) constituent binary systems shows liquid immiscibility, but in the ternary system on section A_xB_y to C, a new miscibility gap, closed upon itself, occurs in the liquid condition i.e the binary miscibility gap does not enter into the ternary miscibility gap as shown in Fig 7.1(b).
CASE III:- In this case, one of the constituent binaries does show a liquid immiscibility gap, but the ternary liquid immiscibility starts

before the upper temperature limit of the binary immiscibility gap begins, and the ternary liquid immiscibility extends to the binary edge as the temperature decreases. This is shown in Fig 7.1(c), where the A-B binary system shows liquid immiscibility but the ternary immiscibility starts at a higher temperature and finally touches the immiscibility gap of the binary A-B system.

CASE IV:- In this case, a huge liquid immiscibility occurs in one of the constituent binary systems and extends over a considerable distance in the ternary as shown in Fig 7.1(d); in some instances the ternary liquid immiscibility extends from one immiscible binary system to the other.

In all the above cases the composition A_xB_y may be a compound, which may or may not form a pseudobinary section with element C. The first three cases are regarded as "true liquid immiscibility". However, case IV will also be discussed separately.

Liquid miscibility: Similarly two types of cases are possible for liquid miscibility of ternary metallic systems A, B and C.

CASE I: Where all the constituent binary systems show complete miscibility in the liquid state and ternary system also shows complete liquid miscibility as shown in Fig 7.2(a).

CASE II:-Where one or two of the constituent edge binary systems do show liquid immiscibility, but this immiscibility does not affect the ternary liquid miscibility on the section $A_xB_y \rightarrow C$ under study as shown in Fig 7.2(b). As before, the composition A_xB_y and element C may or may not form pseudobinary systems.

Two rules have been developed in the present work in an attempt to relate the liquid immiscibility of the ternary systems with certain parameters (or properties) of the constituent elements. They will be described here one by one.

(1) RULE 1 Axon (104) in 1948 and Hildebrand and Scott (57) in 1950 made attempts to predict the conditions required for the formation of liquid immiscibility in binary systems. Axon's (104) work was based on the assumption that liquid immiscibility will occur when there is a wide difference in melting point and atomic size of the components. He examined those binary systems in which no intermediate phases are formed, neglecting those that give complete solid solubility. The systems considered fall into two distinct classes, namely those in which a region of liquid immiscibility is encountered and those which are characterized by the existence of a eutectic. Axon consider the size factor as:

$$\text{Size Factor} = \frac{(L - S)}{S} \times 100$$

Where L and S are the closest distance of approach of the larger and smaller atoms respectively in the pure elements, and the temperature factor as:

$$\text{Temperature Factor} = \frac{\Delta\theta}{1/2\,(\theta_1 + \theta_2)}$$

Where $\Delta\theta$ is the difference between the melting points of the elements and θ_1 and θ_2 are the melting point temperatures on the absolute temperature scale.

Axon (104) plotted the size factor versus the temperature factor on the absolute scale and obtained the Fig 7.3. Region A shows that if the size factor is less than 30% and limited to a temperature factor of 0.175, a eutectic system will form in which the eutectic composition does not vary much from 50 at.%. In region B, where the size factors everywhere are greater than 30%, a miscibility gap will occur in the liquid state. For region C the eutectic moves progressively from 50 at.% as the temperature factor is increased beyond 0.175.

However, this approach was limited to about 80 binary systems of relatively simple form and did not include the systems which showed a limited region of immiscibility.

No suggestion for the condition required for the liquid immiscibility in ternary systems was reported by Axon. However, Mott (105) surmised from Axon's hypothesis that the range of miscibility of two metals could be increased by the addition of a third element for which both atomic size and the melting points were intermediate

between the corresponding properties for the other two. The validity of this hypothesis has not been examined up till now.

In the present work, this hypothesis was considered as one of the bases to establish a rule for the liquid immiscibility/liquid miscibility in ternary systems which is expressed as:

"Liquid immiscibility (true immiscibility) between composition A_xB_y and element C in a ternary metallic system A, B and C will only occur when:

(i) The atomic size of the third component, C, is greater than the atomic size of the other two elements A and B or equal to the size of the larger of the A-B components.

(ii) The melting point of the third component, C, should lie outside the range of the melting points of the other two components A and B or very close to one of them.

(iii) The direction of the tie-line is from A_xB_y to C ($A_xB_y \rightarrow C$).

If all of these conditions are not fulfilled by a ternary system, then no liquid immiscibility would be expected, i.e liquid miscibility will occur".

This rule was applied to the 17 ternary systems in which true liquid immiscibility (case I, II and III, as described earlier) is known to occur in the ternary alloys; and the direction of the tie-lines in the immiscible region is known. These systems are given in Table 5 along with the direction of tie lines given by arrow head, and shown

in Figs 7.4 to 7.20. Liquidus projection/ternary immiscible sections for systems, other than those examined in the present work, were obtained from references (50, 65, 101, 106-117) supplied by Prof. A. Prince (118). Most of these figures are taken from the original works. In addition, the data for the melting points and atomic sizes were taken from references (80) and (82,119) respectively.

Sixteen of these systems agreed with the predicted behavior, as listed in Table 5. However, the Mg-Al-Sb ternary system did not agree with the rule [i.e no. 4 in the Table 5]. The reported liquid immiscibility in the Mg_3Sb_2 to Al section in the Mg-Al-Sb ternary system (Fig 7.7) is in conflict with the speculated behaviour in the present study.

The present theory suggested that this system would be a miscible system. The melting point condition is obeyed by this system, but nevertheless it does exhibit ternary liquid immiscibility and some other reason must be found to explain it. One possibility is suggested by high degree of stability of the compound Mg_3Sb_2 as shown by its melting point (1228°C) and enthalpy of formation, 300 kJ/mole (9).

This would seem to indicate a strong tendency of Mg and Sb atoms to cluster even in the liquid state, perhaps sufficient to withdraw Mg and Sb atoms from solution in the liquid Al with which the Mg and Sb rich liquid appears to be immiscible.

One other ternary system, which is given at the end of the Table 5 (no. 18), Fig 7.21, also showed ternary liquid immiscibility. This is the Pd-Ag-Zr ternary system, which satisfied the melting point condition, but not the size factor. However, the evidence of liquid immiscibility has not been confirmed by other investigators and, in the published work, the direction of the tie-lines in the proposed region of liquid immiscibility has not been determined.

The present theory suggested that liquid immiscibility could be expected in this system if the direction of the tie-line is from PdAg to Zr. However, if the direction of tie-line is in any other direction i.e from PdZr to Ag or AgZr to Pd, no liquid immiscibility will occur and system would be miscible in the liquid state.

The validity of this rule was also tested for those systems where one or two of the constituent edge binary systems showed extensive liquid immiscibility and this immiscibility extended a considerable distance into the ternary; in some instances the ternary liquid immiscibility extended from one immiscible binary system to the other, (case IV). There were 8 such types of known systems given in Table 6, along with the direction of tie-lines, given by arrow head. [See also Appendix 15]. Data for systems other than those studied in the present work were taken from references (118-123) and are shown in Figs 7.22 to 7.29. Out of these 8 systems two did not agree with the rule [Table 6, no. 3 and no. 6], i.e Au-Pb-Ga and Pb-Fe-Te ternary systems.

The Au-Pb-Ga ternary system was investigated in the present study and showed liquid immiscibility in the AuGa-Pb and $AuGa_2$-Pb sections. It should be noted that this system agreed with the atomic size condition, which is the primary condition. However, if the melting point of the Pb (327.65°C) is considered to be close to the melting point of Ga (29.92°C), then the predicted behaviour would agree with the experimental evidence. Otherwise, it may be considered that this system is on the borderline between the agreement and disagreement, having a great tendency towards agreement.

The other system which does not show agreement with the present theory is the PbTe to Fe section of the Pb-Fe-Te ternary system. This system only fulfilled the melting point condition and did not satisfy the atomic size condition. It should be noted here that the Fe-Pb binary system showed a huge liquid immiscibility over a wide range of composition, so obviously ternary immiscibility would also be expected. Present theory suggested that the addition of Te should reduce the liquid immiscibility range of the binary Fe-Pb binary system. The only data published for this system is the join PbTe to Fe, which indicates liquid immiscibility for Fe-rich solutions.

To check the validity of this rule for systems showing liquid miscibility in ternary systems, i.e systems of the type shown in Fig 7.2(a) and 7.2(b). 36 known pseudobinary systems which showed

miscibility in the liquid state were tested. The direction of the tie-lines were also known for these systems [shown by arrow head in Table 7]. It was found that all these systems agreed with the above rule; i.e 13 systems showed agreement due to both atomic size and melting point conditions, whereas in the 18 systems the third component, C, has smaller atomic size than one or both the other two components, A and B, while for 5 systems the melting point of the third element, C, was intermediate between the melting points of the other two, A and B. All these pseudobinary systems are given in Table 7. Data for these systems, other than those investigated in the present work were provided by Prof. A. Prince (118).

From the above discussion it can be concluded that the theory presented here showed an excellent agreement with the experimental evidence for miscible ternary systems.

Briefly, out of 18 known systems, which showed true liquid immiscibility, 2 systems do not agree with the predicted behaviour, but the experimental evidence for liquid immiscibility in one of these systems is deficient, as indicated above, whilst the other may be regarded as an exception which cannot at present be explained quantitatively. The value of this rule lies mainly when liquid immiscibility of a system is well defined along with the direction of the tie-line. The implementation of this rule on 36 known pseudobinary systems showing liquid miscibility were found to be in agreement for all systems.

Hence, with the present theory it is possible with reasonable certainty to describe whether three metals will be miscible or immiscible in the liquid state. Further, it can be used as a guide for the systems showing disputed (doubtful) liquid immiscibility or miscibility in ternary metallic alloys.

(2) RULE 2 Hildebrand and Scott (57) related the liquid immiscibility of the binary systems to the heat of vapourization of the components, (which is defined as a measure of the binding energy) and their atomic volume. They defined the condition for liquid immiscibility as:

$$1/2\left(V_A + V_B\right)\left[\sqrt{\frac{\Delta H_A^V}{V_A}} - \sqrt{\frac{\Delta H_B^V}{V_B}}\right]^2 < 2RT$$

Where V_A and V_B are the atomic volumes of A and B respectively ΔH_A^V and ΔH_B^V are the heats of vapourization of A and B respectively, R is the universal gas constant and T is the absolute temperature.

The term $\left[\sqrt{\frac{\Delta H_A^V}{V_A}}\right]$ was considered to be a measure of the binding energy of component A and was called the solubility parameter, δ_A. Therefore the condition for immiscibility becomes:

$$1/2\left(V_A + V_B\right)\left[\delta_A - \delta_B\right]^2 < 2RT$$

For the non-polar liquids, this relationship proved to be a useful guide to predict liquid behaviour. It showed a nominal agreement for immiscibility, but indicated a poor agreement for miscible systems.

Mott (105) suggested that this failure of the Hildebrand rule was due to the effect of electronegativity. So Mott introduced a new factor in the Hildebrand equation to give the following relation to predict immiscibility:

$$\frac{1/2\left(V_A + V_B\right)\left[\delta_A - \delta_B\right]^2 - 2RT}{23060\left(X_A - X_B\right)} > n$$

where n is the number of electrons available for bonding (i.e the valency of the component) and X_A and X_B are the electronegativities of A and B respectively. The figure 23060 is the Faraday's constant. Mott called the left hand factor K, so the equation reduces to:

K > n for immiscibility.

Because six is the maximum number of valence electrons that can participate in metallic bonding, the maximum value of n is 6. So, according to Mott:

If K > 6 liquid immiscibility will occur.

If K < 2 the alloys will be completely miscible in the liquid state.

For systems with intermediate values of n, the possibility of liquid immiscibility gaps is less apparent.

These conditions defined by Mott are usually successful in predicting liquid immiscibility in binary systems of pure elements, but lack of appropriate data limits application to binary systems involving other than pure elements.

Mott extended this hypothesis to ternary systems. According to Mott liquid immiscibility in alloys of two metals, A and B, can be reduced by appropriate selection of third element, C. The choice of the third element should be such that its solubility parameter ,δ_C, should preferably be in the range of δ_A and δ_B or not greatly different from δ_A or δ_B, and the electronegativity of the C element should differ markedly from the electronegativities of A and B. Very little data are available on the effect of a third element on the immiscibility range of two metals. Prior to this investigation, the hypothesis had been tested and justified for only three ternary systems:

(i) addition of Cd to Bi-Zn alloy.

(ii) addition of Sn to Pb-Zn alloy.

(i) addition of Zr to U-Th alloy.

No published work is available on why the liquid immiscibility (true) is encountered for ternary metallic systems. In the present study the Mott hypothesis was considered to be the basis and a rule

was derived which relates the liquid immiscibility of a ternary system. The rule can be stated as:

"In a ternary metallic system, A, B and C, true liquid immiscibility between composition A_xB_y and pure element C will occur if the solubility parameter of element C (δ_C) lies out side the range of the solubility parameters of the other two elements A and B (δ_A and δ_B), and the electronegativity of C is in between the range of the electronegativities of A and B or very close to A or B and the direction of the tie-line in the immiscible liquid is from A_xB_y to C ($A_xB_y \rightarrow C$). If these conditions are fulfilled, liquid immmiscibility will occur in the ternary system".

The data for the solubility parameters for the present study were taken from the original work of Hildebrand (57) except for some elements, Se, Fe, Pb, Te, Zn, Nb and Co, which are not given in the Hildebrand work or showed a marked difference with recent values for heats of vapourization, densities and atomic weights. The solubility parameters for these elements were calculated in the present study.

Several investigators, including Haissinsky (124), Walsh (125) and Gordy (126) examined the electronegativities of the elements by their own methods, but none of them assessed all the elements. However, Pauling (127) critically assessed the electronegativities values for all elements. For the present purpose the Pauling

electronegativities values were considered, as given by Mott (105) and for some elements (Cu, Pd, Sb, Pb, Fe, Co, Mn, Ni and Cd) values are taken from the original work of Pauling (127).

The above rule was applied to the 17 ternary systems, given in Table 8 [the same systems as described previously in Table 5], which showed true liquid immiscibility in the liquid state. Out of these 17 systems, 15 conformed fully with the rule, while two of the systems showed slight disagreement [AuCd-Pb and ZnTe-Bi system, no. 10 and no. 17 in the Table 8 respectively]. Additionally the Pd-Zr-Ag system fitted this model, which is given at the end of the Table 8 [no. 18].

The AuCd-Pb system obeyed the electronegativity condition, but not the solubility parameter. The analysis shows that the solubility parameters of Cd and Pb are very close to each other, having values of 92 and 96 $(J/cm^3)^{1/2}$ respectively. Similarly the other system ZnTe-Bi does agree with the electronegativity condition, but not the solubility parameter. Again the solubility parameters for Zn and Bi are 108 and 98 $(J/cm^3)^{1/2}$ respectively are close to each other. According to Mott's (105) point of view, the uncertainties in the experimental determination of the latent heat of vapourization of a metal and in the extrapolation of the solubility parameter to high temperatures give rise to errors in the solubility parameter. For many systems the difference between the solubility parameters of two metals could reasonably be in error by $\pm$ 10 $(J/cm^3)^{1/2}$, and it may be higher than this value in some cases. When possible errors

of this magnitude are taken into consideration, the difference between predicted and observed behaviour for these two systems could be explained. Only the predicted behaviour for the Cd-Se-Bi system [no.12 in Table 8] is affected when the uncertainty limits are applied to the other 17 systems considered here.

This rule was applied also to those immiscible systems which showed huge immiscibility in one of the edge binary systems and this immiscibility extended a considerable distance into the ternary. There were 8 such types of ternary systems, given in the Table 9, which are the same systems tested for the previous rule. [See also Appendix 15]. Out of these 8 systems, 6 systems fully agreed with the predicted behaviour, while 2 of the systems, Cu-Bi-Te and Cu-Bi-Se [no. 7 and no. 8 respectively in Table 9], do not show agreement. Both systems were found to be in agreement with the electronegativity condition, and not with the solubility parameter factor. However, again two of the elements showed similar values for solubility parameter but the difference was greater than the suggested uncertainty.

To check the validity of this rule for systems showing complete liquid miscibility in ternary systems. 36 known pseudobinary systems were tested, as presented in Table 10 [the same systems as those tested for previous rule], 27 were found to be in agreement, 20 due to the solubility parameter condition and 7 due to the electronegativity factor. Out of 36 systems, 9 systems did not show

agreement with the rule, 6 showed slight disagreement, whereas 3 of them showed marked disagreement [Table 10]. Careful analysis shows that these 9 systems indicate disagreement only due to very small differences in the solubility parameter or electronegativity values.

Now the question is, why there are many exceptions to this rule in the case of miscible systems. From Mott's (105) point of view the error occurred not only in the solubility parameter values, as described above, but the electronegativity values may also cause this problem. According to Mott (105) electronegativity values are generally expressed to the nearest 0.1 electron volt so that the possible error between the difference of any two elements may be ± 0.2. However, the electronegativity of a given element depends upon the valency it assumes and can therefore vary with the nature of the alloying elements. At the moment no satisfactory basis exists for assessing the probable variation. Small error in the electronegativity values would not affect the predicted immiscible behaviour for these systems which fit the model. Hence, the disagreement with the present theory, shown mainly by the ternary miscible systems, is attributed to the error incurred in the calculation of solubility parameters and variation in the electronegativity values.

When Hildebrand and Scott (57) applied their rule, as described previously, to the liquid phase of binary systems, out of 47

immiscible binary systems 40 obeyed the relationship, 2 were on the borderline and 5 showed marked disagreement. On the other hand, nearly 50% of the alloys which are known to be miscible in the liquid state, should be immiscible according to Hildebrand's rule. Later on, Mott (105) suggested some modifications in Hildebrand's rule (as described in the early part of this chapter).

Mott applied the modified form of Hildebrand's rule to 99 immiscible binary systems and compared his results with those predicted by the original Hildebrand rule. 88 obeyed Hildebrand rule, 72 agreed with modified form of this rule, given by Mott. A total of 430 miscible binary systems were also considered by Mott. Out of these only 224 binary systems obeyed the simple Hildebrand rule, but 206 did not. Mott considered those 206 miscible systems which did not agree with the simple Hildebrand rule and found that 130 of the binary systems can be brought into line with the modified rule.

In addition to these binary systems considered above (99 + 430 = 529), there were 22 for which the experimental evidence at that time was either conflicting or insufficient to draw any definite conclusions as to the existence of liquid immiscibility. According to the Mott theory the immiscibility could be expected in 8 of these systems. Data for one of these 8 systems, (i.e Te-As) has been used in the present study. However, for the present purpose it is considered to be a miscible binary system according to the most recent evaluation (100). For the remaining 14 systems, analysis

indicates no immiscibility, which is in general agreement with most recent investigations. Out of these 14 binary systems, 2 systems i.e Cu-Fe and Ag-Ti have been used in the present study and considered to be the miscible systems.

From the above discussion it can be concluded that disagreement of certain systems is imposed by the lack of precise information on the properties which determined the solubility parameter and its variation with temperature and by the difficulties in providing a precise figure for the electronegativity differences for a given system. Despite this, it is suggested that the rule based on the solubility parameter and electronegativity can be applied to predict the liquid immiscibility of a ternary metallic system which will give a reasonably good agreement with the observed behaviour. However, the rule showed a poor agreement for miscible systems, due to the problem discussed above. This is analogous to the fact that both the rule for the binary metallic liquid miscibility, given by Hildebrand and its modified form given by Mott, based on the solubility parameter and electronegativity, also showed a poor agreement. Further, it should be noted that the percentage of predictability in case of ternary metallic systems, as presented here, were much better than those as predicted by Hildebrand and Mott for binary metallic systems.

When these possible errors, as described above, are taken into consideration, many miscible systems which appear to be

exceptions to the rule can be brought into agreement. For example, if the electronegativity values of Sb, Ge are considered to be 1.8 and 1.6 respectively, instead of values used in present study of 1.9 and 1.7 respectively, then the systems no. 25, 23 and 14 in Table 10 will show agreement with the rule.

Similarly, if the solubility parameters of As, In and Ge are considered to be 132, 120 and 150 $(J/cm^3)^{1/2}$ instead of values taken here as 135, 123 and 155 $(J/cm^3)^{1/2}$ respectively, then the systems no. 31, 19 and 18 in Table 10 can be brought into line. However, these changes will not affect the fit for other immiscible and miscible system considered in which any of these elements participate.

There are still some systems which can not be explained on this basis. Hence it can be concluded that more accurate data is required so that liquid miscibility or liquid immiscibility can be defined reasonably well in the ternary metallic system.

It should be noted that no ternary system considered was in disagreement with both of the rules. Hence, if liquid immiscibility in a ternary system is predicted by both rules, then one can assume with confidence that liquid immiscibility will occur.

(7.1.1) Direction of Tie Line:

The direction of the tie-line within the two-liquid (immiscible) region determined which of the constituent elements was designated as the 'C' element for the application of the rules. Thus in Fig 7.30 if the tie-lines run from 'a' to 'b', then the 'C' element lies at the apex of the triangle.

(7.1.2) Elements from Group IV of the Periodic Table:

Phase equilibria have been studied between AuX compounds and two elements, Ge and Pb, from group IV of the periodic table. AuX-Ge alloys showed complete miscibility in the liquid state at all compositions, whereas the AuX-Pb, alloys showed extensive liquid immiscibility. This behaviour can be attributed to the progressive increase in the number of electron shells and hence the atomic size of the element and progressive decrease in the electronegativities and solubility parameters of the elements as the period number is increased down this group IV. Sn lies between Ge and Pb in the IVth group of the periodic table, but data are not available for liquidus surfaces to show whether or not true immiscibility or imminent immiscibility occurs on the corresponding AuX-Sn sections. So it can be speculated that the AuX-Sn sections in the Au-Sn-X ternary system will show an intermediate trend of liquid immiscibility. By considering this speculation as a first approximation, a periodicity trend towards unmixing would be expected in the ternary alloys such that, when the intermediate congruent melting compound AuX (where X are the elements of IIB and IIIB group of the periodic table) mixed with the elements of

group IV, there is a trend towards liquid immiscibility as the period number of the group IV elements is increased.

(7.2) SOLID SOLUBILITY

The principle factors which govern the extent of solid solubilities were formulated by Hume-Rothery (23). According to this argument the solid solubility of one metal in another will depend upon the difference in their atomic diameters, their relative valency effect and their electrochemical nature. Hume-Rothery postulated that if the the diameter of solvent and solute differ by more than about 13–14% of that of solvent, the 'size factor' is unfavourable, and the solid solubility does not exceed a few atomic percent.

In the present study the solid solubilities of AuX-Ge sections in the Au-Ge-X ternary systems were determined and are given in the Table 11. The size factors are also given in the Table 11. It can be seen that in the Au-Ge-X ternary systems the experimental determinations obey the Hume-Rothery rule, suggesting that the other factors (electrochemical and relative valency factor) are not affecting the solid solubilities.

(7.3) VAN`T HOFF EQUATION AT HIGHER CONCENTRATION OF THE SOLVENT

It has been found in the present study that the liquidus for the AuX-Ge pseudobinary eutectic systems follow the Van`t Hoff equation (equation 6.1) at the higher concentration of 85–95 at.% of the solvent. The application of equation (6.1) for the initial slopes of the liquidus curves and for the eutectic compositions at higher concentration of solvent gave excellent agreement with the experimental results for the AuX-Ge pseudobinary eutectic systems. Hence this equation is recommended for the same application with other eutectic systems, when sufficient thermochemical data are not available.

(7.4) POSSIBLE CONSTITUTION OF THE Au-Pb-X SYSTEMS

The AuGa-Pb and $AuGa_2$-Pb sections in the Au-Pb-Ga ternary systems were not found to have pseudobinary characteristics as shown in Fig 6.19 and 6.21 respectively. However, $AuGa_2$-Pb is nearly a pseudobinary section. The possible reaction scheme is presented in Table 12 from the thermal analysis data obtained in the present study for these two sections. Both sections, i.e AuGa-Pb and $AuGa_2$-Pb can be interpreted as shown in Figs 7.31(a) and 7.31(b) respectively. The probable liquidus projection of the Au-Pb-Ga system is presented in Figs 7.32(a) and 7.32(b). The details of various reactions involved are given in Fig 7.33(a) to 7.33(d). The triangulation of this system is illustrated in Fig 7.33(e). However,

these interpretations require further experimental support.

(7.5) PROBLEMS ENCOUNTERED, ACCURACY AND REPRODUCIBILITY

At the commencement of this work, it was decided to aim for an accuracy of better than $\pm 3^{o}C$ in all thermal measurements. Appropriate procedures were adopted to ensure that this accuracy was attained.

According to Prince (69) the alloys should be melted and quenched in to cold water prior to placing in the furnace for detailed thermal analysis, as described in the previous chapter. Then for thermal analysis the alloys should be homogenized for a short period (20-30 min) for thermal equilibrium to be established prior to examining the lowest arrest temperature by heating. Then again a second short period of homogenization should be allowed prior to examining the same arrest temperature by cooling. This technique of quenching alloys followed by cyclic thermal analysis has been shown (69,128) to be effective in reducing the heterogeneity within the specimen and consequently eliminating any spurious effects. In the present study, it could be done only for the Pb-containing alloys. Unfortunately, quenching into cold water for the preparation of alloys prior to thermal analysis, was not possible for Ge-containing alloys, owning to the risk involved of cracking the silica crucible.

Cracking is associated with the expansion of germanium on solidification. Therefore conventional alloying techniques were adopted. The alloys were melted and homogenized within the thermal analysis rig, followed immediately by thermal analysis. So, for Ge containing alloys thermal analysis was started from the liquidus arrest by a cooling run as described earlier. However, for In alloys containing Ge it was possible to quench the alloys into hot water to counter the tendency of the silica crucible to crack when quenched into cold water. Further, as the amount of In increased in the alloys, the cracking was less pronounced (i.e AuIn-Ge alloys were more prone to crack as compared to $AuIn_2$-Ge alloys), which suggested that the expansion of Ge is compensated by the large amount of In contraction on solidification. But severe problems of cracking the silica crucibles were still encountered for higher Ge contents in these In-containing alloys. A similar phenomenon was observed for Ga, Zn and Cd containing alloys; as the amount of these elements increased, the expansion on solidification of the alloy became less pronounced.

Severe problems were encountered for all alloys containing high Ge contents; more than 50 (60 at.%). So the liquidus and solidus curves in all systems were experimentally determined up to 50 or 60 at.% Ge, and both these curves were extrapolated from 50 (or 60 at.% Ge) to the pure Ge axis, as described in the earlier part of the thesis.

In the study of the AuCd-Ge section, the investigation was complicated not only by the cracking of the silica crucibles on

expansion of Ge on solidification, but also by the high vapour pressure of Cd which caused an additional problem of volatilization at elevated temperature. So the thermal analysis technique was altered again, as described in the experimental portion, where constituents were allowed to homogenize above the estimated liquidus temperature for only 15-20 min under a charcoal atmosphere, to avoid any Cd volatilization. With alloys containing up to about 15% Ge the melts were heated to a maximum temperature of 700°C. When the alloys were removed from the furnace after solidification, the upper walls of the crucible and the thermocouple sheath showed slight discolouration, indicative of Cd volatilization, but good reproducibility of the arrest temperatures on repeated heating and cooling indicated that only very minor changes in the composition had occurred. However, a new alloy was made for each composition to avoid any error due to the possibility of cumulative Cd volatilization. To check the extent of the loss of Cd from the alloys, the specimens containing 10 and 30 at.% Ge were subjected to microprobe analysis after completion of the thermal analysis. The 10 at.% Ge alloy showed negligible Cd loss and 30 at.% Ge alloy showed a maximum loss of 0.7 at.% Cd.

For alloys containing higher concentrations of Ge, the maximum temperature had to be increased because of the progressive increase in the melting temperature with Ge content. Discolouration was then more pronounced and the arrest temperatures changed during repeated thermal cycling. So, the results were checked by

thermal analysis of alloys sealed in an evacuated silica crucible of approximately the same internal dimensions as those used in the rest of work, as described in the experimental section. A longer hold above the melting point was allowed to compensate for the lack of stirring. No discolouration was found with the evacuated silica crucibles. The first thermal cycle with the open crucible arrangement (under charcoal) agreed within ± 5°C with those obtained with the evacuated crucibles.

The exponential increase in the vapour pressure of cadmium with increase in the liquidus temperature required to melt the alloys was only partially compensated by the decrease in Cd concentration as the Ge content of the alloys was increased. The volume expansion on solidification invariably resulted in cracking of the silica crucibles at high Ge contents. Because of this additional limitation, the liquidus curve in Figure 6.6 was determined experimentally only up to 50 at.% Ge and extrapolated to intersect the pure germanium axis at the melting point of Ge.

Metallographic examination of various alloys showed only two phases, AuCd and Ge and no evidence of a third phase, confirming that the section is a pseudobinary. SEM examination of 10 and 30 at.% Ge alloys confirmed that the phases present were AuCd and Ge.

However, for AuCd-Pb alloys, prior to the thermal analysis, quenching was possible, as the absence of Ge allowed quenching

without the risk of cracking the silica crucible.

The arrest temperatures for the solidus line were obtained from heating and cooling curves. All results for the solidus lines were reproducible with an accuracy of ± 3°C, except for two Cd-containing alloys having more than 30 at.% Ge, where the accuracy was ± 5°C. Arrest temperatures for the liquidus were taken only from the cooling curves. The high accuracy of liquidus temperatures obtained in a cooling run has been emphasized by Hume-Rothery (31). On the heating run, the alloys are passing through a continuous melting region and the thermal changes are very small as the end of melting is approached. Also during heating alloys can cnot be stirred easily.

The alloys were stirred continuously during cooling to the liquidus temperature. The importance of this agitation has been emphasized by several investigators (31,65,69). This stirring reduces the extent of under cooling and hence the accuracy of the liquidus temperature determination is increased. So supercooling was minimal and the change in slope of the $\partial T/\partial t$ vs T graph was more clearly defined on cooling than on heating. Stirring during a cooling run was also possible with some semisolid alloys which contained a large proportion of the liquid phase. The liquidus arrests became sharper and more clearly defined as the Ge contents increased (i.e as the composition moved further from the eutectic point). However, the solidus reaction became also relatively stronger with the increase of Ge, and the extent of undercooling on the solidus line tended to

increase.

When the liquidus temperature changed slowly with composition, the reproducibility was ± 1°C. However, where the liquidus temperature changed rapidly with composition and the phase boundary became more steep (i.e near to the invariant reaction) the thermal arrests were small, due to the small heat effects, and were not well defined. Repetitive heating and cooling runs through these transformations gave an estimated accuracy of ± 3°C for the liquidus temperature.

There were generally two types of errors that are likely. One is compositional errors and other is temperature measurements. After thermal analysis reweighing of the sample showed negligible variances as a result of melting which was confirmed by SEM results. Therefore, the alloys composition quoted are the nominal compositions based on the initial weights of the components.

The other error of temperature may arise due to the variation of cold junction box temperature, which were of the order of ± 0.2°C, and to thermocouple behavior. The thermocouple was calibrated against the known melting points of pure elements and was recalibrated at frequent intervals. No significant change in calibration was found after extended periods of use. However, the reproducibility was excellent; for the liquidus temperatures it was considered to be within ± 1°C and for solidus temperature ±3 °C, as described earlier, while the overall accuracy was of the order of

$\pm 1^{o}C$.

(7.6) COMPARISON OF EXPERIMENTAL AND THERMODYNAMICALLY COMPUTED SECTIONS AND ISOTHERMS

The various experimentally derived and thermodynamically calculated sections in the Au-Ge-In ternary system were shown previously [Figs 6.1, 6.2, 6.8(a), 6.8(b) and 6.28 to 6.31]. The comparison of these vertical sections is shown here in Figs 7.34 to 7.37.

The comparison of the AuIn-Ge section (Fig 7.34) showed that the calculated eutectic temperature is $18^{o}C$ lower than that obtained experimentally ($488^{o}C$), with a composition of 4.0 at.% Ge, which is twice that found experimentally.

Similarly the comparison of $AuIn_2$-Ge section (Fig 7.35) indicated that the computed eutectic temperature is $9^{o}C$ lower than the experimentally determined eutectic temperature of $522^{o}C$, while the eutectic composition is 4.4 at.% higher than that found experimentally (4.1 at.% Ge).

The comparison of the $Au_{41.5}In_{58.5}$ to Ge isopleth showed a temperature difference of $10^{o}C$ between the calculated and

experimentally investigated temperature for the monovariant line, whereas the computed ternary eutectic temperature, 460°C, is 11°C lower than that experimentally obtained.

So, from the above discussion it is clear that the computed and experimentally determined sections and isopleth showed a maximum difference of ± 9°C.

The calculated ternary eutectic composition was 8.05 at.% Ge, 44.84 at% Au and 47.11 at% In, while experimentally it is estimated to be 3.5 at.%Ge, 43.25 at% Au and 53.25 at% In.

The comparison of the liquid isotherms is shown in Fig 7.38. Here the computed and experimentally determine isotherms on the liquidus surface showed a maximum difference of ± 4 at.% Ge.

In the present work, the vertical isothermal sections and isotherms on the liquidus surface were computed from assessed data for the relevant binary diagrams and were not modified to fit the experimental data found for the pseudobinary sections. Although, in principle, experimental measurement should be more reliable, the simple computer assessment can be used to supplement the experimental data for this system with sufficient accuracy for most purposes. However comparison of these diagrams shows that both the data and the assumptions used in computing these equilibria are fairly good.

(7.7) Au-Sn BINARY PHASE DIAGRAM

The Au-Sn binary phase diagram has been studied by many investigators (128-132). The most recent evaluation of this system is reported by Okamoto and Massalski (132); Fig (7.39). The enlarged Au-rich portion of this diagram is given in Fig (7.40). The equilibria in the Au-rich portion of the Au-Sn phase diagram are still uncertain, and are shown by dotted lines in Fig (7.40). However, Legendre, Prince and co-worker found two peritectic reactions at 530°C and 519°C respectively, Fig (7.41) but did not study equilibria below 400°C. To clarify the uncertainty of the low-temperature equilibria, a series of alloys covering the appropriate range of compositions (as described in the previous part of the thesis) were heat treated isothermally at four selected temperatures given as 140°C, 220°C, 300°C and 380°C. Two temperatures, 140°C and 380°C, were studied at UMIST by Dr. Hayes and co-workers, while the other two temperatures i.e 220°C and 300°C were examined in the present work.

The heat-treatment time, temperatures, compositions and resultant phase/phases formed for the Au-rich portion of the Au-Sn binary phase diagram are given in Table 2; Fig.6.44 (as described in results section).

For simplicity the specimens heat treated at 300°C with

compositions 7.5, 10.5, 12.0, 14.5 and 16.0 at.% Sn are numbered as (1), (2), (3), (4) and (5) as shown in Fig 6.44 and the micrographs of these samples are given in Fig 6.33 to 6.37 respectively. Similarly the specimens heat treated at 220°C with compositions 7.5, 12.0, 14.5, 16.0, 17.5 and 20.0 at.% Sn are numbered as (6), (7), (8), (9), (10) and (11) as shown in Fig 6.44 and the micrographs of these samples are given in Fig 6.38 to 6.43 respectively. The lines drawn (thick lines) from the results in the present study are numbered by (a), (b), (c) and (d) respectively.

The interpretation of the microstructures was complicated by the extensive porosity, particularly in specimen no. 9, 10 and 11, which developed during the isothermal treatment. In fact, the microstructures were more clearly differentiated under the microscope than is apparent from the micrographs.

It can be seen from the micrographs, Fig 6.33, of the specimen (1) that it contained a two phase structure i.e Au and β. SEM, Electron Microprobe Analysis, results indicated that the β has a composition of 9.1 at.% Sn, confirming the value given by Okamoto and Massalski (132). Sample (2); Fig 6.34 also showed a two phase structure, β and ζ. Again Electron Microprobe Analysis indicated that the β phase has a composition of 9.1 at.% Sn as described above. All the other specimens (3), (4) and (5) showed a single phase structure of ζ ; Fig 6.35, 6.36 and 6.37 respectively. The ζ phase has a homogeneity range between about 10 and 18.5 at.% Sn (132).

The sample (6) revealed a structure having two phases, β and Au, as shown in Fig 6.38. Specimen (7) and (8) gave a single phase ζ structure, while samples (9), (10) and (11) were found to have two phase structures (ζ + AuSn compound). The amount of AuSn, increased from samples (9) to (11).

The present work has confirmed that β phase has a composition of 9.1 at.% Sn, so the position of line (b); Fig 6.44, could be fixed. The careful study of the micrographs indicated that the samples (1) and (6), which have two phase structures, contained equal amounts of each phase (i.e ≅50% for each). Now the location of line (a) in Fig 6.44 was fixed by applying the Lever Rule with these microstructures of specimens (1) and (6). By applying the Lever Rule, the same amount of area for both phases in specimen (1) suggested that the distance of lines (a) and (b) from (1) should be same. The same is true for the specimen (6). As the line (b) has already been fixed, line (a) was located accordingly. Further, the similarity of the microstructures for specimens (1) and (6) is evidence that no phase change occurred at 250°C, as suggested by Okamoto and Massalski (132), as shown in Fig 7.40. If such a reaction does occur, then it must be at a temperature below 220°C.

The specimen (2) had a two phase structure, β and ζ, as shown in Fig 6.34. The microstructure of this specimen indicated that about 30% of the structure is covered by β phase. Application of the Lever

Rule suggested the position of the line (c) as shown in Fig 6.44, was located correctly by Prince and co-worker. The samples (3), (4), (5), (7) and (8) gave single phase ζ structures. The application of the Lever Rule with samples (9), (10) and (11) gave rise to the position of line (d). The upper end of this line was drawn to coincide with the established line [bold in Fig 6.44] at 279.5°C, and from here the direction of this line is such that if it is extended it should pass between the specimen (12) and (13) in Fig 6.44. These specimens were studied at UMIST. Unfortunately, most of the specimens studied at UMIST did not reach equilibrium and a result was obtained only for the specimen (13). This specimen showed a small amount of liquid had been present at the equilibration temperature. Hence, the high temperature portion of this line was probably located correctly by Prince and co-workers (dotted lines in Fig 6.44).

It should be noted here that the position of line (a) is more accurate as compared to line (d). Because, if there is a chance of 5% error in the estimate of the amount of the phases present in the microstructure, then the position of line (a) will not be affected significantly. Whereas the position of line (d) is very sensitive to the estimated amounts of the small regions of AuSn compound. Further, in the light of the above results and discussion it is probable that the Au solvus line is located as shown by the chain line in Fig 6.44. The probable extension to lower temperature of the ζ/AuSn + ζ phase boundary is shown also as a chain line in the Figure.

Thus the present work has substantiated, at least in part, the version of the Au-Sn binary diagram proposed by Prince and co-worker, and confirms that the constituent of the Au- rich alloys suggested by Okamoto and Massalski is incorrect.

CHAPTER 8

CONCLUSIONS

(1) The partial constitutions of Au-Ge-X ternary systems have been investigated, where Au forms stable intermediate congruent melting compounds with the elements 'X' belonging to the IIB and IIIB groups of the periodic table. These compounds include AuIn, $AuIn_2$, AuGa, $AuGa_2$, AuZn and AuCd. Pseudobinary eutectic systems were found between the above stable compounds and Ge. The solubility of Ge in the AuX compounds was 1.3 at.%Ge for Zn and Cd containing alloys and less than 1.0 at.% Ge for In and Ga containing alloys at the eutectic temperatures, which is in accordance with the Hume-Rothery rule. All Au-Ge-X systems show complete miscibility in the liquid state for all compositions. The liquidus curves for higher concentrations of solvent obey the Vant Hoff equation in these pseudobinary systems.

The examination of the AuIn-$AuIn_2$-Ge partial ternary system showed the presence of a ternary eutectic with an estimated composition of 3.5 at.% Ge, 43.25 at.% Au and 53.25 at.% In at 471°C. Also the presence of a degenerate ternary eutectic located very close to the In corner at a temperature of 156°C was detected in the $AuIn_2$-Ge-In partial ternary system.

The study of the AuGa-Ge-$AuGa_2$ partial system also showed the presence of a ternary eutectic with an estimated composition 3.2 at.% Ge, 41.8 at.% Au and 55.0 at.% Ga at 438°C.

(2) The constitutions of the Au-Pb-X ternary systems have also been investigated, where X has the same meaning as described above. The stable compounds AuX did not exhibit pseudobinary eutectic systems with Pb (AuIn-Pb and $AuIn_2$-Pb sections have already been investigated prior to this study, where AuIn-Pb section forms a pseudobinary system, but $AuIn_2$-Pb section does not form pseudobinary system). The investigation of AuX-Pb sections in Au-Pb-X ternary systems, showed extensive liquid immiscibility over a wide range of compositions; immiscibility was easily seen on metallographic sections. This contrasts with the pseudobinary eutectic nature of AuX-Ge sections.

(3) Prior to this study, it had been shown that the liquid immiscibility which occurs in a number of binary systems can be predicted from the enthalpies of vapourization and electronegativities of the constituents elements. The extension of this theory to ternary equilibria is shown here. The presence of liquid immiscibility and complete liquid miscibility in ternary systems is reasonably predicted using atomic size factor and melting points. Rather a poor predictability is given by using a combination of the electronegativity and a solubility parameter for miscible ternary systems. However, good agreement is indicated for

liquid ternary immiscible systems. Hence, if liquid immiscibility in a ternary system is predicted by both rules, then it can assumed with confidence that the liquid immiscibility will occur.

(4) Thermodynamic calculations of various sections in the Au-Ge-In ternary system and isotherms of the AuIn-Ge-In partial sub-ternary system showed good agreement with experimental determination. These thermocalculations were made by using the optimized data of the binary systems involved in the Au-Ge-In system by the Lukas (38) method.

(5) Smith Thermal Analysis equipment, which was originally develop to determine the enthalpy of phase transformation and heat capacity of the alloys as a function of temperature, was used to the determine phase boundaries. The STA apparatus proved to be excellent for the determination of phase boundaries. This apparatus provided the specimens with thermal conditions which are favourable for preserving the metallurgical equilibrium.

(6) The lower temperature equilibria, which was uncertain before this study, for the Au-rich portion of the Au-Sn binary phase diagram, has been partially amended.

CHAPTER 9

SUGGESTIONS FOR FURTHER WORK

(1) The AuX-Pb sections (AuGa-Pb, $AuGa_2$-Pb, AuZn and AuCd-Pb) in the Au-Pb-X ternary system do not form pseudobinary eutectic systems and possible interpretation, with the existing experimental data obtained in the present study is presented here. However, further experimental determination is needed to confirm these systems.

(2) The AuX-Si sections (where X = In, In_2, Ga, Ga_2, Zn and Cd) in the Au-Si-X ternary system may form pseudobinary eutectic systems, which require experimental confirmation. Also $AuAl_2$-Ge, and Au_2Al-Ge sections may form pseudobinary eutectic systems, which can be investigated experimentally.

(3) The AuIn-Ge-Au and AuGa-Ge-Au partial ternary systems in the Au-Ge-In and Au-Ge-Ga ternary systems respectively require further determination to establish the complete description of these systems.

(4) The optimization of the AuIn-Ge and $AuIn_2$-Ge sections in the Au-Ge-In ternary system can be obtained by the combination of phase boundary results obtained in the present study, with the data

for the edge binary systems by using the Lukas optimization programme. Furthermore, the full thermodynamical description of the Au-Ge-In system can be obtained.

(5) The pseudobinary AuGa-Ge, $AuGa_2$-Ge, AuZn-Ge and AuCd-Ge sections in the Au-Ge-X ternary system, which have been determined in the present investigation, should be calculated on a thermodynamical basis, which, in turn, demands thermodynamical data for all the edge binary phase diagrams involved in each ternary system. The Au-Ga, Au-Zn and Au-Cd binary data are not available and require to be calculated. The rest of the thermodynamical data for the other binary phase diagrams involved are available. By acquiring data for all these binary phase diagrams, all the above experimentally examined pseudobinary sections can be computed thermodynamically and hence can be optimized.

(6) Similarly all the AuX-Pb sections in the Au-Pb-X ternary systems required thermodynamical calculations for all sections in the same way from the edge binary optimized data, as described above; again all these binary phase diagrams involved, still have to be optimized except for the Au-Pb binary system.

(7) The lower temperature equilibria for the Au-rich portion of the Au-Sn binary system determined so far is not sufficient to describe it completely and hence there is need for further research.

REFERENCES

(1) J. L. Haughton, J. Inst. Met., 1947, 73, 693-704.

(2) F. J. Dunkerley and G. J. Mills, "Thermodynamic in Physical Metallurgy", Am. Soc. Metals, Cleveland, Ohio 1950.

(3) C. D. Thurmond, J. Phys. Chem. 1953, 57, 827.

(4) H. Seltz, J. Am. Chem. Soc., 1934, 56, 307-311.

(5) H. Seltz, J. Am. Chem. Soc., 1935, 57, 391-395.

(6) G. Scatchard, J. Am. Chem. Soc.,1940, 62, 2426-2429.

(7) R. Hultgren, T. Desai, D. T. Hawkins, M. Gleise, K. K. Kelley and D.Wagman,"Selected Values of Thermodynamics Properties of the Elements", ASM, Metals Park, Ohio, 1973.

(8) R. Hultgren, T. Desai, D. T. Hawkins, M. Gleise, K. K. Kelley and D.Wagman, "Selected Values of Thermodynamics Properties of Binary Alloys", ASM, Metals Park, Ohio, 1973.

(9) O. Kubaschewski and C. B. Alcock, "Metallurgical Thermochemistry", 5th Edittion, Pergamon Press, Oxford, 1979.

(10) CALPHAD, Calculation of Phase Diagrams (Computer Coupling of Phase Diagram and Thermochemistry ed. L. Kaufman, Pergamon Press, Oxford, New York and Frankfurt).

(11) SGTE, (Scientific Group Thermodata Europe).

(12) L. Kaufman, H. Bernstein, "Computer Calculations of Phase Diagrams", Academic Press, New York and London,1970.

(13) D. S. Evans and A. Prince, Mat. Res. Bull., 1982, 17, 681-687.

(14) A. Prince, (The use of phase diagrams in the joining of metals), "Phase Diagrams", vol. 2, A. M. Alper, Academic Press, New York, 1970, 319-338

(15) A. Prince, J. Less Common Metals, 1967 12, 107-116.

(16) M. M. Karnowsky and F. G. Yost, Met. Trans., A, 1976, 7(8), 1149-1156.

(17) F. G. Yost, F. P. Ganyard and M. M. Karnowsky, Met. Trans., A, 1976, 7(8),1141-1148.

(18) F. G. Yost, Gold Bull., 1977, 10, 94-100.

(19) D. S. Evans and A. Prince, "The reaction of 80 wt.% Au 20 wt.% Sn solder alloy with Gallium", Presented at one day meeting on phase diagrams, Marseilles, 1986.

(20) J. C. Chaston, Int. Met. Rev.,1977 (March), 25-38.

(21) M. Antler, Gold Bull., 1983, 16(1), 2-7.

(22) M. L. McGluschan, "Physcio-Chemical Quantities and Units", Royal Inst. of Chemistry Monographs for Teachers No. 15, London, 1968

(23) W. Hume-Rothery, R. E. Smallman and C. W. Haworth,"The Structure of Metals and Alloys", Monograph and Report. Series No. 1, 5th ed.(rev.), Institute of Metals, London, 1988.

(24) L. S. Palatnik and A. I. Landau, Zh. Fiz. Khim., 1955, 29, 1784 and 1956, 30, 2399

(25) F. N. Rhines, "Phase Diagrams in Metallurgy", McGraw-Hill, New York, 1956.

(26) A. Prince, "Alloy Phase Equilibria", Elsevier, Amsterdam 1966.

(27) A. M. Alper, "Phase Diagrams", Academic Press, New York and London, 1970

(28) D. R. F. West, "Ternary Equilibrium Diagram", Chapman and Hall, New York and London, 1982.

(29) D. A. Porter and K. E. Easterling, "Phase Transformations in Metals and Alloys", Van Nostrand Reinhold, London, 1981.

(30) P. Gordon, "Principles of Phase Diagrams in Material Systems", McGraw Hill, New York, 1968.

(31) W. Hume-Rothery, J. W. Christian and W. B. Pearson, "Metallurgical Equilibrium Diagrams", The Institute of Physics, London, 1952.

(32) O. Kubaschewski and T. G. Chart, J. Inst. Met., 1964-65, 93, 329-338.

(33) L. Kaufman and H. Nesor, Metall. Trans., 1974, 5, 1617-1629.

(34) T. G. Chart, J. F. Counsell, G. P. Jones, W. Slough and P. J. Spencer, Inst. Metall. Rev.,1975, 20, 57.

(35) T. G. Chart, F. H. Putland and A. T. Dinsdale , "The Calculation of Multicomponent Alloy Phase Diagrams" at National Physical Laboratory, NPL Report Chem. 91.

(36) T. G. Chart and F. Putland, CALPHAD, 1979, 3(1), 9-18.

(37) I. Ansara, Int. Met. Rev., 1979, 24, 20-45.

(38) H. L. Lukas, E. Th. Henig, and B. Zimmermann, CALPHAD, 1977, 1(3), 225-236.

(39) P. Dorner, E. Th. Henig, H. Krieg, H. L. Lukas and G. Petzow, CALPHAD, 1980, 4(4), 241-254.

(40) J. L. Murray, Metall. Trans. A, 1984, 15A, 261-268.

(41) J. Nemela, G. Effenberg, K. Hack and P. J. Spencer, CALPHAD,1986, 10, 77-89.

(42) B. Jansson, Report Series D, No. 55, Division of Physical Metallurgy Royal Institute of Technology, 1984.

(43) I. Ansara, in "Metallurgical Chemistry", Proc. Symp. Brunel University, NPL 1971.

(44) E. Bonnier, R. Caboz and C. R. Hebd, Seances Acad. Sci., 1960, 250, 527.

(45) G. Toop, Trans. Metall. Soc. AIME, 1965, 232, 850-855.

(46) F. Kohler, Montash. Chem., 1960, 91, 738-740.

(47) C. Colinet, DES. Fac. Sci. Univ. Grenoble, France, 1967.

(48) Y. Muggianu, M. Gambino and J. Bros., J. Chem. Phys.1975, 72, 83-88.

(49) H. Lukas, J. Weis and E. Heing, CALPHAD, 1982, 6(3), 229-251.

(50) F. H. Hayes and W. T. Chao, UMIST, Private Communication, 1988.

(51) F. H. Hayes, H. L. Lukas, G. Effenberg and G. Petzow, Z, Metallkde., 1986, 77, 749-754.

(52) A. T. Dinsdale, Ph.D Thesis, Brunel Univ.1984.

(53) R. A. Oriani and C. B. Alcock, Trans. Metall. Soc. AIME., 1962, 224, 1104-1115.

(54) M. L. Kapoor, Inst. Metall. Rev., 1975, 20, 150-165.

(55) J. H. Hildebrand, Proc. Nat. Acad. Sci., 1927, 13, 267-272.

(56) J. H. Hildebrand, J. Amer. Chem. Soc., 1929, 51, 66-80.

(57) J. H. Hildebrand, and R. L. Scott, "The Solubility of Non-Electrolytes", 3rd ed., Rheinhold, New York, 1950.

(58) R. C. Mackenzie, "Differential Thermal Analysis" vol. 1, Academic Press, London,1970.

(59) R. J. W. Mclaughlin, "Physical Method of Determining Mineralogy" (J. Zussmaned), Academic Press, New York, 1967.

(60) A. Blazek, (Translation editor J. F. Tyson) "Thermal Analysis", Van Nostrand Reinhold Ltd., London, 1973.

(61) G. V. Raynor, "Physical Metallurgy" (R. W. Cahn, ed.) North. Holland Publ., Amsterdam, 1965.

(62) C. Plato and A. R. Glasgow, Anal. Chem., 1969 ,41, 330.

(63) C. S. Smith, Trans. AIME, 1940, 137, 236-245.

(64) W. Hagel, G. Pound and R. Mehl, Acta Metall., 1956, 4, 37-46.

(65) G. Humpston and D. S. Evans, Mater. Sci. Tech., 1987, 3, 621-627.

(66) G. Humpston and B. L. Davies, Mater. Sci. Tech. 1985, 1(6), 433-441.

(67) G. Humpston and B. L. Davies, Metal Science, 1984, June, 18, 329-331.

(68) D. S. Evans and A. Prince, Metal Science, 1978, Aug., 386-387.

(69) D. S. Evans and A. Prince, Thermochim. Acta., 1982, 58, 199-209.

(70) D. S. Evans and A. Prince, Metal Science, 1978, Dec, 12. 600-602.

(71) D. S. Evans and A. Prince, Metal Science, 1983, March, 17. 117-121.

(72) D. S. Evans and A. Prince, Metal Science, 1977, Dec, 597.

(73) C. Maxwell, UMIST, Private Communication, 1988.

(74) M. T. Z. Butt and C. Bodsworth, Mater. Sci. Tech., 1990, 6(2), 134.

(75) M. T. Z. Butt, C. Bodsworth and A. Prince, Scripta Met., 1989, 23(7), 1105.

(76) M. T. Z. Butt, C. Bodsworth and A. Prince, J Less-Common Metals, 1989, 154, 229.

(77) M. T. Z. Butt, C. Bodsworth and A. Prince, Scripta Met.,1990, 24(3), 481.

(78) M. T. Z. Butt, C. Bodsworth and A. Prince, To be published.

(79) C. R. M. Grovenor, Thin Solid Films, 1983, 104, 409.

(80) Private Communication from T. G. Chart, National Physical Laboratory, U.K (SGTE Pure Component Transition Data, March, 1988).

(81) P. C. Wallbrecht, R. Blachnik and K. C. Mills, Thermochimica Acta, 1981, 48, 69-82.

(82) E. A. Brandes, Smithells Metal Reference Book (6th ed.), Butterworth and Co. Ltd., London, 1983.

(83) H. Okamoto and T. B. Massalski, Bull. Alloy Phase Diagrams, 1984, 5(6), 601-610.

(84) S. Hassam, M. Gambino, M. Gaune-Escard, J. P. Bros, and J. Agren, Met. Tran. A, 1988, 19A, 409-416.

(85) R. W. Olesinski, N. Kanani and G. J. Abbaschian, Bull. Alloy Phase Diagrams, 1985, 6(6), 581.

(86) V. K. Nikitina, A. A. Babitsyna and Yu. K. Lobanova, Izv.

Akad. Nauk. SSSR, Neorg. Mater., 1971, 7(3), 421-427, in Russian; TR: Inorg. Mater.,1971, 7(3), 371-376.

(87) O. Kubaschewski and F. Weibke, Z. Elektrochem.,1938, 44, 870-877.

(88) K. Itagaki, J. Japan Inst. Metals, 1976, 40(10), 1038-1046.

(89) S. E. R. Hiscocks and W. Hume-Rothery, Proc. Roy. Soc., London, 1964, A282, 318-330.

(90) R. W. Olesinski and G. J. Abbaschian, Bull. Alloy Phase Diagrams, 1985, 6(3), 287.

(91) C. J. Cooke and W. Hume-Rothery, J Less-Common Metals, 1966, 10, 42.

(92) M. Hansen and K. Anderko, Constitution of Binary Alloys, McGraw-Hill, New York 1958.

(93) R. W. Olesinski and G. J. Abbaschian, Bull. Alloy Phase Diagrams, 1985, 6(6), 583.

(94) H. Okamoto and T. B. Massalski, "Phase Diagrams of Binary Gold Alloys", ASM, Metals Park, Ohio 1987.

(95) R. Alderdice and D. B. Dowine, Scripta Met., 1972, 6, 837.

(96). H. Ipser and R. Krachler, Scripta Met., 1988, 22, 1651.

(97) R. W. Olesinski, and G. J. Abbaschian, Bull. Alloy Phase Diagrams, 1986, 7(2), 189.

(98) H. Okamoto and T. B. Massalski, Bull. Alloy Phase Diagrams, 1986, 7(1), 52.

(99) H. Okamoto and T. B. Massalski, Bull. Alloy Phase Diagrams. 1984, 5(3), 276.

(100) H. Okamoto and T.B. Massalski, Binary Alloy Phase Diagrams. ASM, Metals Park, Ohio 1986.

(101) A. Prince, G. V. Raynor and D. S. Evans, "Phase Diagrams of Ternary Gold Alloys", Institute of Metals, London, (1990).

(102) R. D. Pehlke and K. Okajima, Trans. Metall. Soc. AIME, 1967, 239, 1354.

(103) C. T. Heycock and F. H. Neville, J. Chem. Soc., 1894, 65, 65.

(104) H. J. Axon, Nature, 1948, 162, 997.

(105) B. W. Mott, Phil. Mag., 1957, 2, 259-283.

(106) Y. A. Chang, D. Goldberg and P. G. Neumann, J. Phys. Chem. Ref. Data, 1977, 6, 621-627.

(107) E. G. Eroshenhova, V. G. Olencheva and L. A. Petrova, "Diagrammy Sostoyaniya Metallicheskikh Sistem", 1975 21, 92.

(108) N. Parravano and E Viviani, Atti Accad. Naz., Cl. Sc. Fis. Mat. Nat., Rend., 1910, 19(1), 835.

(109) W Guertler and A. Bergmann, Z. Metallk., 1933, 25(81), 111.

(110) Y. Hosoi, J. Japan Inst. Metals, 1952, 16, 555.

(111) R. Vogel and D. Horstmann, Arch. Eisenhuttenwesen, 1953, 24, 435.

(112) N. K. Rao and H. Wintehager, Trans. Indian Inst. Metals, 1956-57, 10, 139.

(113) A. A Sher, I. N. Odin and A. V. Novoselova, Russian Journal of Inorganic Chemistry, 1979, 24(9), 1393.

(114) G. Zwingmann and R. Vogel, Arch. Eisenhuttenwesen, 1957, 28, 591.

(115) J. J. Jacobs, R. H. Maes and R. E. de Strycker, Trans. Metall. Soc. AIME, 1967, 239, 1166.

(116) S. Briesemeister, Z. Metallk., 1931, 23, 225.

(117) V. V. Marugin, I. N. Odin and A. V. Novoselova, Russian Journal of Inorganic Chemistry, 1984, 29(6), 894.

(118) A. Prince, Private Communication.

(119) C. S. Barrett, "Structure of Metals", McGraw-Hill Book Co. New York, 1943.

(120) P. G. Rustamov, A. Z. Gadzhieve and B. N. Mardakhaev, Russian Journal of Inorganic Chemistry, 1976, 21(2), 279.

(121) E. G. Eroshenhova, V. G. Olencheva and L. A. Petrova, "Diagrammy Sostoyaniya Metallicheskikh Sistem", 1977 23, 82.

(122) F. Wald and R. W. Stormount, Trans. Metall. Soc. AIME, 1968, 242, 72.

(123) B. Gather and R. Blachnik, J. Less Common Metals, 1976, 48, 205.

(124) M. Haissinsky, J. Phys. Rad., 1946, 7, 12.

(125) A. D. Walsh, J. Chem. Soc., 1948, part I, 398-406.

(126) W. Gordy, Phys. Rev., 1946, 69, 604 and 69, 130.

(127) L. Pauling, "The Nature of the Chemical Bond", 3rd ed., Cornell University Press, New York, London, 1967.

(128) E. A. Owen and E. A. O'Donnell Roberts, J. Inst. Met., 1945, 71, 213-254.

(129) R. Vogel, Z. Anorg. Chem., 1905, 46, 60-75.

(130) H. A. Davies and J. S. Leach, J. Inst. Met., 1968, 96(7), 220-221.

(131) E. Hayer, K. L. Komarek., J. P. Bros and M. Gaune-Escard, Z.

Metallkd., 1981, 72(2), 109-115.

(132) H. Okamoto and T. B. Massalski, Bull. Alloy Phase Diagrams, 1984, 5(5), 492-503.

FIGURES

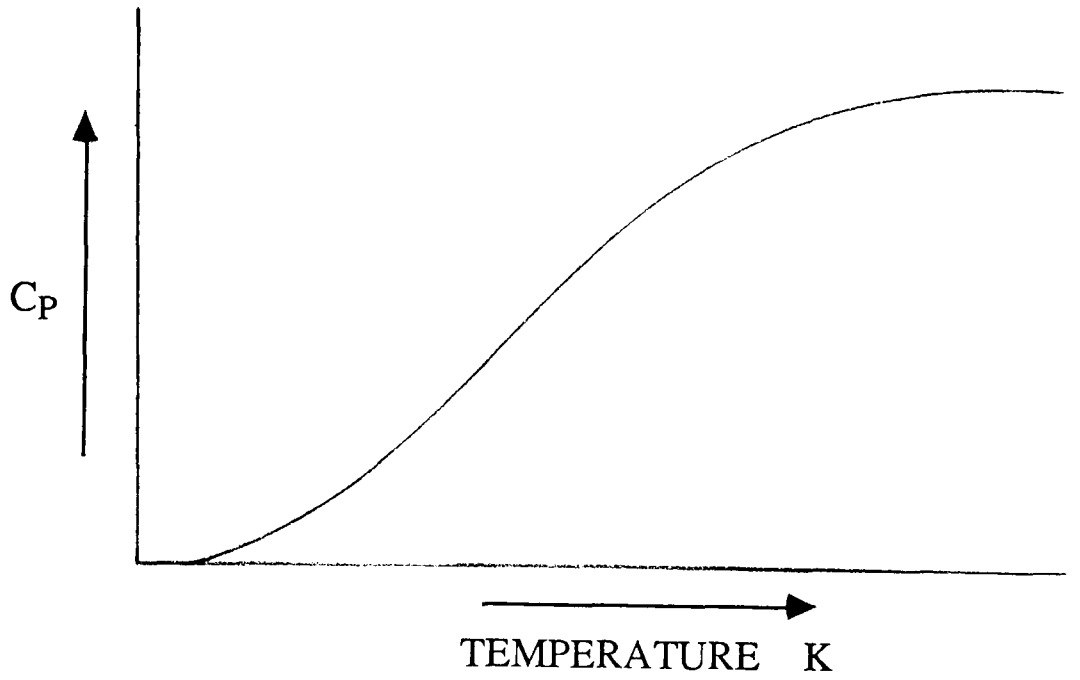

Fig 2.1:- Variation of C_P with temperature.

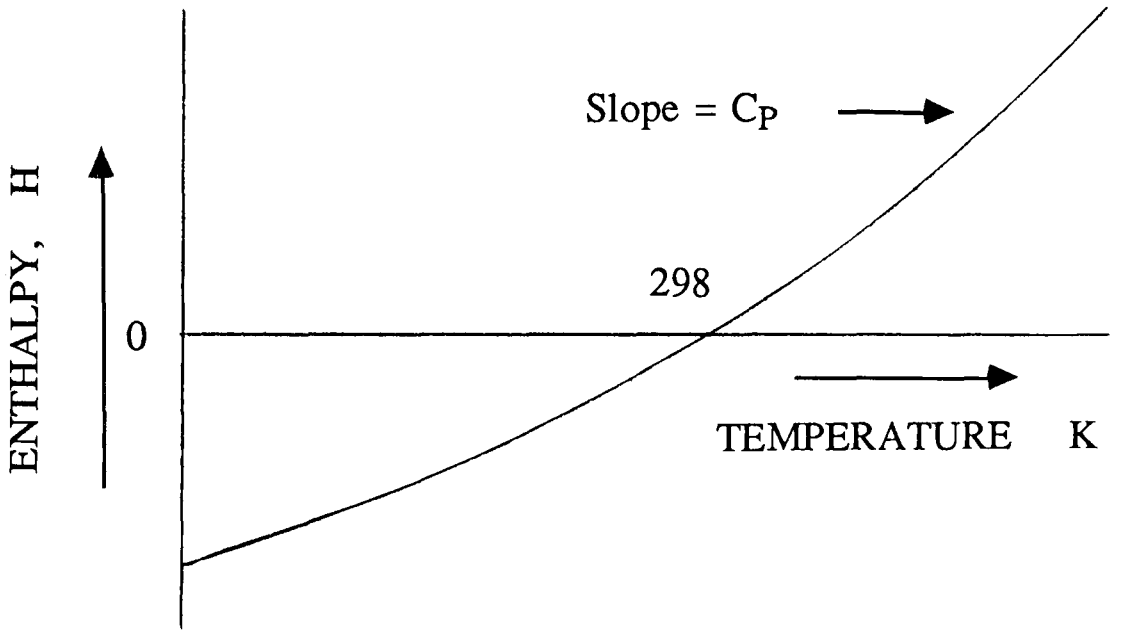

Fig 2.2:- Variation of enthalpy with temperature.

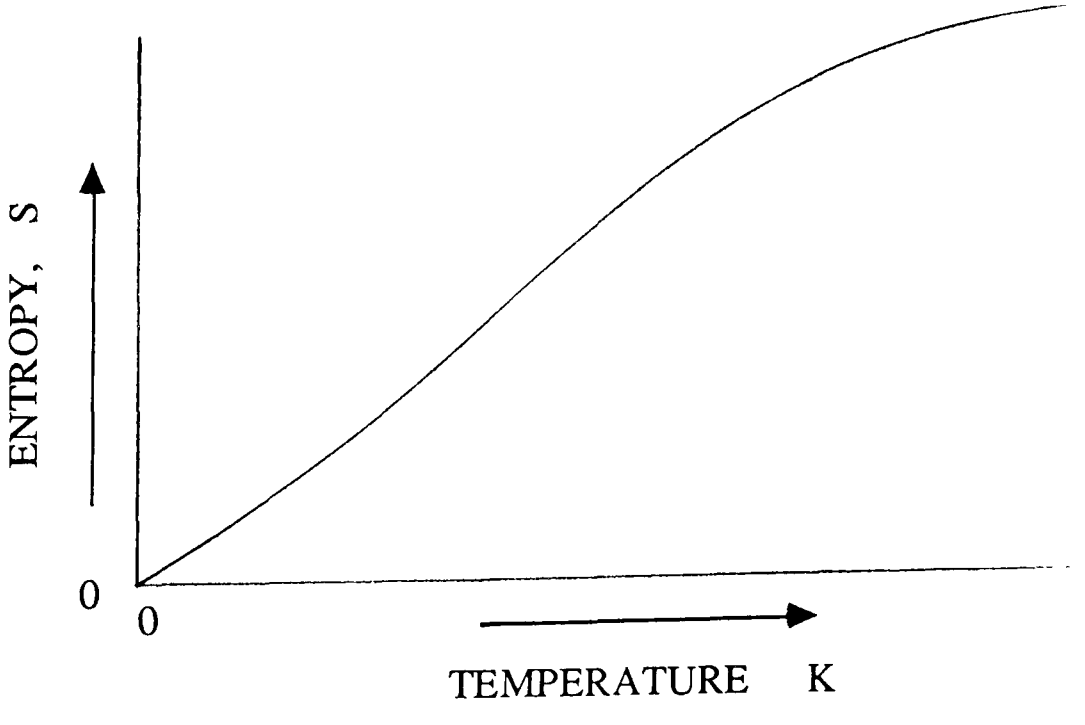

Fig 2.3:- Variation of entropy with temperature.

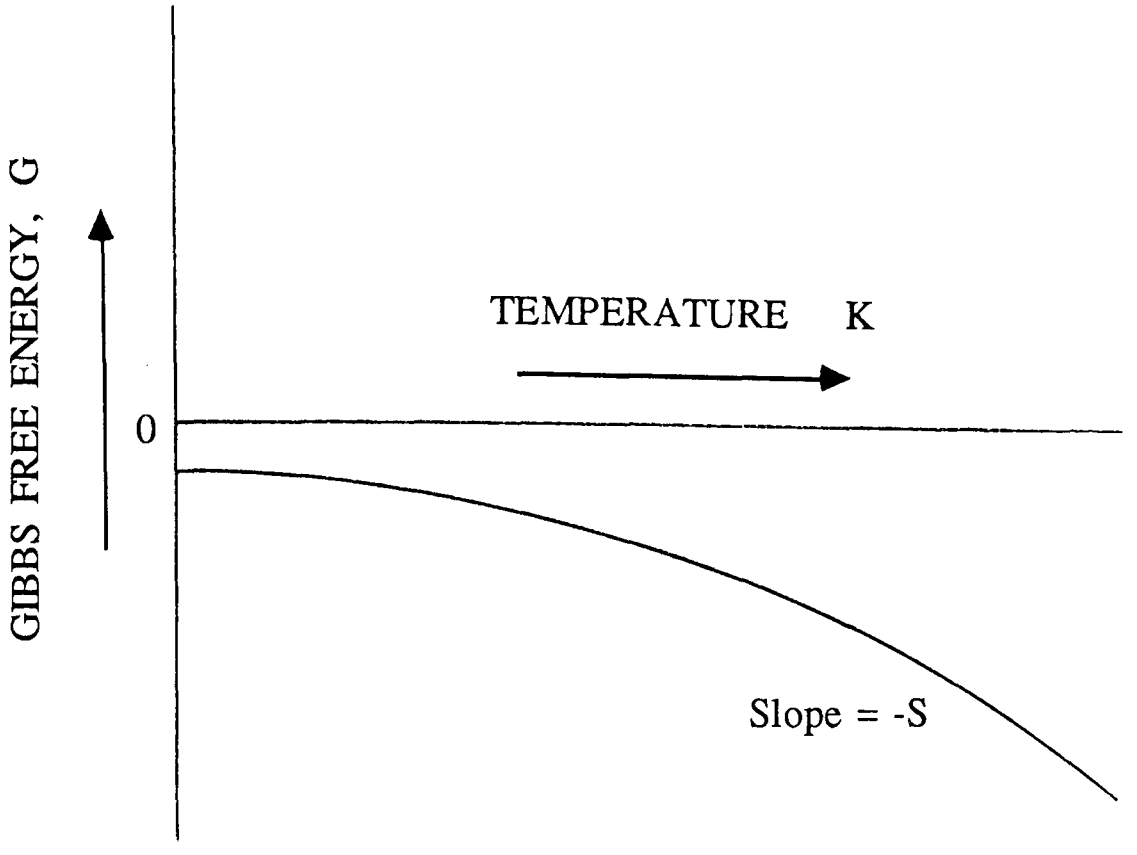

Fig 2.4:- Variation of G with temperature.

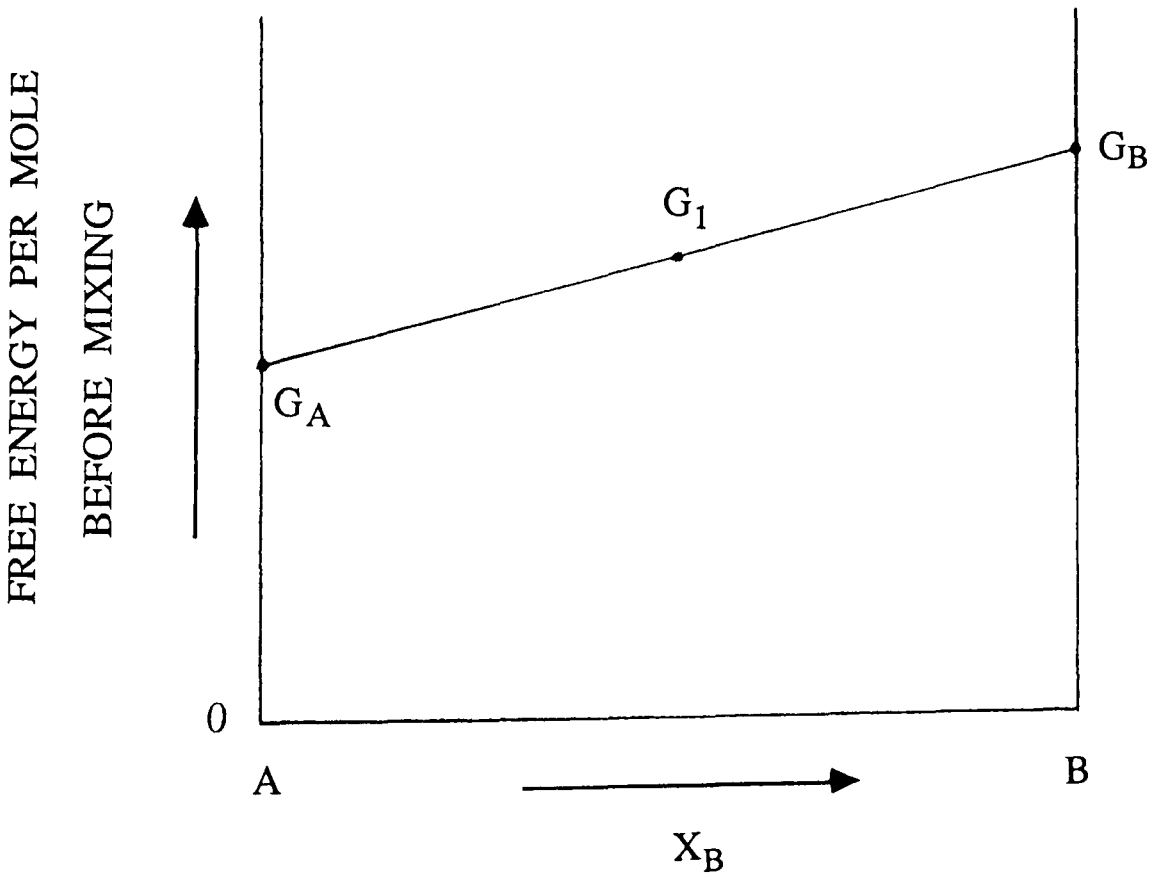

Fig 2.5:- Variation of free energy before mixing.

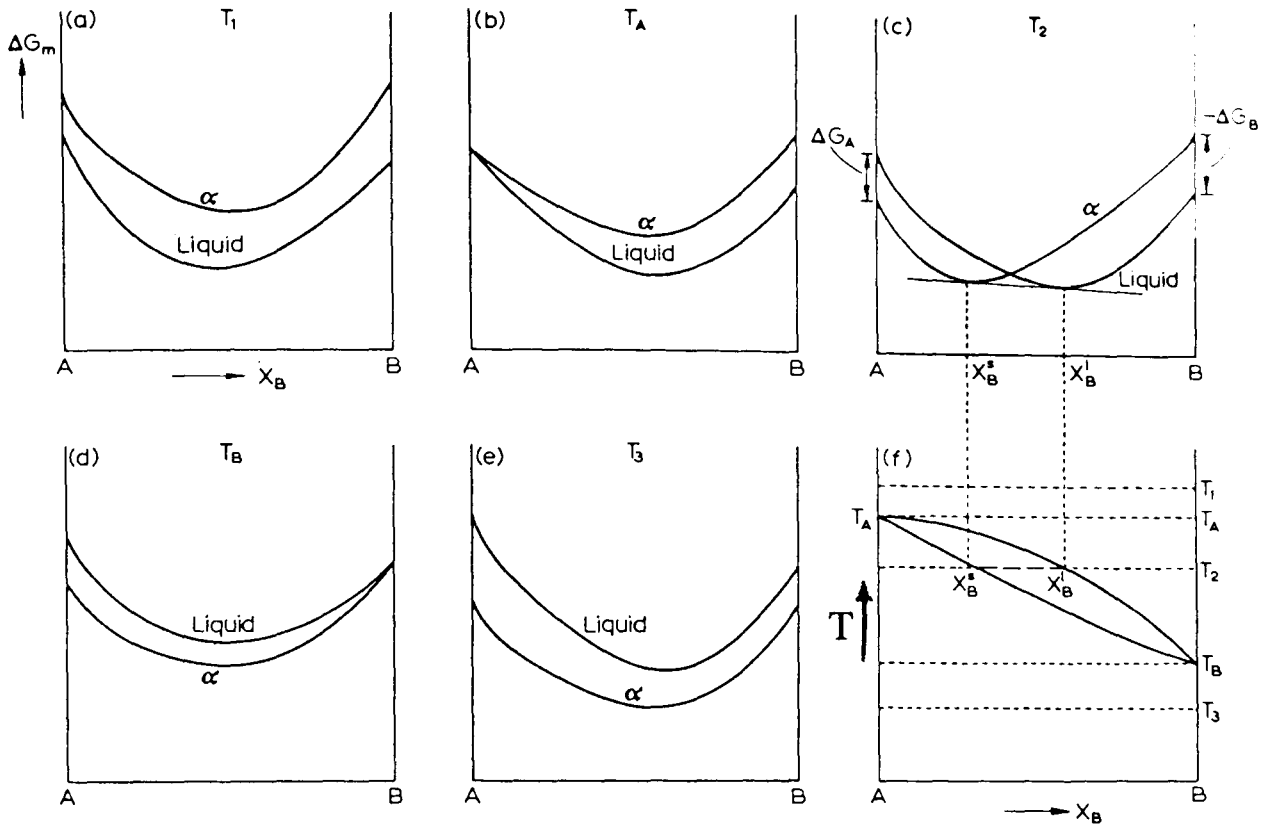

Fig 2.6:- Derivation of the phase diagram from the free energy curves (26).

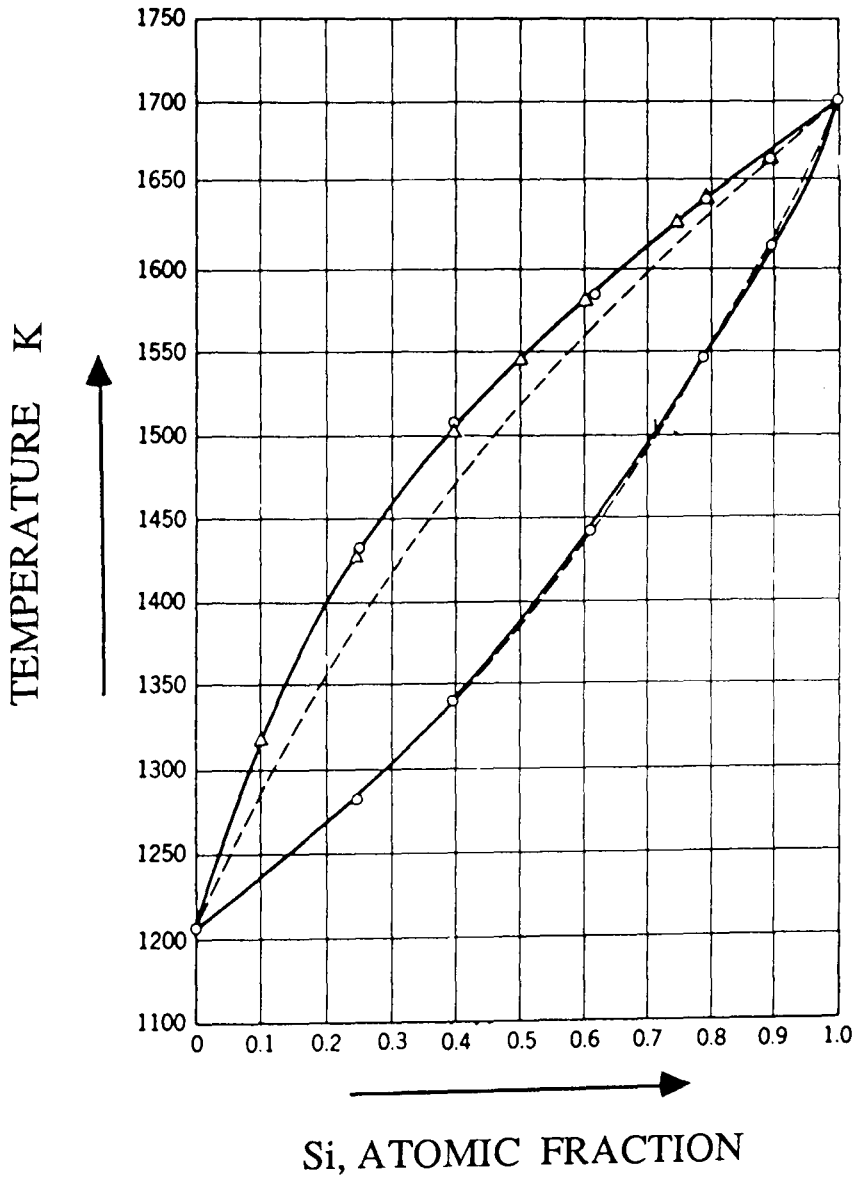

Fig 2.7:- Phase diagram for Ge-Si system. Solid line, experimental and dashed line, calculated (3).

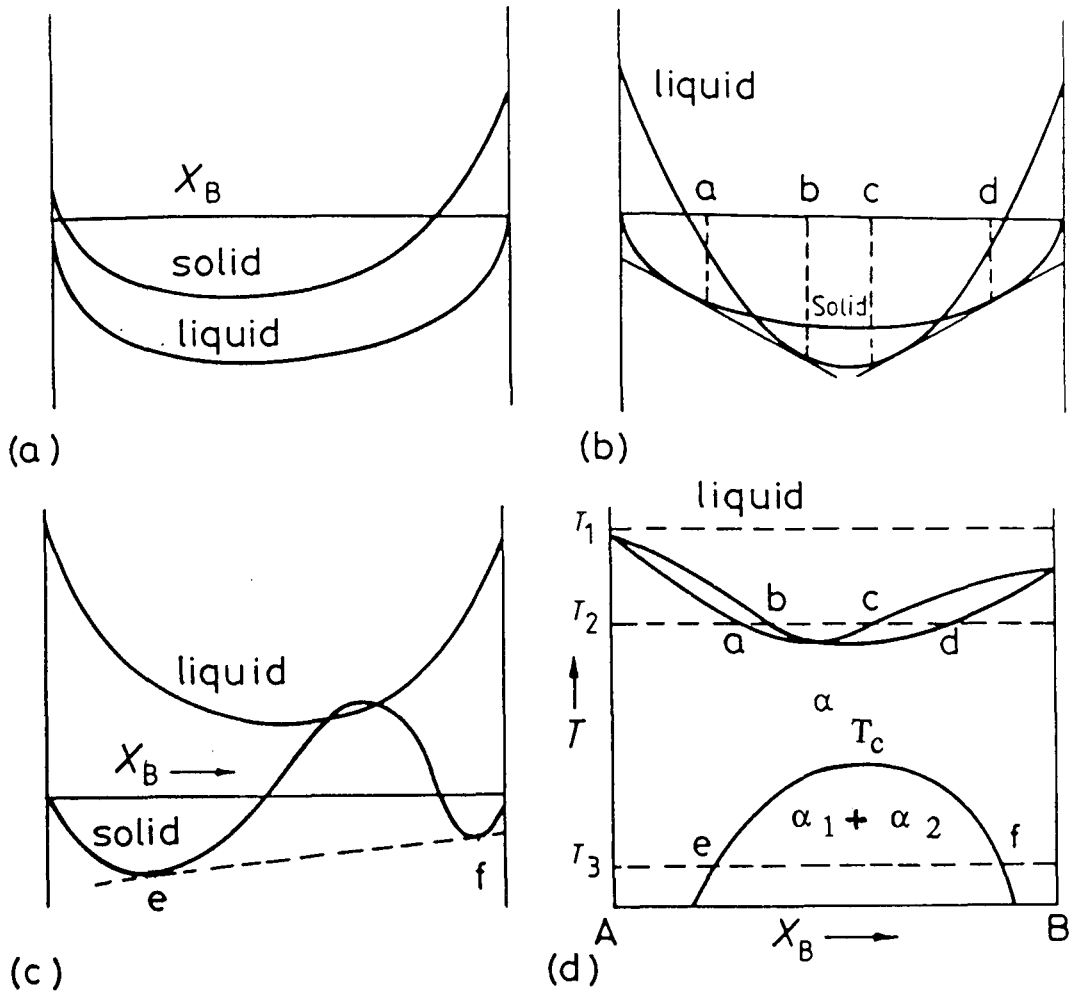

Fig 2.8:- The derivation of a phase diagram showing minima, where $\Delta H^{S}_{mix} > H^{l}_{mix} = 0$ (a), (b), (c) are the free energy vs composition curves at T_1, T_2 and T_3 respectively, and (d) shows the derived phase diagram, temperature vs composition (29).

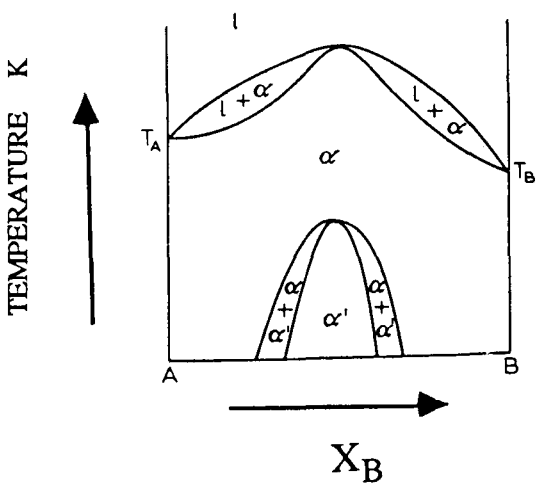

Fig 2.9:- Phase diagram showing maxima when $\Delta H^{S}_{mix} < 0$ (26).

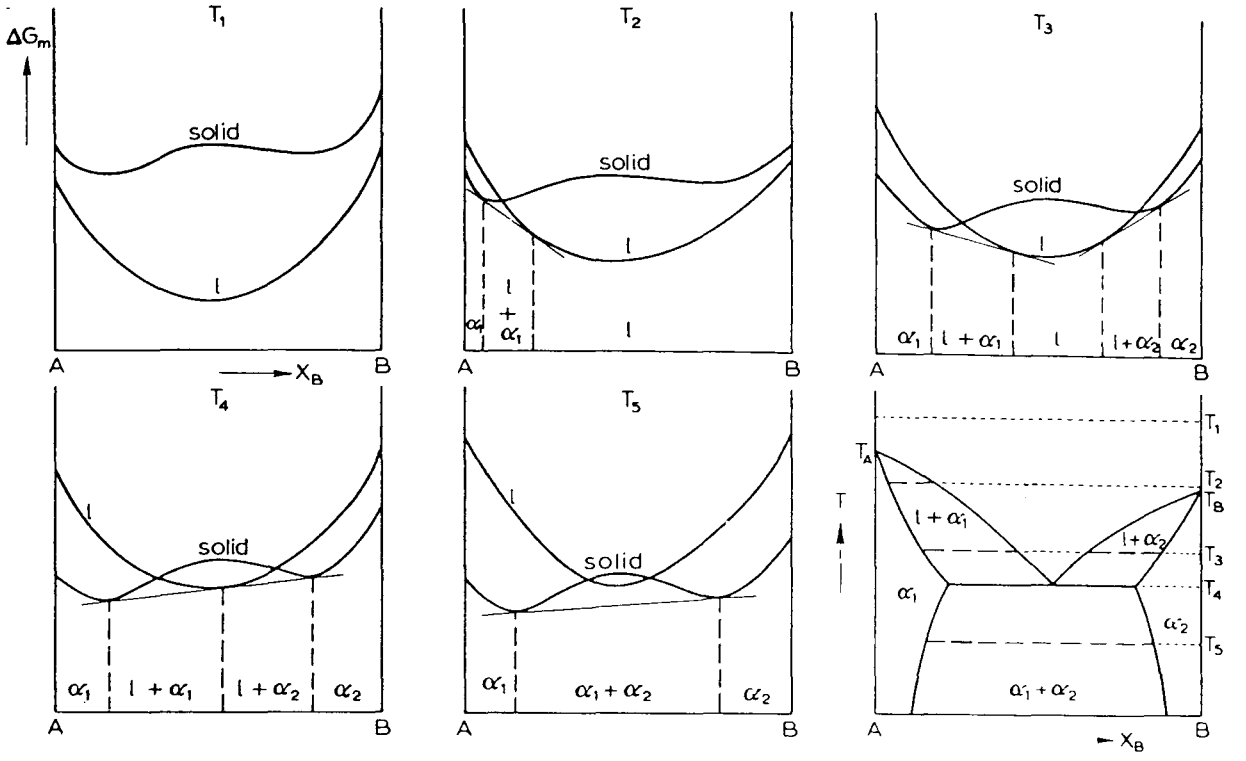

Fig 2.10:- The derivation of eutectic phase diagram from the free energy curves for the liquid and solid phases, when A and B both have same crystal structure (26).

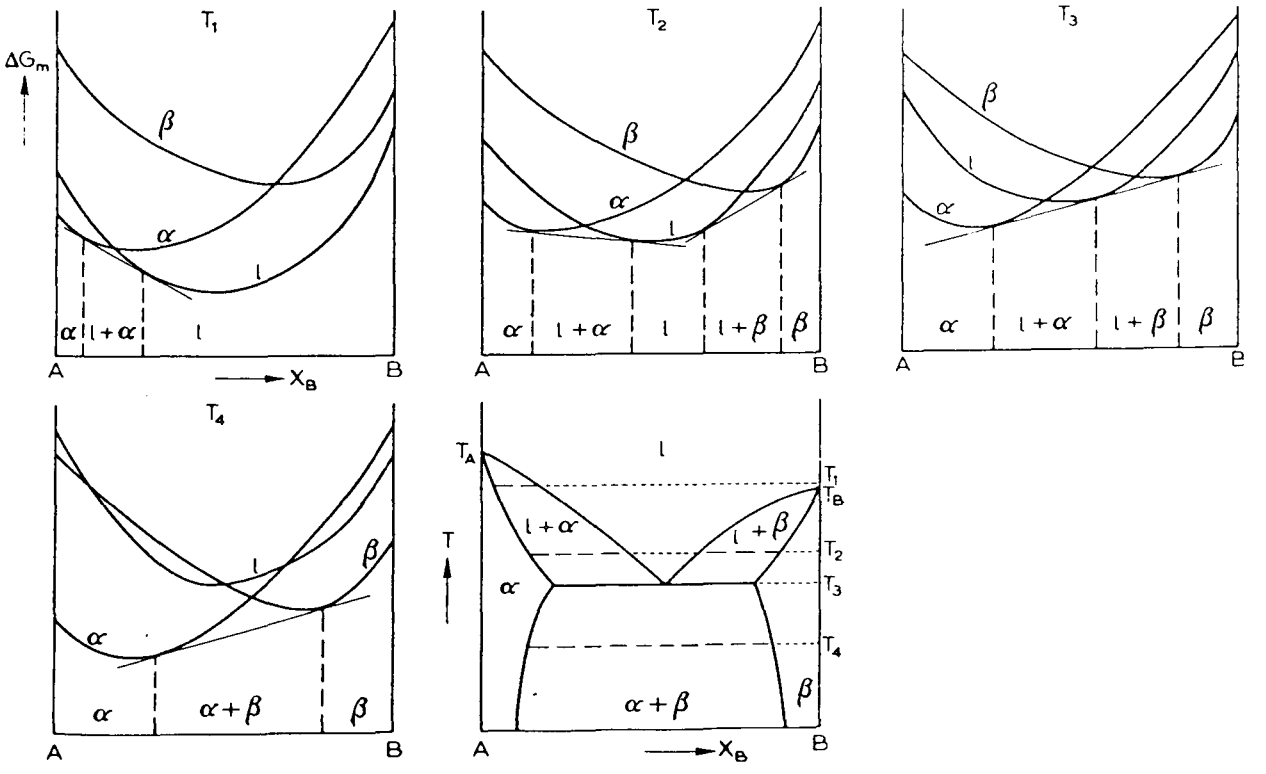

Fig 2.11:- The derivation of eutectic phase diagram from the free energy curves for the liquid, α and β phases, when A and B both have different crystal structure (26).

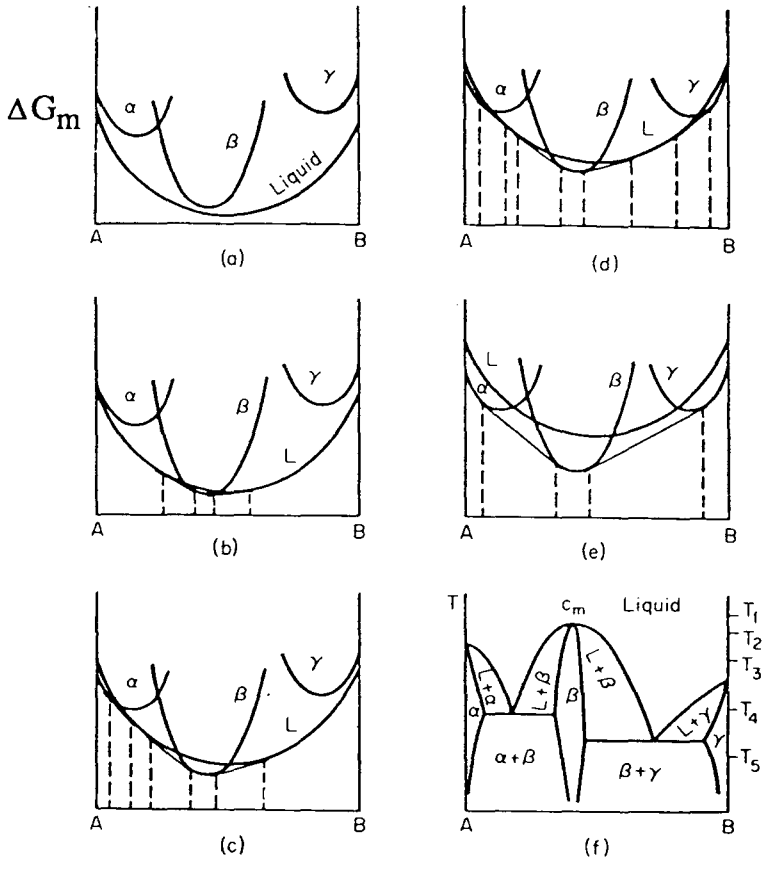

Fig 2.12:- The phase diagram, showing the intermediate phase, derived from the free energy curves (After Cottrell).

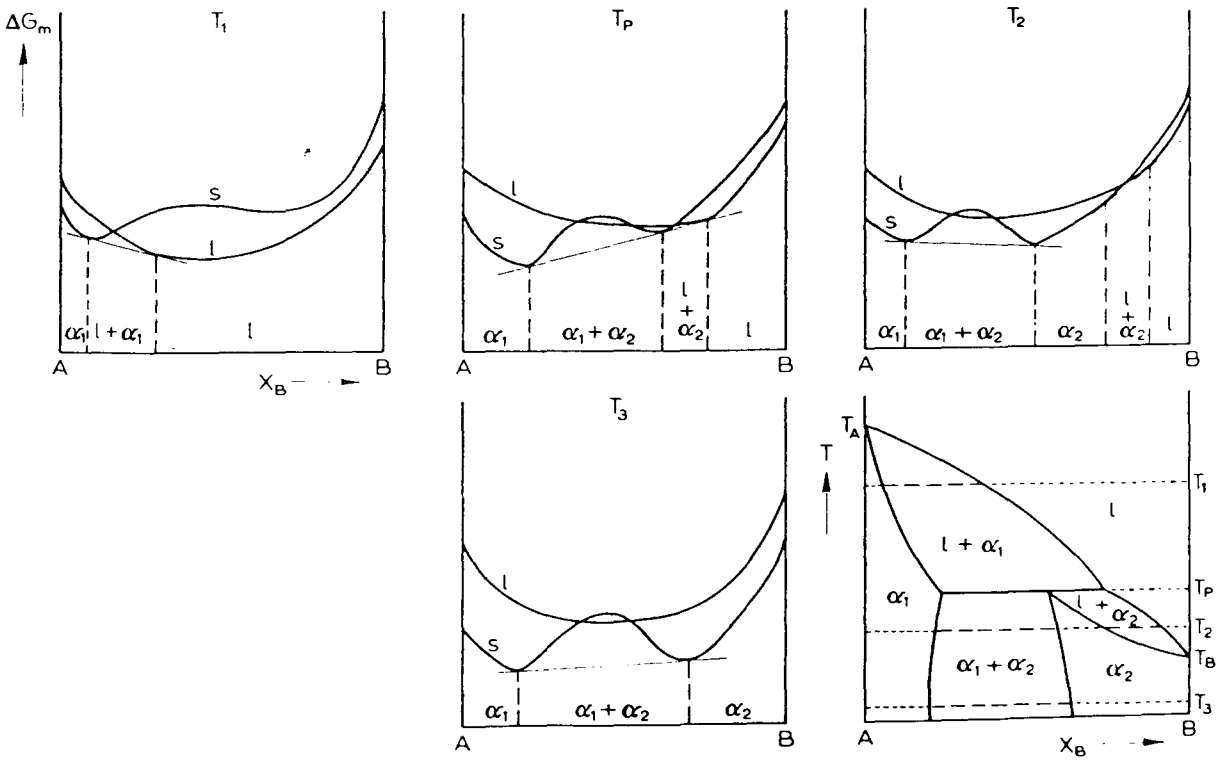

Fig 2.13:- Derivation of the peritectic phase diagram, from the free energy curves for the liquid and the solid phases (26).

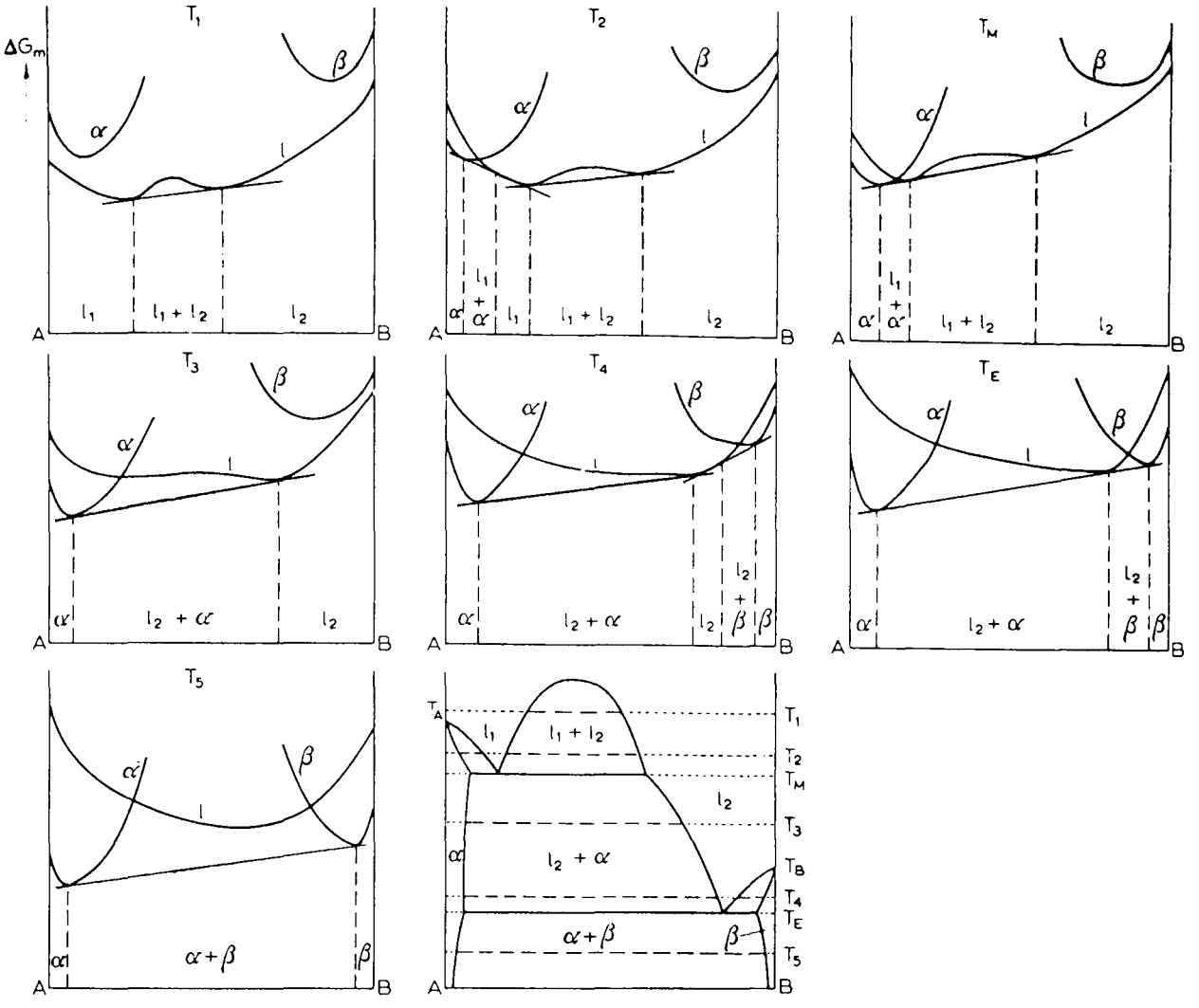

Fig 2.14:- The derivation of the monotectic phase diagram from the free energy curves (26).

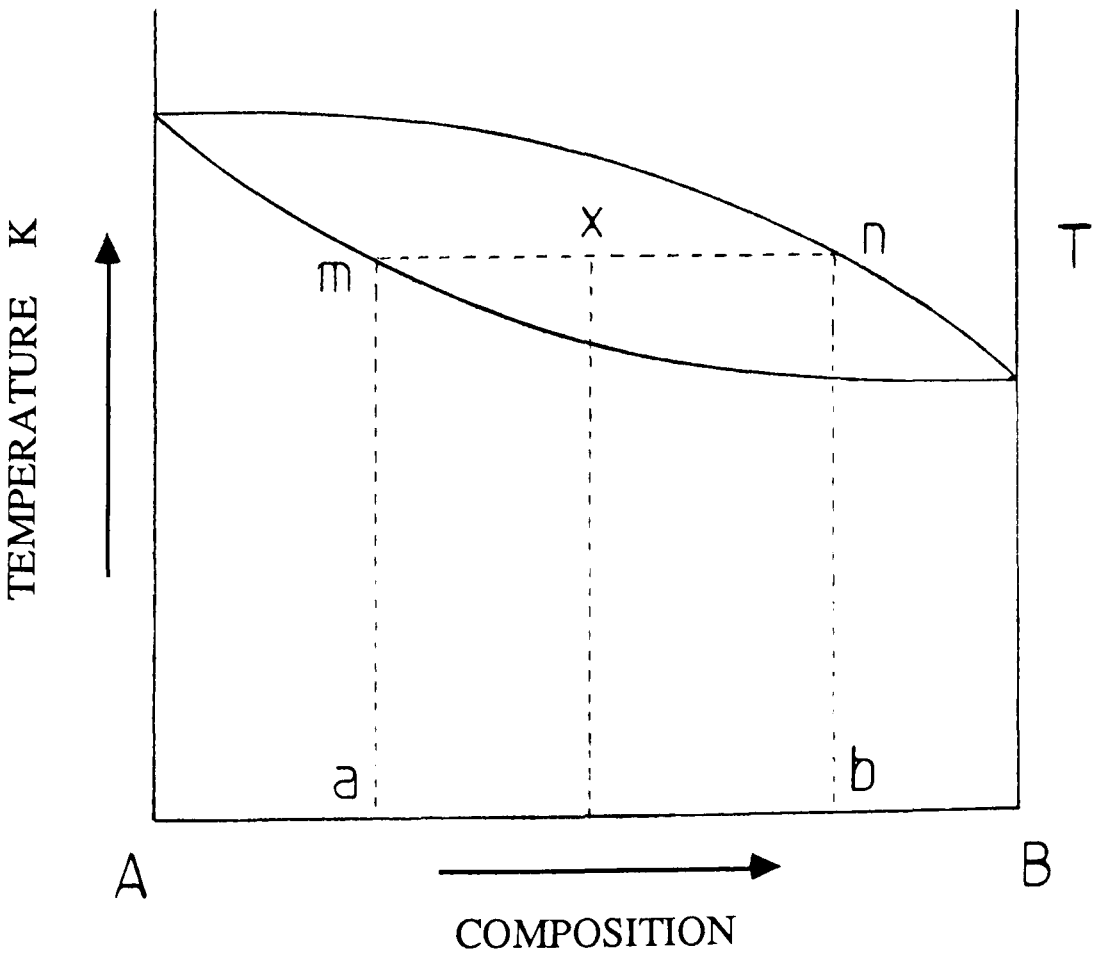

Fig 2.15:- Diagram showing the tie-line 'mn' at temperature T.

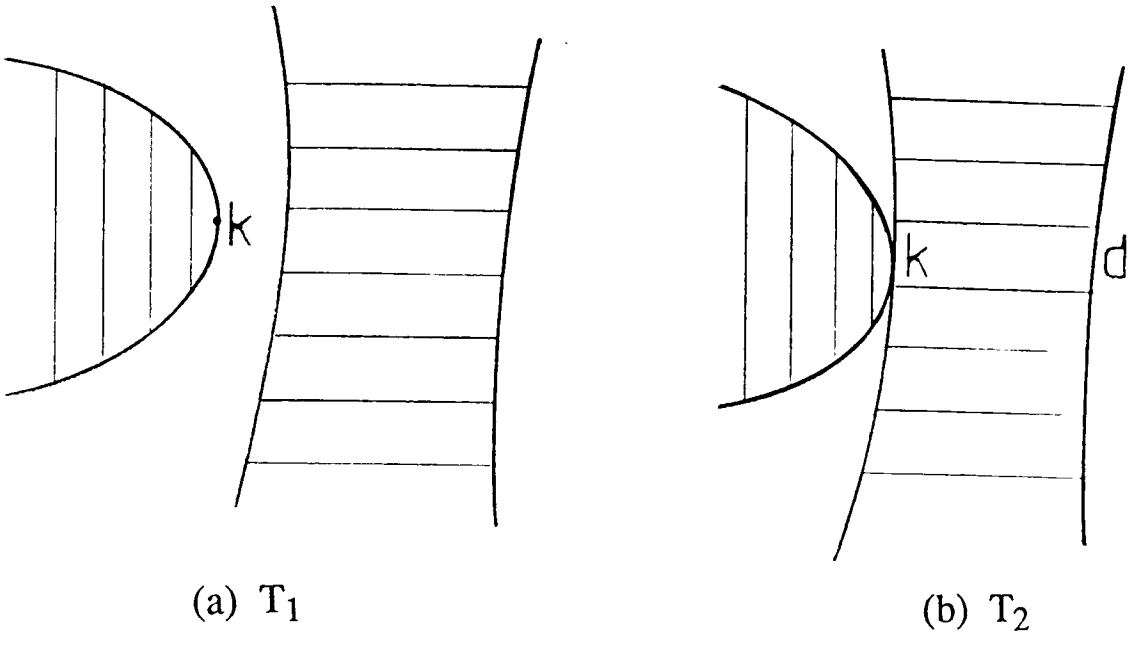

(a) T_1 (b) T_2

(c) T_3

Fig 2.16:- production of a ternary three-phase eqilibrium by the coalescence of two two-phase regions ($T_1 > T_2 > T_3$).

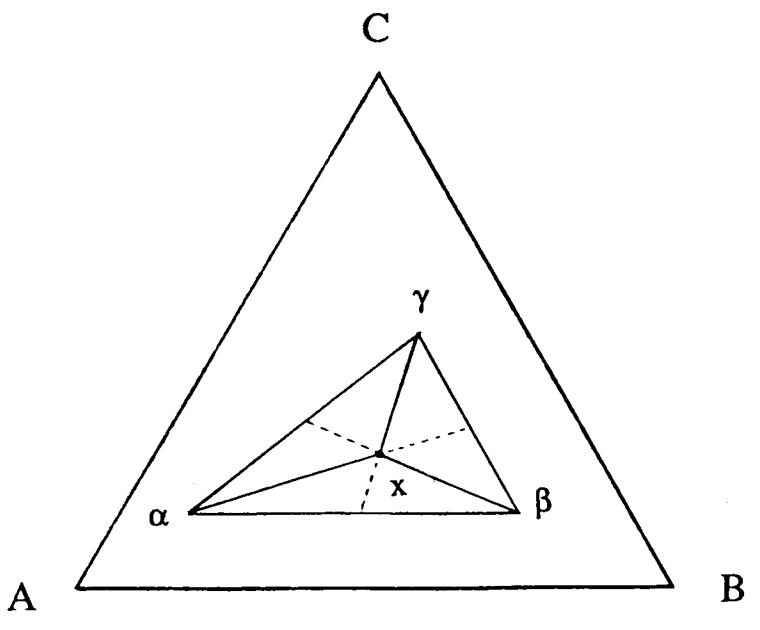

Fig 2.17:- Diagram showing tie-lines and tie-triangle.

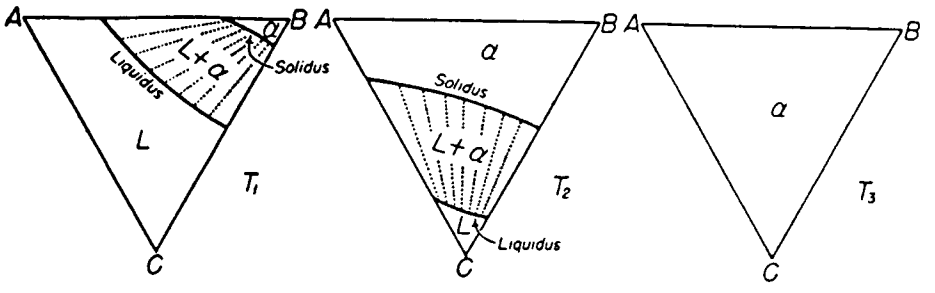

Fig 2.18:- Isotherms through the ternary isomorphous phase diagram, as derived from Fig 2.19. Dotted lines are showing the tie-lines (25)

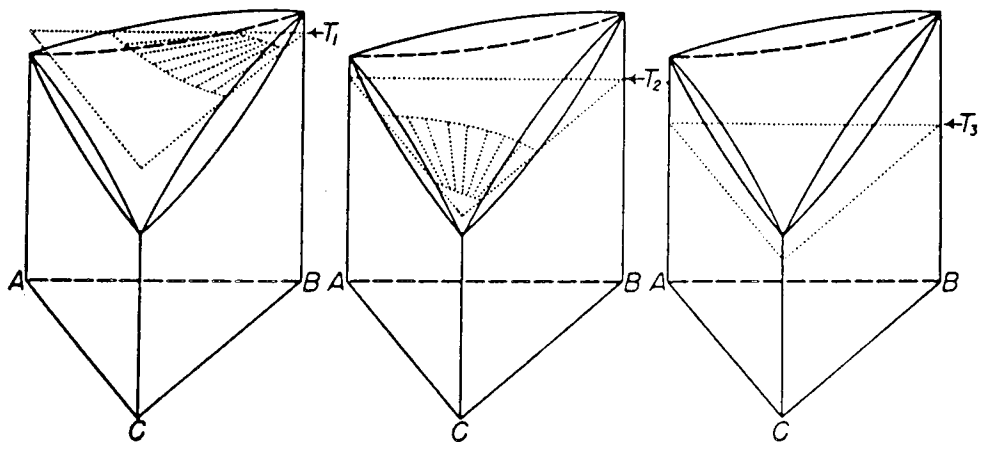

Fig 2.19:- Diagrams showing the development of isotherms at T_1, T_2 and T_3 (25).

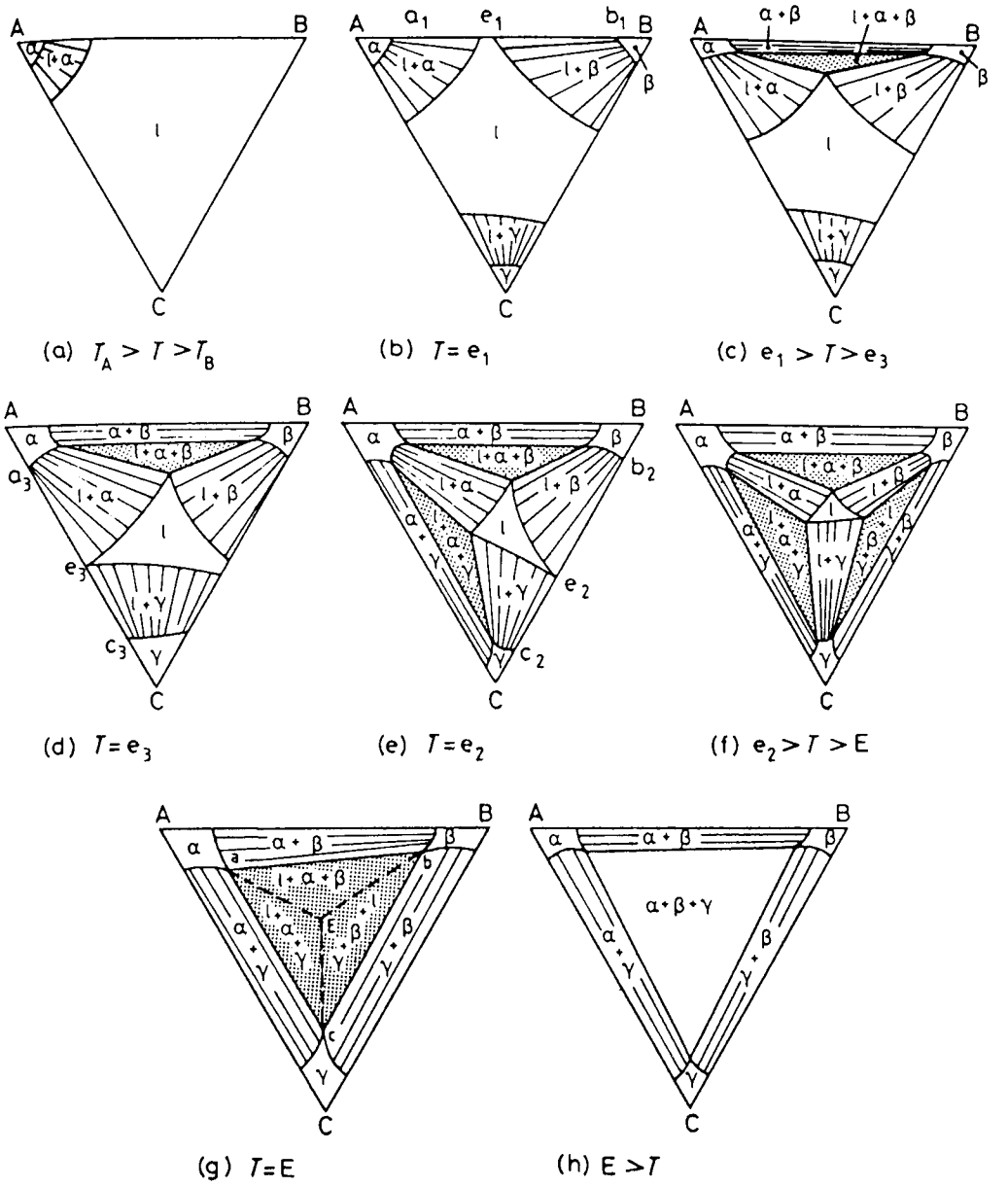

(a) $T_A > T > T_B$ (b) $T = e_1$ (c) $e_1 > T > e_3$

(d) $T = e_3$ (e) $T = e_2$ (f) $e_2 > T > E$

(g) $T = E$ (h) $E > T$

Fig 2.20:- Isotherms through the ternary eutectic system (from Fig 2.21) at various temperatures (26).

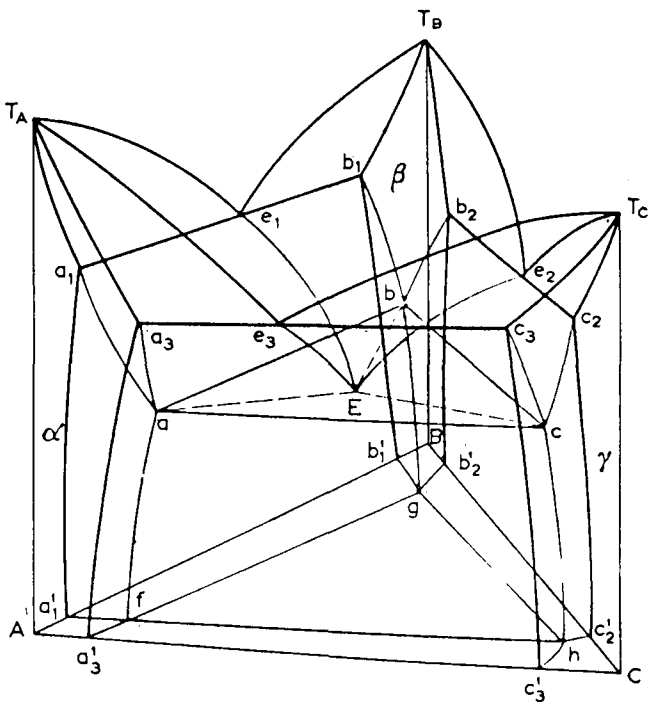

Fig 2.21:- The ternary eutectic system (26)

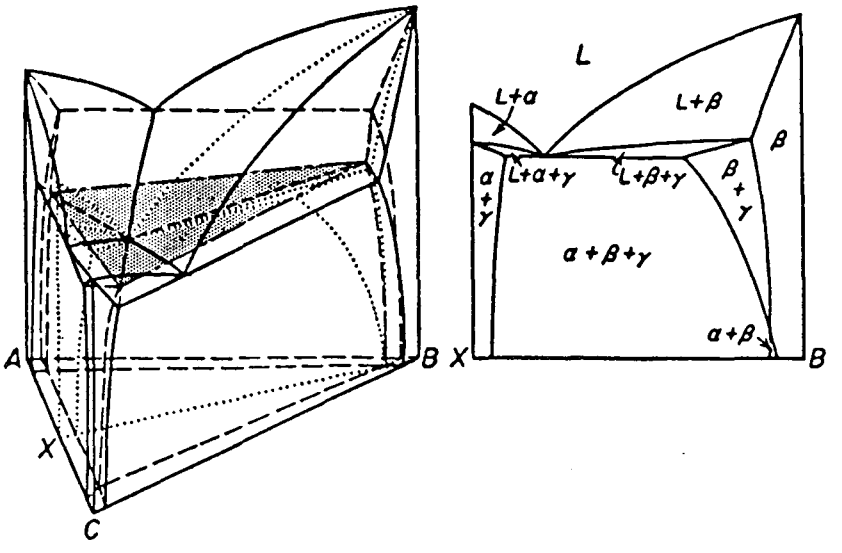

Fig 2.22:- Vertical sectioning through a ternary eutectic system representing the constant composition ratio of two components A and B (25).

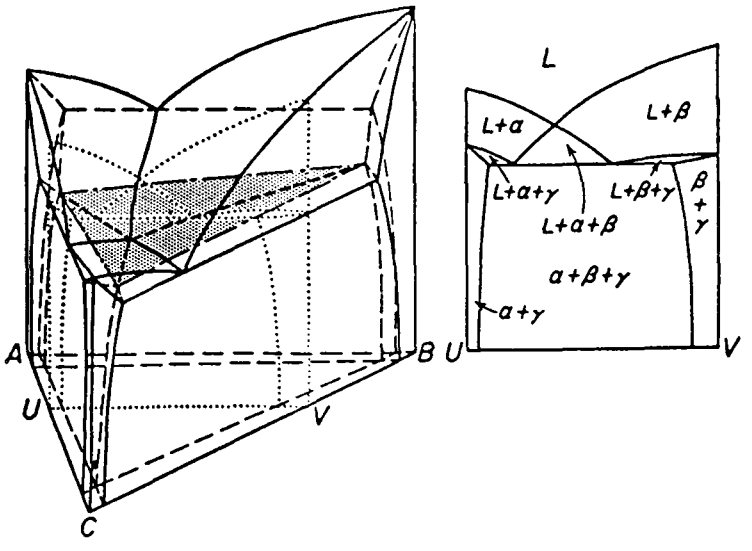

Fig 2.23:- Vertical sectioning through a ternary eutectic system representing the constant composition of one component (25).

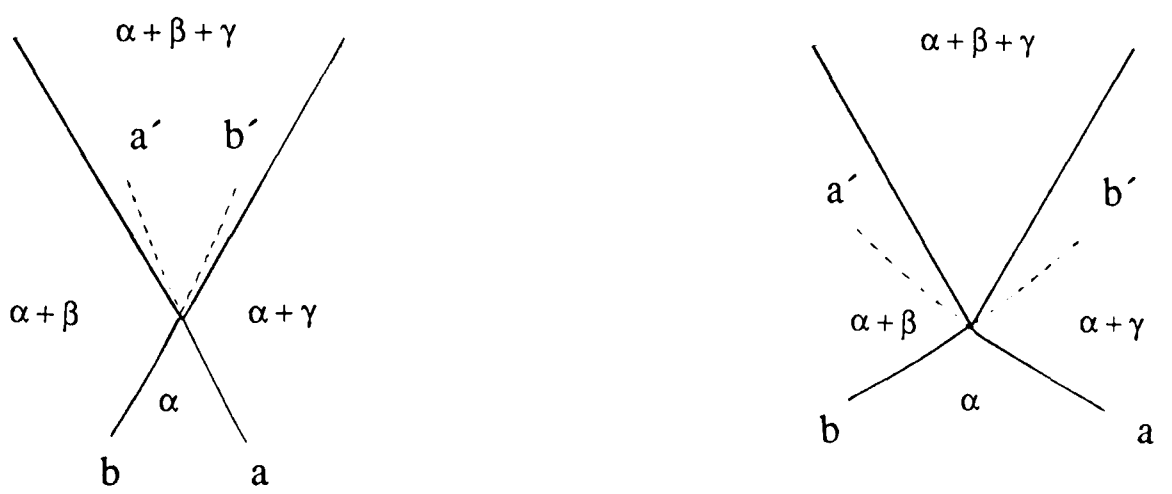

Fig 2.24:- Disposition of phase boundaries in isothermal sections of ternary systems containing three-phase region.

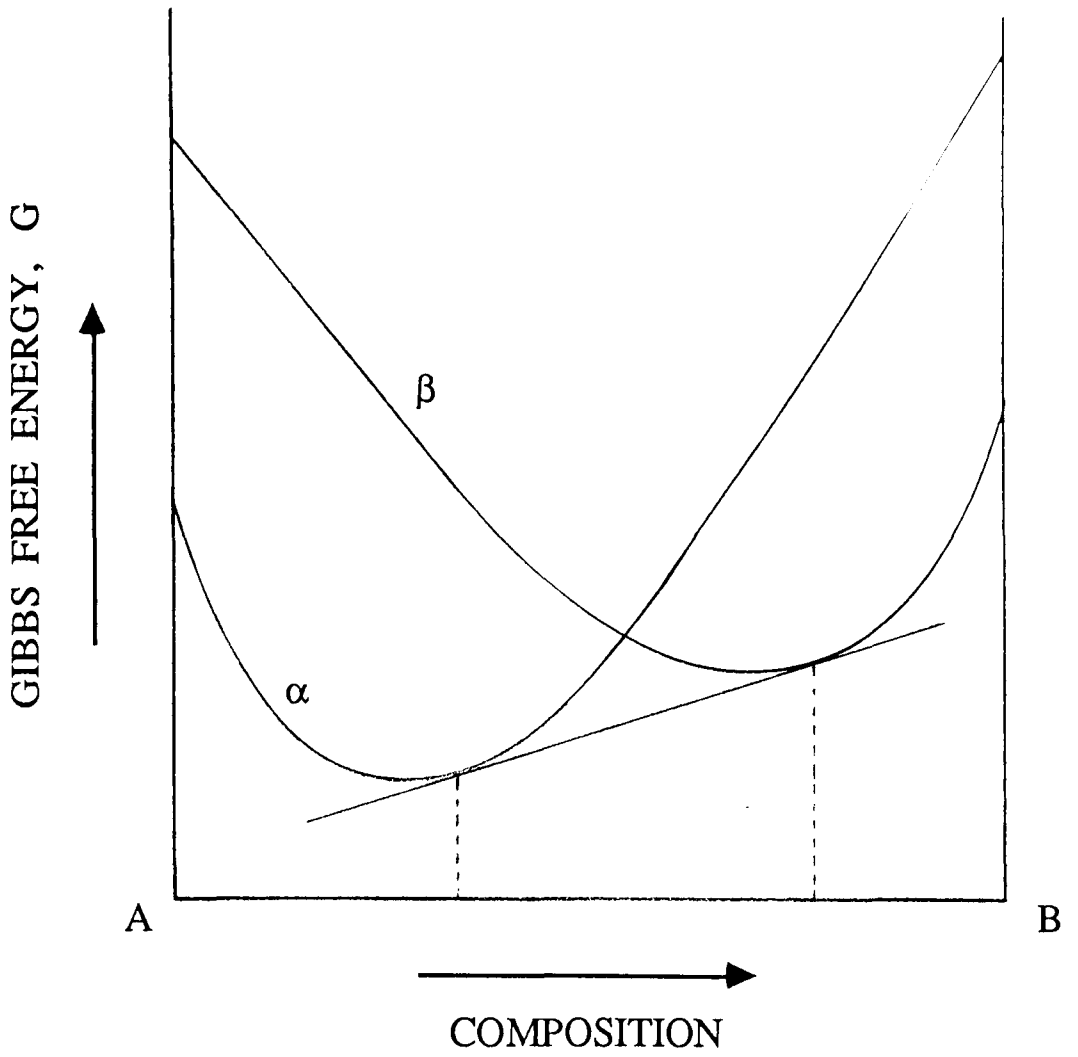

Fig 3.1:- Occurrence of two-phase equilibrium when two phases intersect.

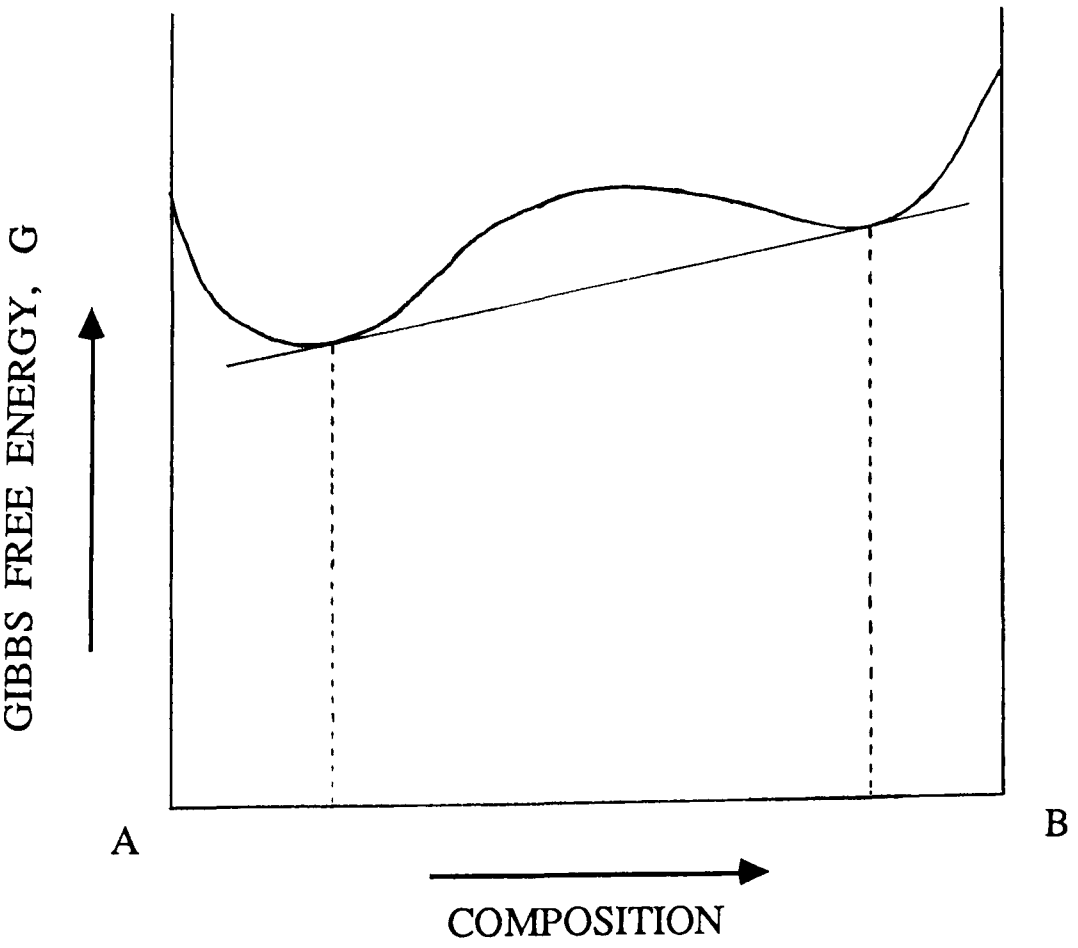

Fig 3.2:- Occurrence of two-phase equilibrium in a single phase showing two minima.

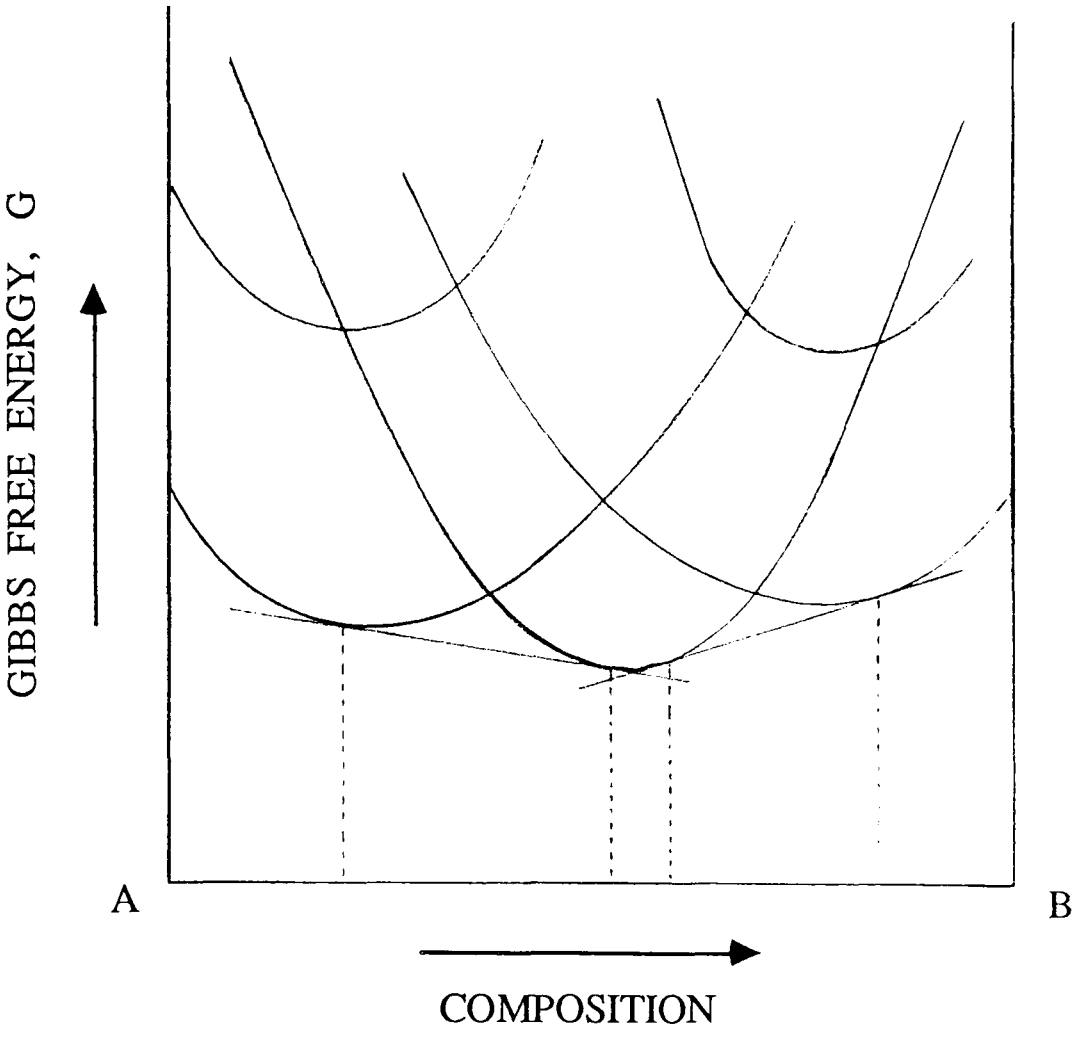

Fig 3.3:- Most stable combination of two-phase equilibria with lowest Gibbs free energy.

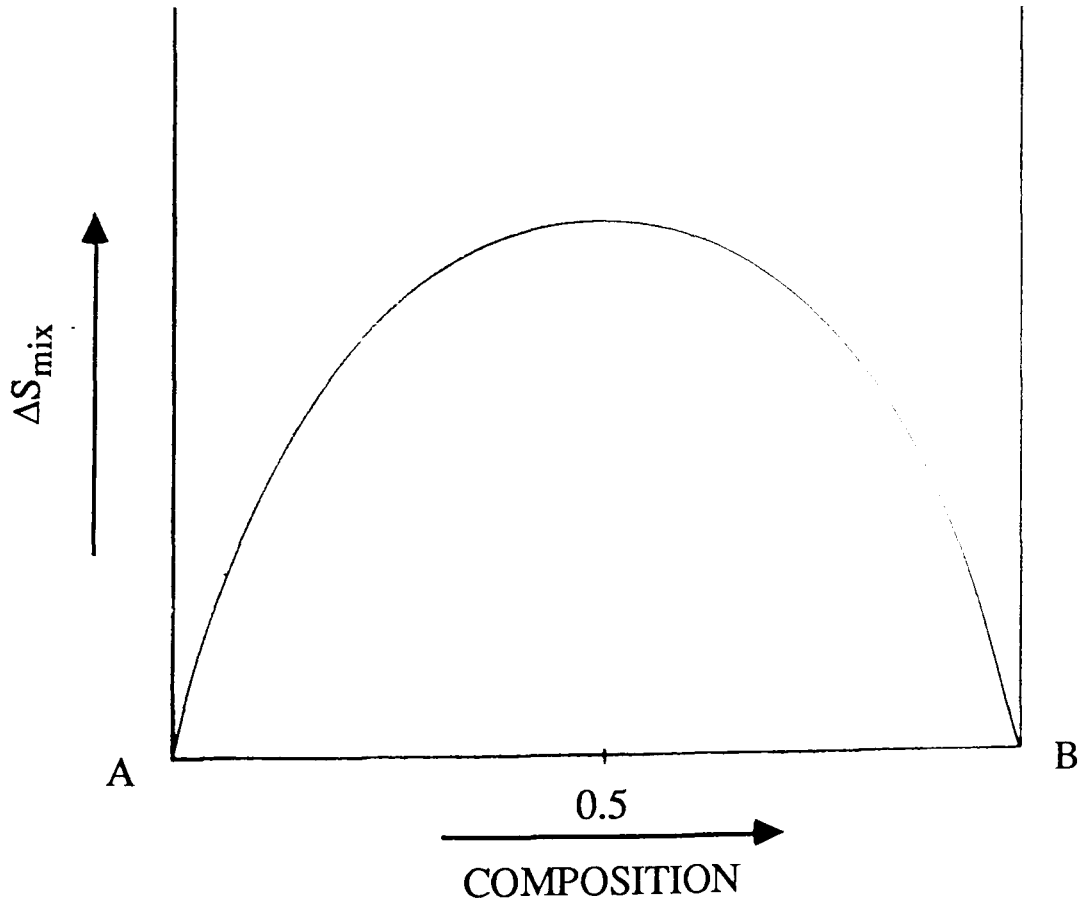

Fig 3.4:- Variation of Entropy of mixing with composition.

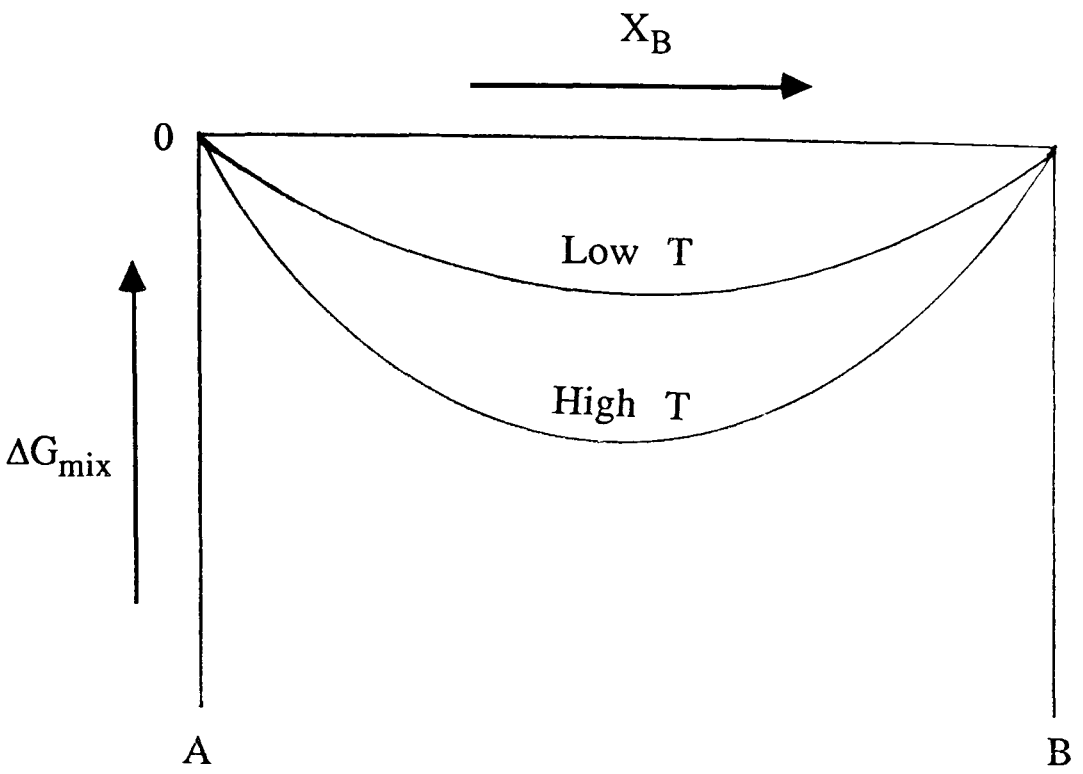

Fig 3.5:- Free energy of mixing of an ideal solution.

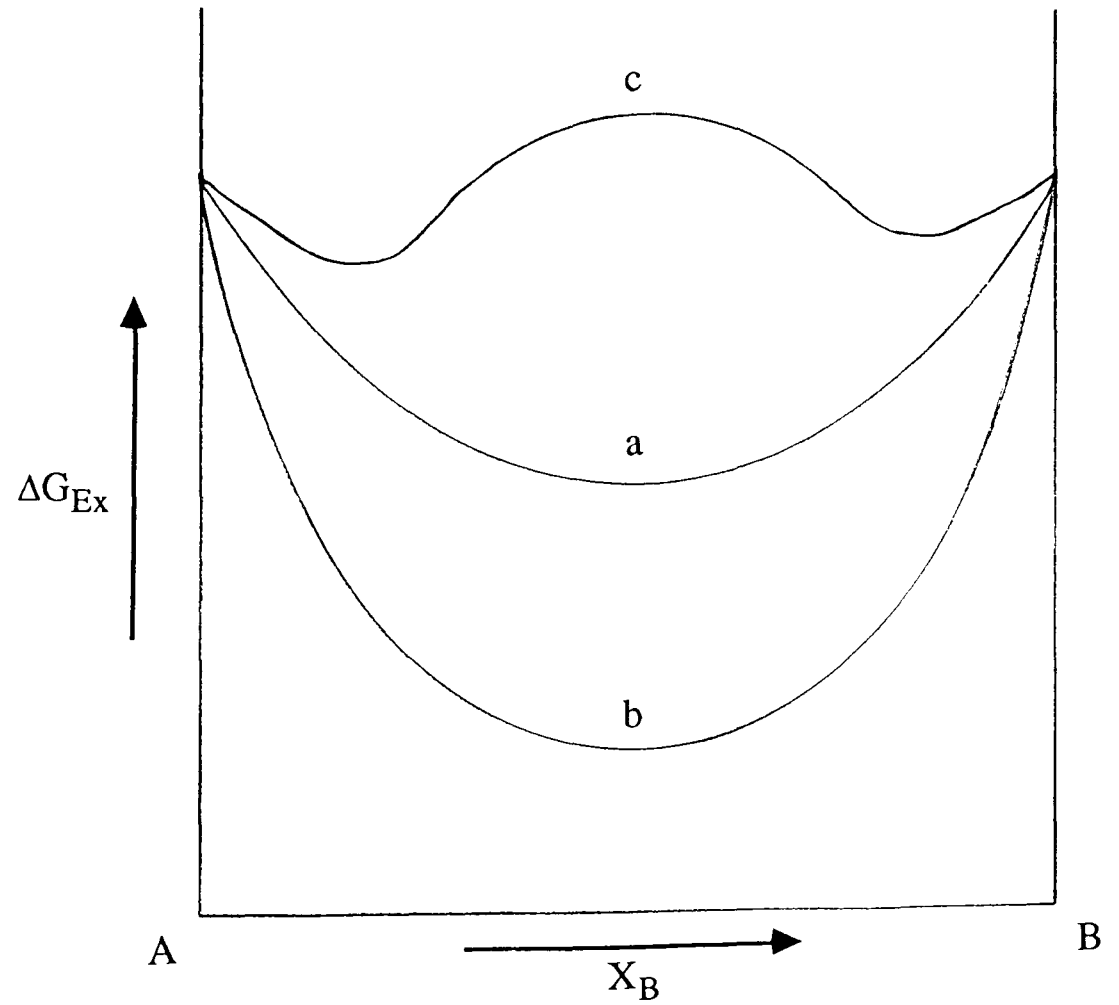

Fig 3.6:- Gibbs energies of formation, curves showing:

(a) Ideal solution, when $\Omega = 0$

(b) Negative Gibbs energy, when Ω = –ve (formation of a compound)

(c) Positive Gibbs energy, when Ω = +ve (showing two minima leading to immiscibility)

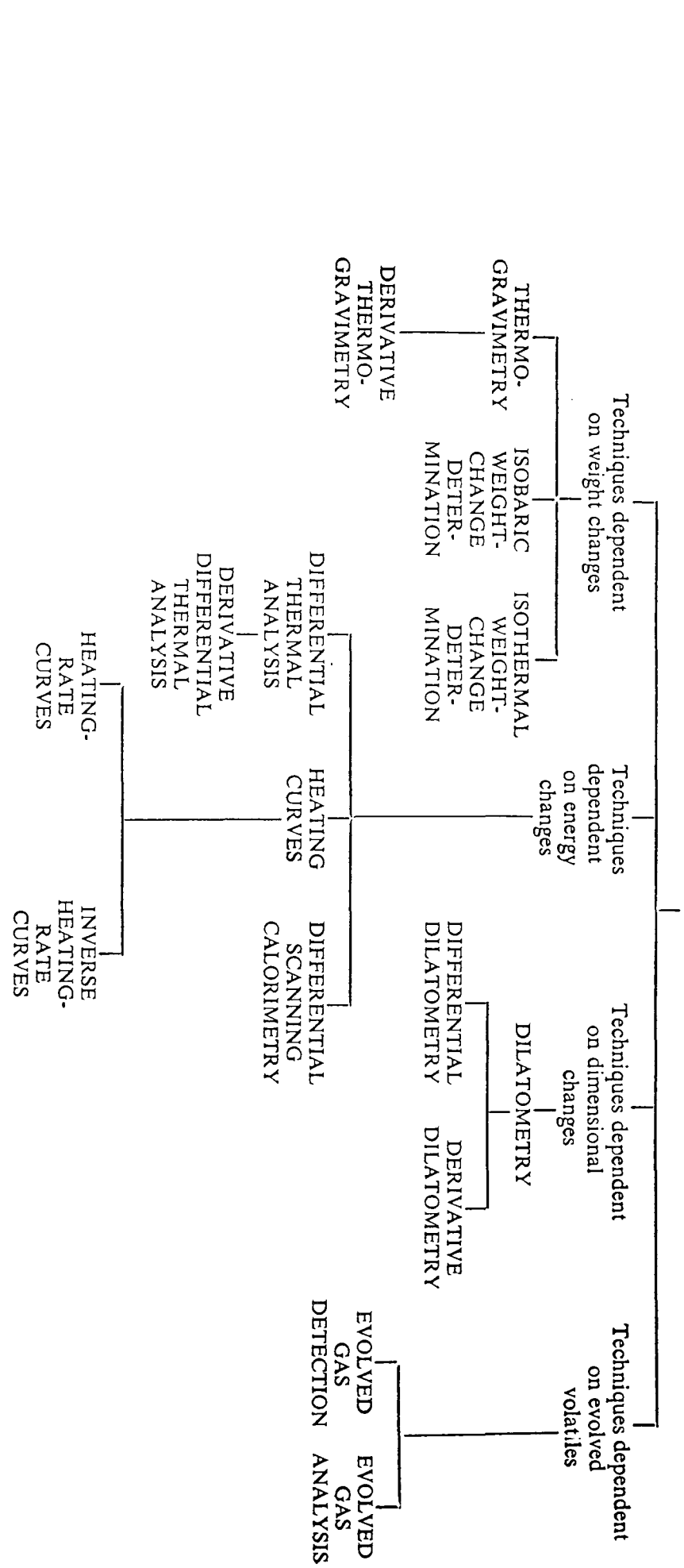

Fig 4.1:- Principle techniques of thermal analysis (After Mackenzie).

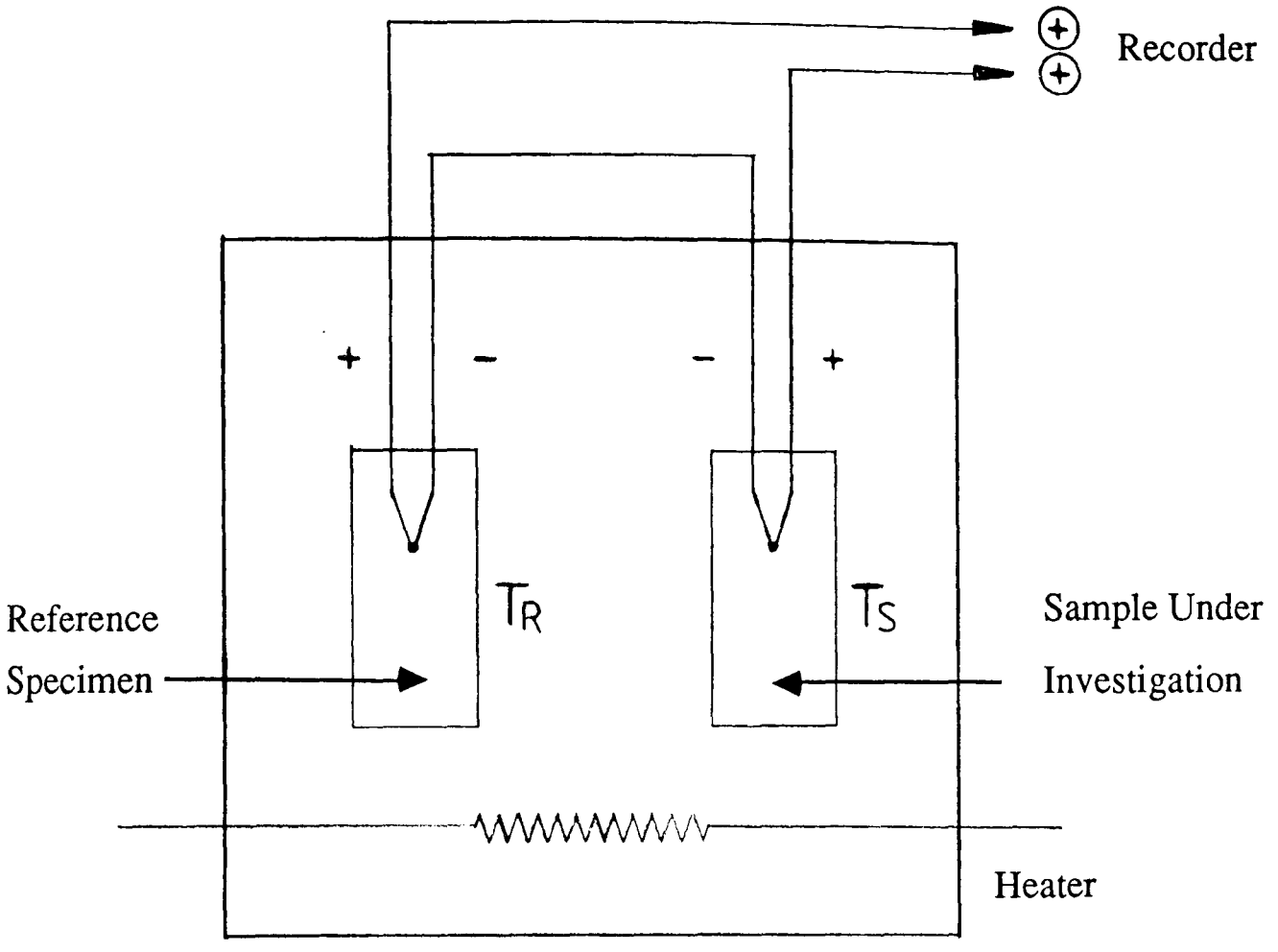

Fig 4.2:- DTA thermocouples arrangement.

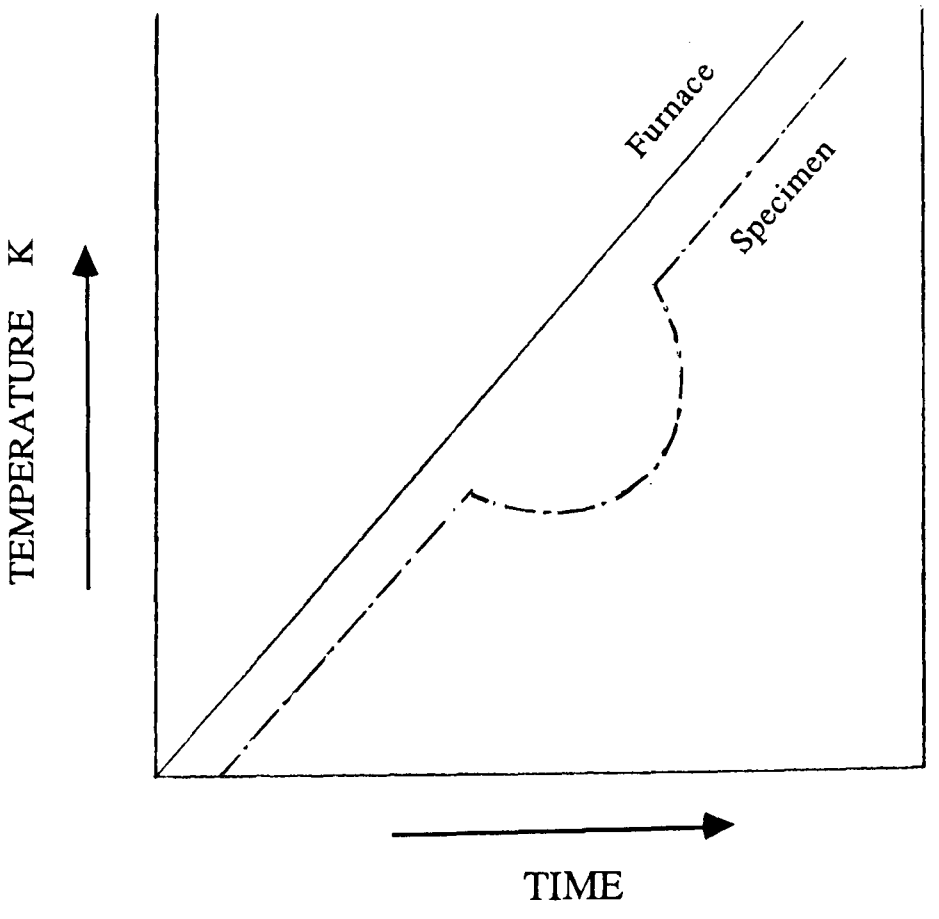

Fig 4.3:- DTA time/temperature curve shows that the furnace temperature is independent of specimen temperature.

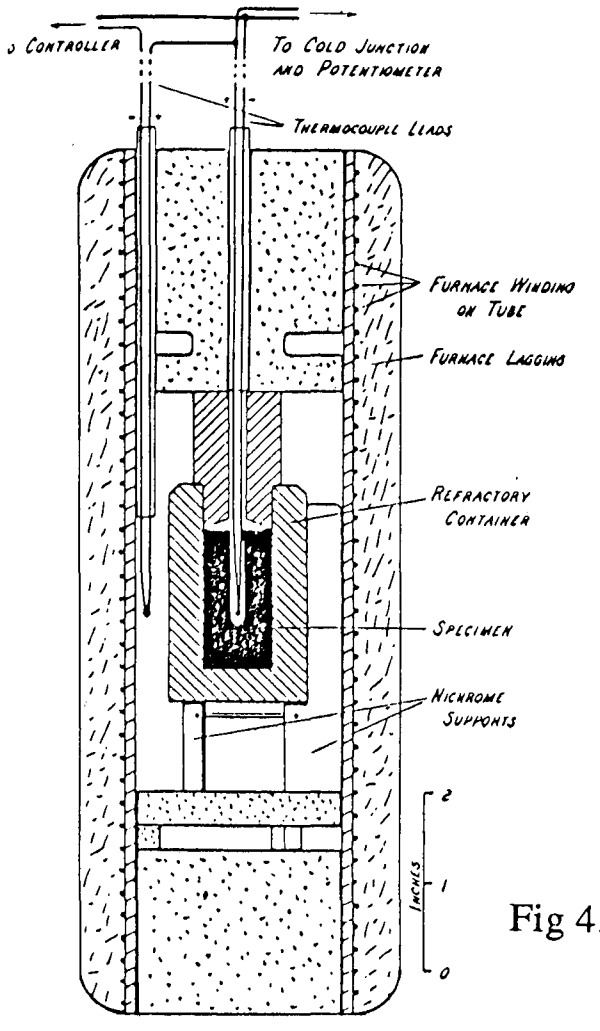

Fig 4.4

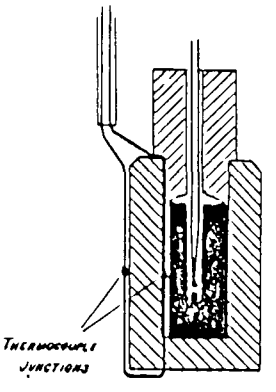

Fig 4.5

Fig 4.4:- Thermocouple arrangement in Smith Thermal Analysis. (After Smith).

Fig 4.5:- Arrangement of Differential couple for controlling temperature gradient across container thermocouple. (After Smith).

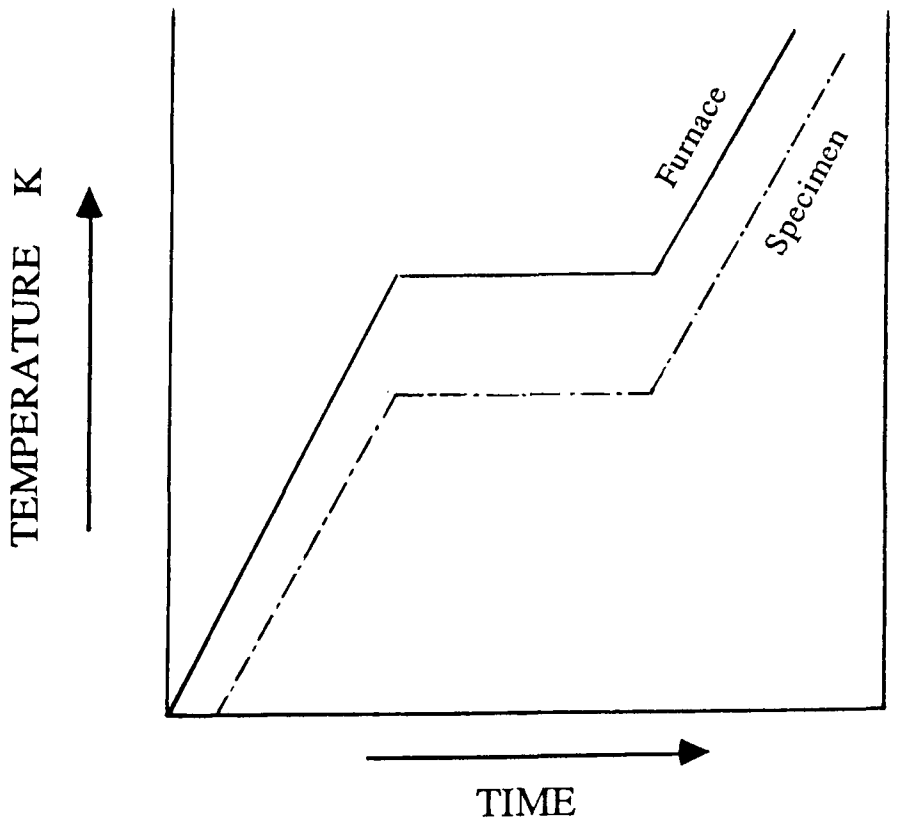

Fig 4.6:- STA time/temperature curve shows that the furnace temperature is governed by specimen temperature.

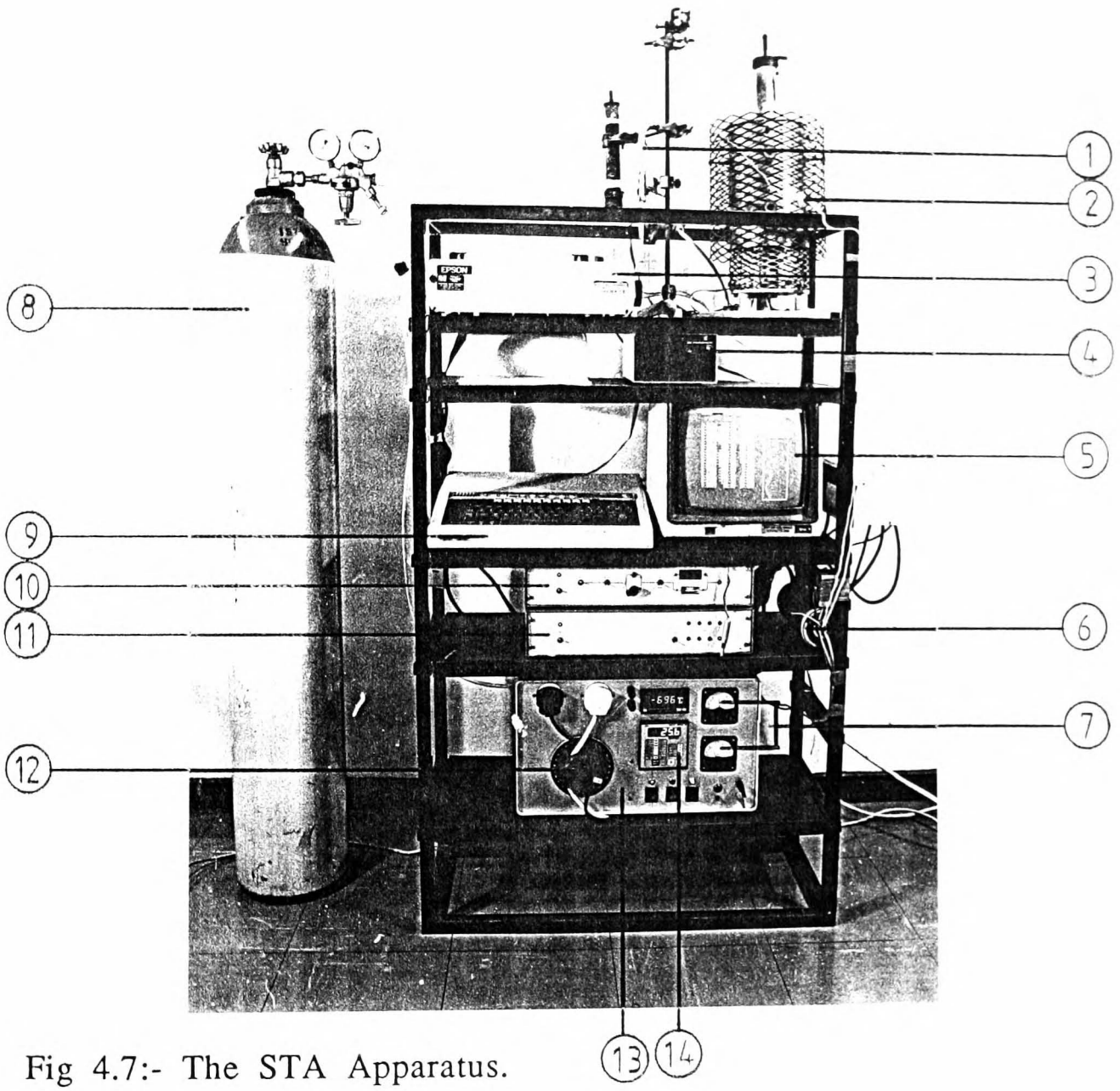

Fig 4.7:- The STA Apparatus.

1. Rota Meter
2. STA Furnace
3. Printer
4. Disc Drive
5. VDU Screen
6. Cold Junction Box/Furnace
7. Volt and Am. Meters
8. Gas Cylinder
9. Key Board
10. Temperature Controller
11. Amplifier
12. Variac
13. Cold Junction Thermostat
14. Saftey Box

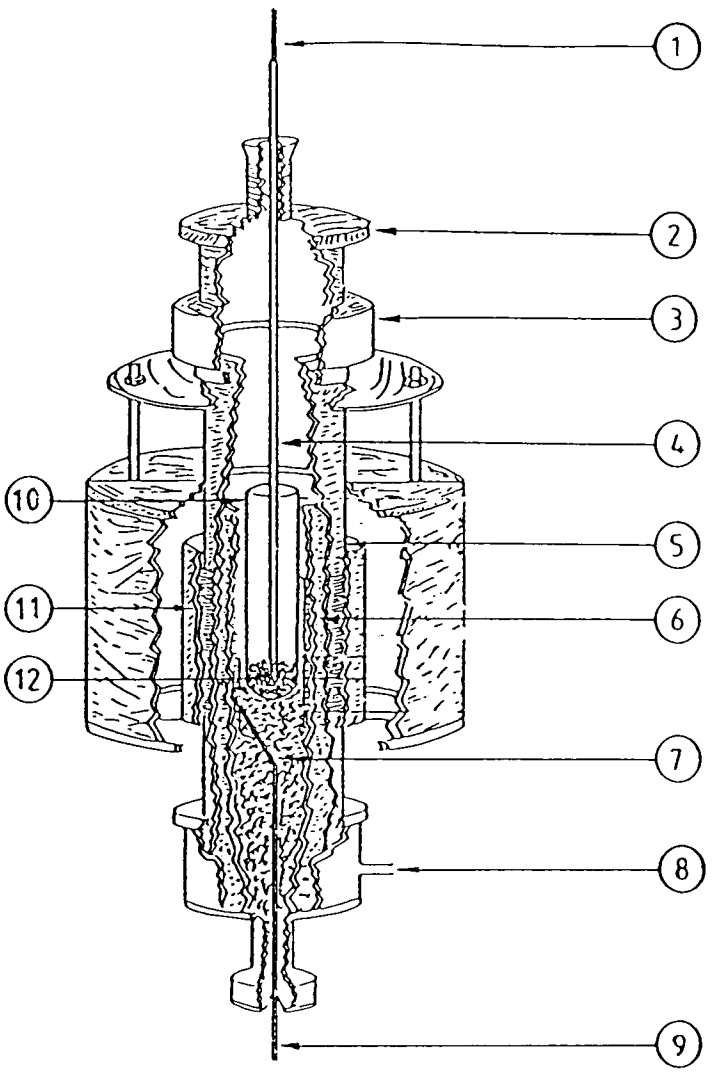

Fig 4.8 Sectioning view of STA furnace.

1. Specimen Thermocouple
2. Top End Cap
3. Water Jacket
4. Silica Thermocouple Sheath
5. Furnace Tube
6. Inner Tube
7. Ceramic Wool
8. Gas Inlet
9. Furnace Thermocouple
10. Silica Crucible
11. Cement Coating Over Resistance Winding
12. Specimen Under Investigation

02SC PURE In 15-1-90

T mV	Prdtn	Slope
5.5743	1.38	-1.759
5.5558	0.57	-1.780
5.5381	-0.09	-1.794
5.5182	0.03	-1.806
5.4993	-0.39	-1.817
5.4808	-1.33	-1.830
5.4613	-1.99	-1.851
5.4440	-3.05	-1.861
5.4249	-3.50	-1.869
5.4060	-3.91	-1.873
5.3879	-4.59	-1.871
5.3698	-4.99	-1.865
5.3524	-5.65	-1.847
5.3337	-5.95	-1.838
5.3165	-6.69	-1.826
5.2985	-7.57	-1.814
5.2797	-7.83	-1.813
5.2611	-8.15	-1.809
5.2434	-8.52	-1.807
5.2253	-8.59	-1.809
5.2072	-8.50	-1.812
5.1906	-8.30	-1.807
5.1733	-8.25	-1.795
5.1552	-7.84	-1.789
5.1379	-7.62	-1.777
5.1207	-7.83	-1.762
5.1043	-8.16	-1.746
5.0862	-8.09	-1.740
5.0816	-11.55	-1.665
5.0812	-16.05	-1.517
5.0799	-20.03	-1.322
5.0791	-23.84	-1.087
5.0765	-27.45	-0.847
5.0737	-30.73	-0.626
5.0722	-34.25	-0.429
5.0713	-37.82	-0.273
5.0707	-41.81	-0.168
5.0695	-42.75	-0.151
5.0676	-40.32	-0.154
5.0643	-35.37	-0.161
5.0630	-29.04	-0.163
5.0609	-21.94	-0.161
5.0596	-15.35	-0.162
5.0587	-9.39	-0.167
5.0563	-4.15	-0.176
5.0561	-1.03	-0.173
5.0541	-0.28	-0.166
5.0525	-0.34	-0.156
5.0521	-0.93	-0.140
5.0513	-1.22	-0.131
5.0494	-1.16	-0.126
5.0487	-1.46	-0.122
5.0481	-1.83	-0.115
5.0466	-2.21	-0.109
5.0445	-1.96	-0.115
5.0432	-1.78	-0.116
5.0412	-1.31	-0.125
5.0169	4.98	-0.262
4.9668	17.49	-0.632
4.9203	28.98	-1.157
4.8788	39.21	-1.763
4.8420	48.37	-2.367
4.8087	56.61	-2.905
4.7753	64.42	-3.346
4.7448	71.72	-3.638
4.7167	78.07	-3.729
4.6891	78.93	-3.589
4.6634	69.38	-3.324
4.6385	52.60	-3.100
4.6158	31.33	-2.912
4.5918	9.50	-2.762
4.5707	-11.40	-2.626
4.5496	-29.44	-2.497
4.5295	-42.87	-2.386
4.5102	-49.63	-2.286
4.4907	-48.27	-2.195
4.4720	-42.49	-2.117
4.4551	-38.06	-2.039
4.4394	-34.72	-1.960
4.4212	-31.72	-1.891
4.4050	-29.33	-1.834
4.3886	-26.89	-1.780
4.3733	-25.06	-1.729
4.3596	-23.75	-1.674
4.3444	-22.19	-1.624
4.3299	-21.05	-1.583
4.3163	-19.95	-1.546
4.3017	-18.32	-1.512
4.2881	-17.18	-1.471
4.2744	-16.27	-1.443
4.2616	-15.60	-1.416

END

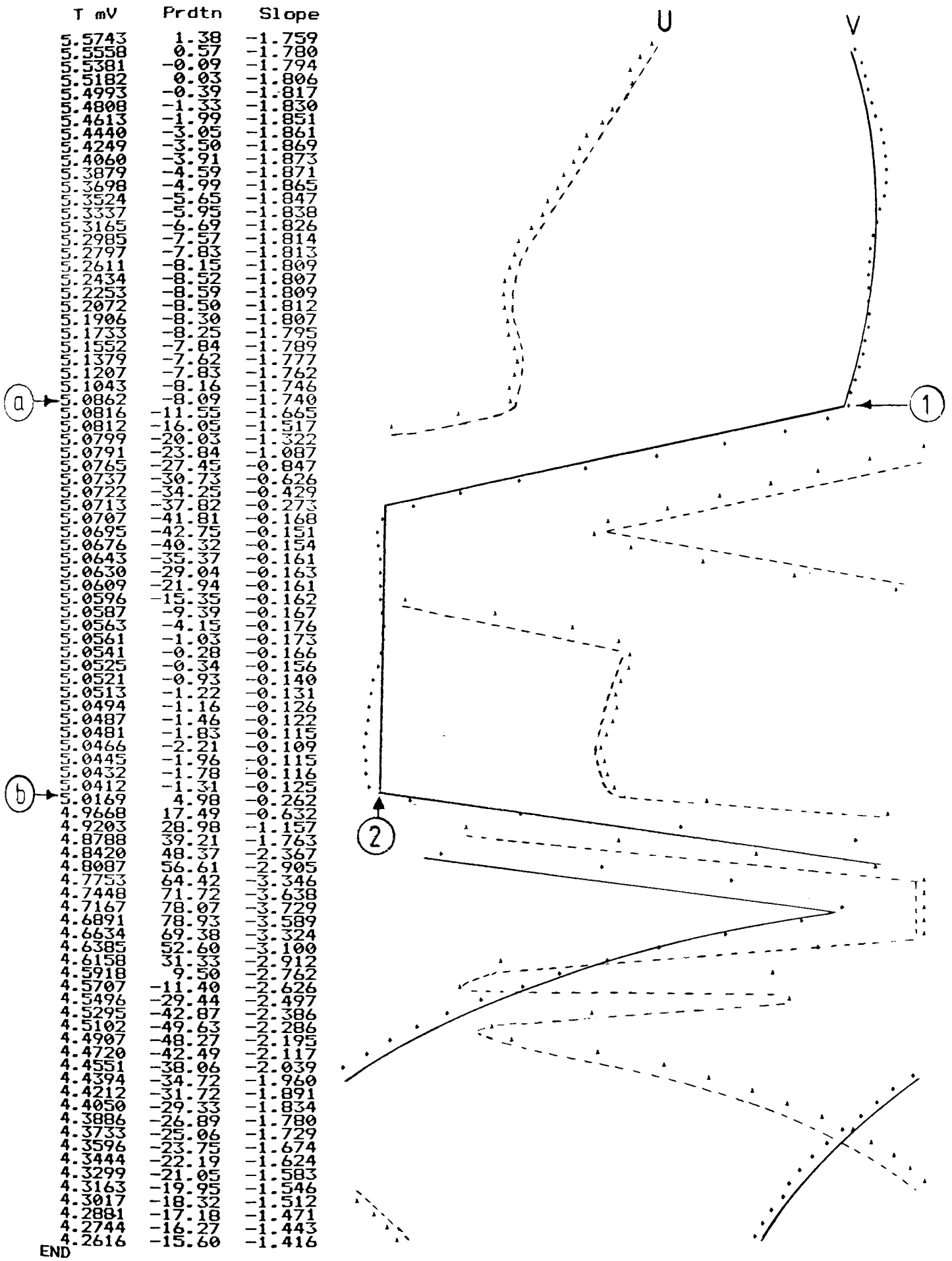

Fig 5.1:- Cooling curve of pure Indium.

01SH PURE In 15-1-90

T mV	Prdtn	Slope
4.5439	-10.72	1.926
4.5631	-10.61	1.920
4.5820	-10.74	1.907
4.5987	-10.92	1.890
4.6181	-10.46	1.876
4.6352	-10.66	1.861
4.6525	-10.78	1.844
4.6711	-10.14	1.835
4.6877	-10.24	1.809
4.7065	-10.06	1.794
4.7241	-10.24	1.783
4.7424	-10.00	1.782
4.7589	-9.93	1.779
4.7765	-9.75	1.769
4.7941	-9.43	1.769
4.8114	-9.08	1.764
4.8278	-9.21	1.750
4.8451	-8.48	1.742
4.8620	-8.24	1.726
4.8787	-8.17	1.716
4.8964	-8.18	1.710
4.9117	-8.68	1.701
4.9276	-8.77	1.684
4.9439	-9.08	1.667
4.9589	-9.55	1.648
4.9748	-9.45	1.631
4.9904	-9.58	1.610
5.0049	-9.74	1.586
5.0209	-9.63	1.569
5.0369	-9.75	1.558
5.0514	-10.00	1.552
5.0661	-9.90	1.540
5.0812	-9.69	1.530
5.0951	-9.61	1.518
5.1100	-9.31	1.504
5.1202	-10.07	1.468
5.1243	-12.14	1.383
5.1274	-14.71	1.249
5.1295	-17.71	1.084
5.1303	-21.17	0.899
5.1321	-24.13	0.707
5.1339	-27.14	0.525
5.1353	-30.12	0.369
5.1369	-32.96	0.249
5.1376	-35.08	0.182
5.1396	-34.73	0.160
5.1415	-32.29	0.152
5.1430	-28.47	0.151
5.1440	-23.59	0.152
5.1462	-17.86	0.153
5.1485	-12.16	0.158
5.1496	-7.38	0.162
5.1508	-3.62	0.162
5.1532	-1.19	0.168
5.1543	-0.59	0.165
5.1552	-0.50	0.160
5.1561	-0.65	0.153
5.1570	-0.81	0.143
5.1578	-1.03	0.128
5.1606	-0.93	0.126
5.1622	-1.08	0.130
5.1625	-1.40	0.127
5.1641	-1.64	0.124
5.1655	-1.58	0.130
5.1686	-1.00	0.144
5.1707	-0.57	0.159
5.1726	-0.09	0.171
5.1764	1.11	0.190
5.2004	6.81	0.322
5.2478	18.16	0.679
5.2893	28.33	1.168
5.3280	37.76	1.716
5.3602	45.30	2.249
5.3924	52.45	2.729
5.4209	58.64	3.111
5.4485	64.67	3.351
5.4755	70.22	3.415
5.4981	69.88	3.261
5.5202	59.82	2.997
5.5421	43.79	2.780
5.5631	24.35	2.598
5.5839	4.65	2.456
5.6021	-14.49	2.317
5.6197	-30.71	2.196
5.6367	-42.42	2.082
5.6537	-48.13	1.983
5.6714	-45.94	1.912
5.6879	-39.92	1.844
5.7022	-35.60	1.772
5.7174	-31.83	1.708
5.7315	-29.34	1.648
5.7461	-26.56	1.602
5.7597	-24.29	1.556
5.7732	-22.02	1.508
5.7878	-19.78	1.469
5.7994	-19.12	1.423
5.8118	-18.24	1.386
5.8251	-16.76	1.361

END

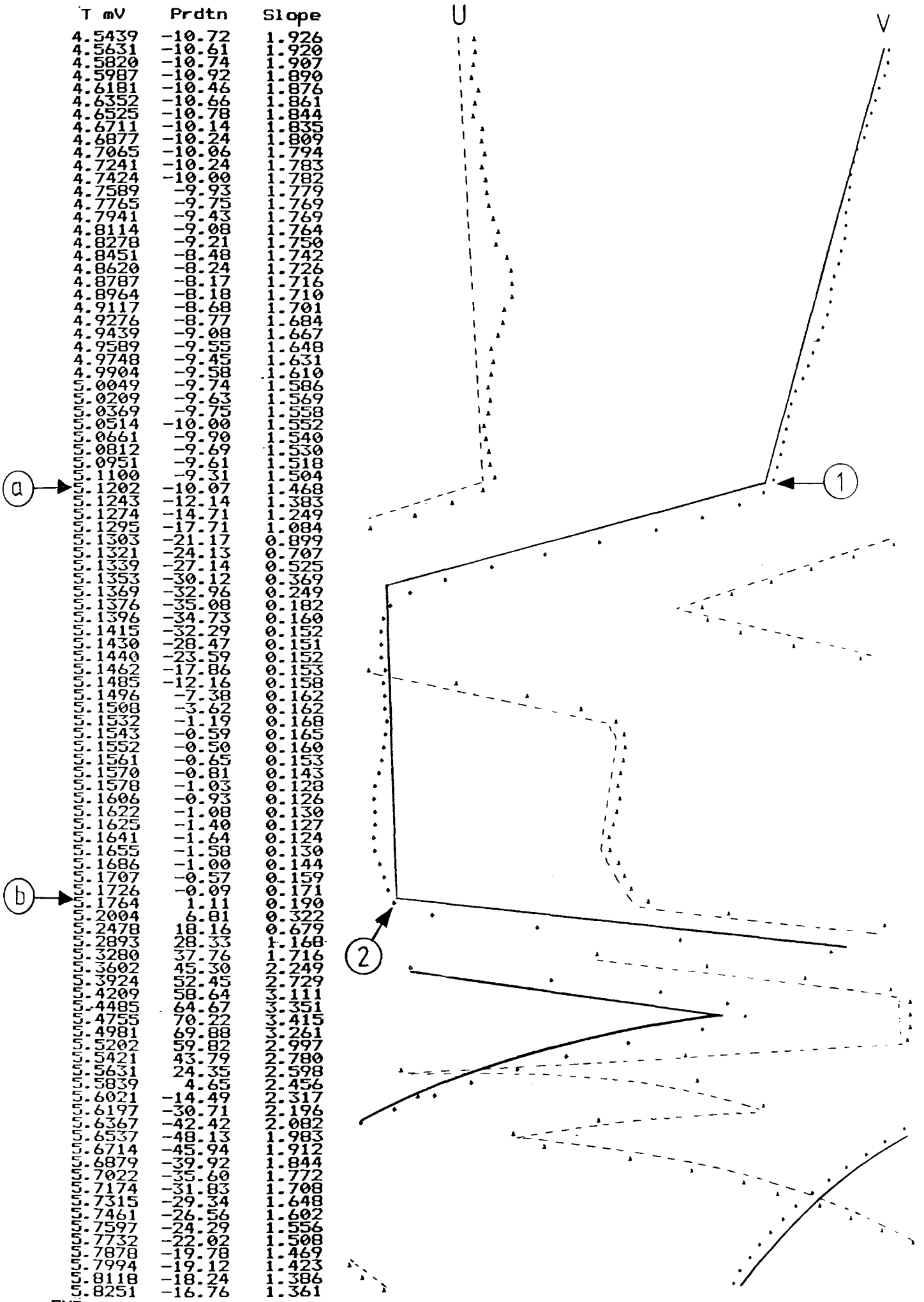

Fig 5.2:- Heating curve of pure Indium.

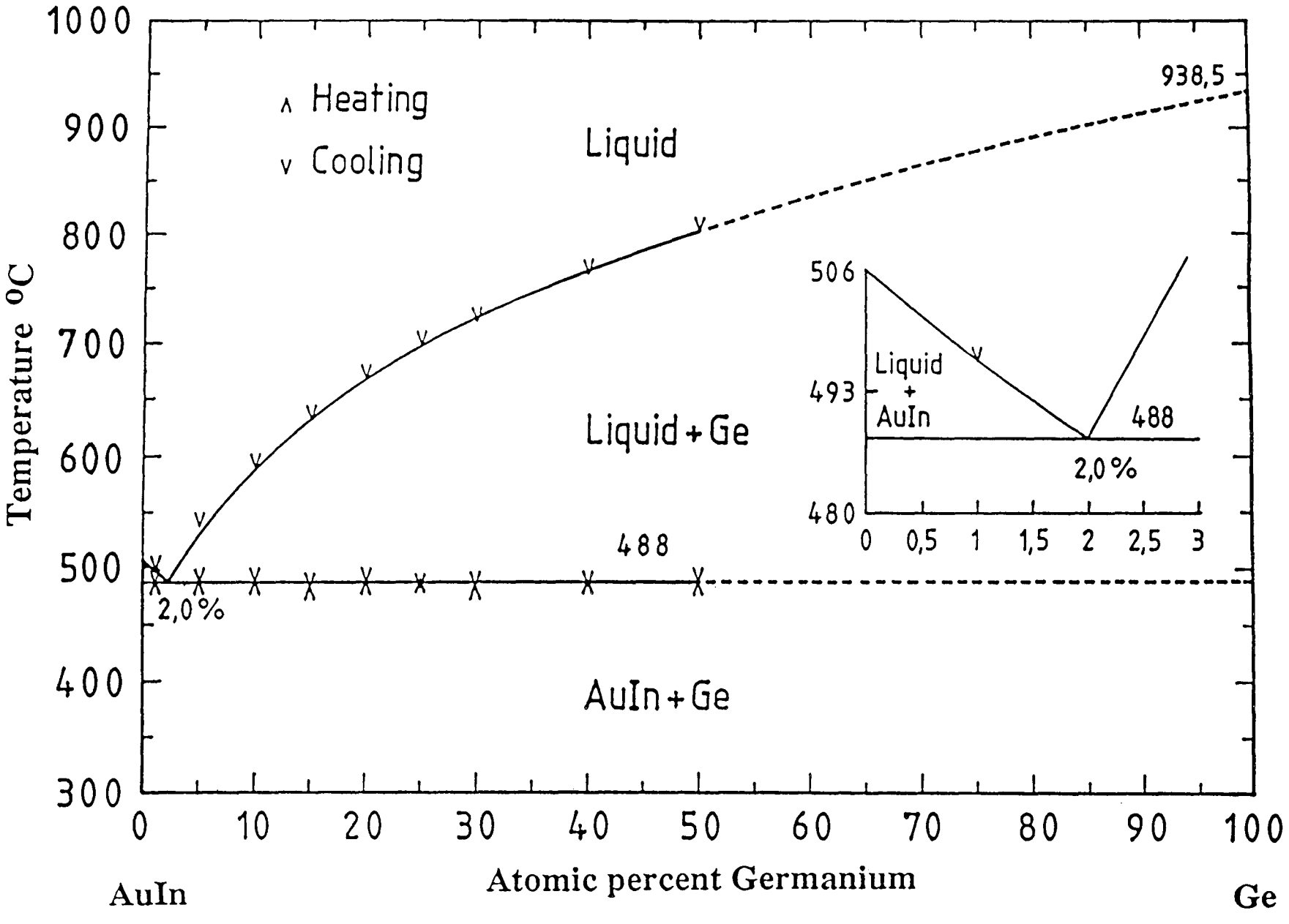

Fig 6.1:- The pseudobinary section AuIn-Ge determined by Thermal Analysis.

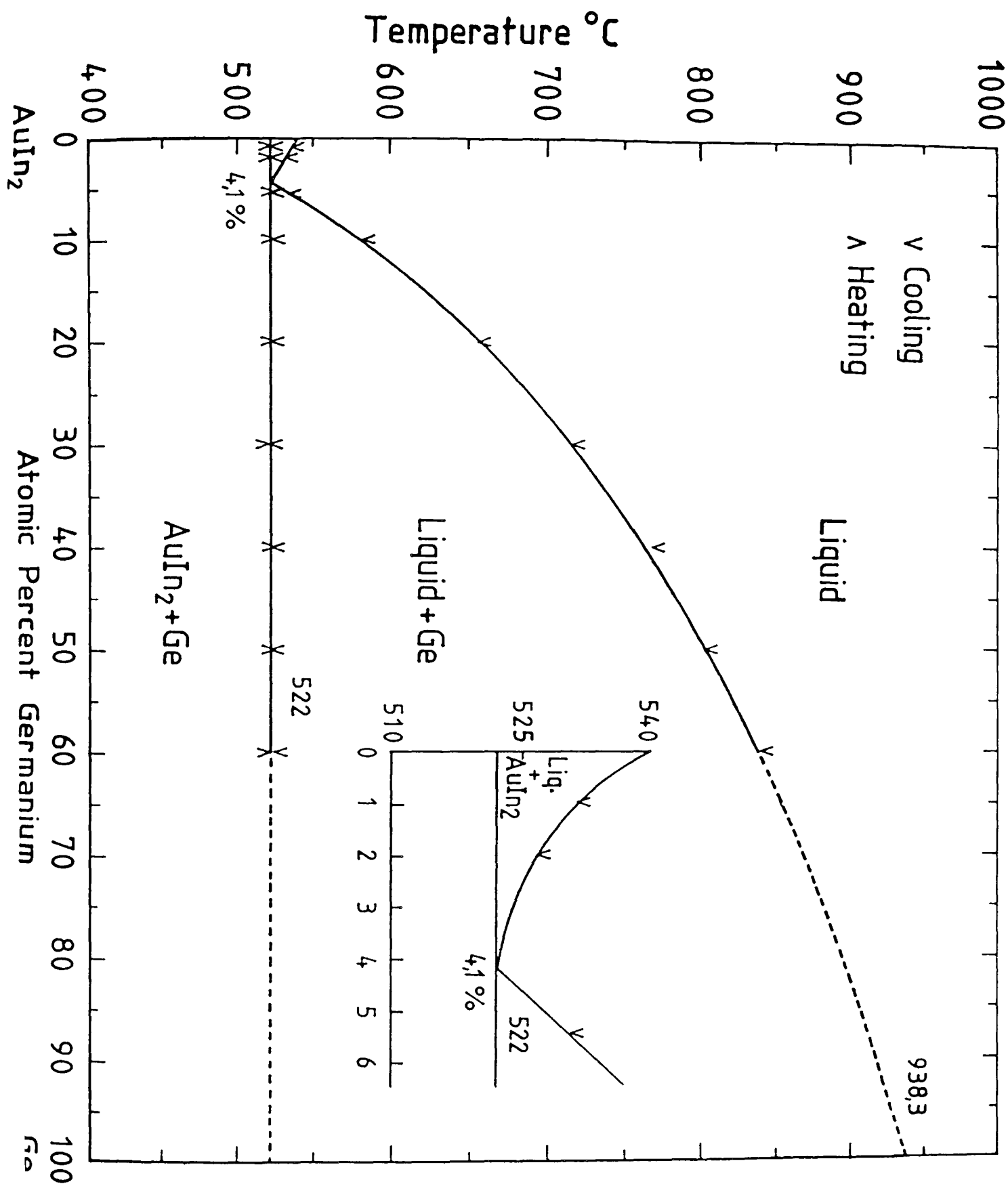

Fig 6.2:- The pseudobinary section $AuIn_2$-Ge determined by Thermal Analysis.

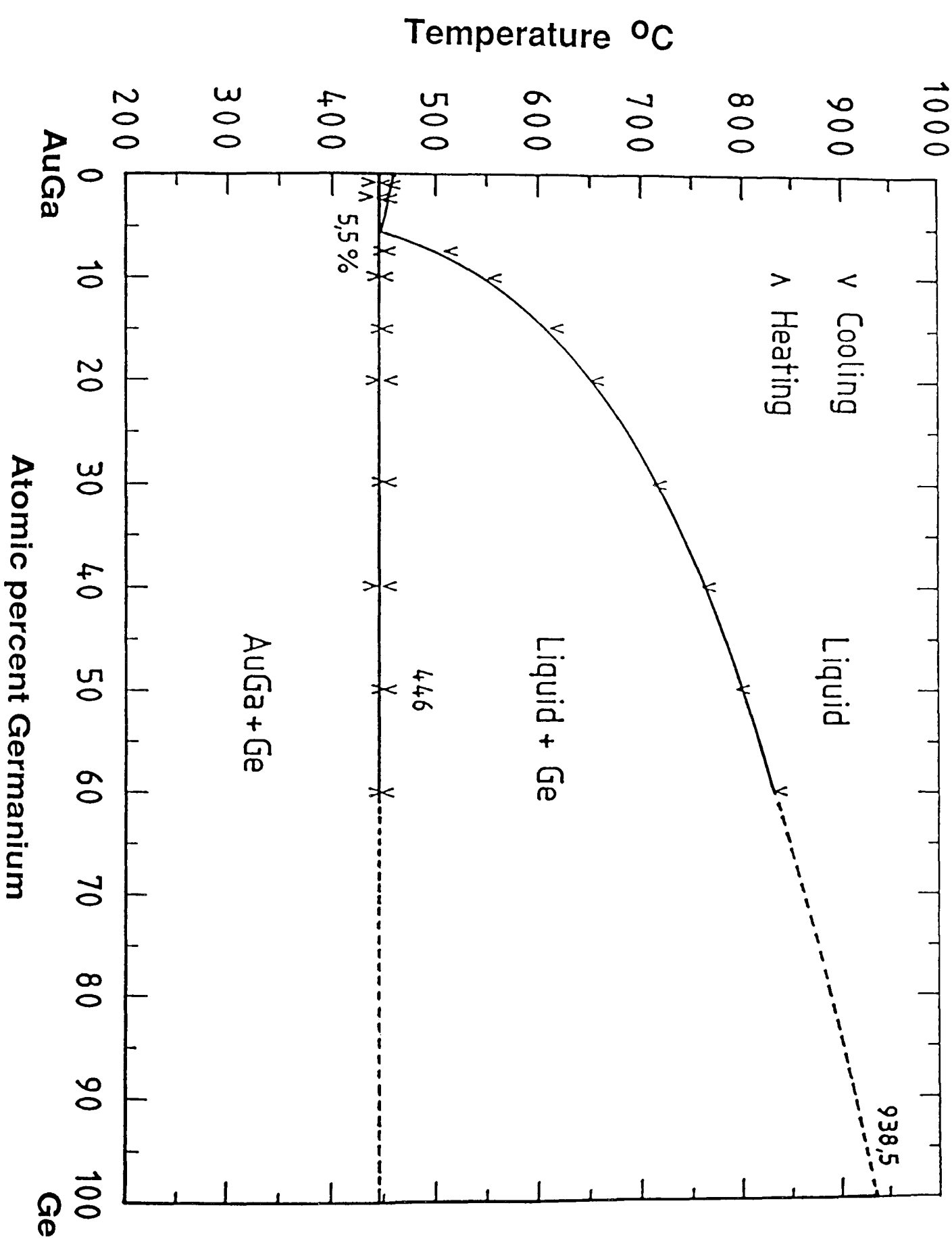

Fig 6.3:- The pseudobinary section AuGa-Ge determined by Thermal Analysis.

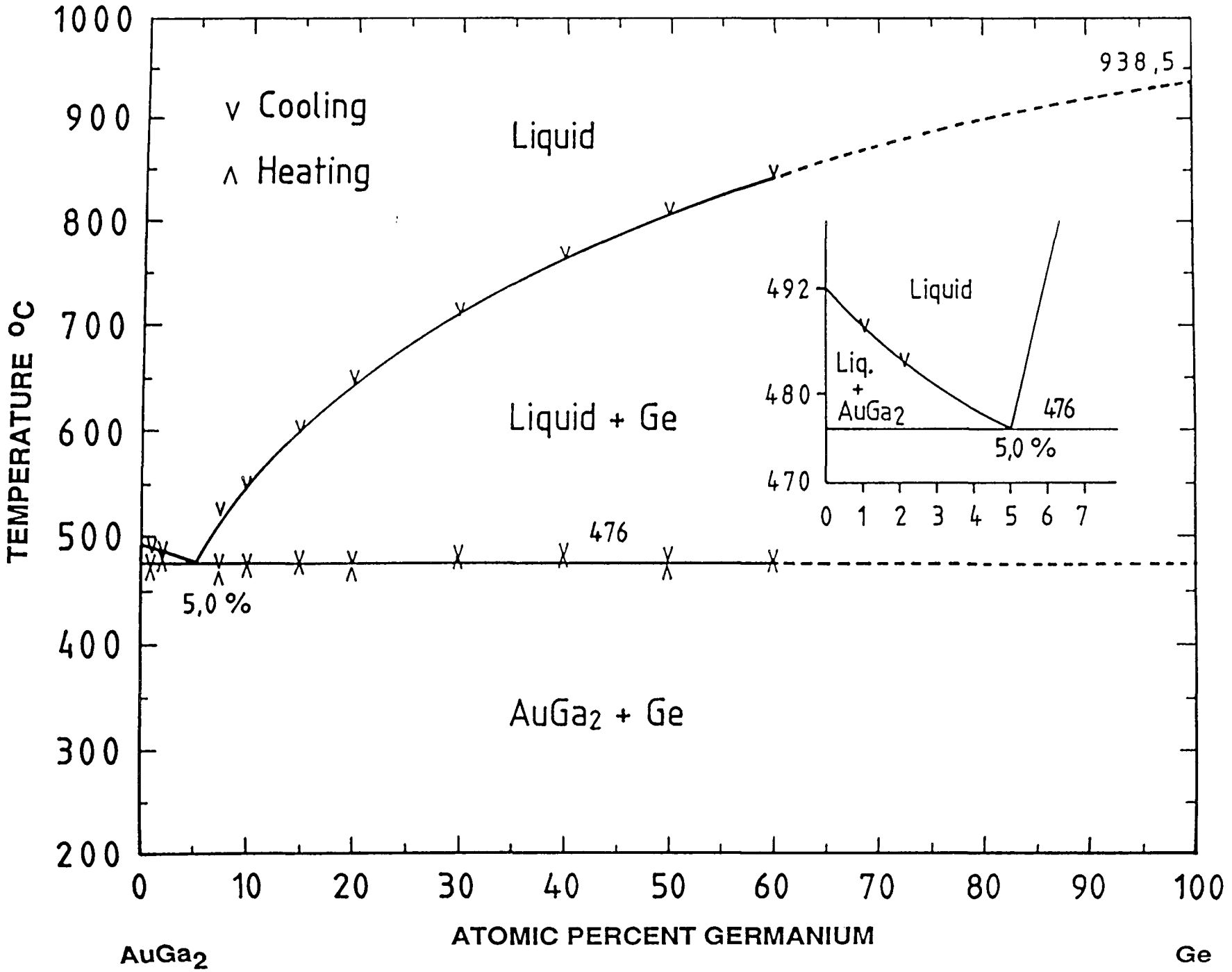

Fig 6.4:- The pseudobinary section $AuGa_2$-Ge determined by Thermal Analysis.

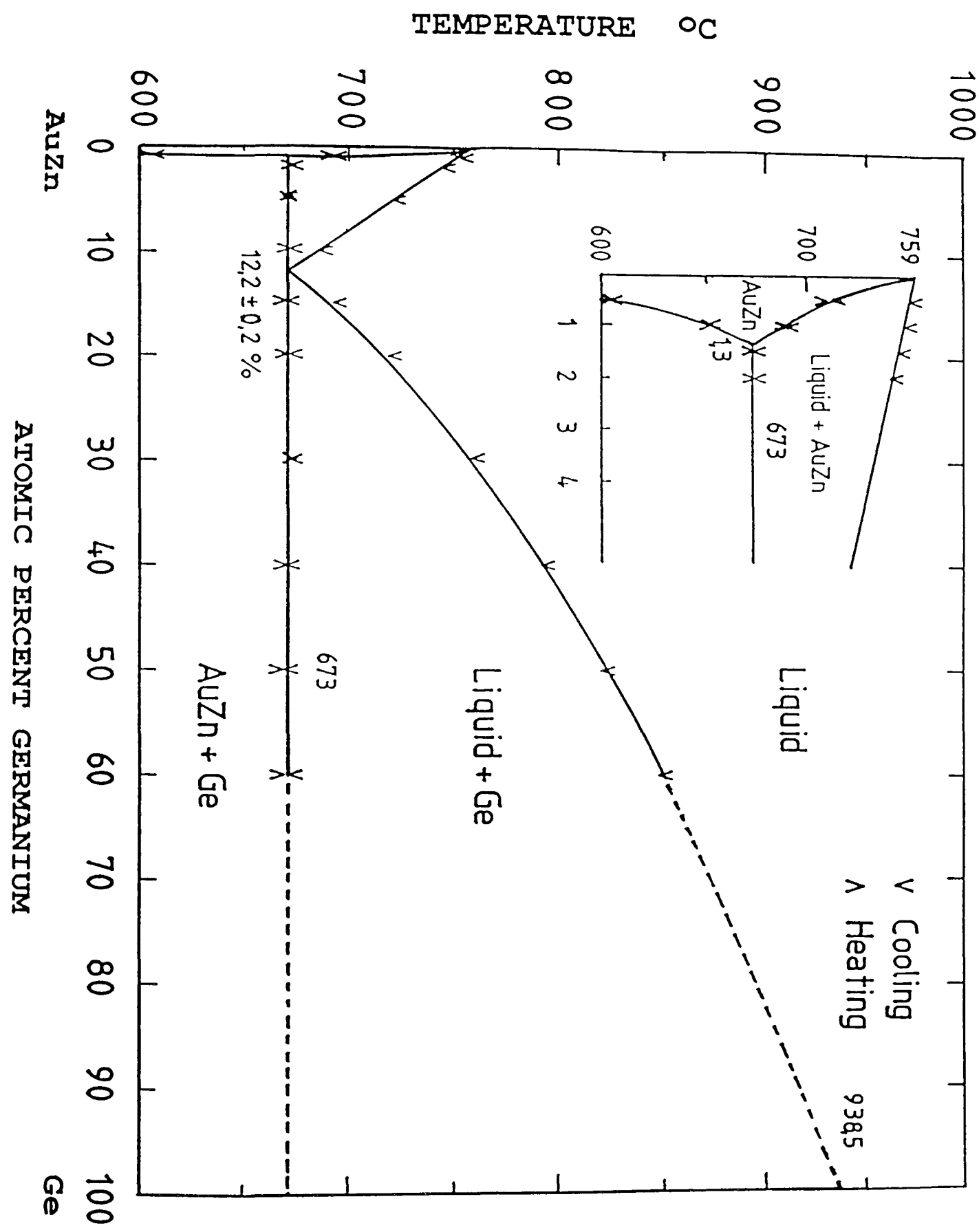

Fig 6.5:- The pseudobinary section AuZn-Ge determined by Thermal Analysis.

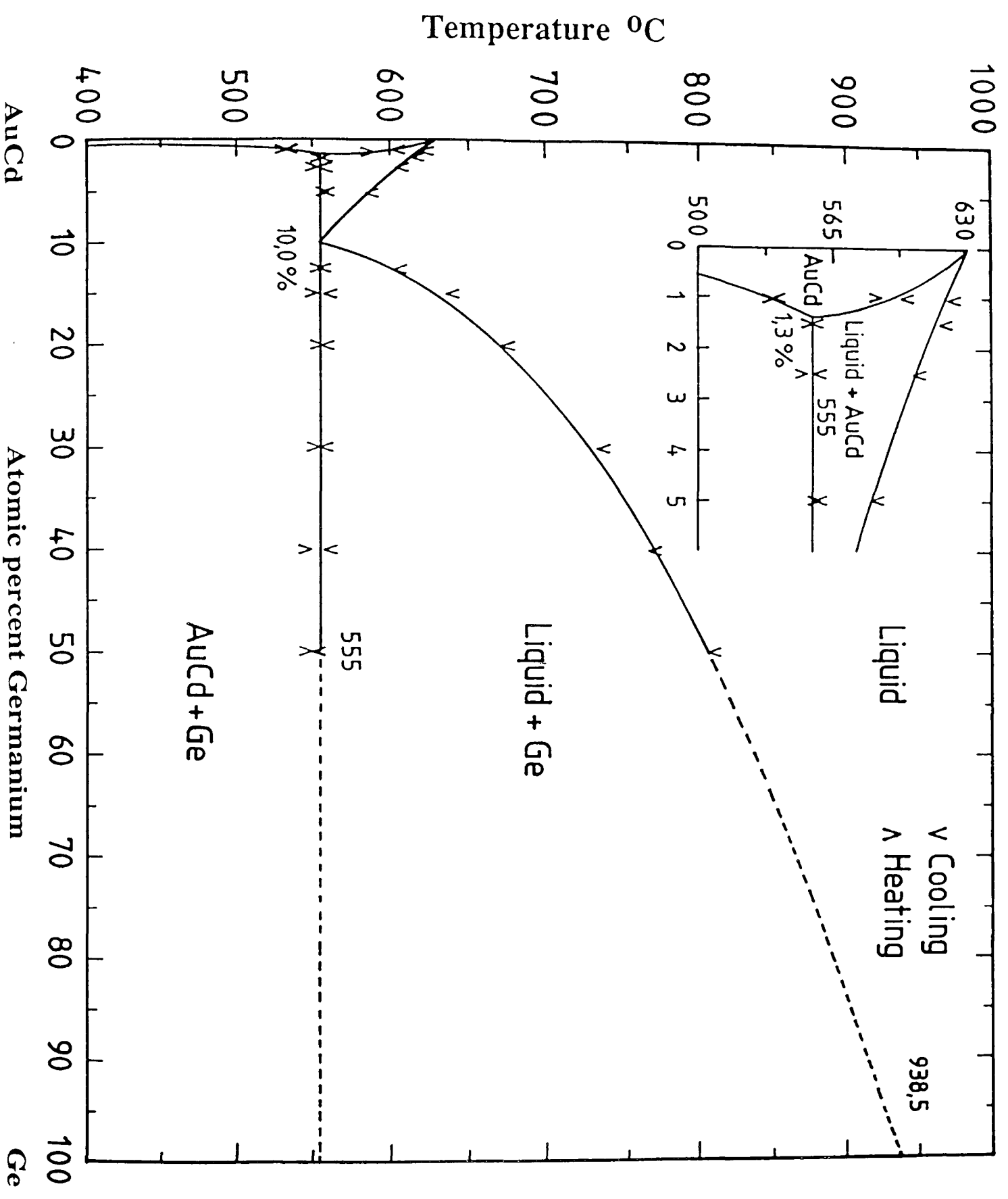

Fig 6.6:- The pseudobinary section AuCd-Ge determined by Thermal Analysis.

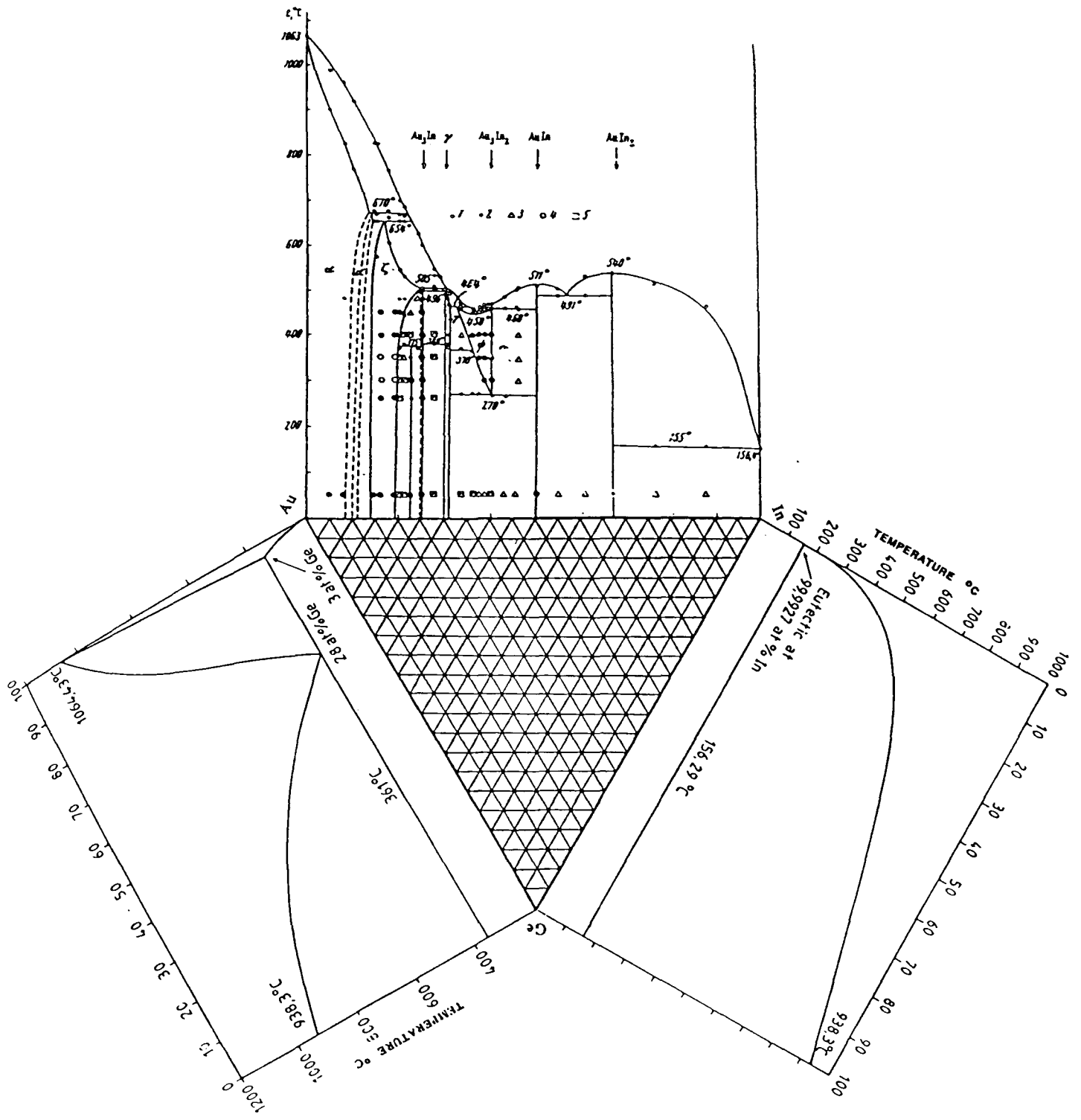

Fig 6.7:- The three edge binary phase diagrams involved in Au-Ge-In ternary system.

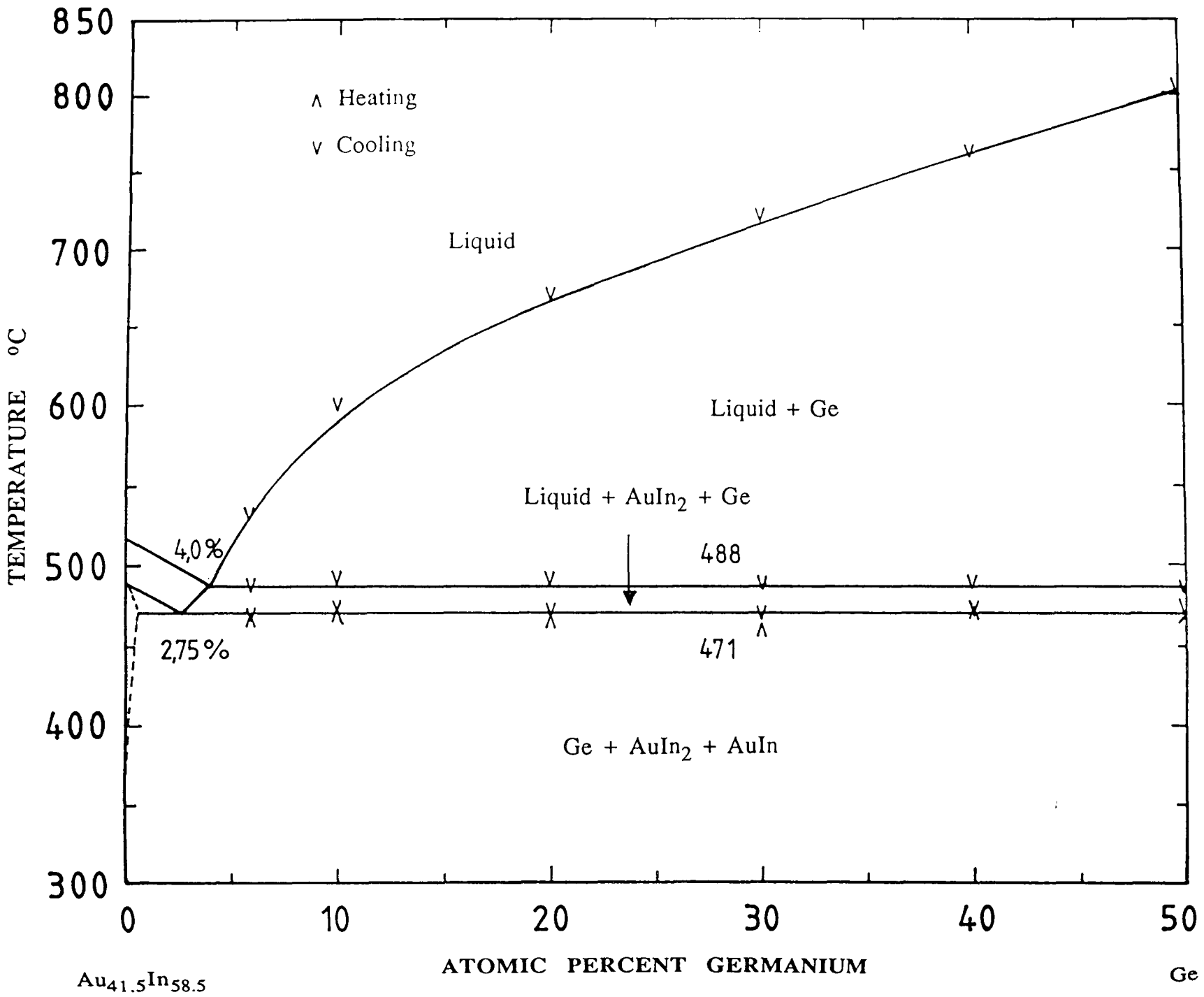

Fig 6.8(a):- Isopleth from $Au_{41.5}In_{58.5}$ to Ge.

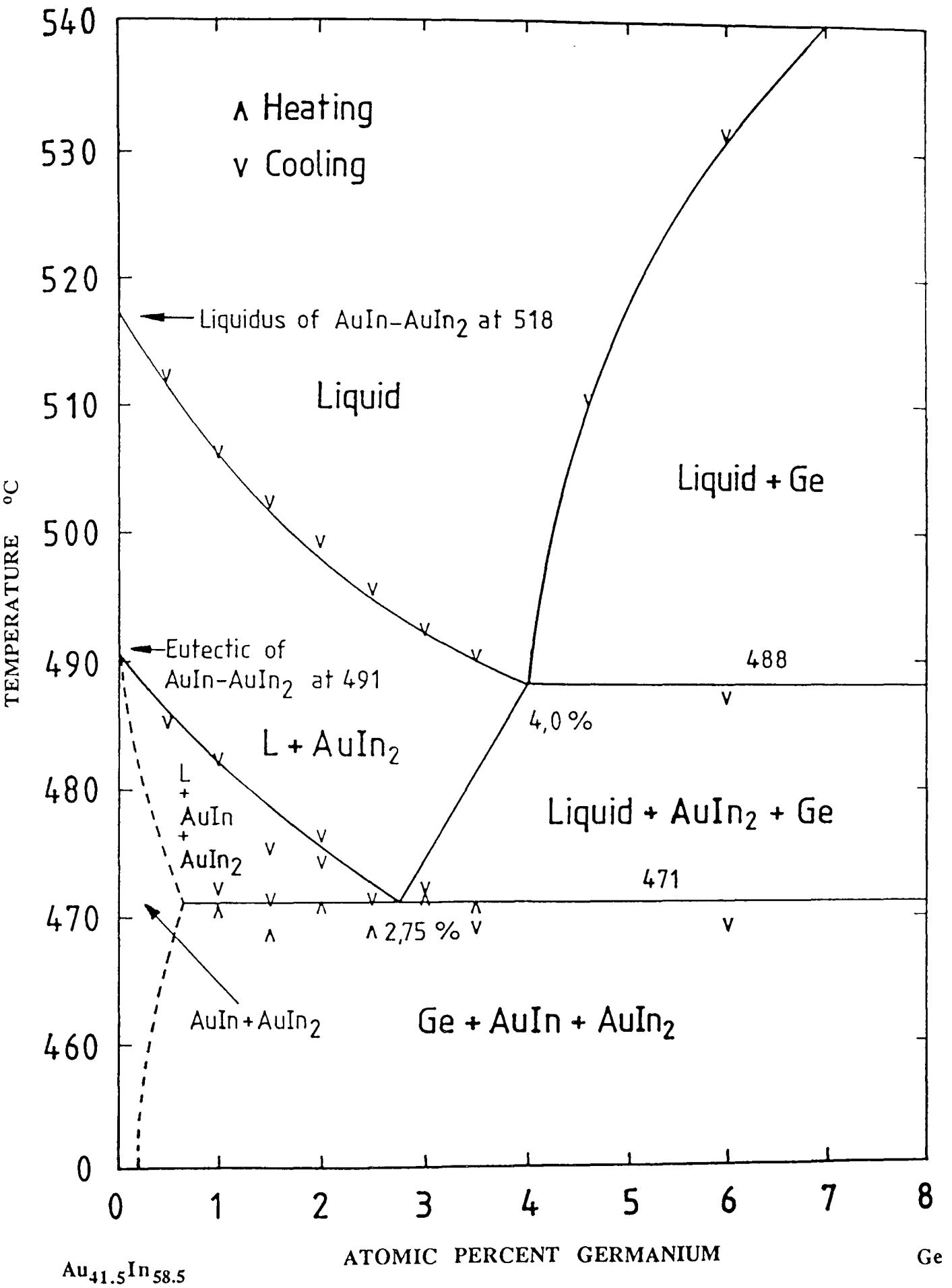

Fig 6.8(b):- Magnified portion of Fig 6.8(a) for alloys containing less than 8 at.% Ge.

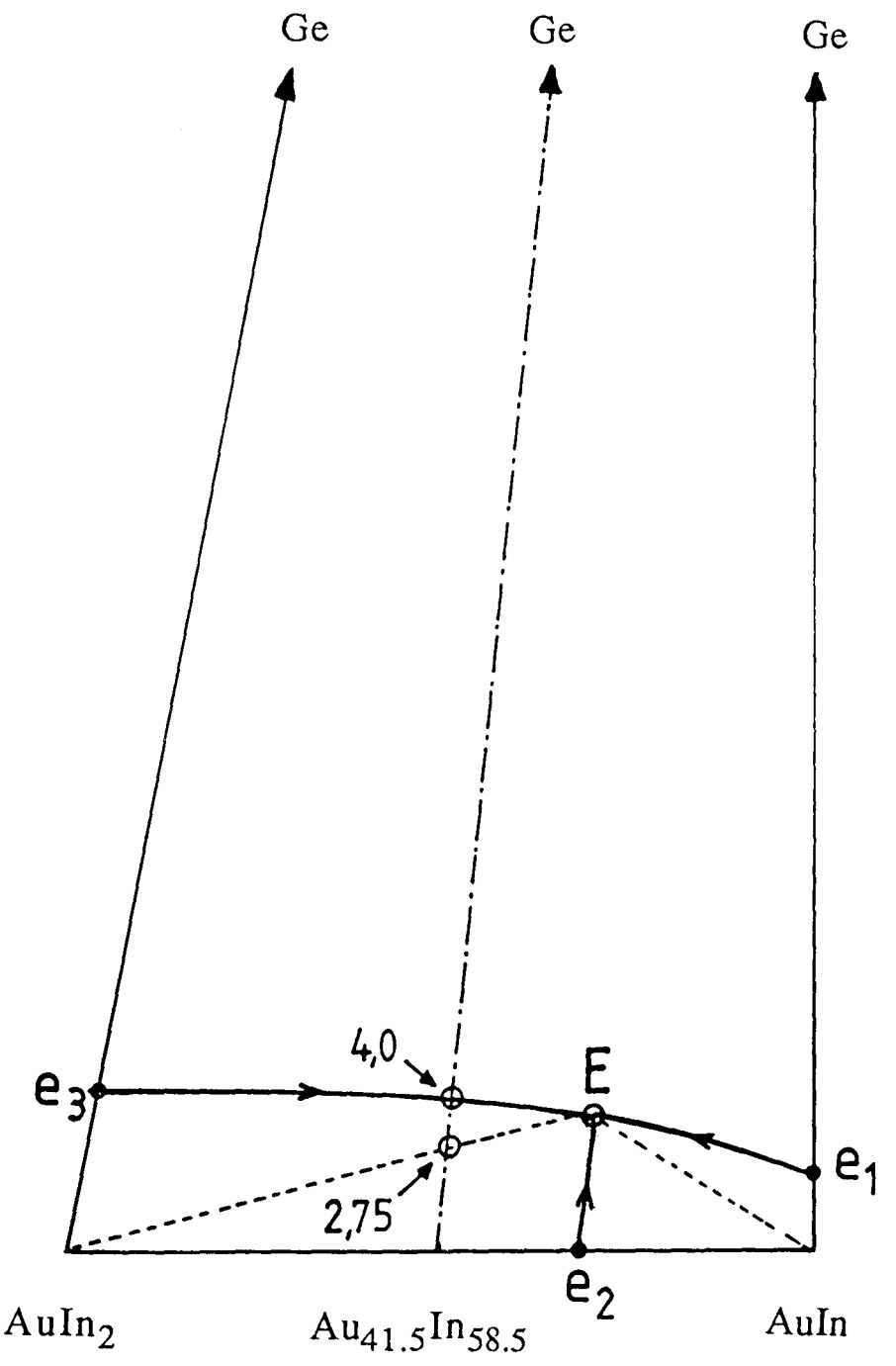

-·-·-= Isopleth Studied, $Au_{41.5}In_{58.5}$ → Ge.

e_1 = Eutectic between AuIn and Ge at 2.0 at.% Ge and 488°C.

e_2 = Eutectic between AuIn and $AuIn_2$ at 56.5 at.% In and 491°C.

e_3 = Eutectic between $AuIn_2$ and Ge at 4.1 at.% Ge and 522°C.

E = Ternary Eutectic Point at 3.5 at.% Ge, 43.25 at.% Au and 53.25 at.% In and 471°C.

Fig 6.8(c):- Liquidus projection of the partial ternary system $AuIn-AuIn_2-Ge$.

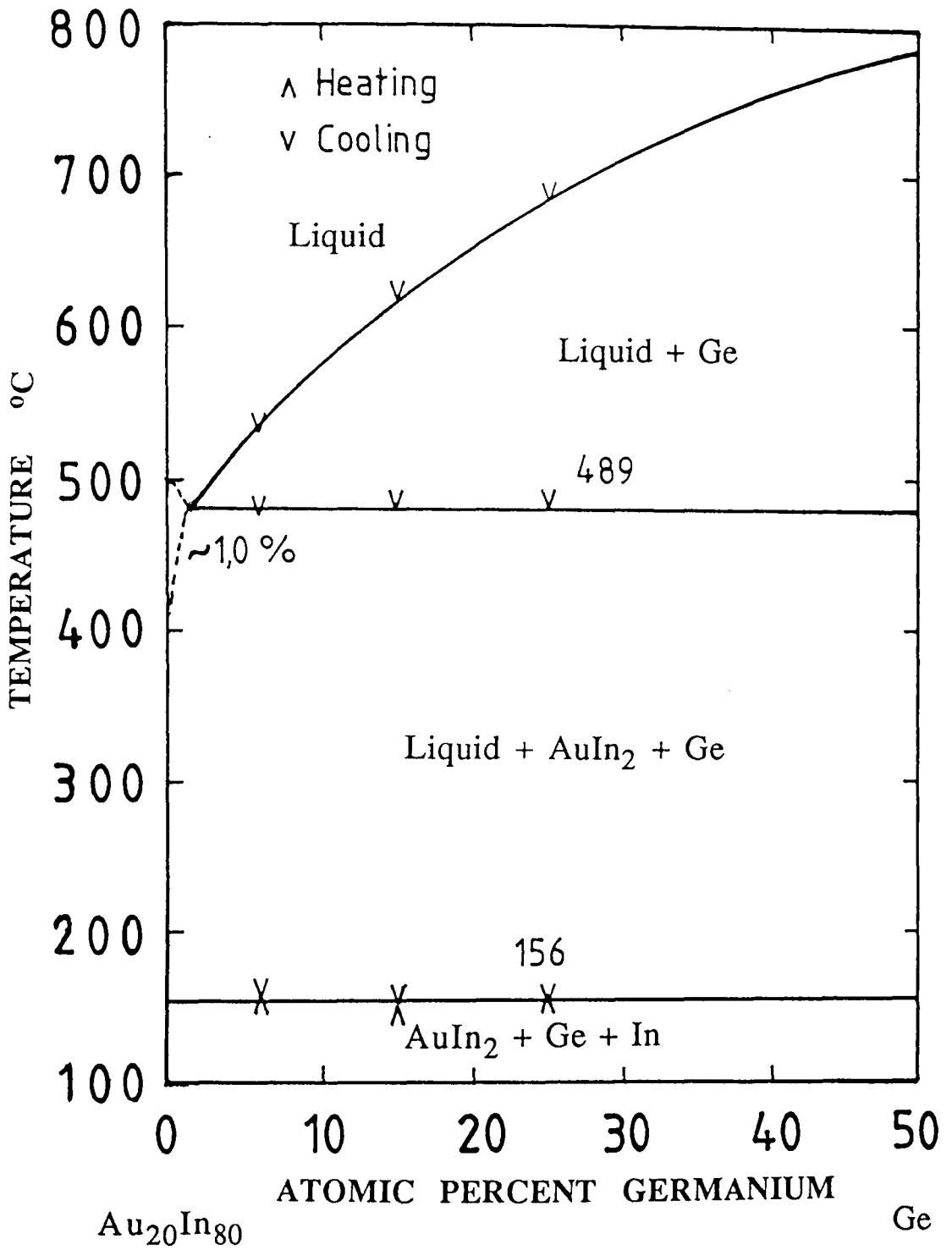

Fig 6.9(a):- Isopleth from $Au_{20}In_{80}$ to Ge.

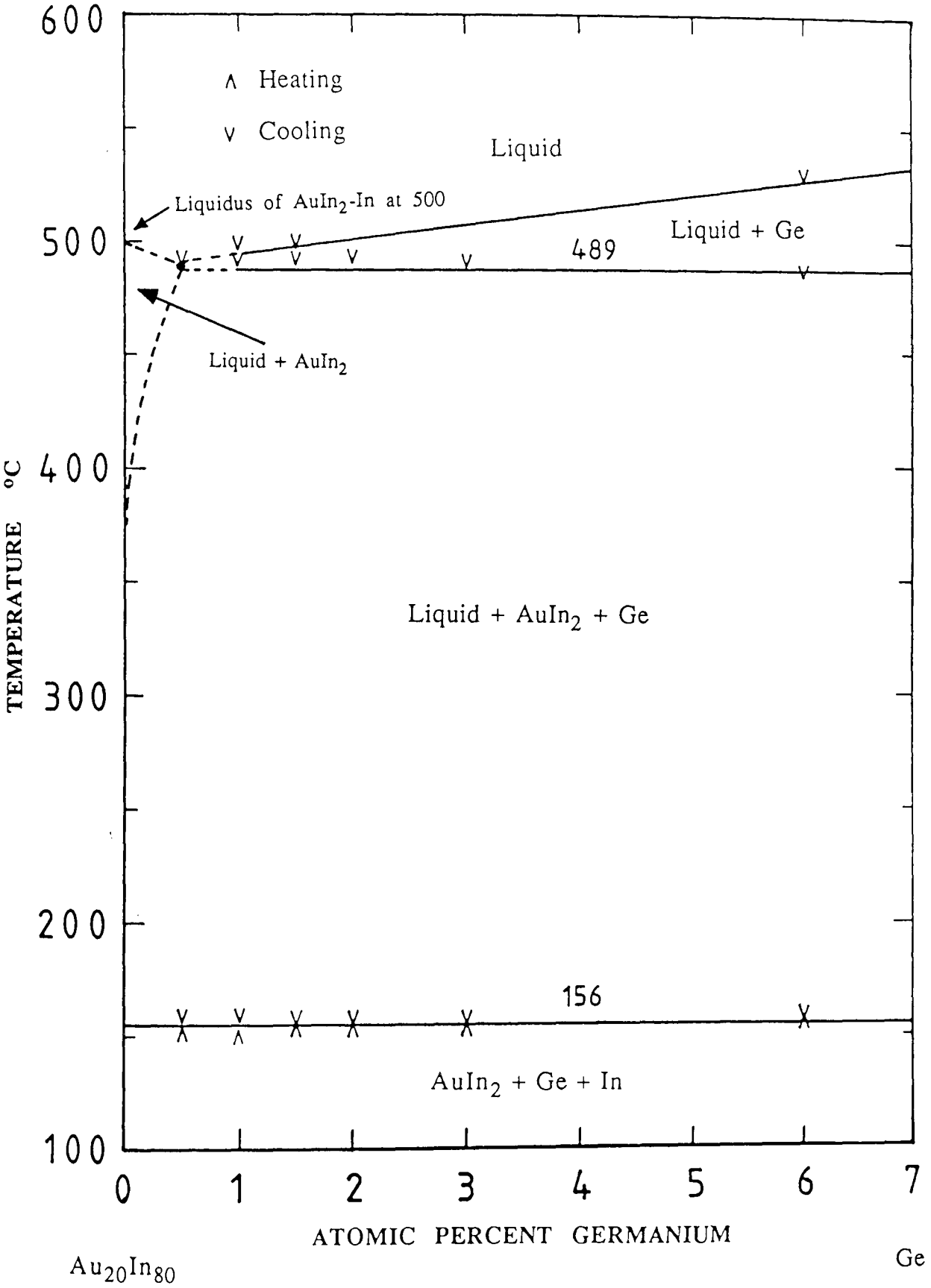

Fig 6.9(b):- Magnified portion of Fig 6.9(a) for alloys containing less than 7 at.% Ge.

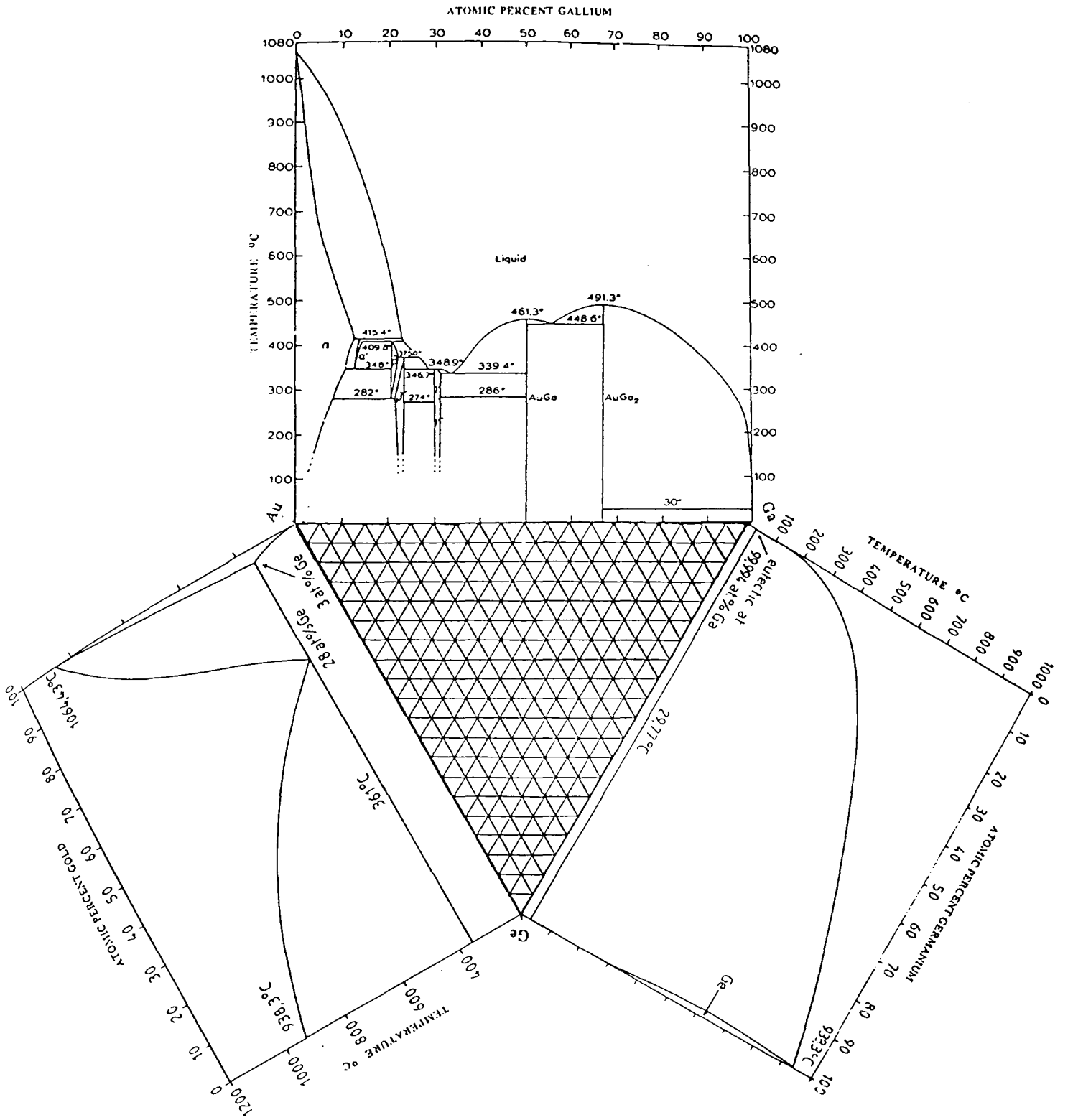

Fig 6.10:- The three edge binary phase diagrams involved in Au-Ge-Ga ternary system.

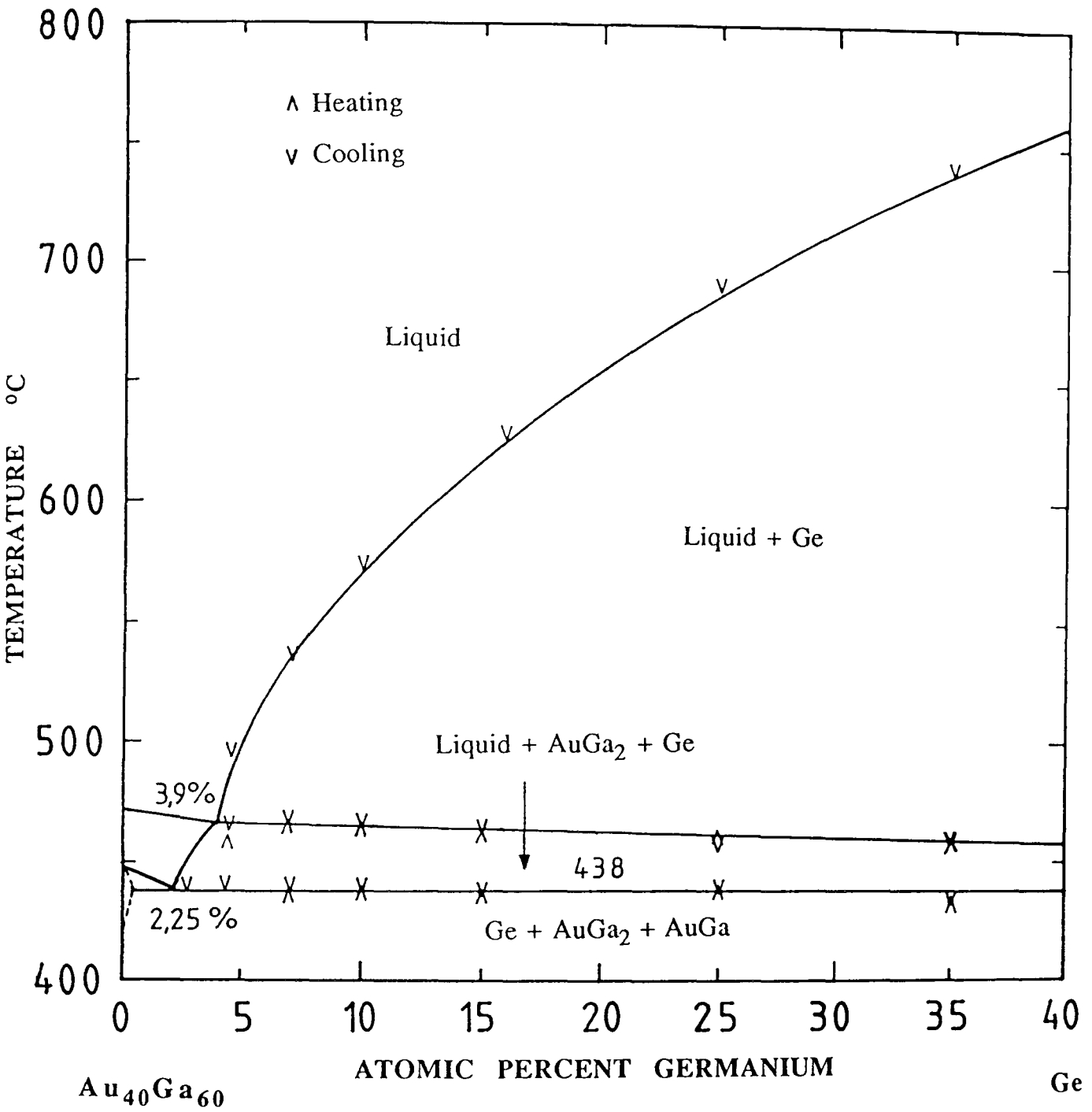

Fig 6.11(a):- Isopleth from $Au_{40}Ga_{60}$ to Ge.

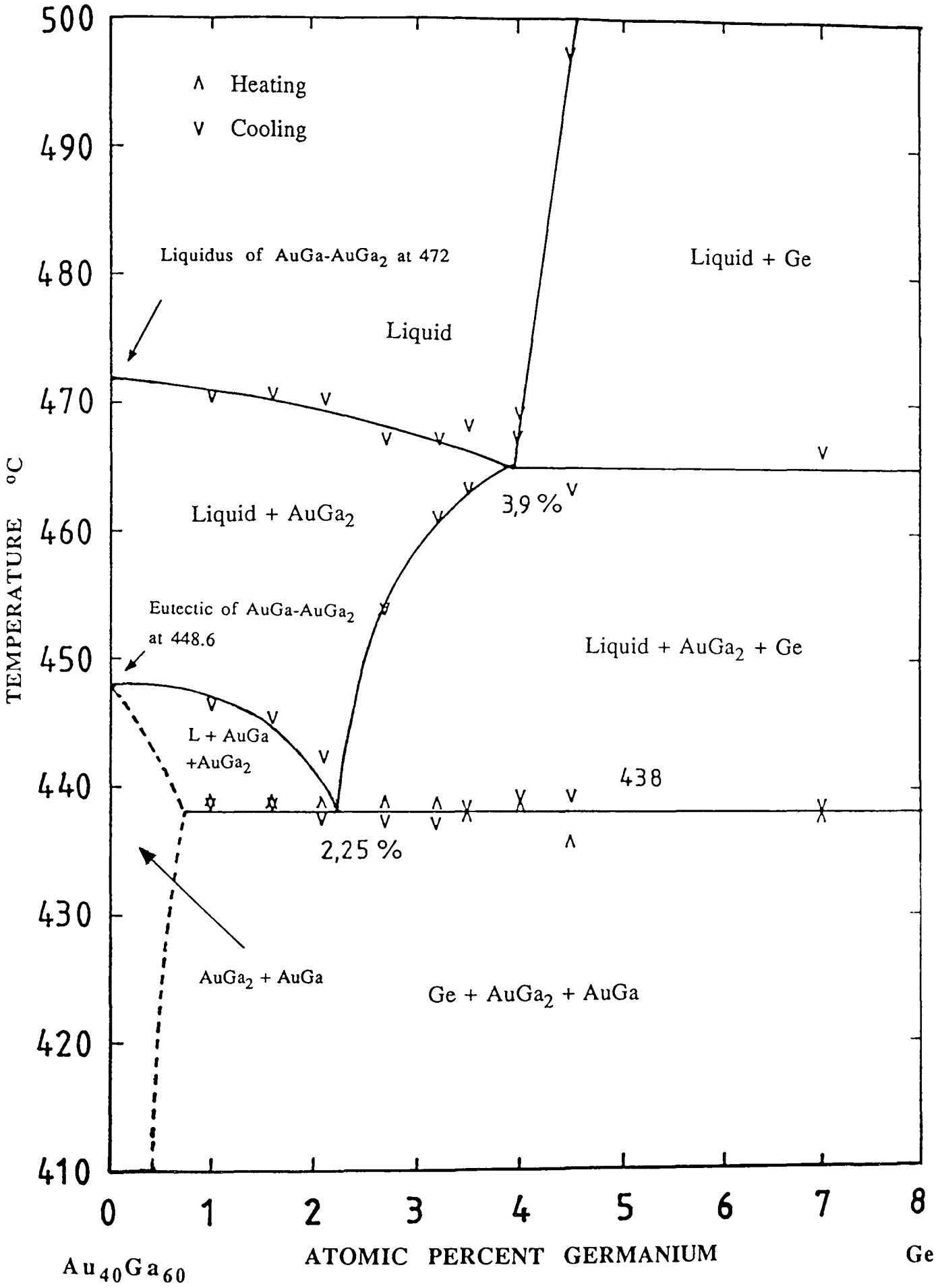

Fig 6.11(b):- Magnified portion of Fig 6.11(a) for alloys containing less than 8 at.% Ge.

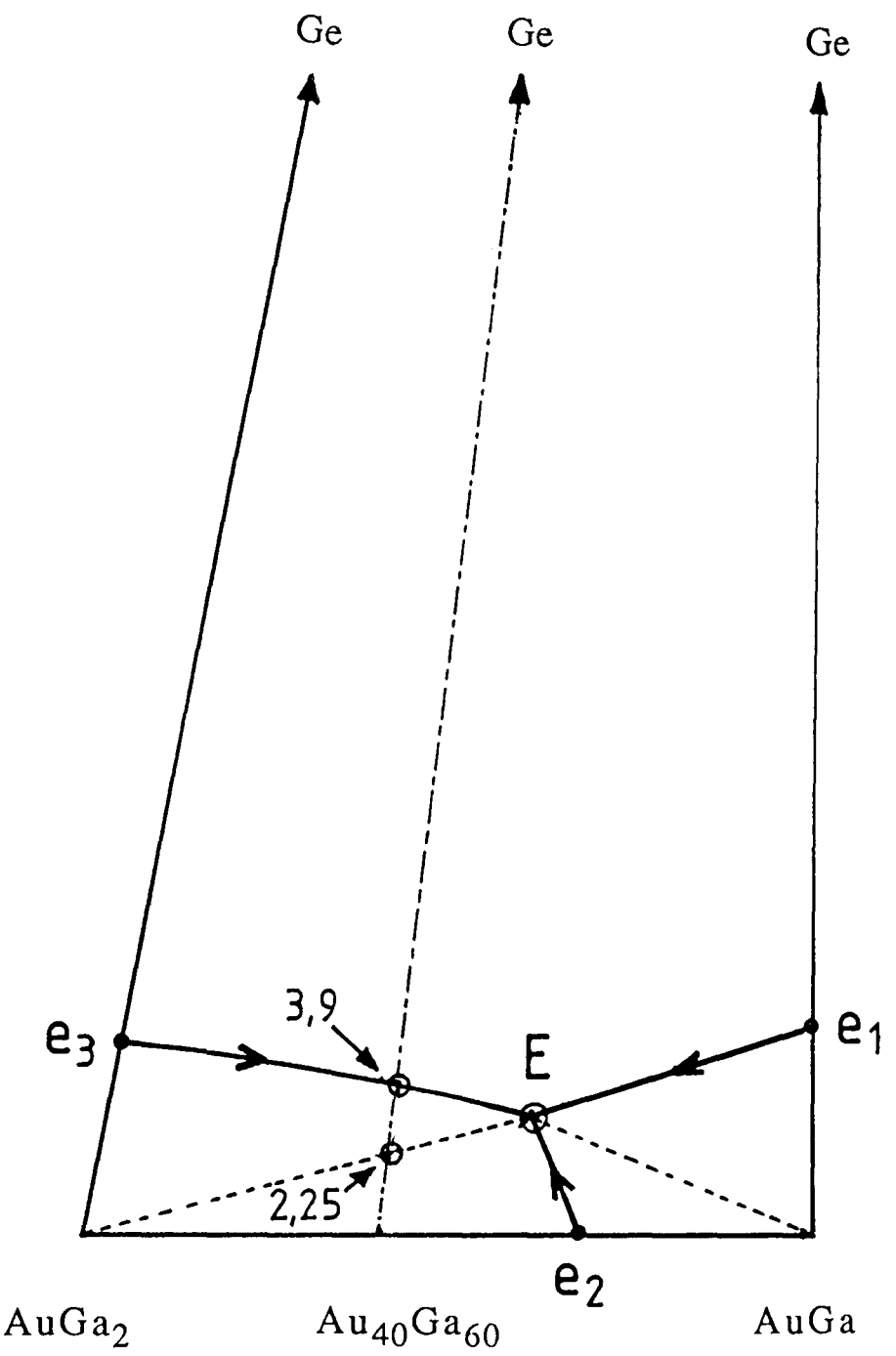

——·—·— = Isopleth Studied, $Au_{40}Ga_{60} \rightarrow$ Ge.

e_1 = Eutectic between AuGa and Ge at 5.5 at.% Ge and 446°C.

e_2 = Eutectic between AuGa and $AuGa_2$ at 55.4 at.% Ga and 448.6°C.

e_3 = Eutectic between $AuGa_2$ and Ge at 5.0 at.% Ge and 476°C.

E = Ternary Eutectic Point at 3.2 at.% Ge, 41.8 at.% Au and 55.0 at.% Ga and 438°C.

Fig 6.11(c):- Liquidus projection of the partial ternary system $AuGa\text{-}AuGa_2\text{-}Ge$.

Fig 6.12(a)

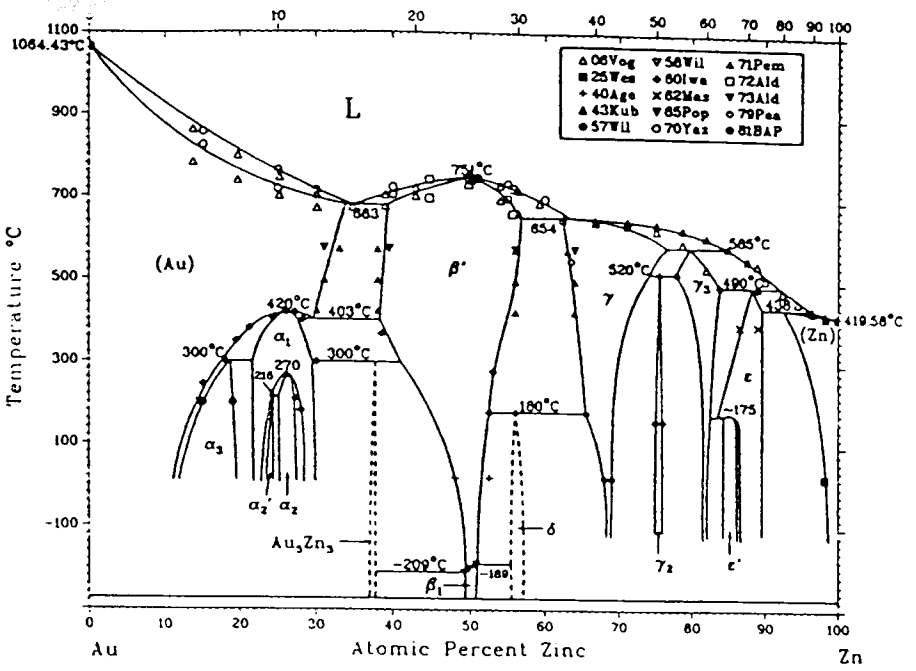

Fig 6.12(b)

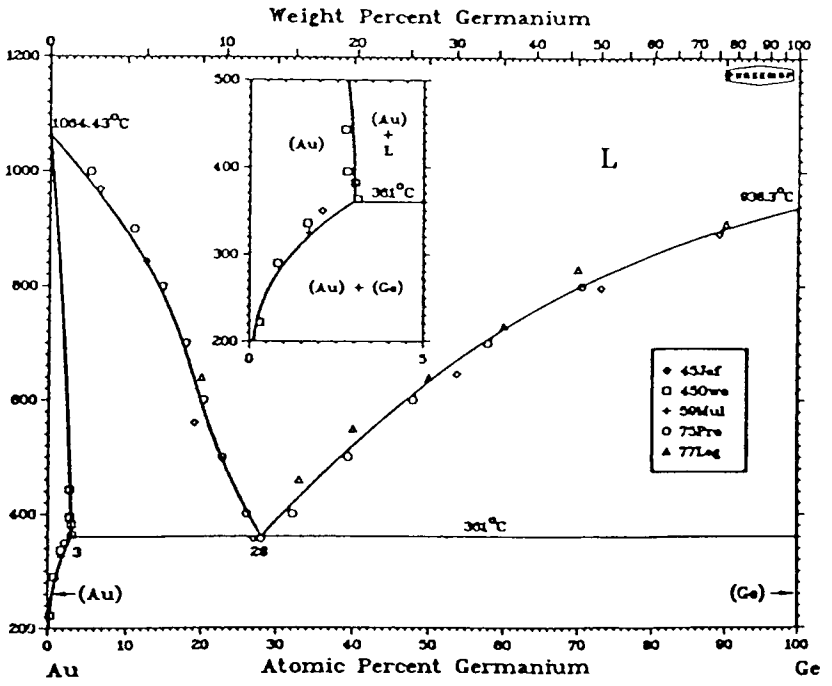

Fig 6.12(c)

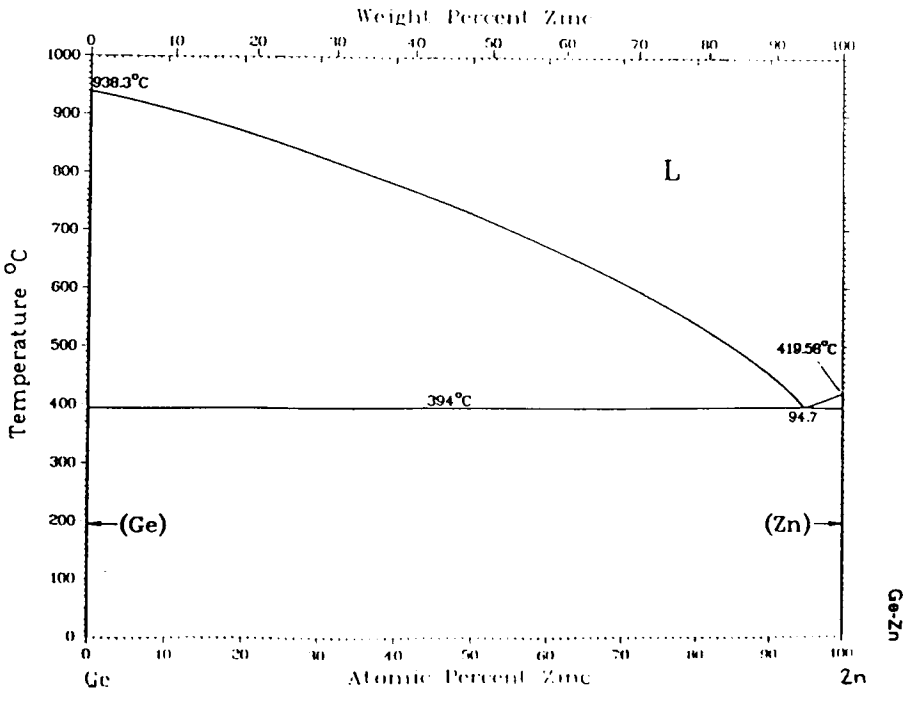

Fig 6.12(a,b,c):- The three edge binary phase diagrams involved in Au-Ge-Zn ternary system.

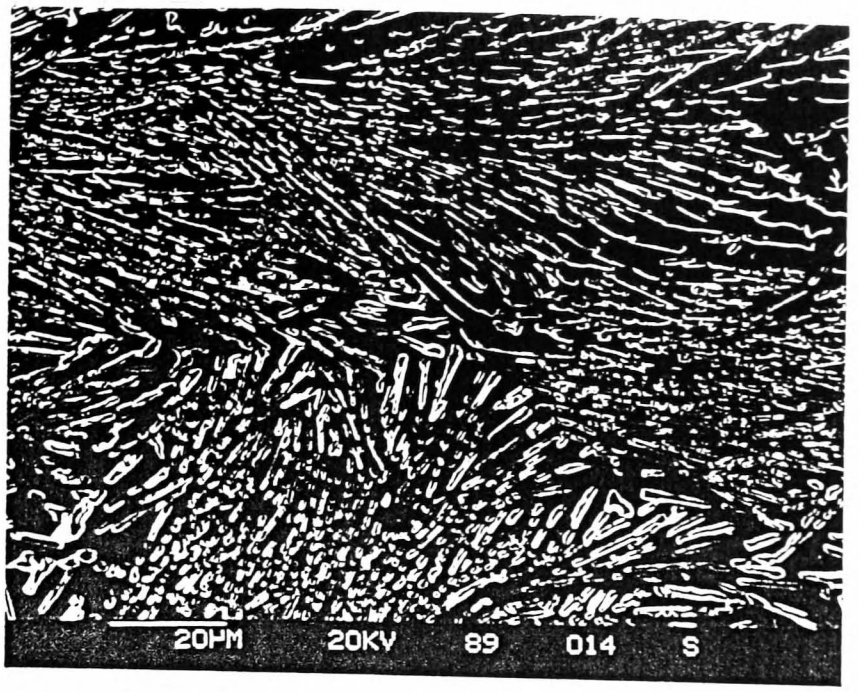

Fig 6.13:- Microstructure of an AuZn-Ge eutectic alloy containing 12.2 at.% Ge (x 800).

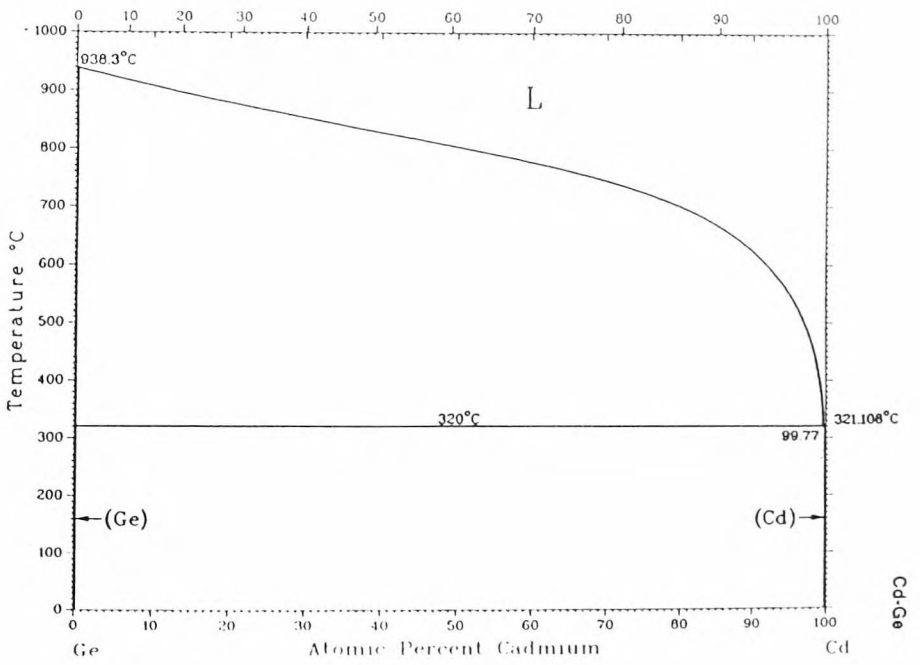

Fig 6.14(a)

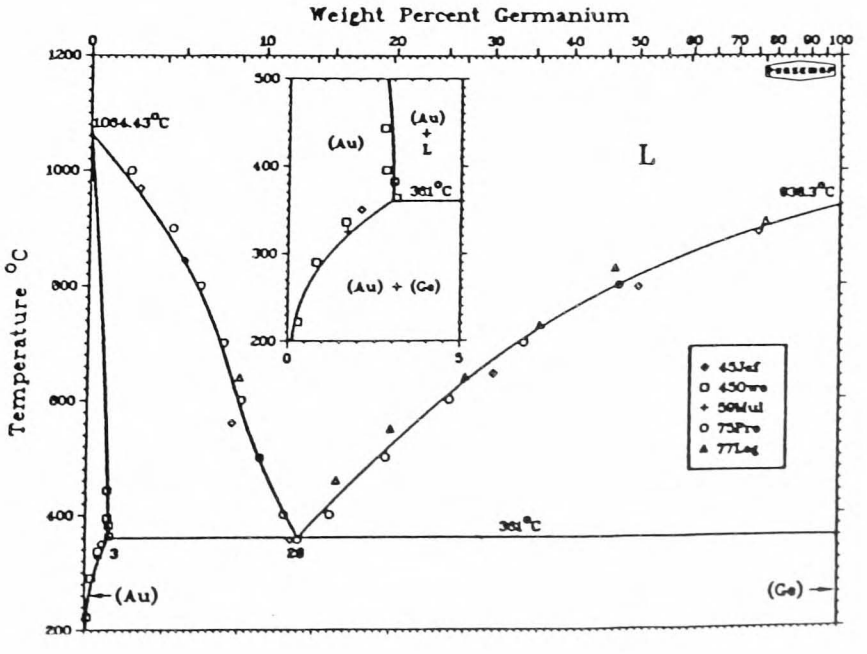

Fig 6.14(b)

Fig 6.14(c)

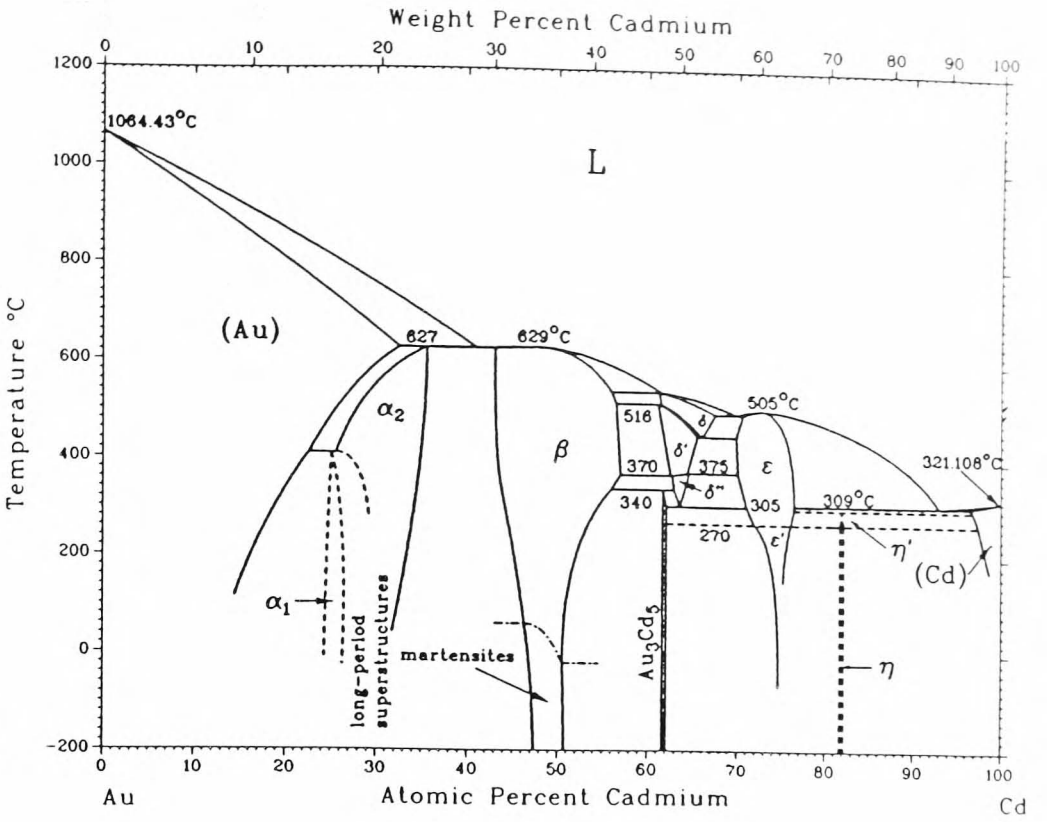

Fig 6.15

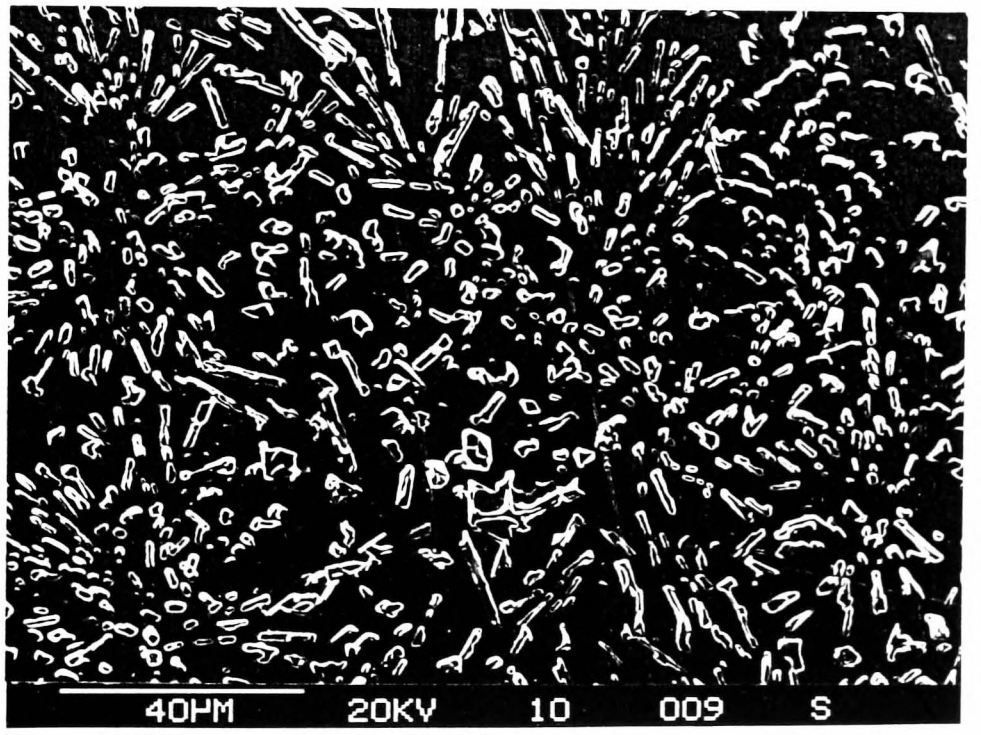

Fig 6.14(a,b,c):- The three edge binary phase diagrams involved in Au-Ge-Cd ternary system.

Fig 6.15:- Microstructure of an AuCd-Ge eutectic alloy containing 10.0 at.% Ge (x 600).

Fig 6.16

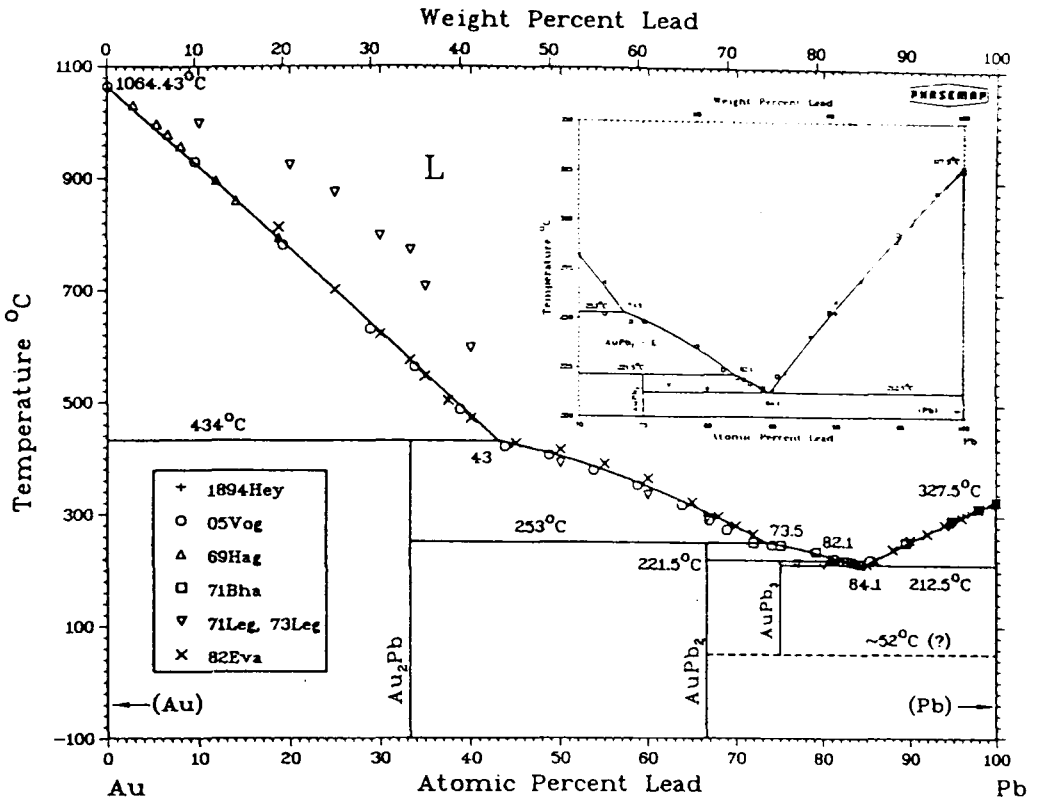

Fig 6.17

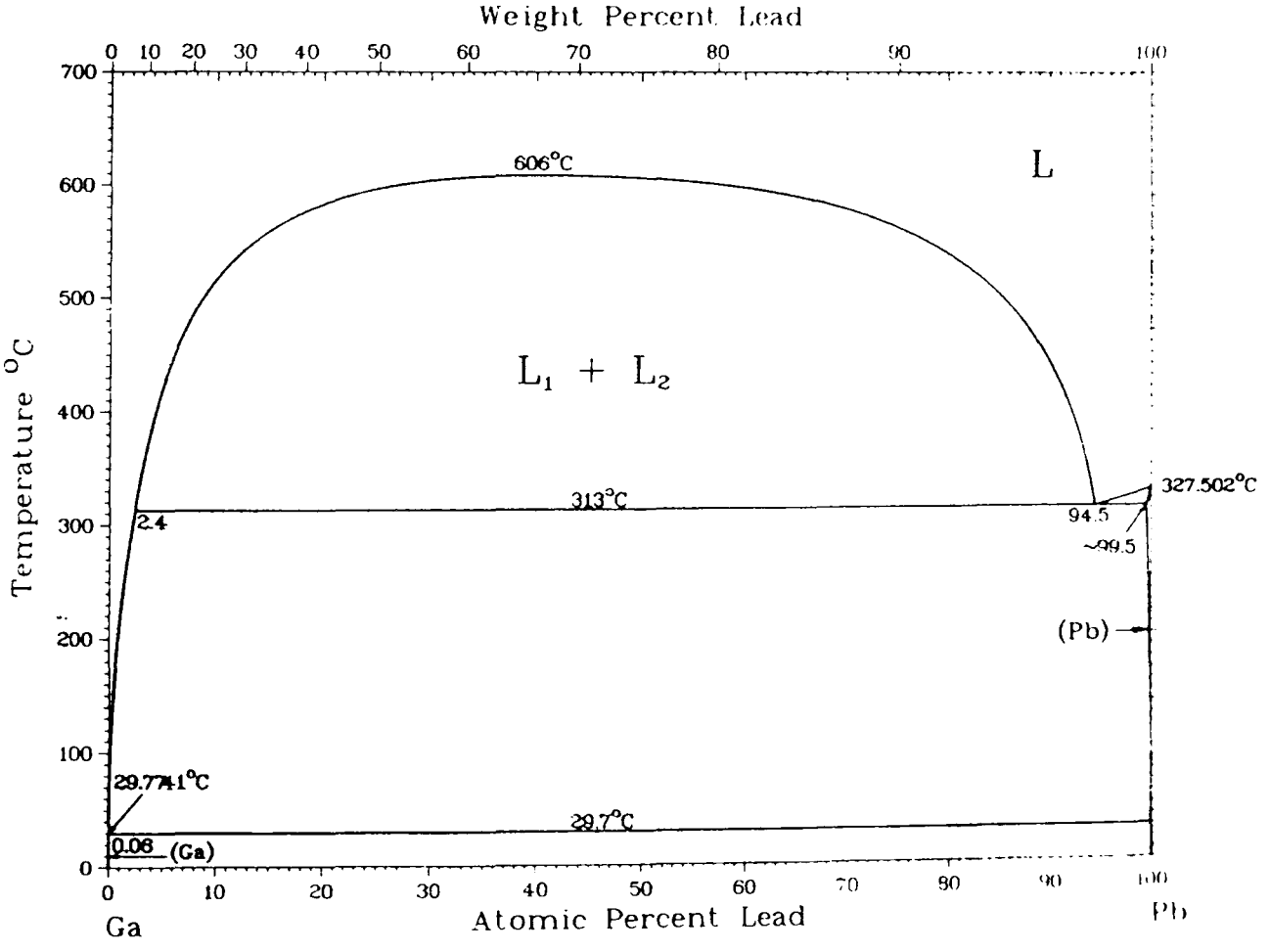

Fig 6.16:- The Au-Pb binary phase diagram (99).

Fig 6.17:- The Ga-Pb binary phase diagram (100).

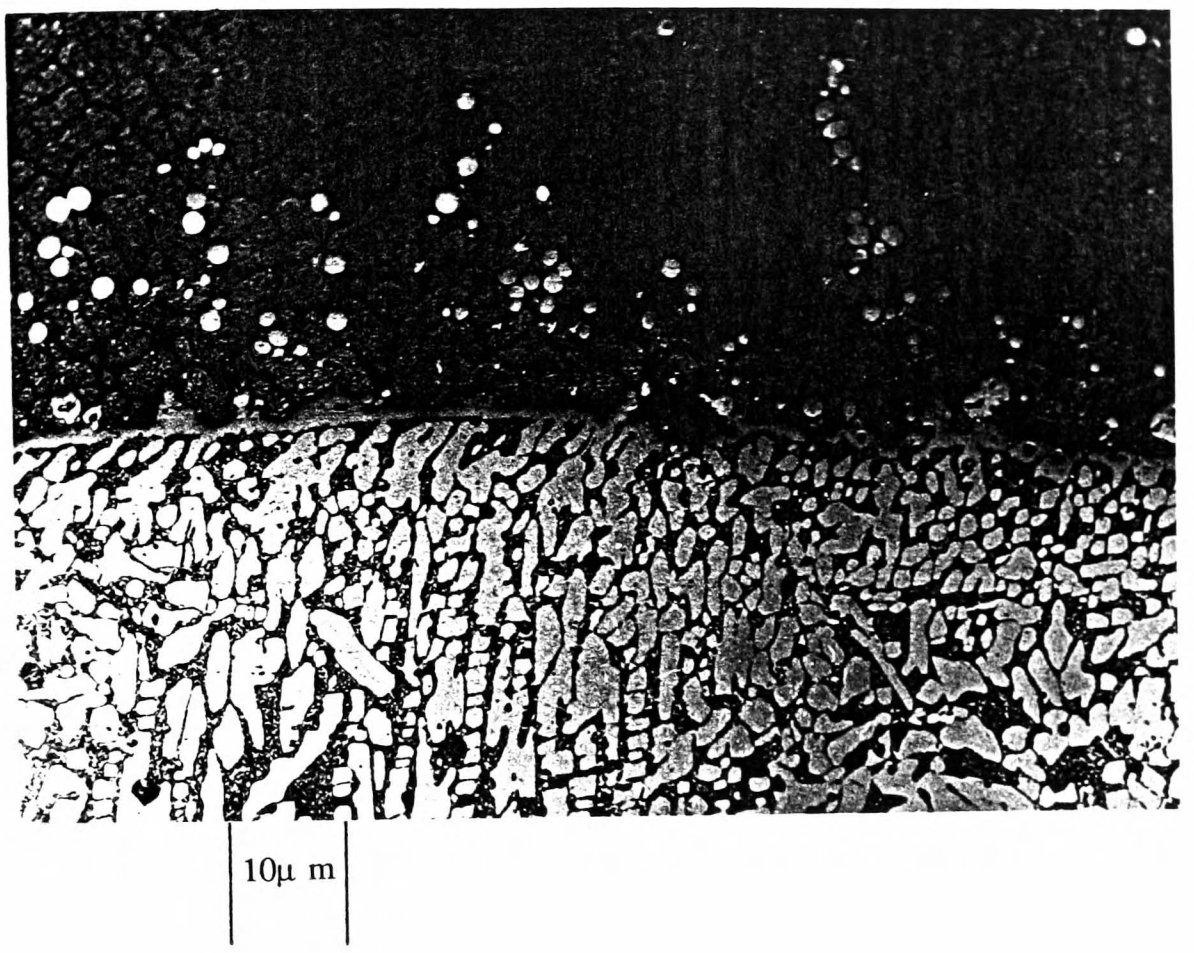

Fig 6.18:- Liquid immiscibility in AuGa-Pb system containing 60.0 at.% Pb and 40.0 at.% AuGa (x 100).

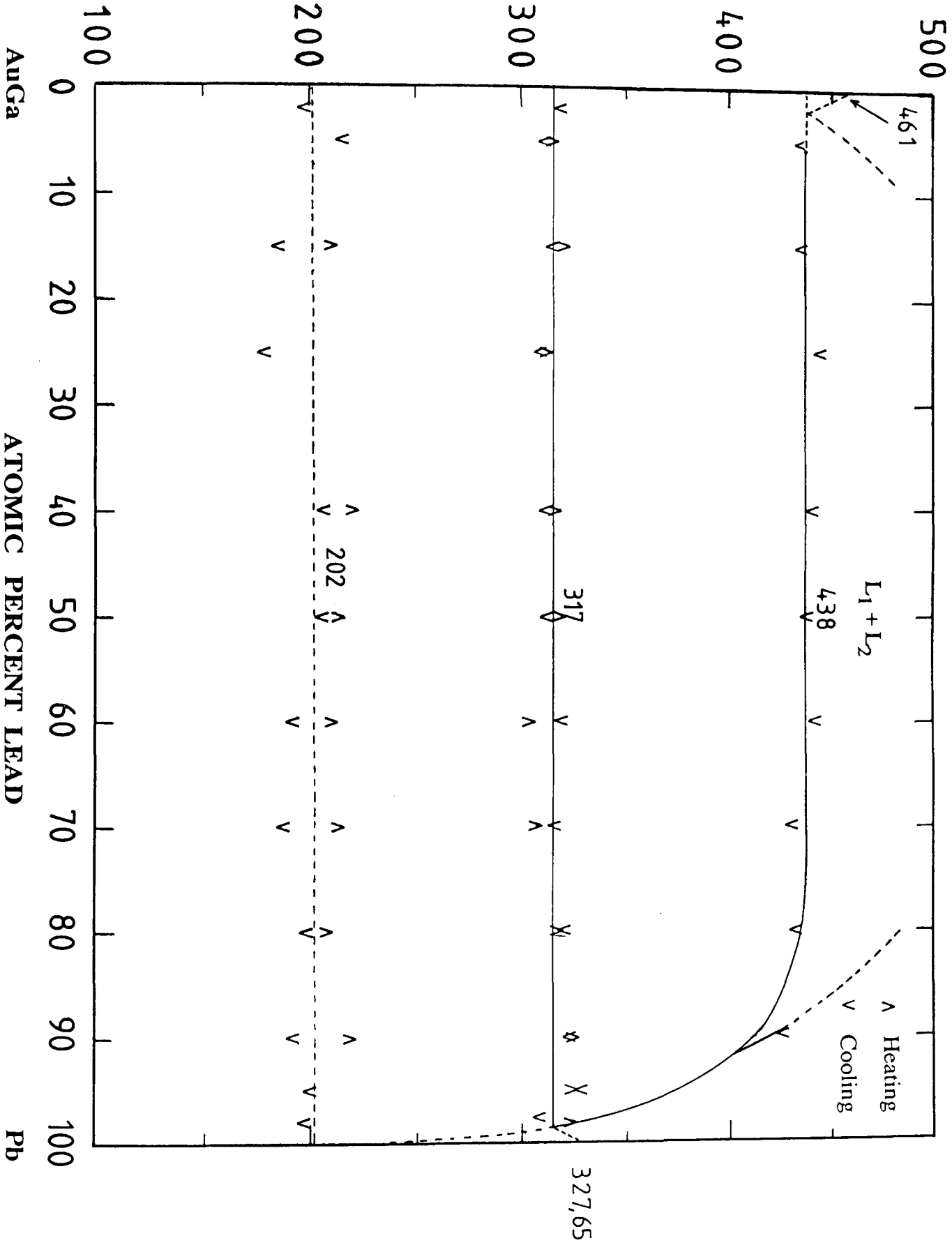

Fig 6.19:- The AuGa-Pb section determined by Thermal Analysis.

[See Fig 7.31(a)]

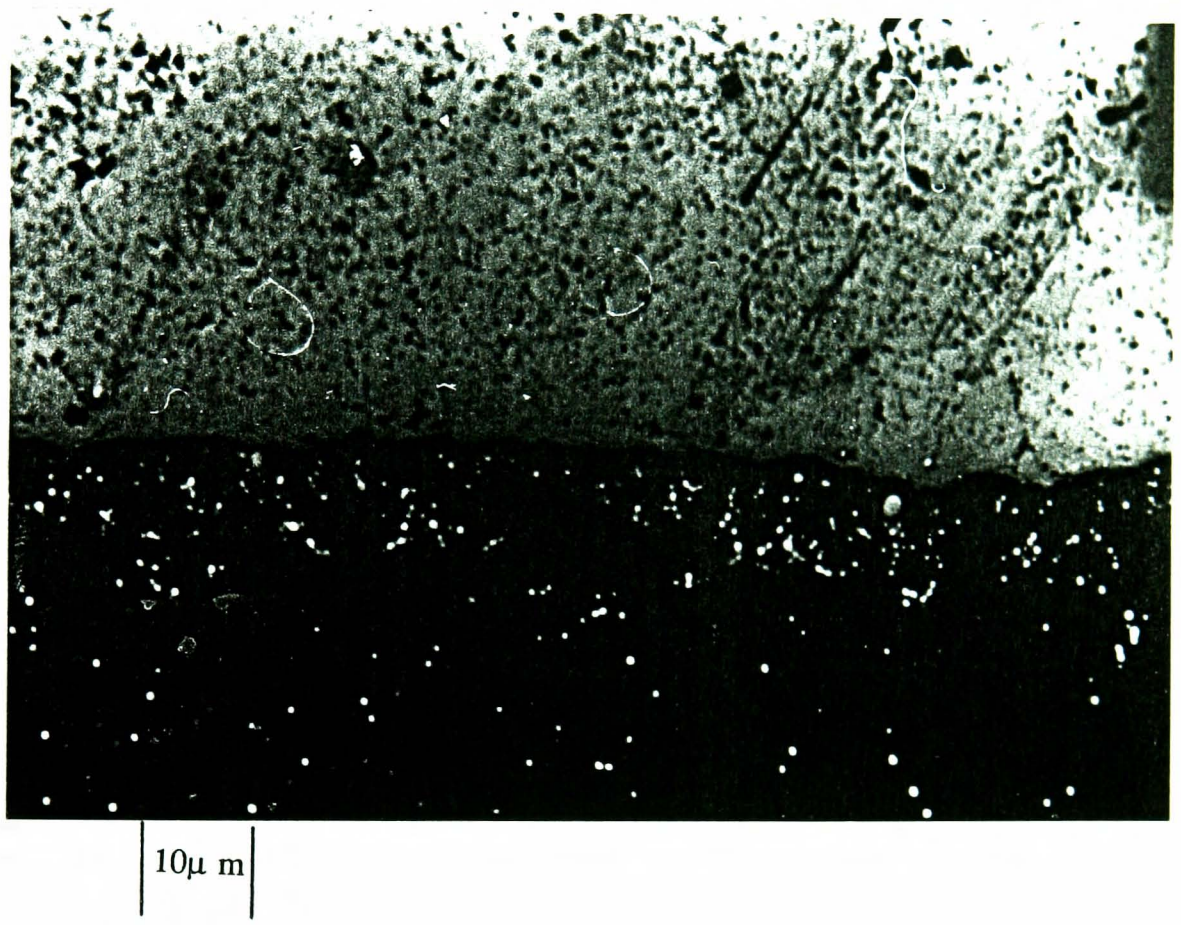

Fig 6.20:- Liquid immiscibility in $AuGa_2$-Pb system containing 50.0 at.% Pb and 50.0 at.% $AuGa_2$ (x 50).

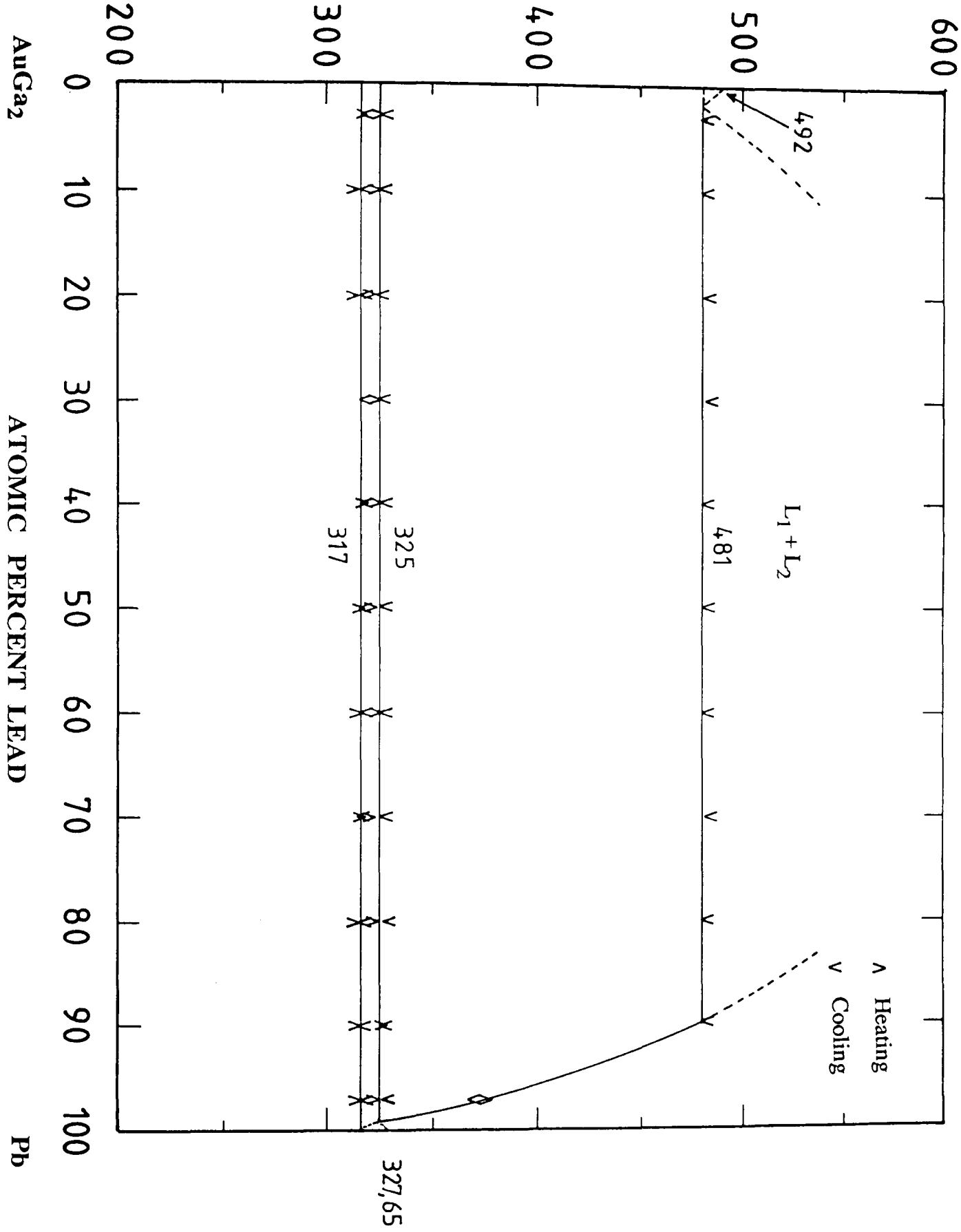

Fig 6.21:- The $AuGa_2$-Pb section determined by Thermal Analysis.

[See Fig 7.31(b)]

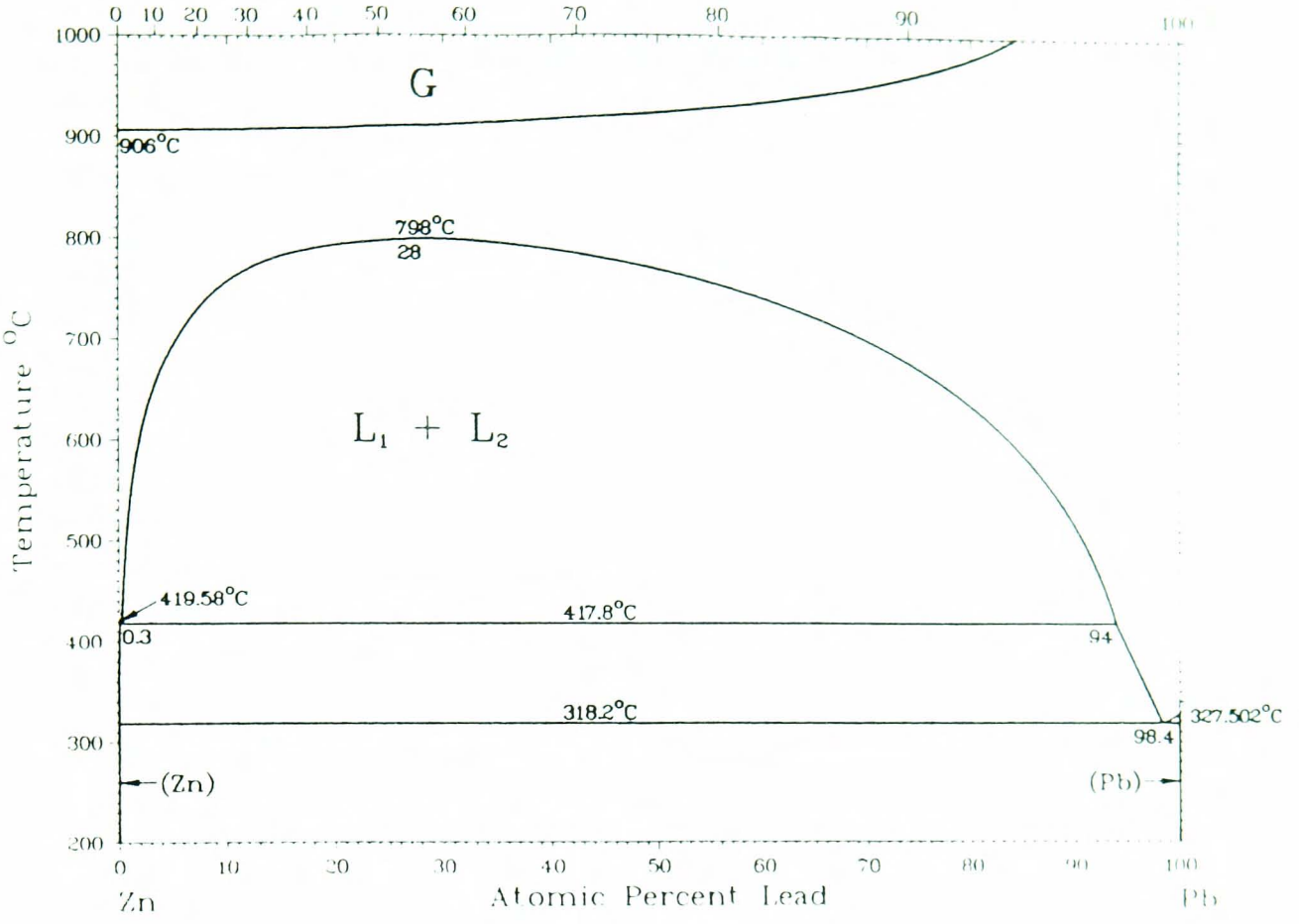

Fig 6.22:- The Zn-Pb binary phase diagram.

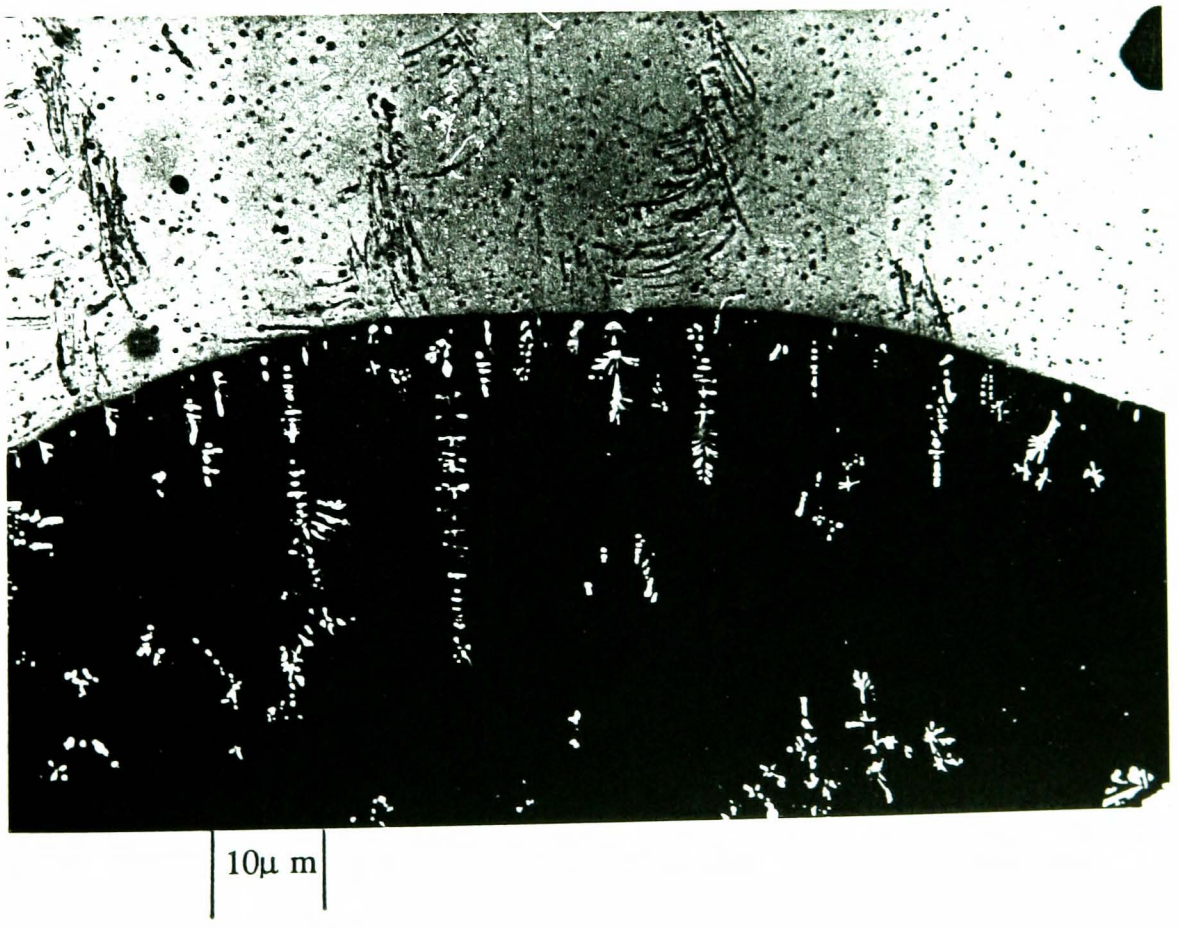

Fig 6.23:- Liquid immiscibility in AuZn-Pb system containing 40.0 at.% Pb and 60.0 at.% AuZn (x 50).

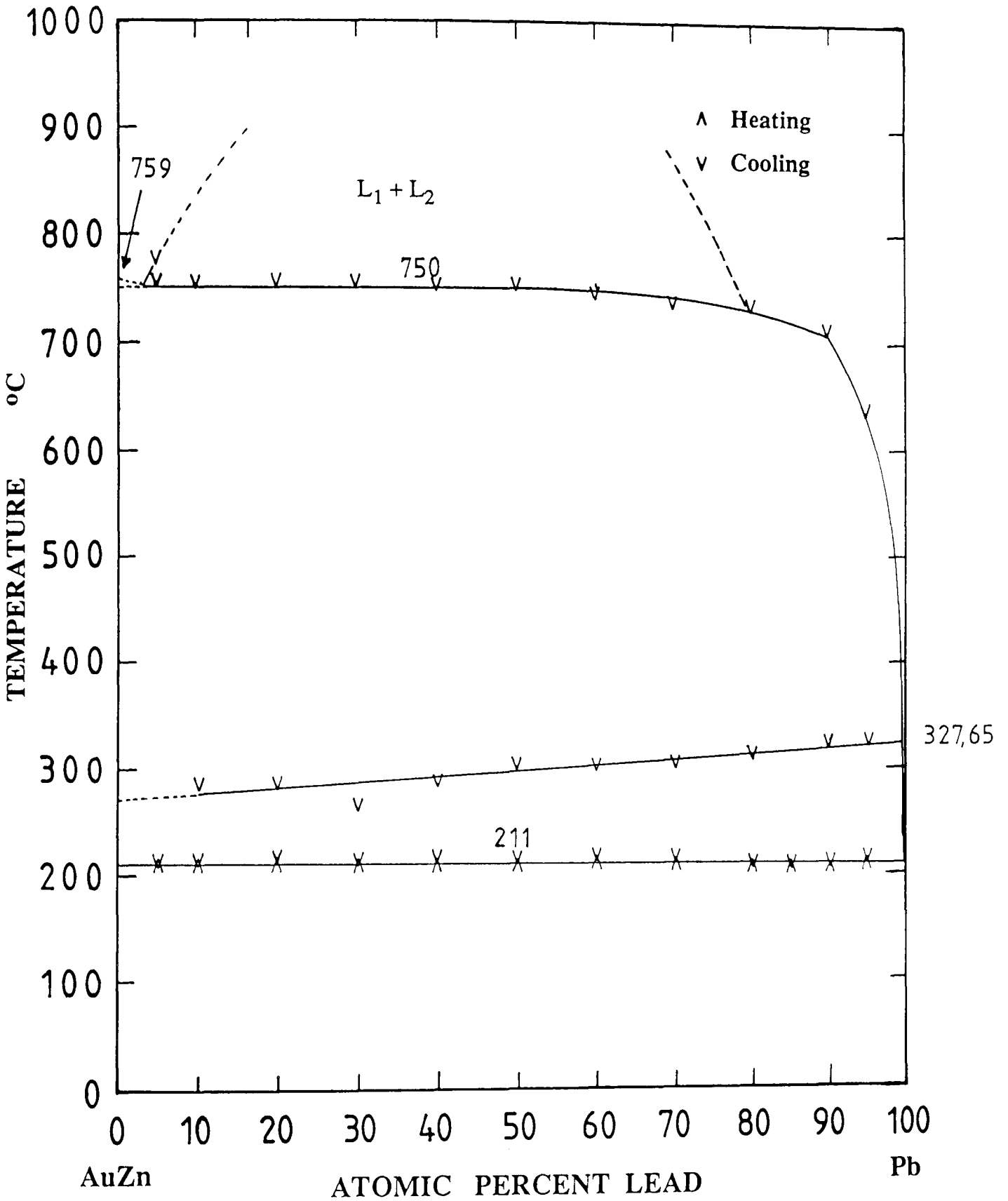

Fig 6.24:- The AuZn-Pb section determined by Thermal Analysis.

Fig 6.25

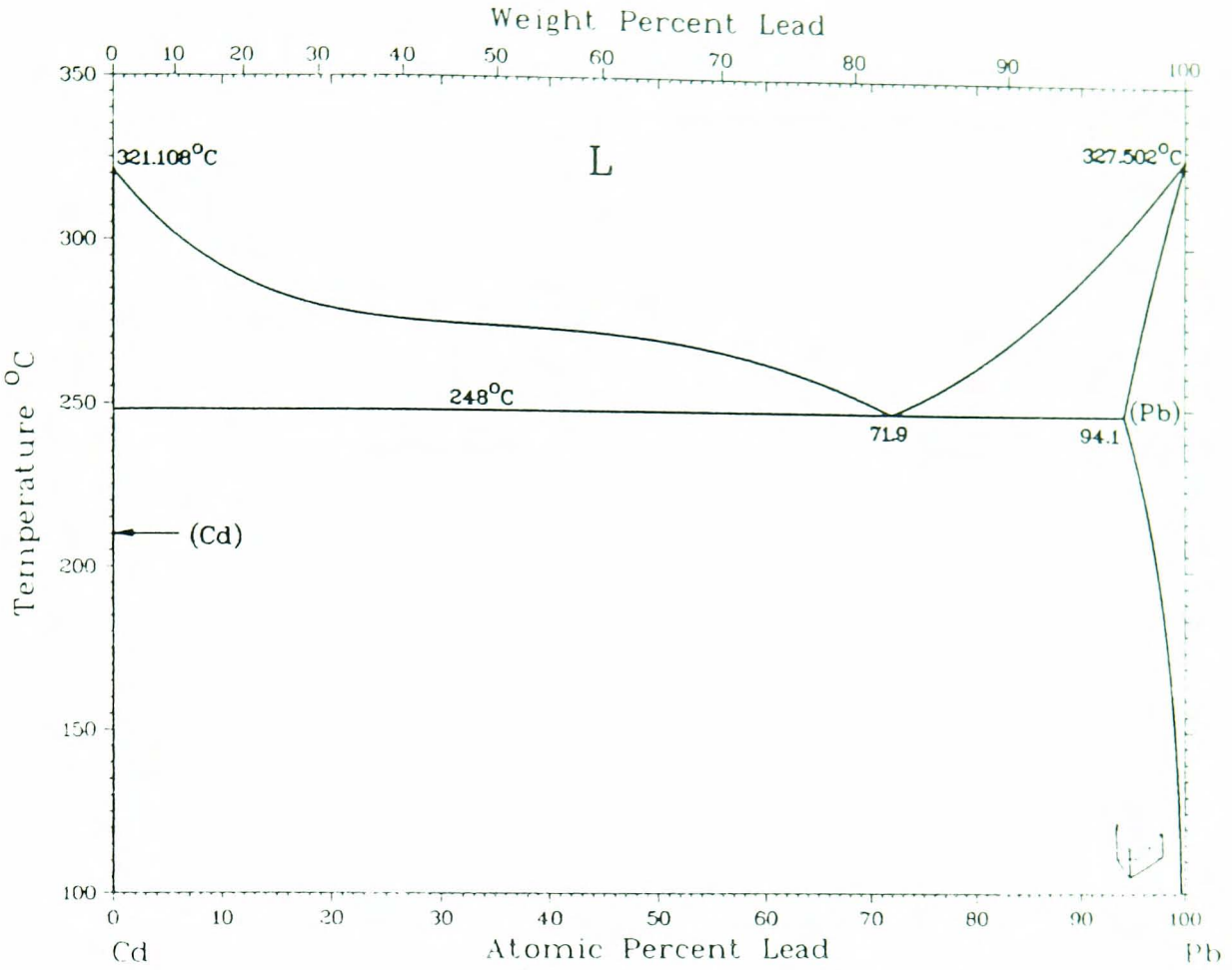

Fig 6.26

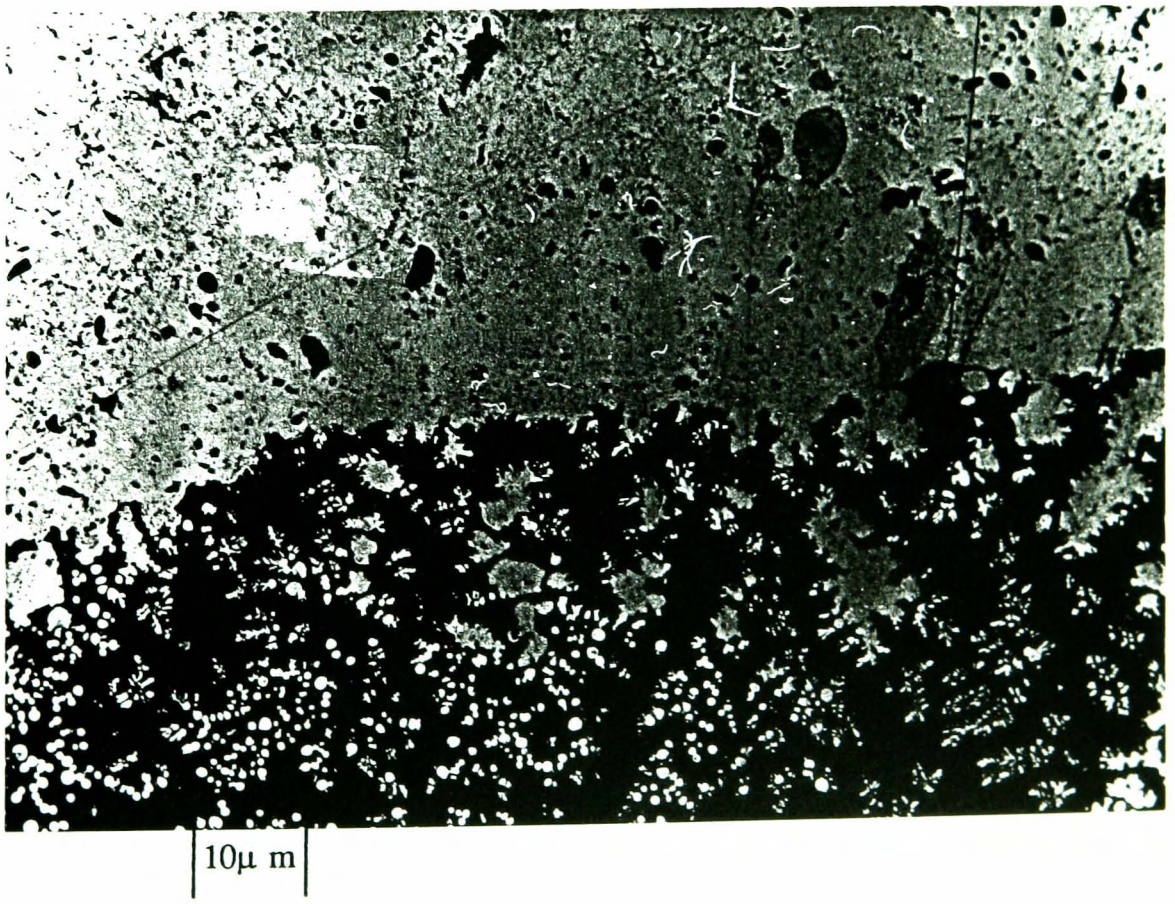

Fig 6.25:- The Cd-Pb binary phase diagram.

Fig 6.26:- Liquid immiscibility in AuCd-Pb system containing 40.0 at.% Pb and 60.0 at.% AuCd (x 50).

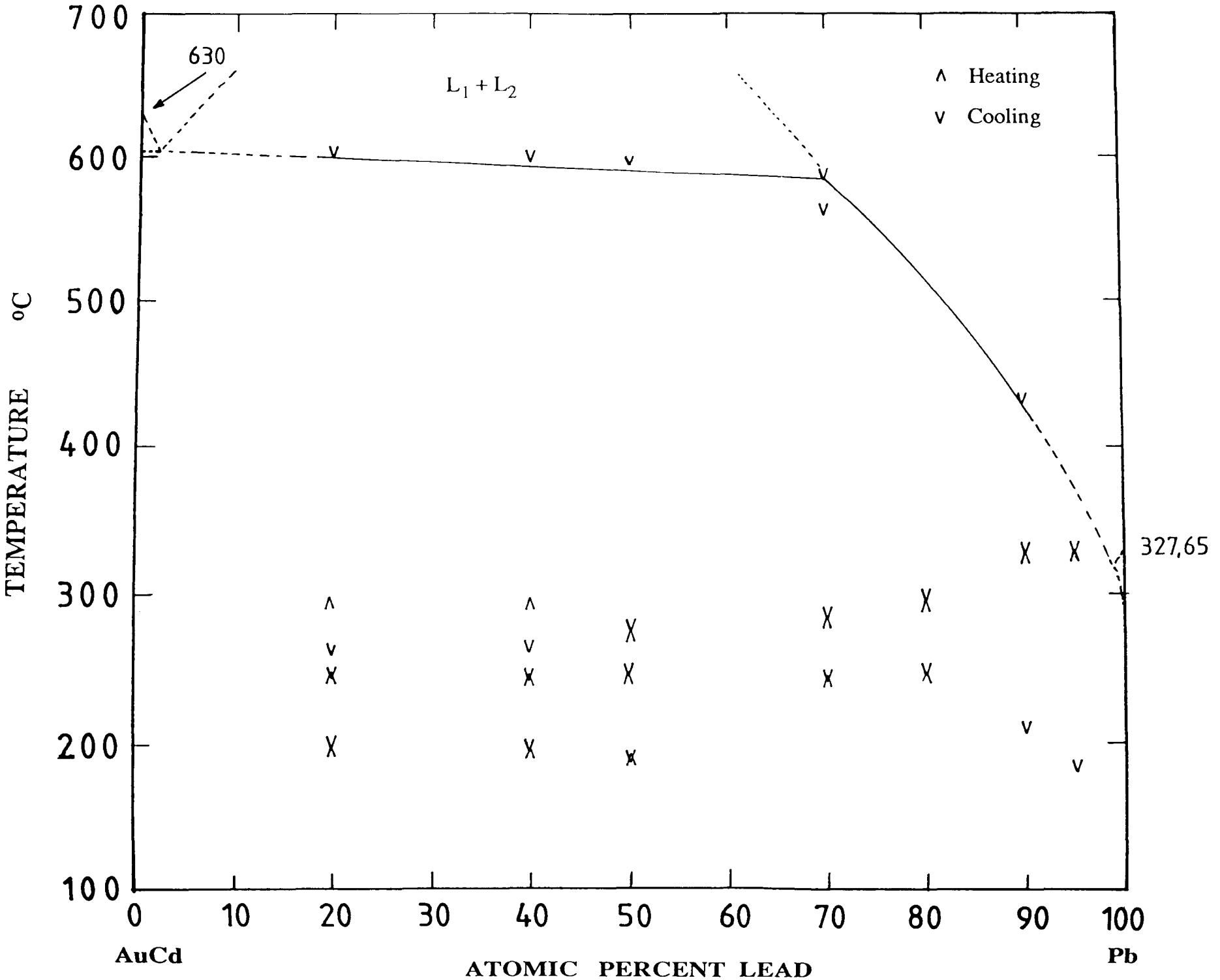

Fig 6.27:- The AuCd-Pb section determined by Thermal Analysis.

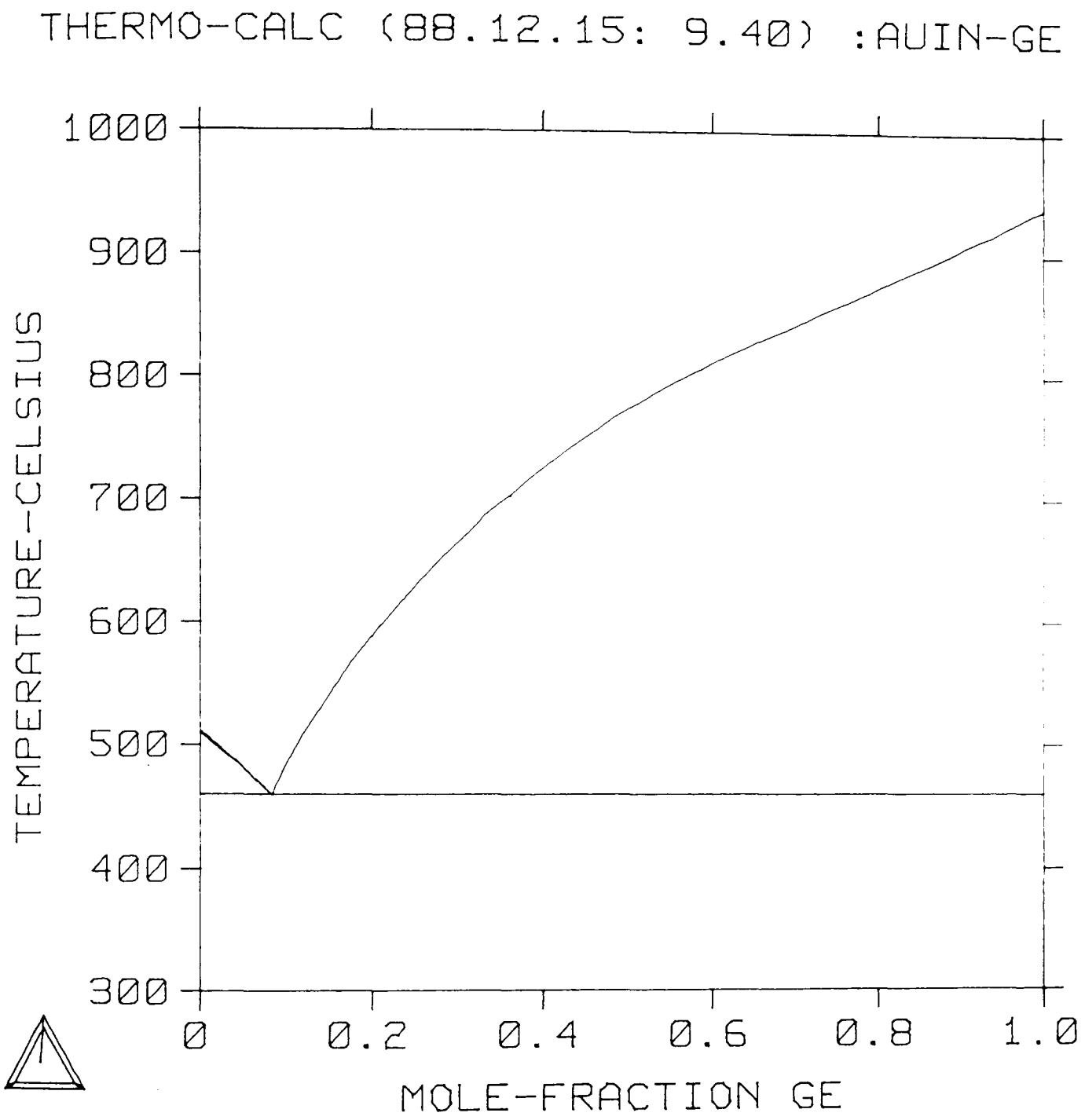

Fig 6.28:-Thermodynamically computed AuIn-Ge section.

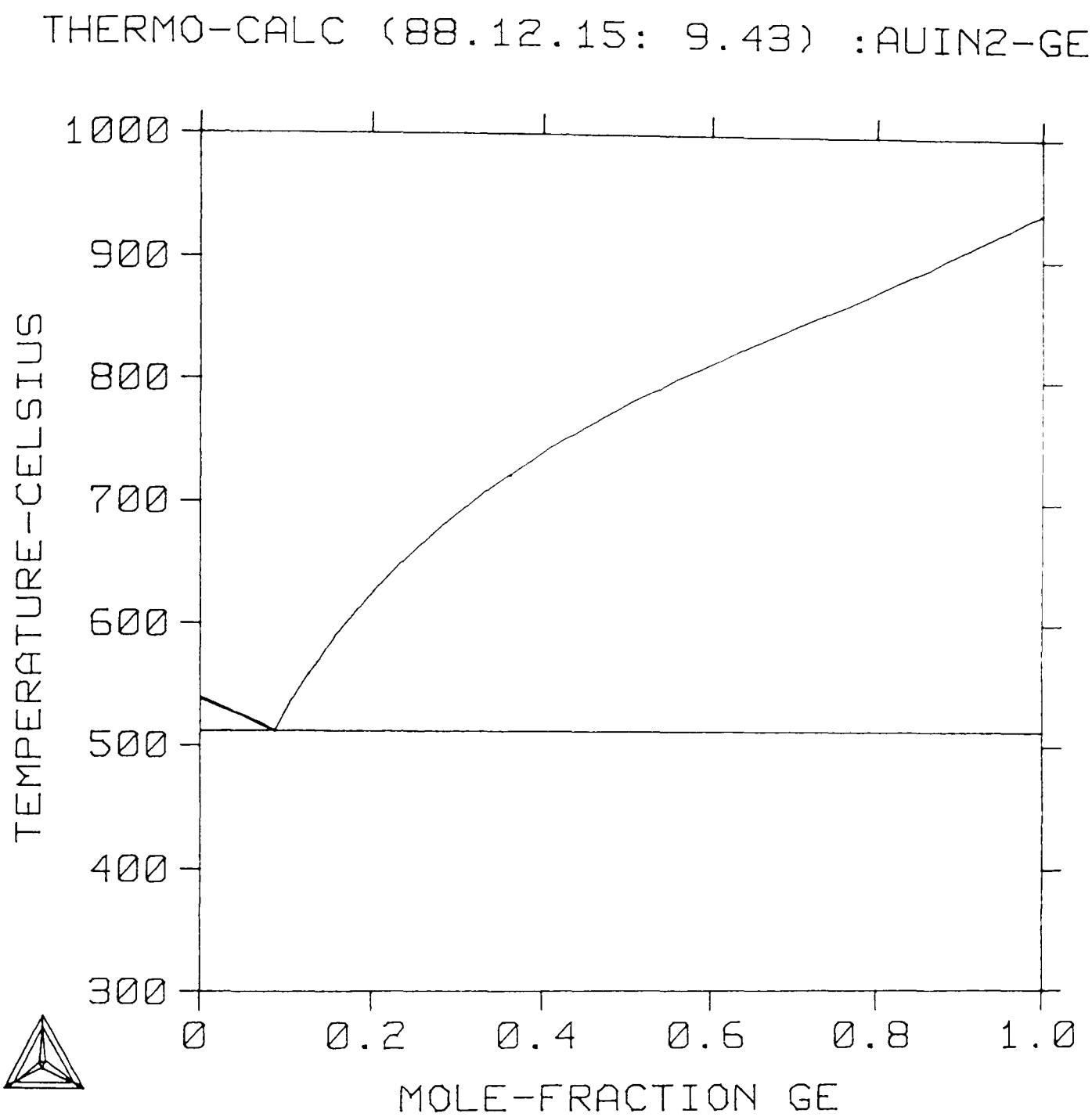

Fig 6.29:-Thermodynamically computed $AuIn_2$-Ge section.

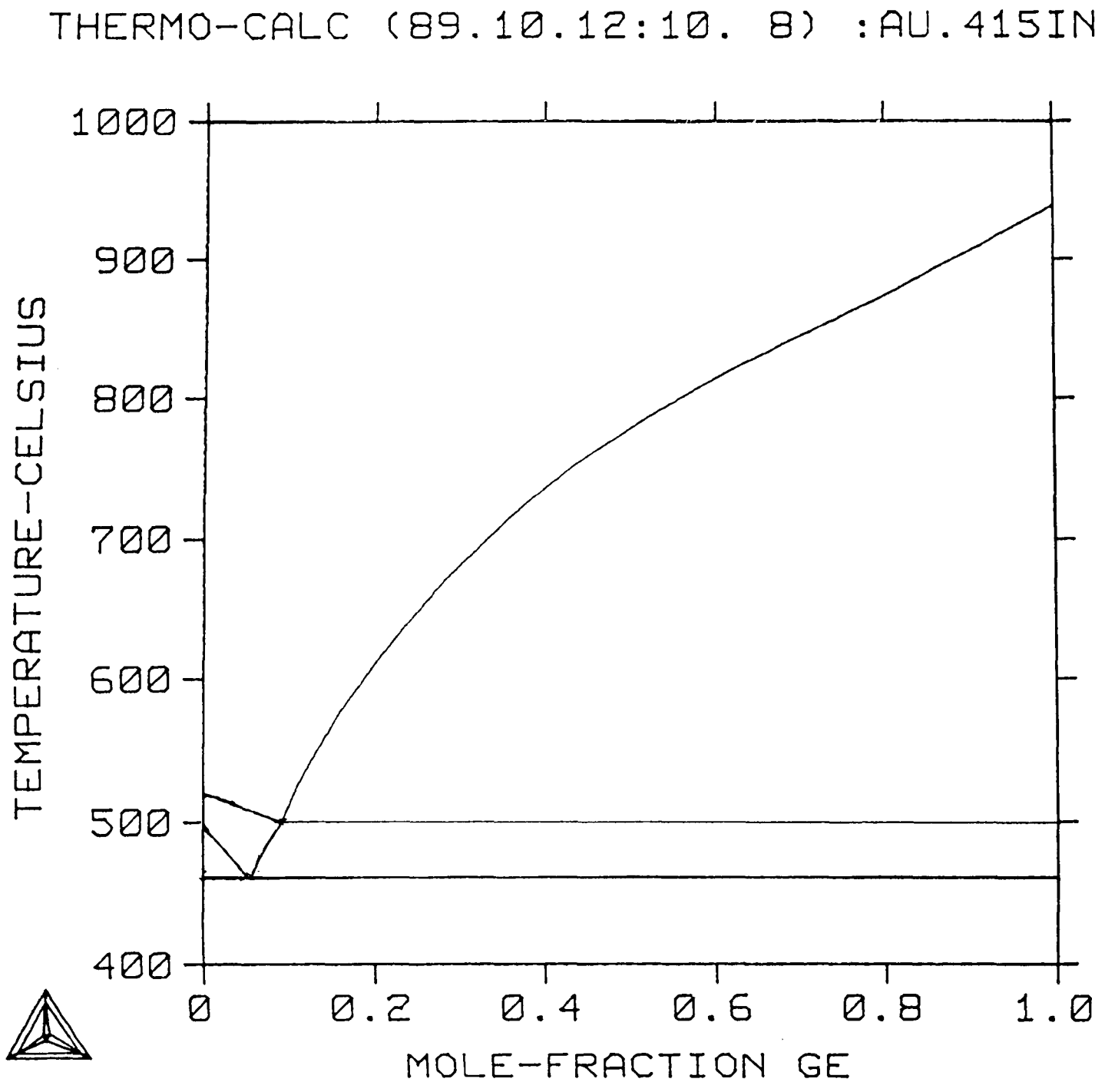

Fig 6.30:-Thermodynamically computed results for the $Au_{41.5}In_{58.5}$ to Ge isopleth.

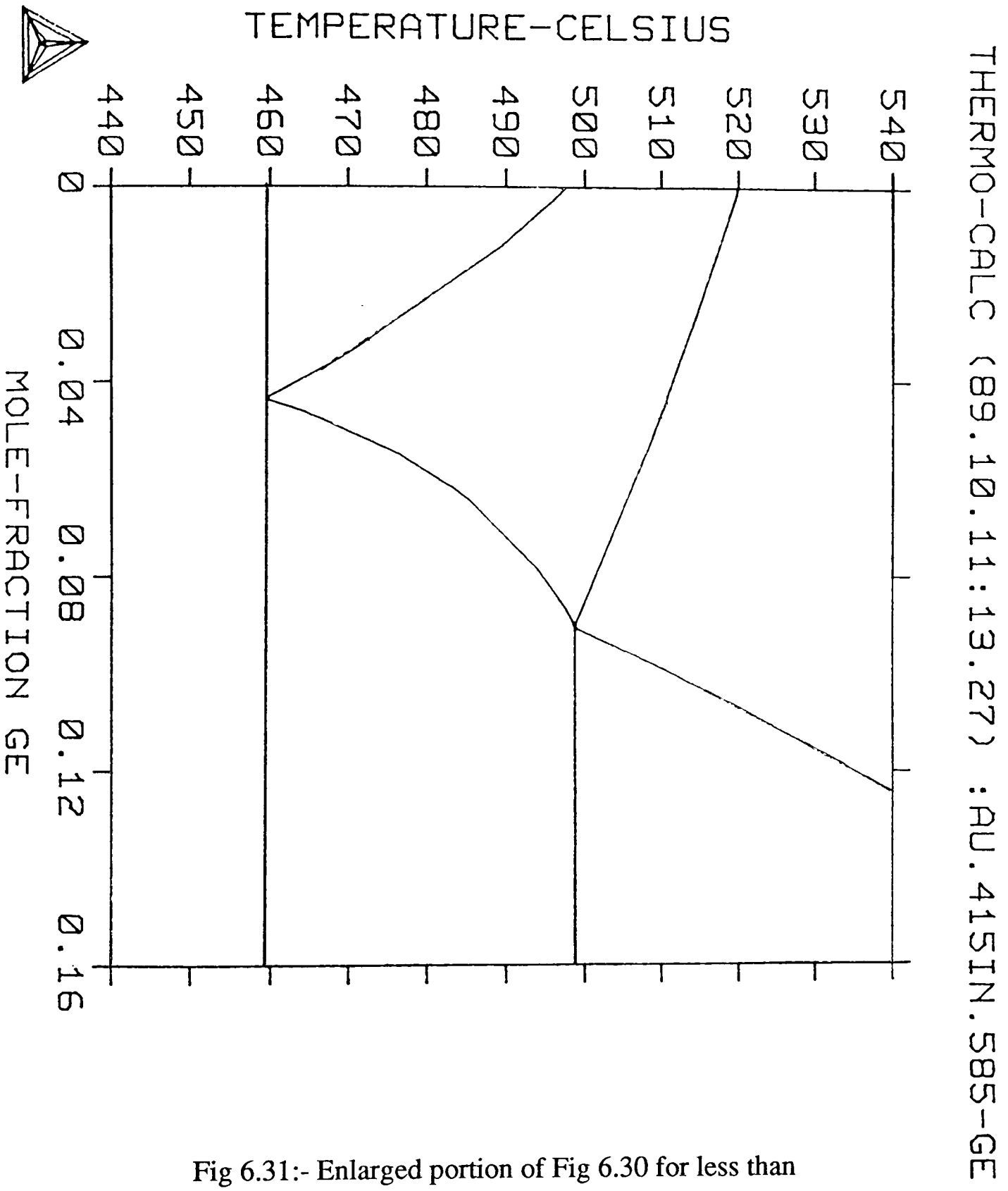

Fig 6.31:- Enlarged portion of Fig 6.30 for less than 16.0 at.% Ge contents.

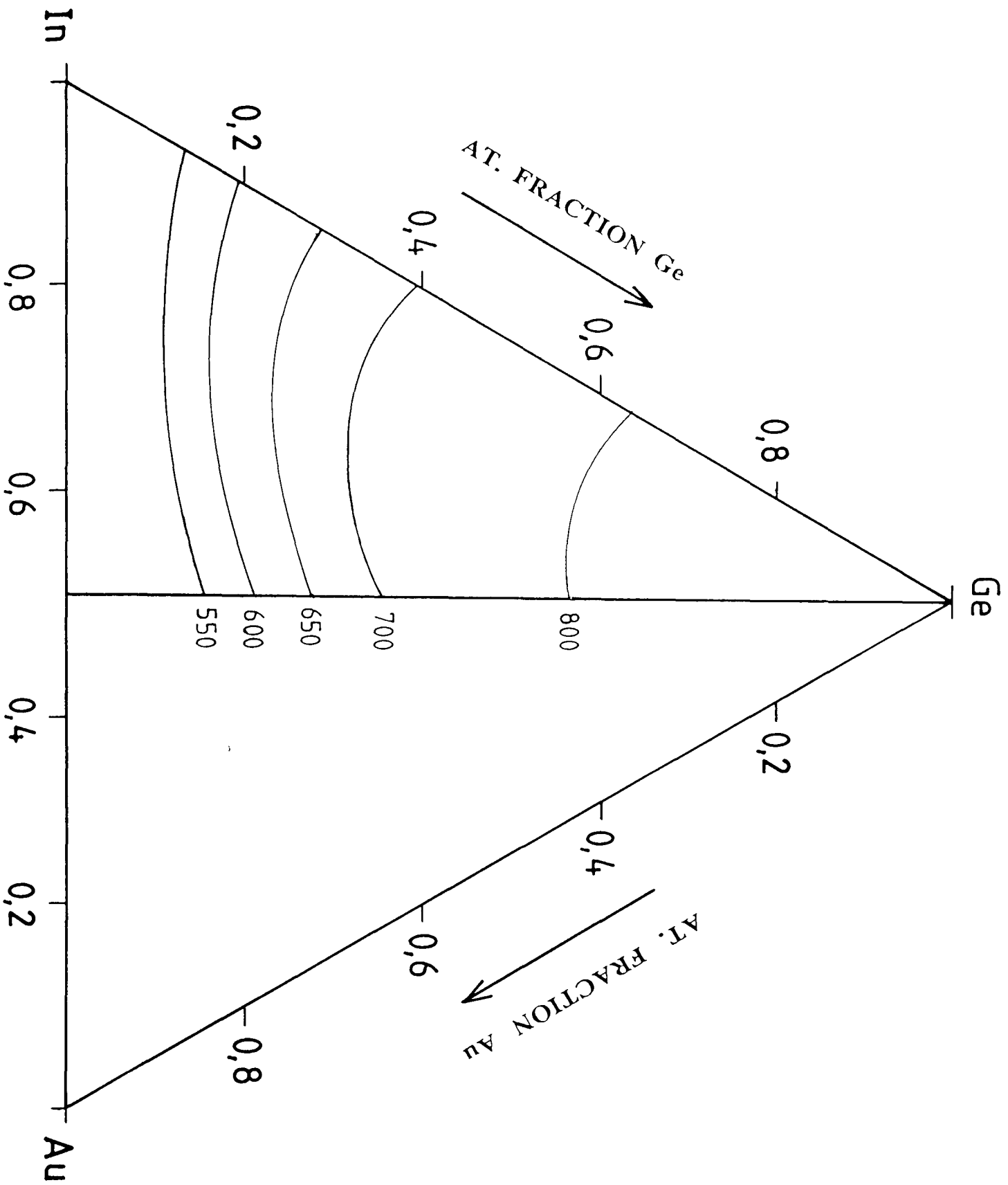

Fig 6.32(a):- Computed isotherms for AuIn-In-Ge partial ternary system at various temperatures.

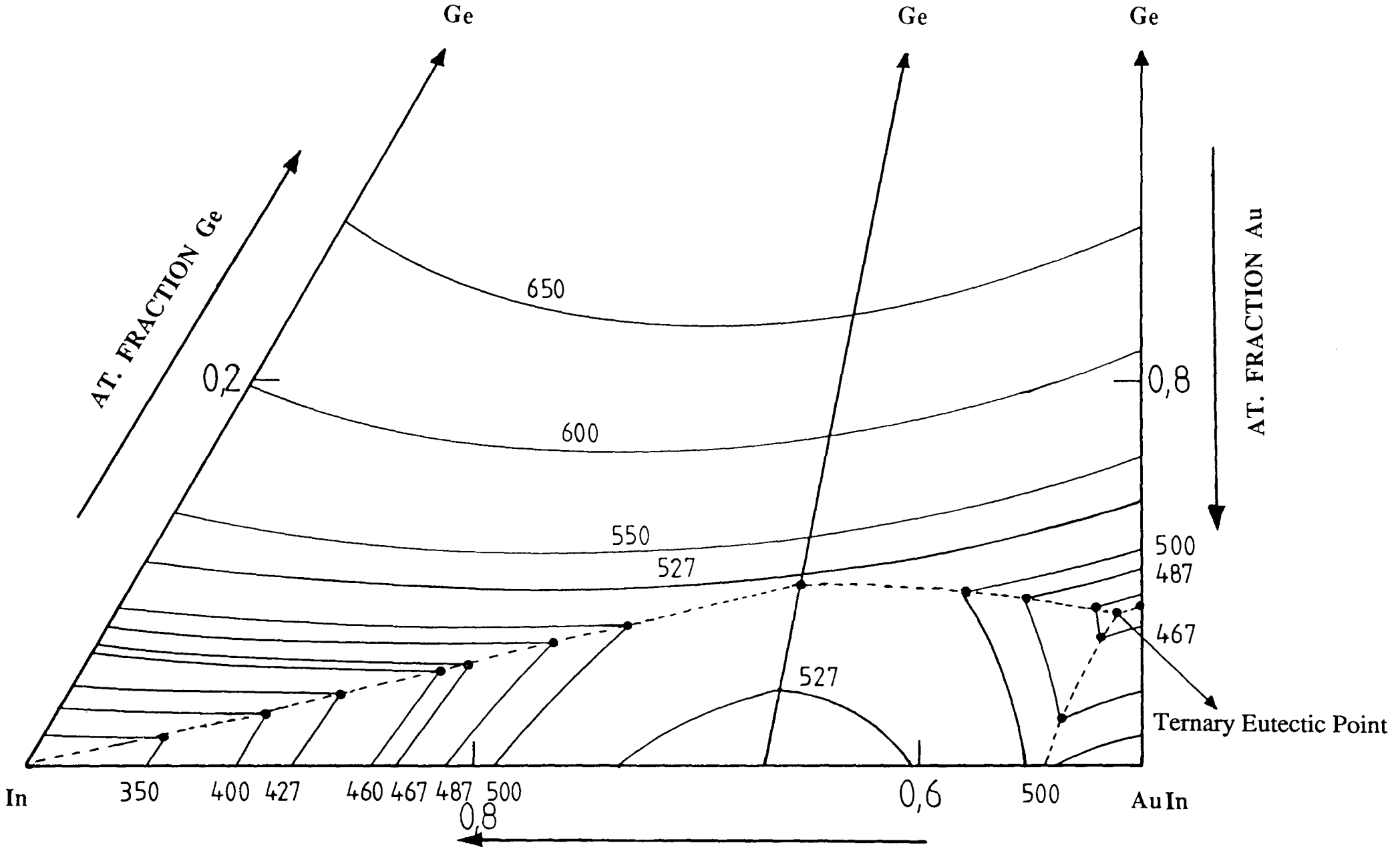

Fig 6.32(b):- Computed isotherms for AuIn-In-Ge partial ternary system at various temperatures.

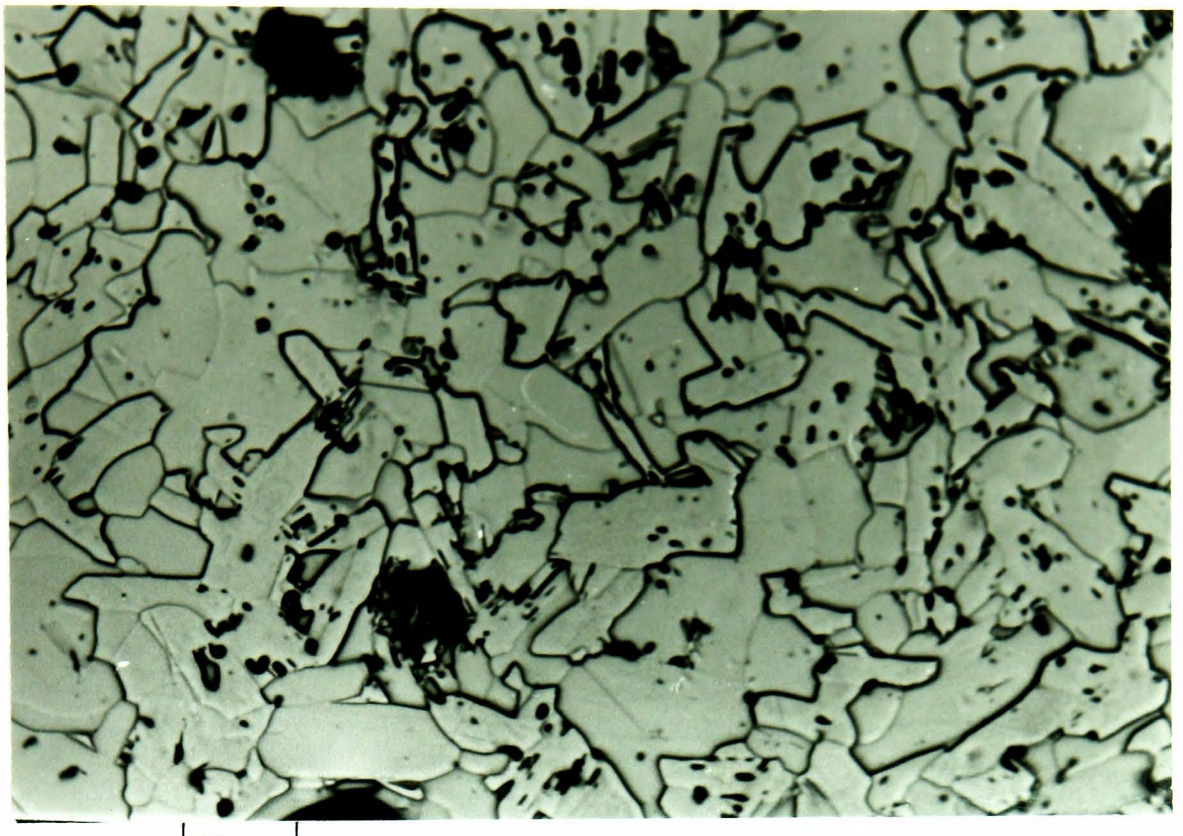

(X 100)

Fig 6.33:-

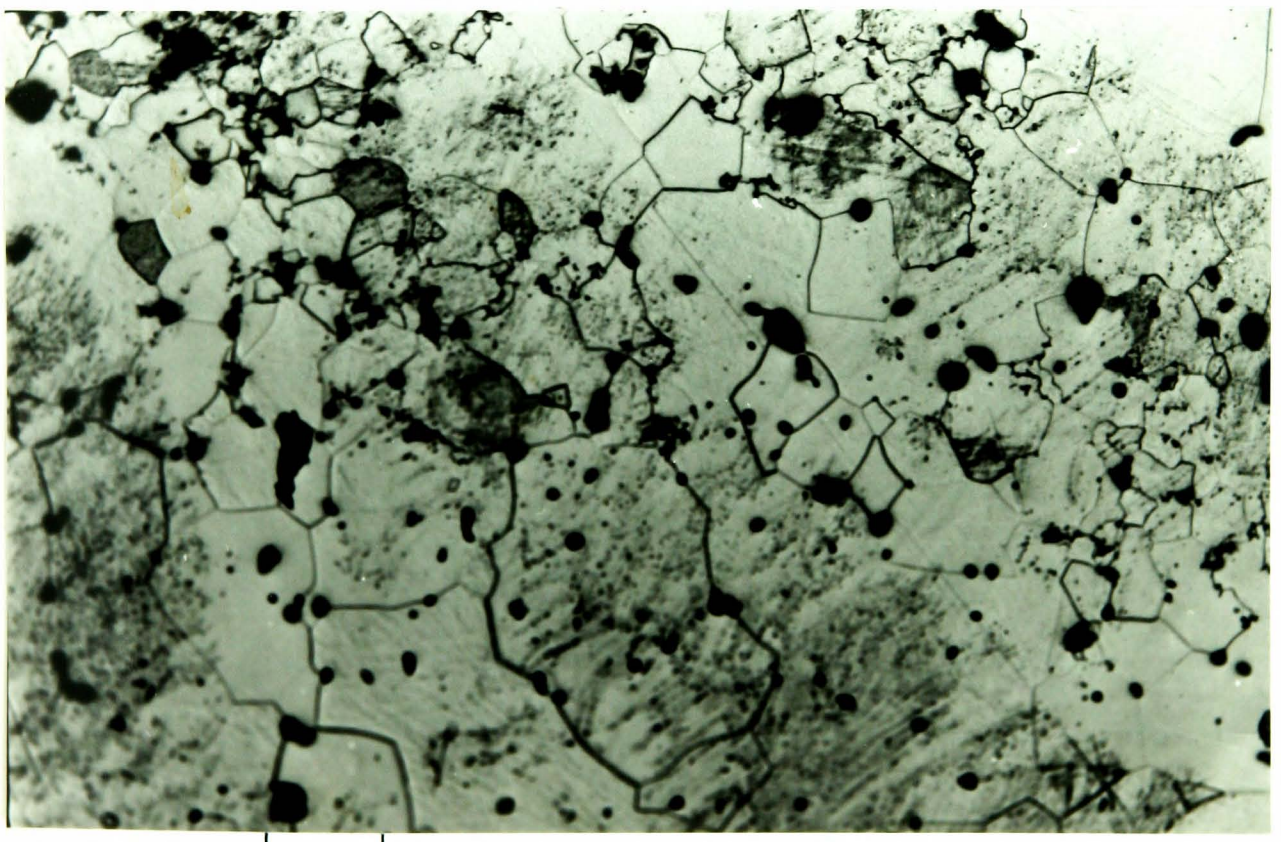

(X 100)

Fig 6.34:-

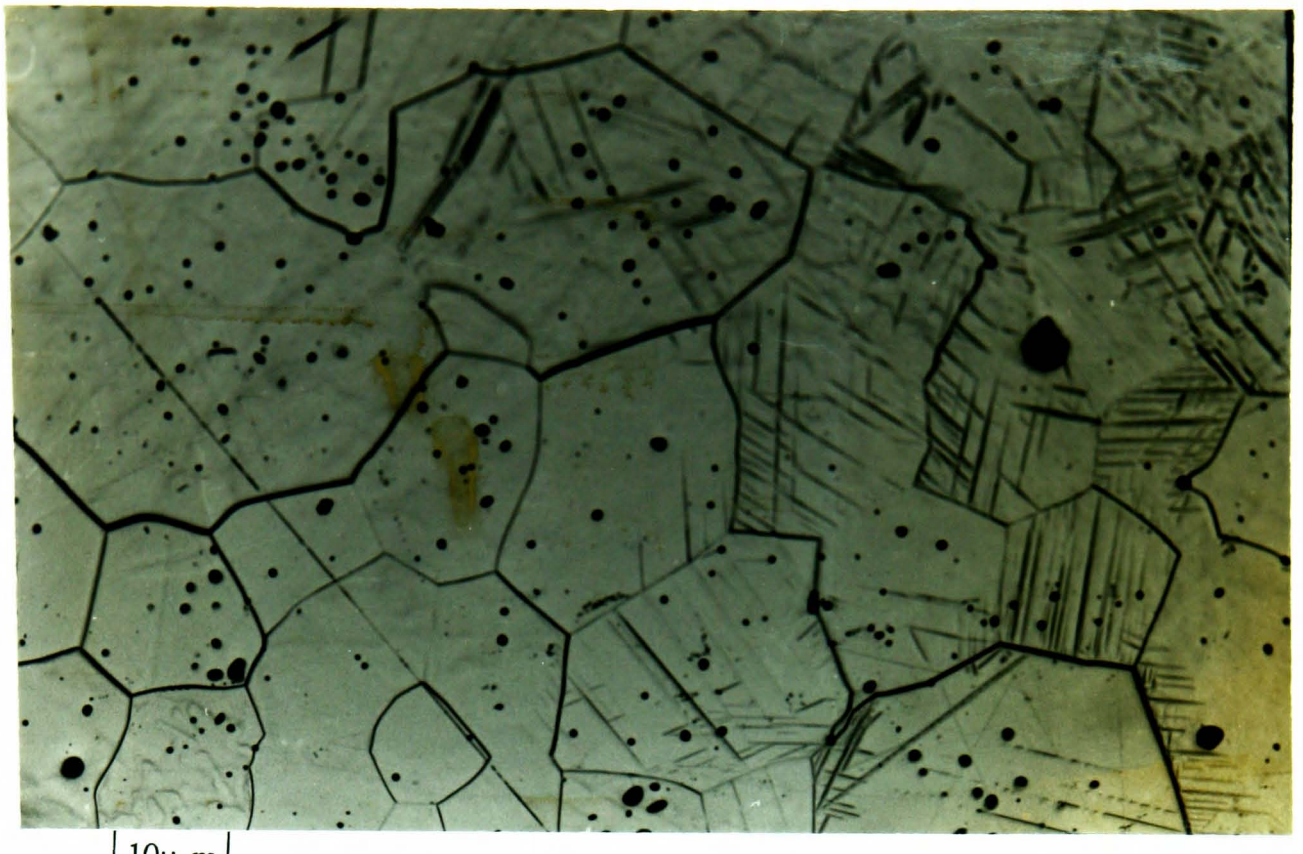

(X 100)

Fig 6.35:-

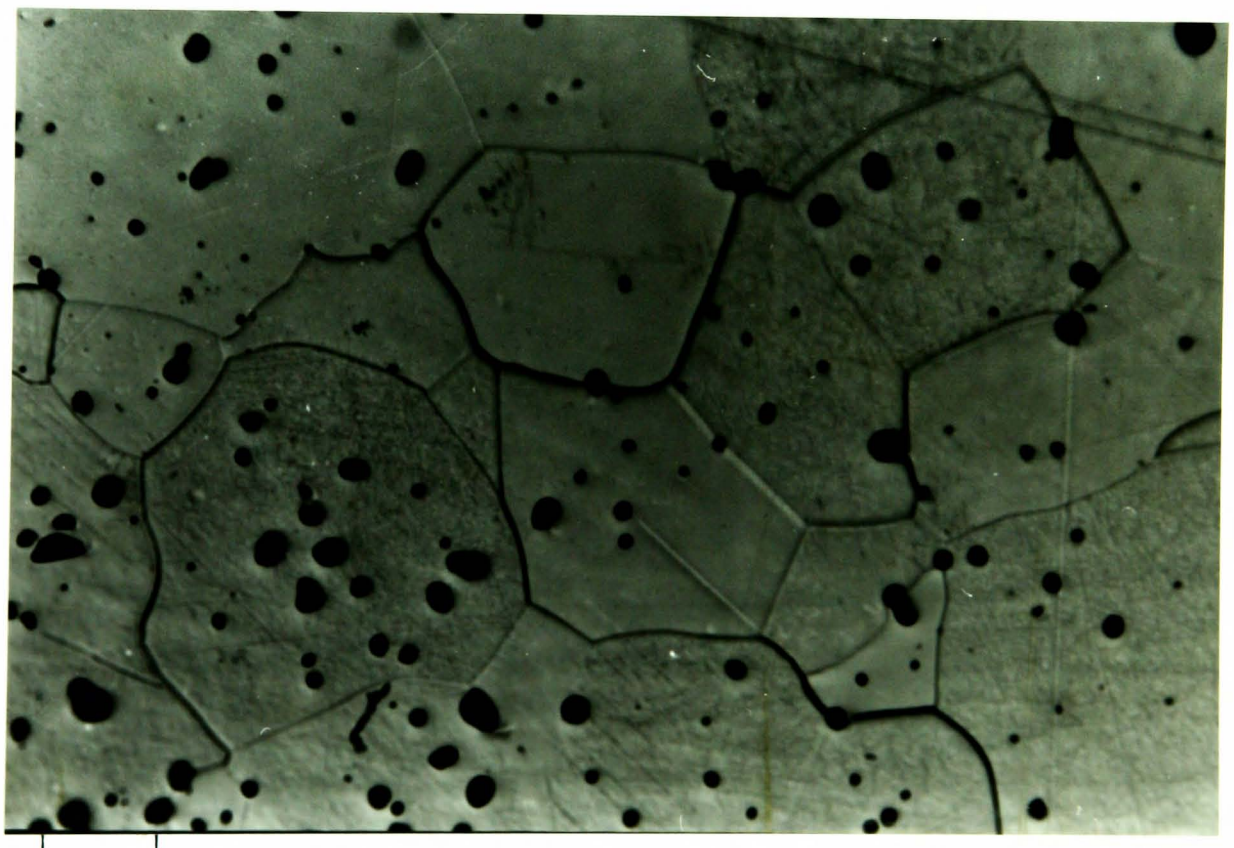

(X 100)

Fig 6.36:-

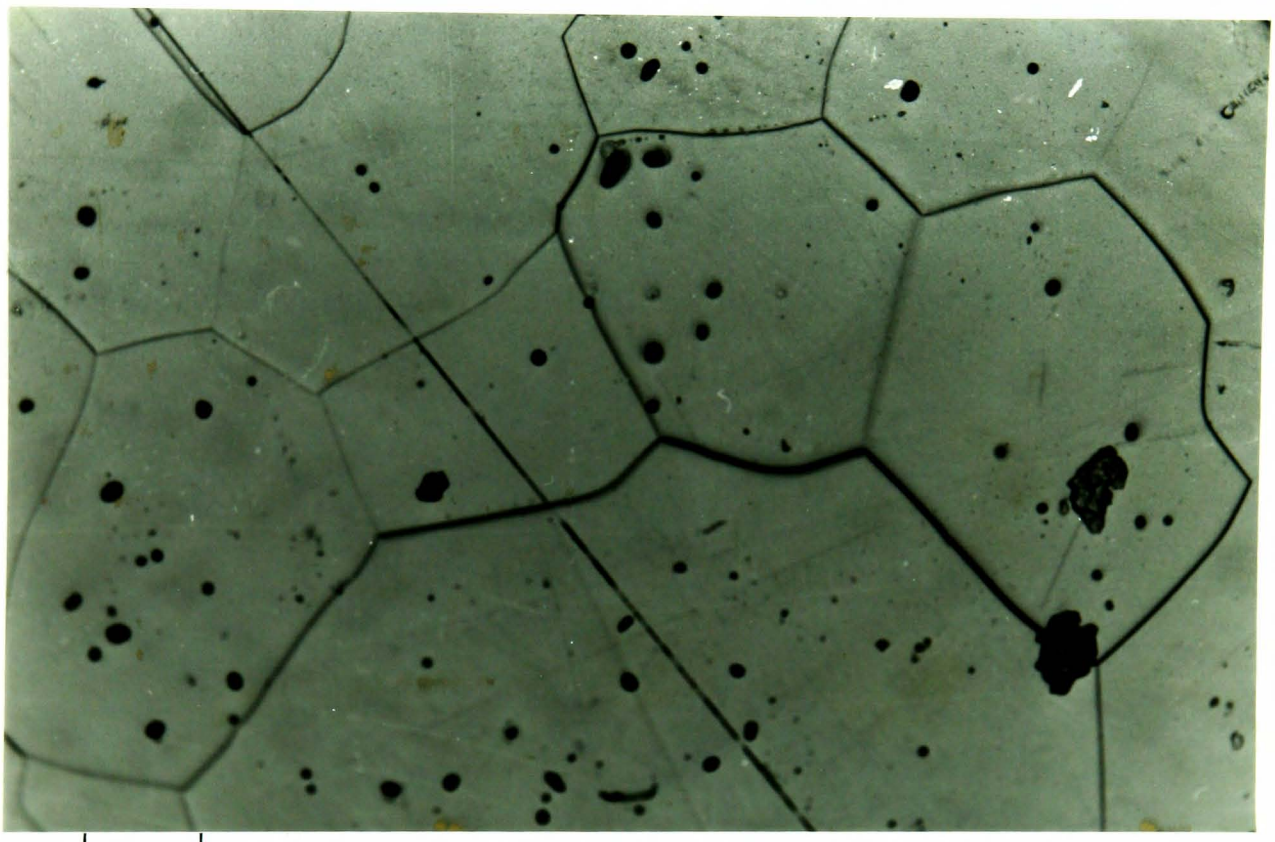

10μ m

(X 200)

Fig 6.37:-

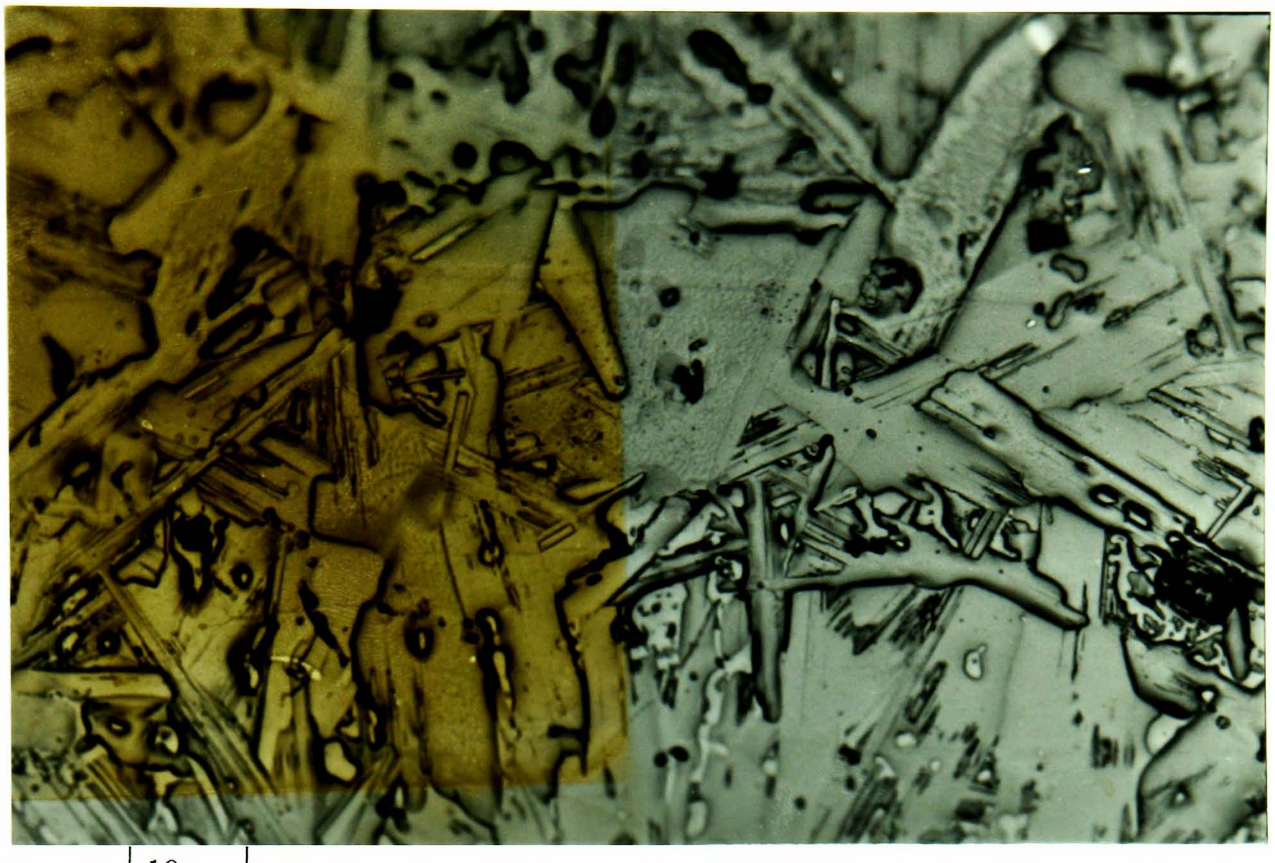

10μ m

(X 100)

Fig 6.38:-

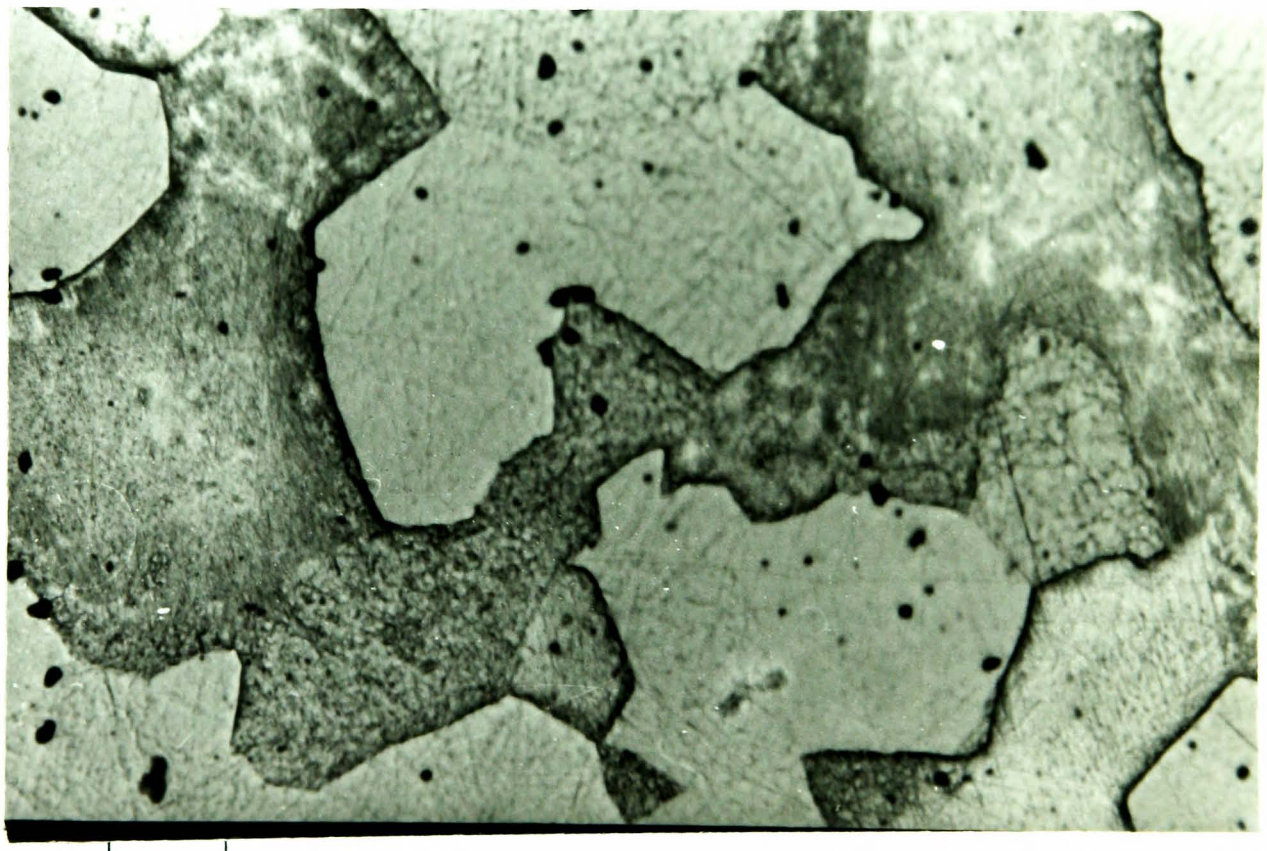

10μ m

(X 100)

Fig 6.39:-

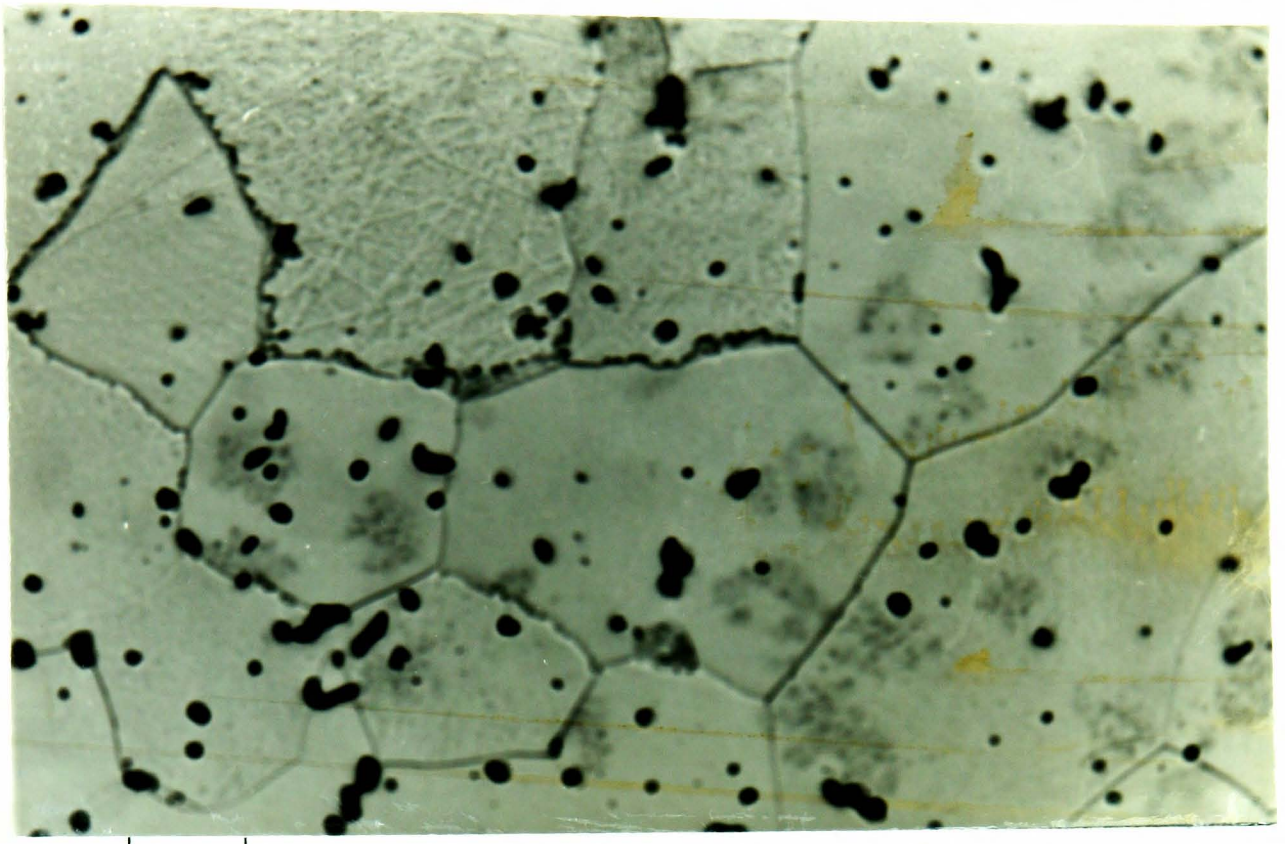

(X 100)

Fig 6.40:-

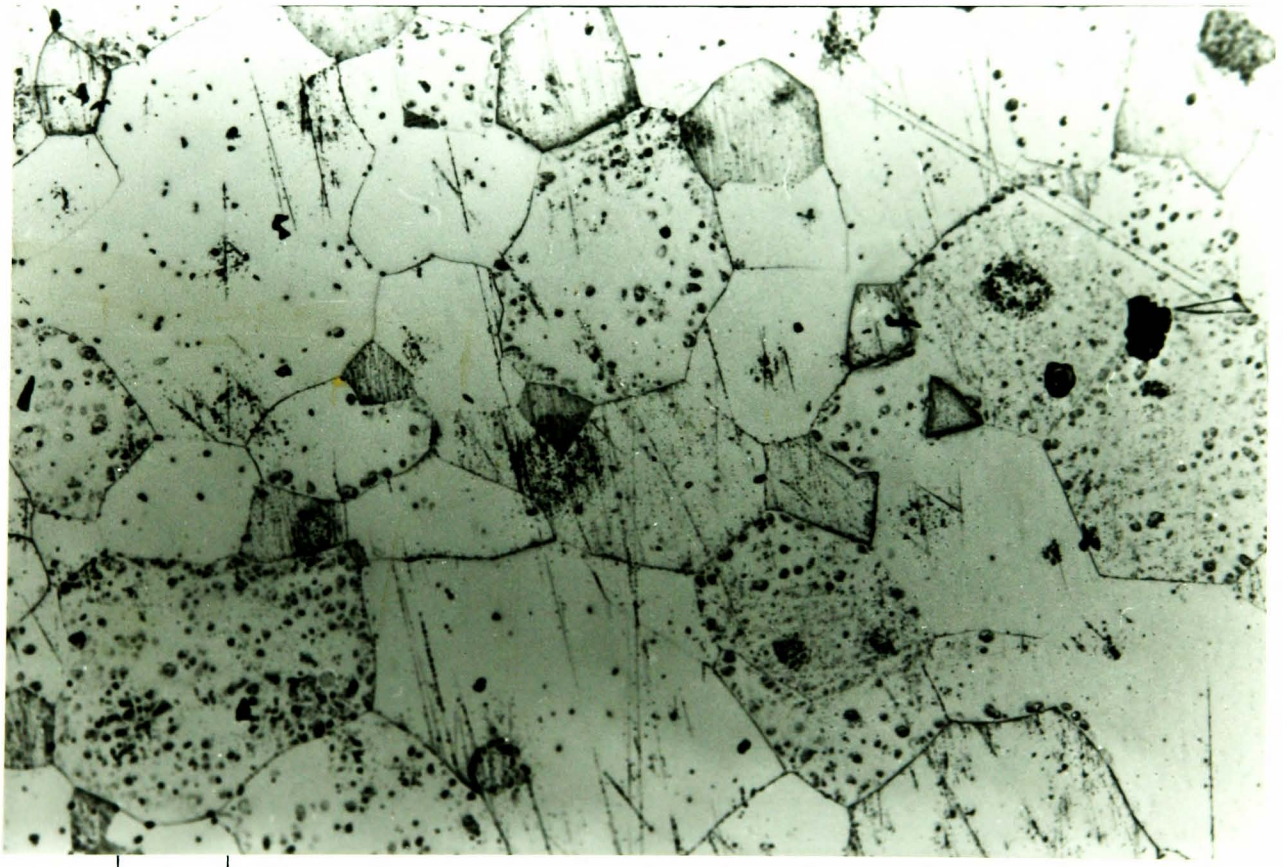

(X 100)

Fig 6.41:-

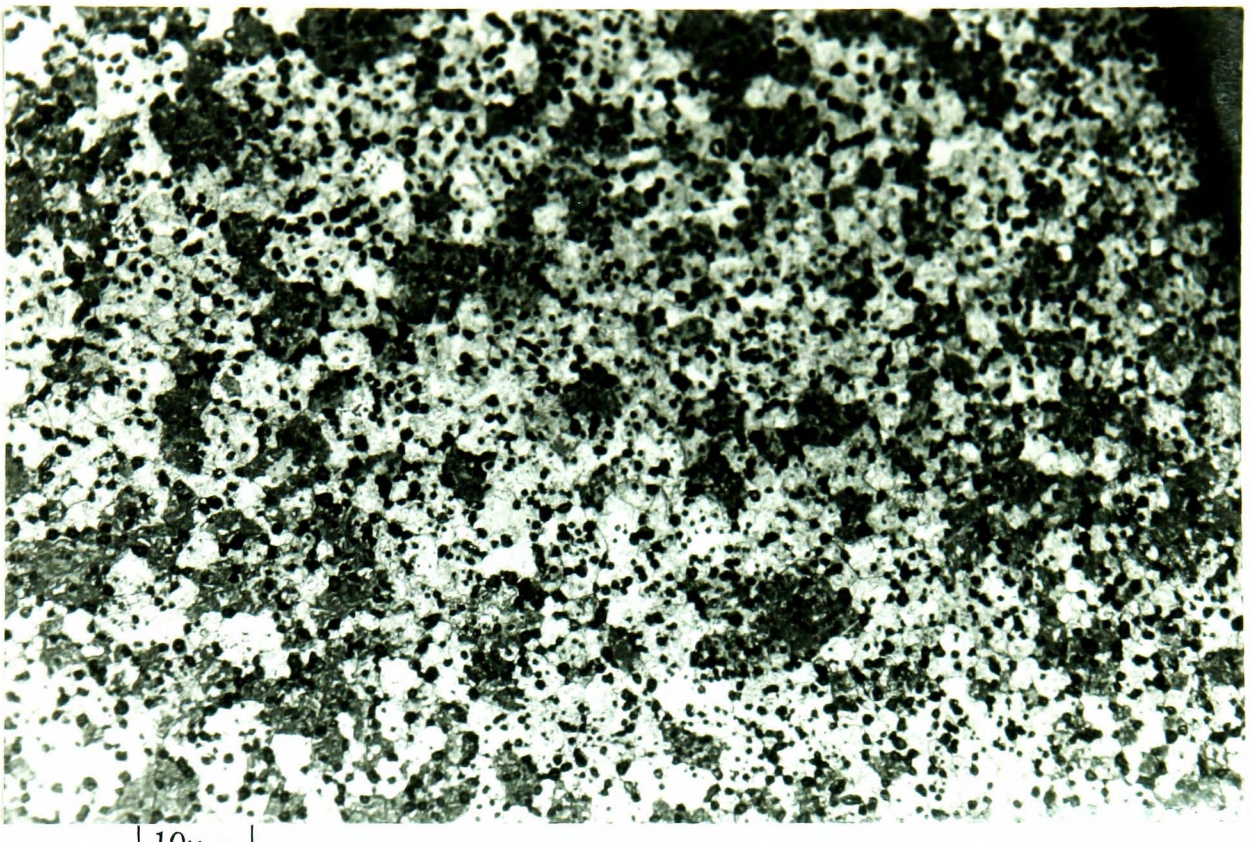

(X 100)

Fig 6.42:-

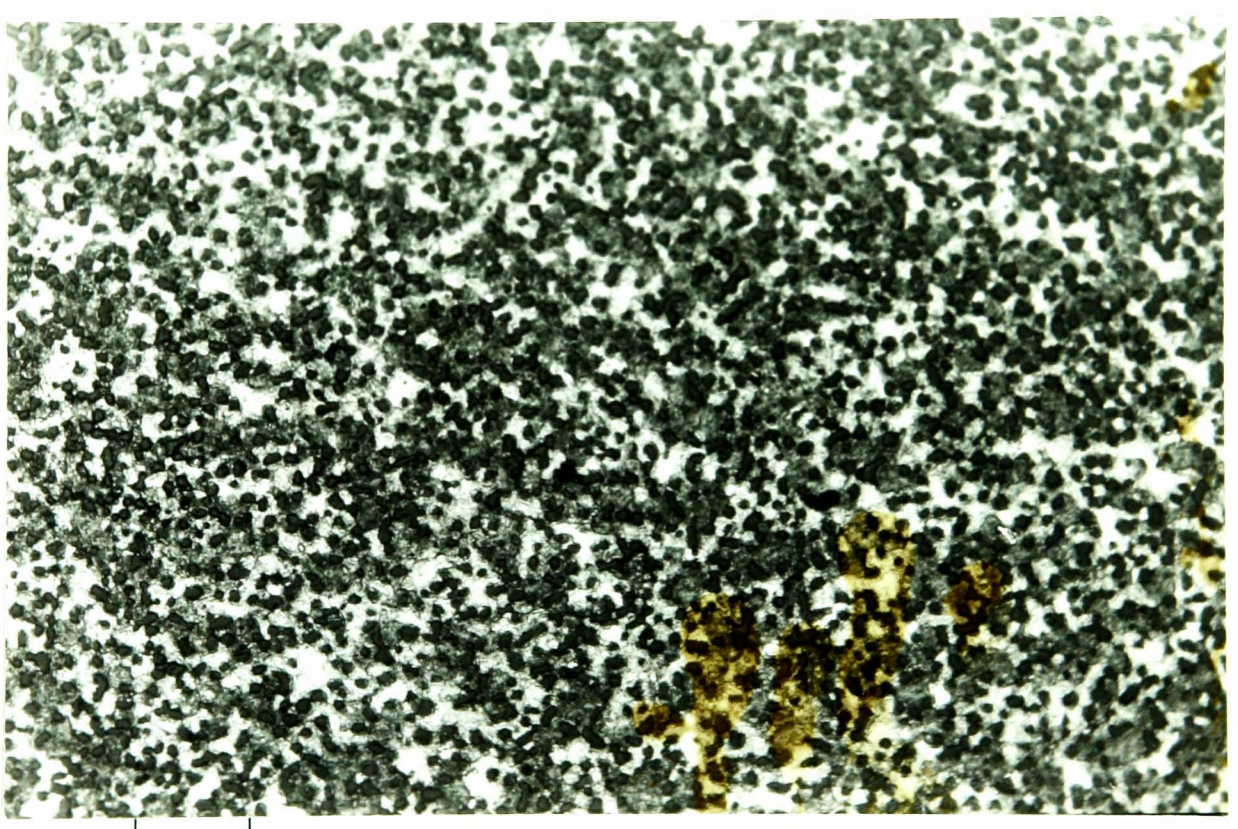

(X 100)

Fig 6.43:-

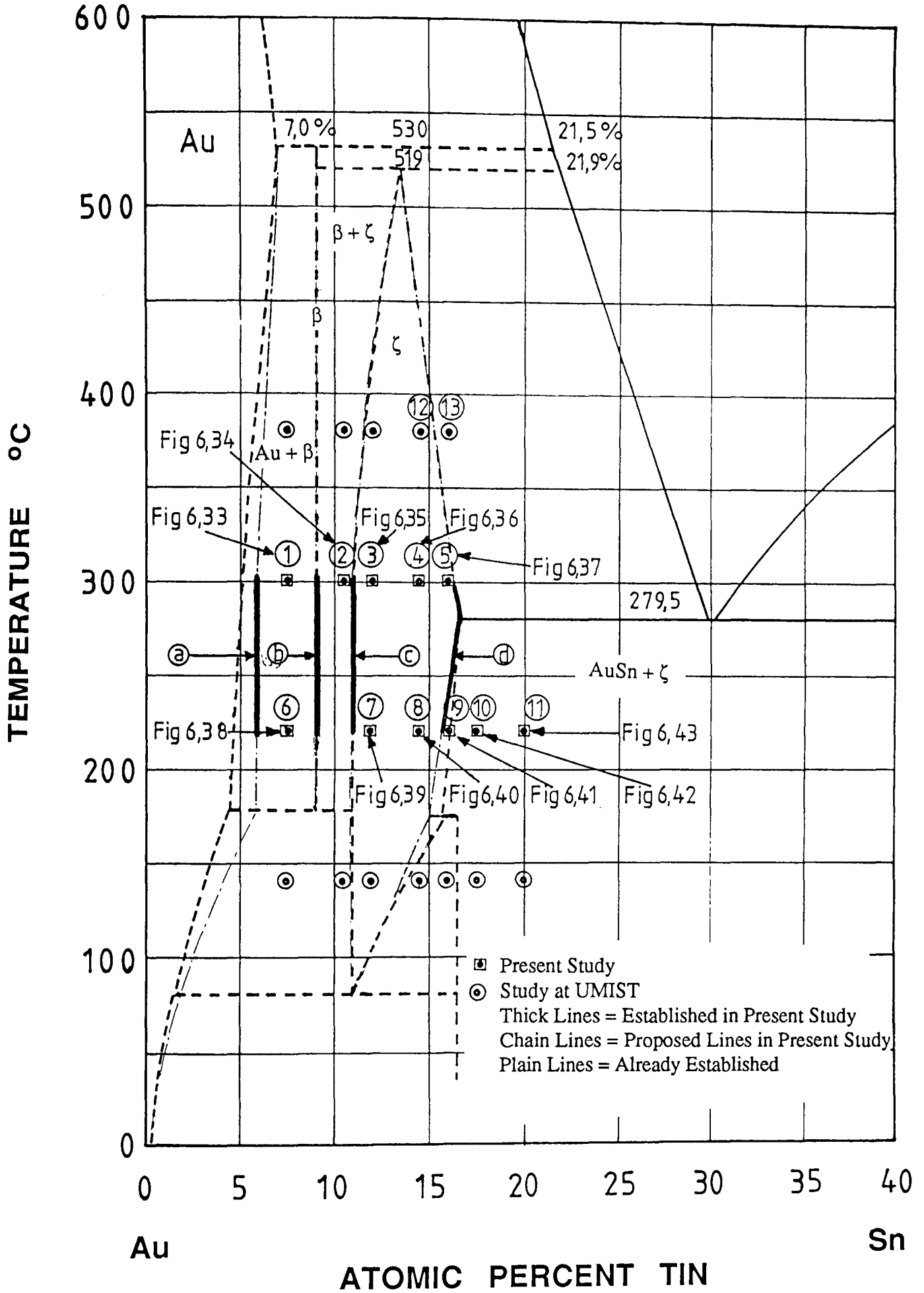

Fig 6.44:- The amended low-temperature region of the Au-rich portion of the Au-Sn binary phase diagram after long term heat treatment at 220 °C and 300 °C.

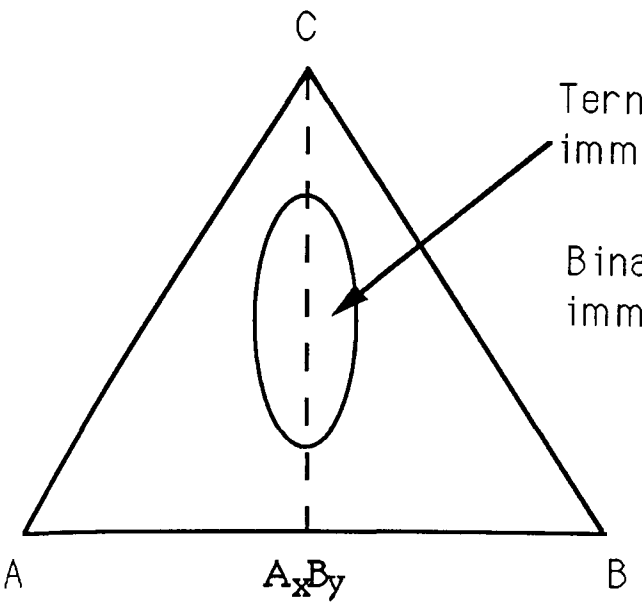

Fig 7.1(a)

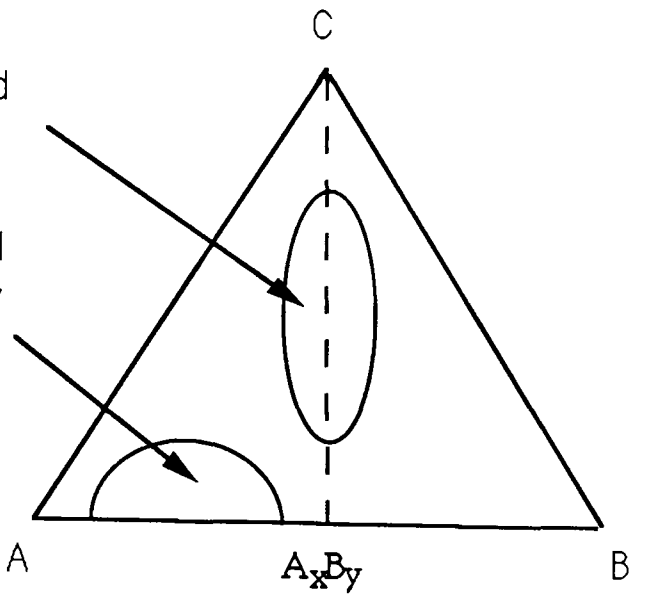

Fig 7.1(b)

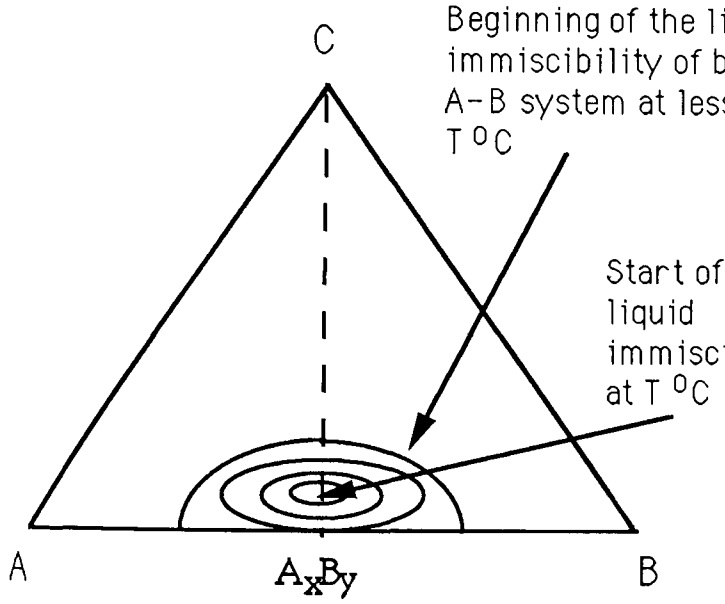

Fig 7.1(c)

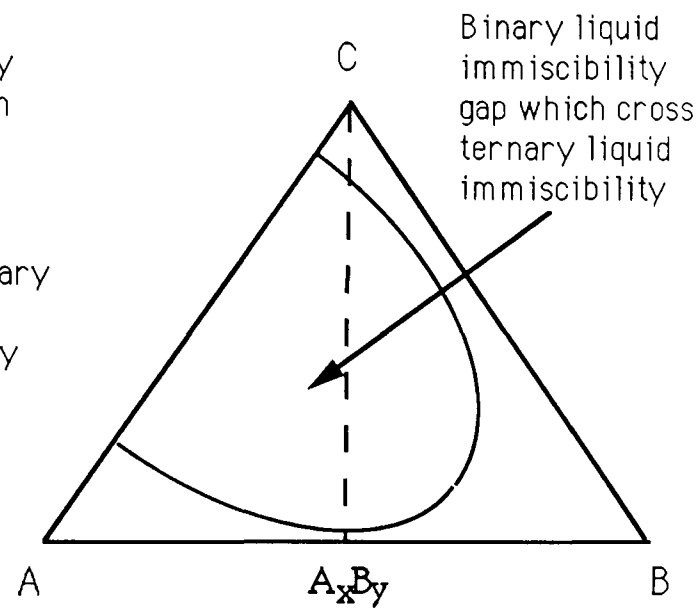

Fig 7.1(d)

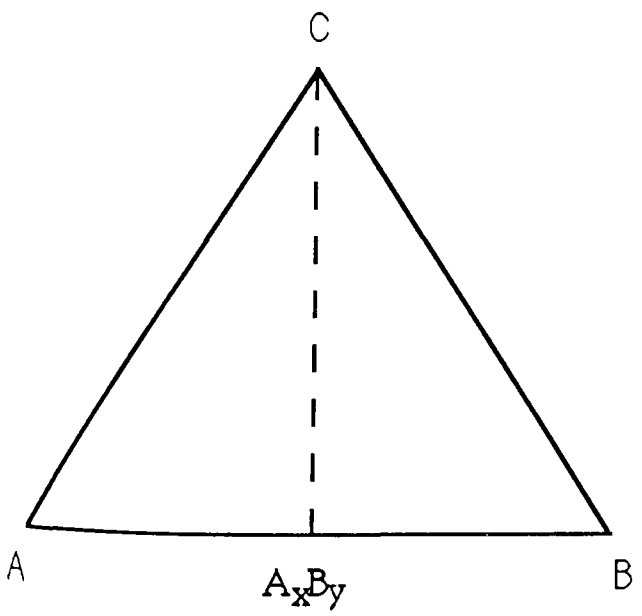

Fig 7.2(a)

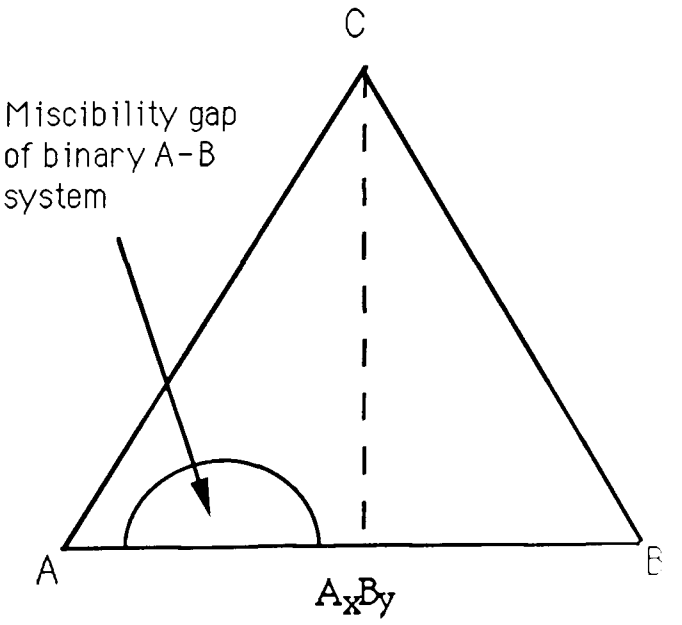

Fig 7.2(b)

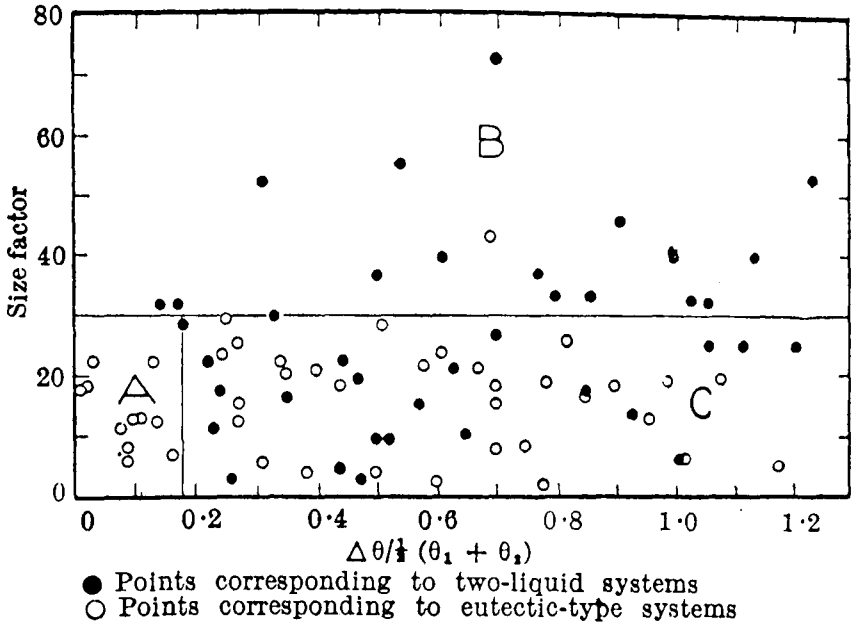

Fig 7.3:- The diagram for liquid immiscibility and eutectic type metallic systems (104).

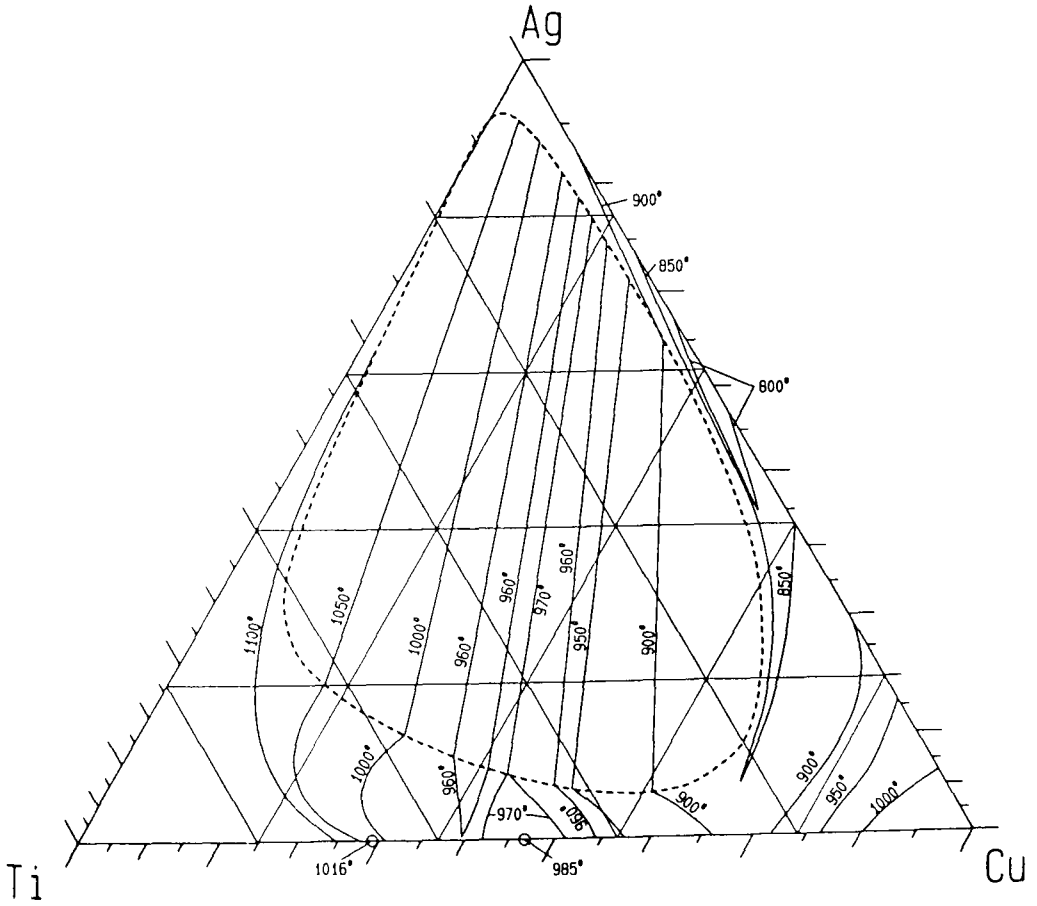

Fig 7.4:- Liquidus Projection of Ag-Cu-Ti Ternary System.

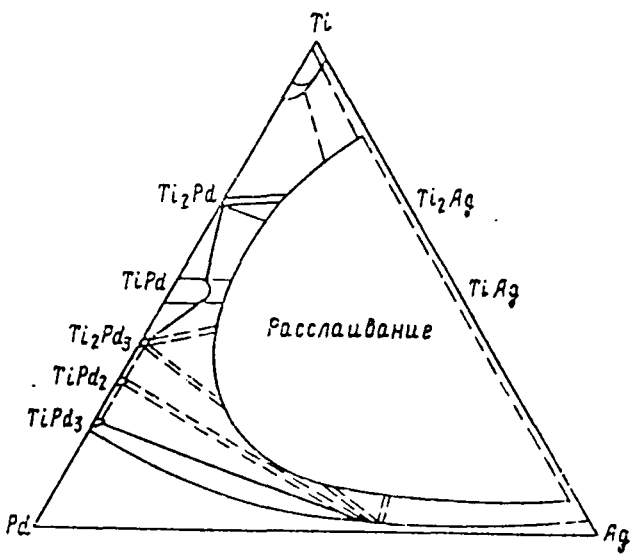

Fig 7.5:- Liquidus Projection of Ag-Pd-Ti Ternary System.

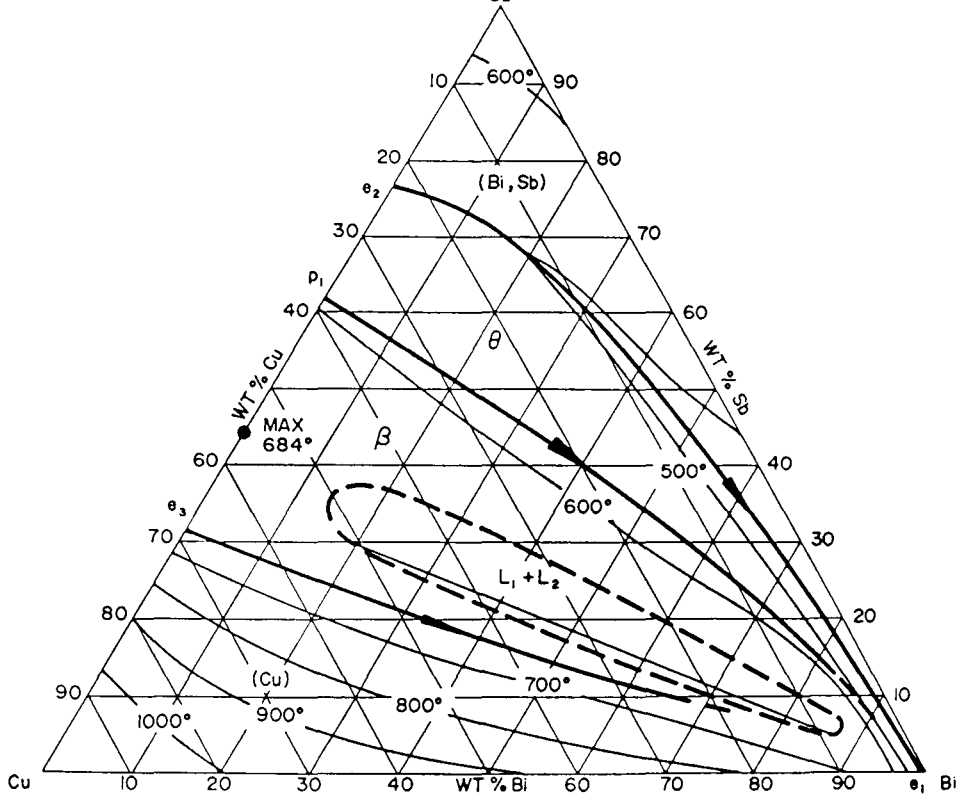

Fig 7.6:- Liquidus Projection of Cu-Bi-Sb Ternary System.

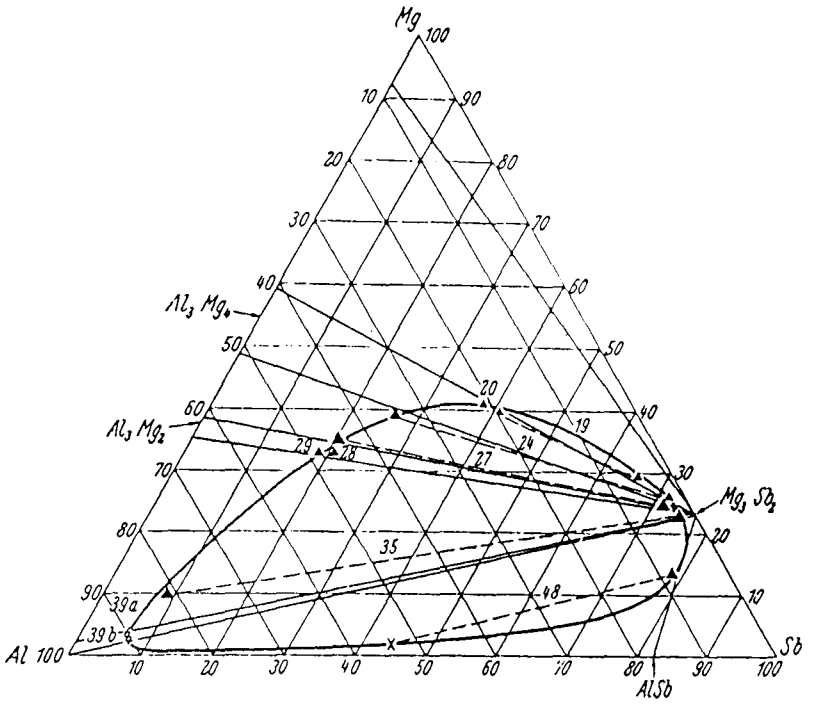

Fig 7.7:- Liquidus Projection of Mg-Al-Sb Ternary System.

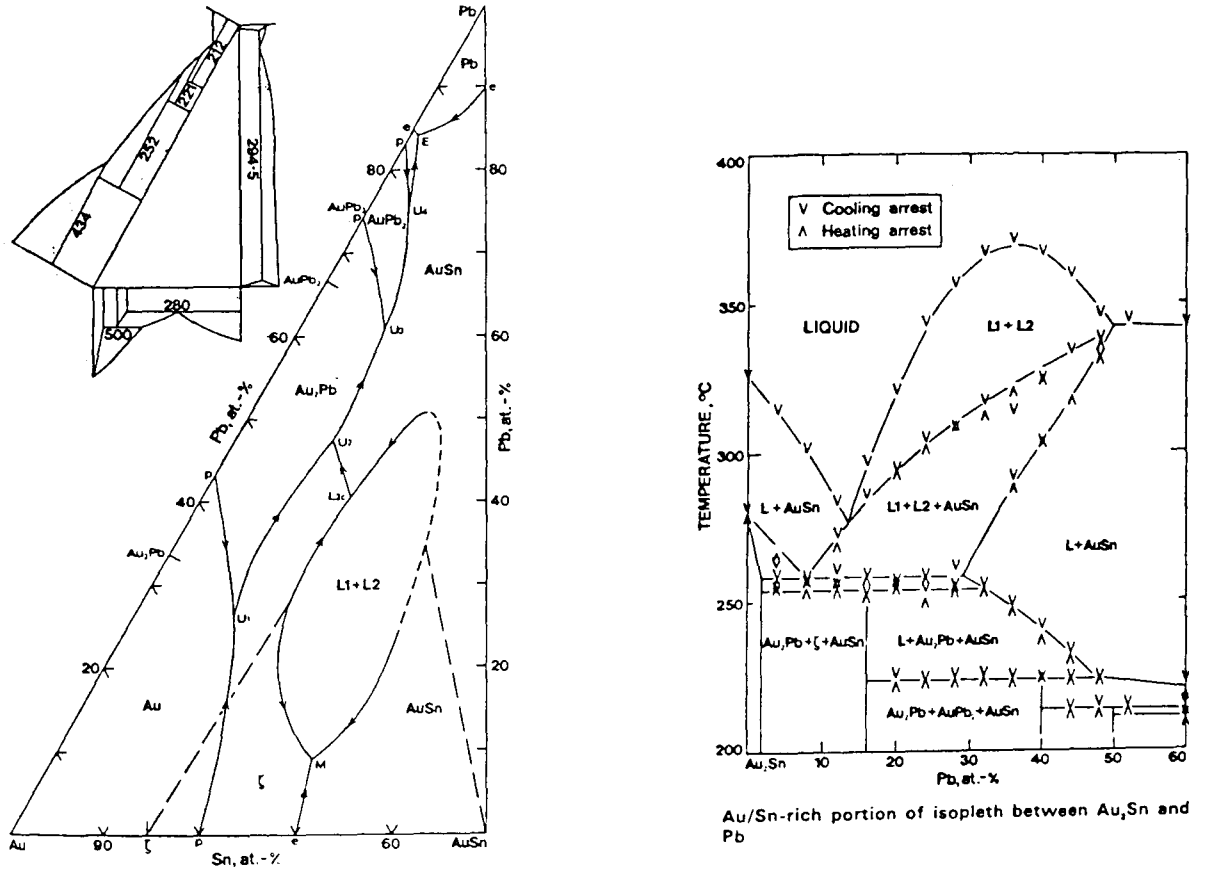

Au/Sn-rich portion of isopleth between Au_3Sn and Pb

Fig 7.8:- Liquidus Projection of Au-Pb-Sn Ternary System.

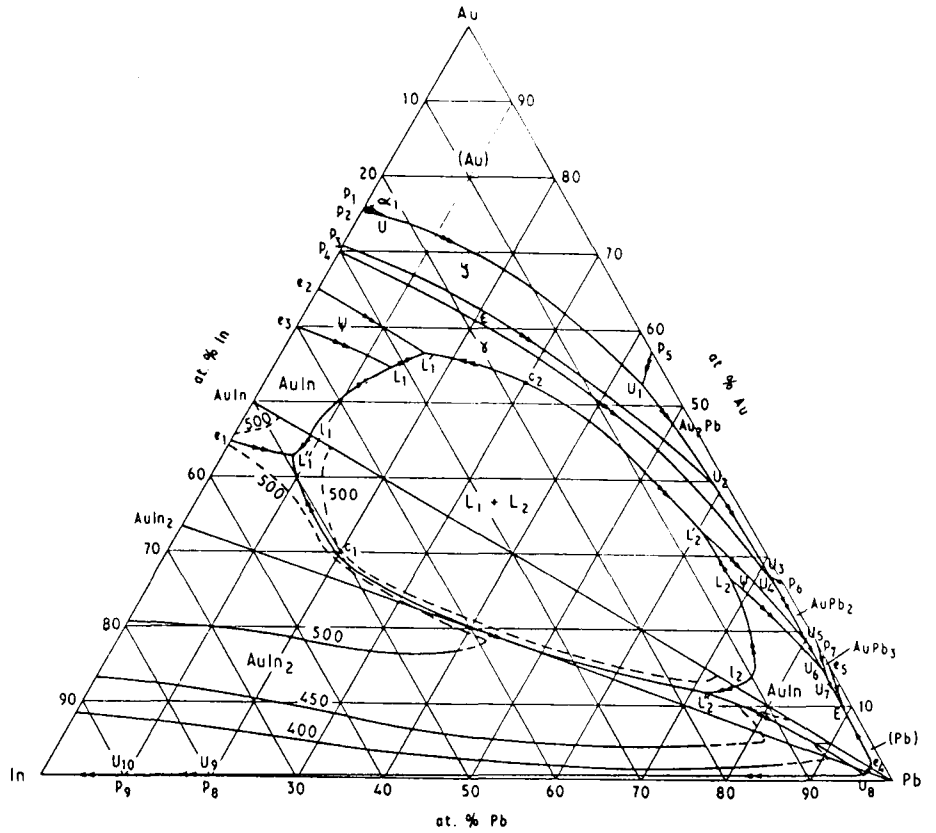

Fig 7.9:- Liquidus Projection of Au-Pb-In Ternary System.

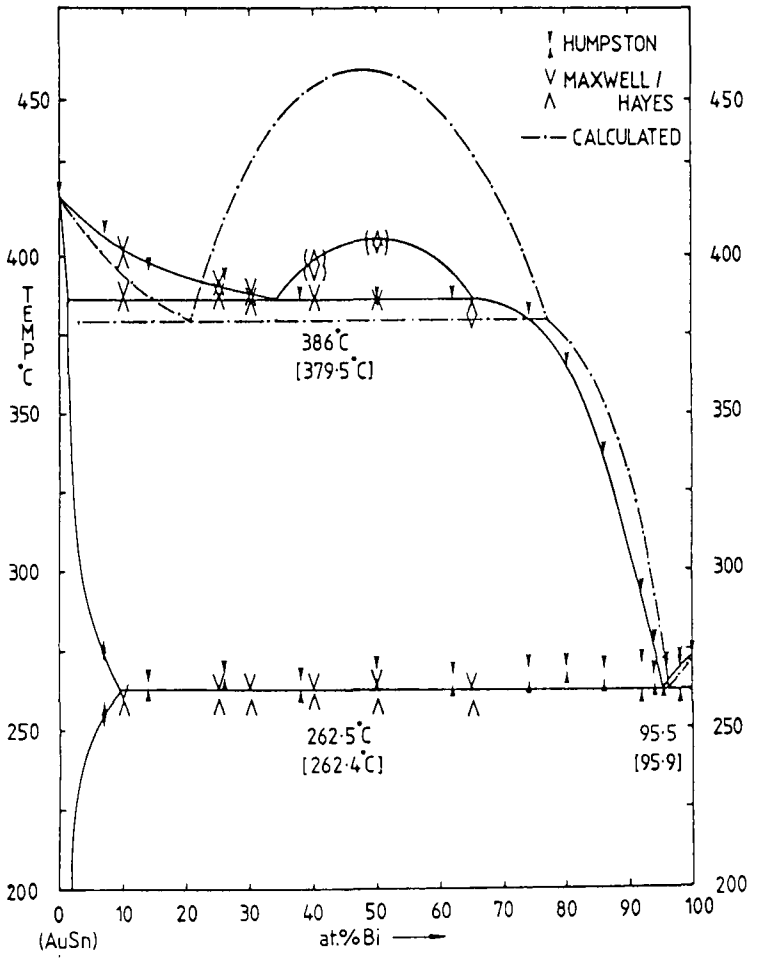

Fig 7.10:- The AuSn-Bi Pseudobinary section showing liquid immiscibility.

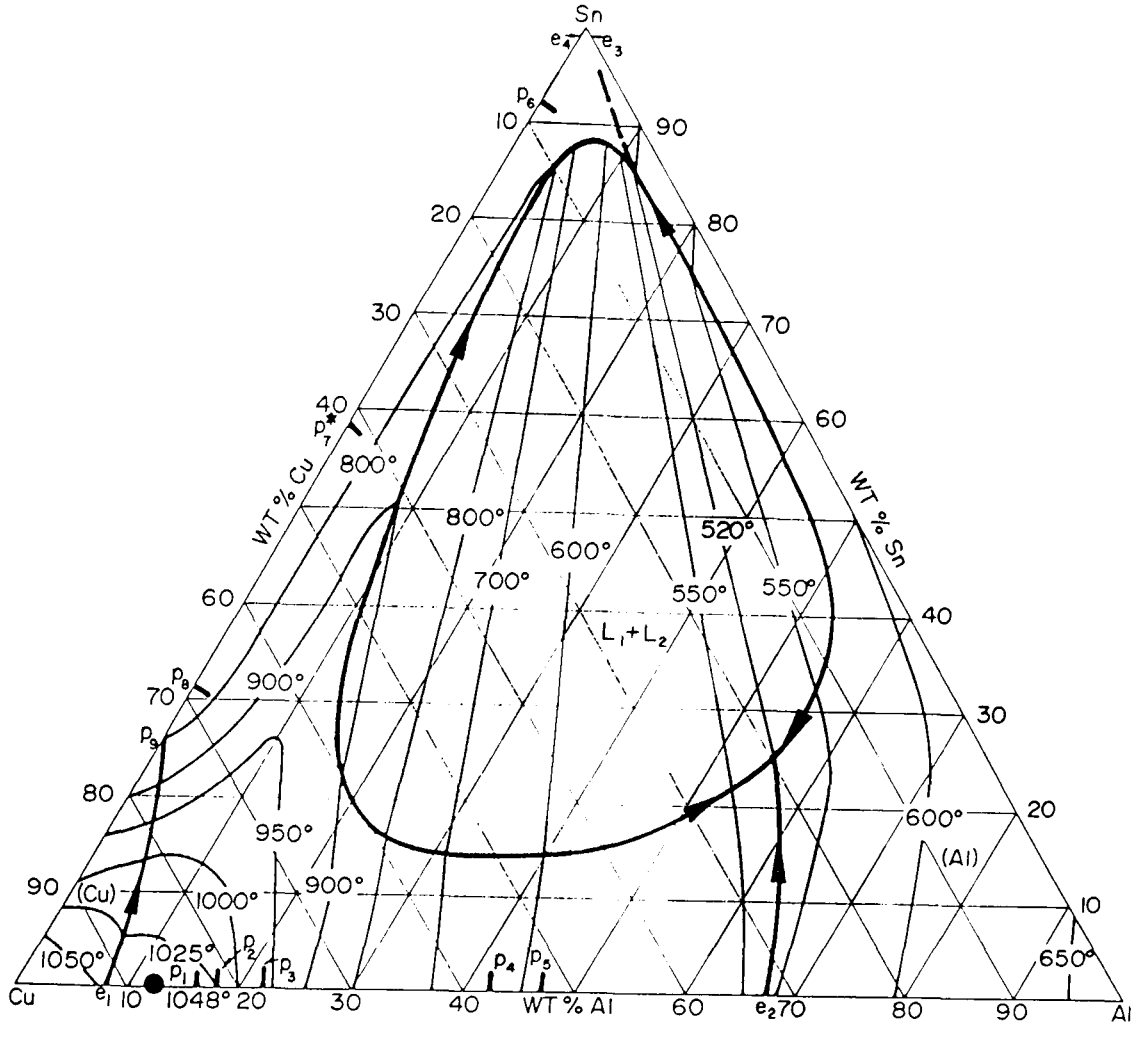

Fig 7.11:- Liquidus Projection of Cu-Al-Sn Ternary System.

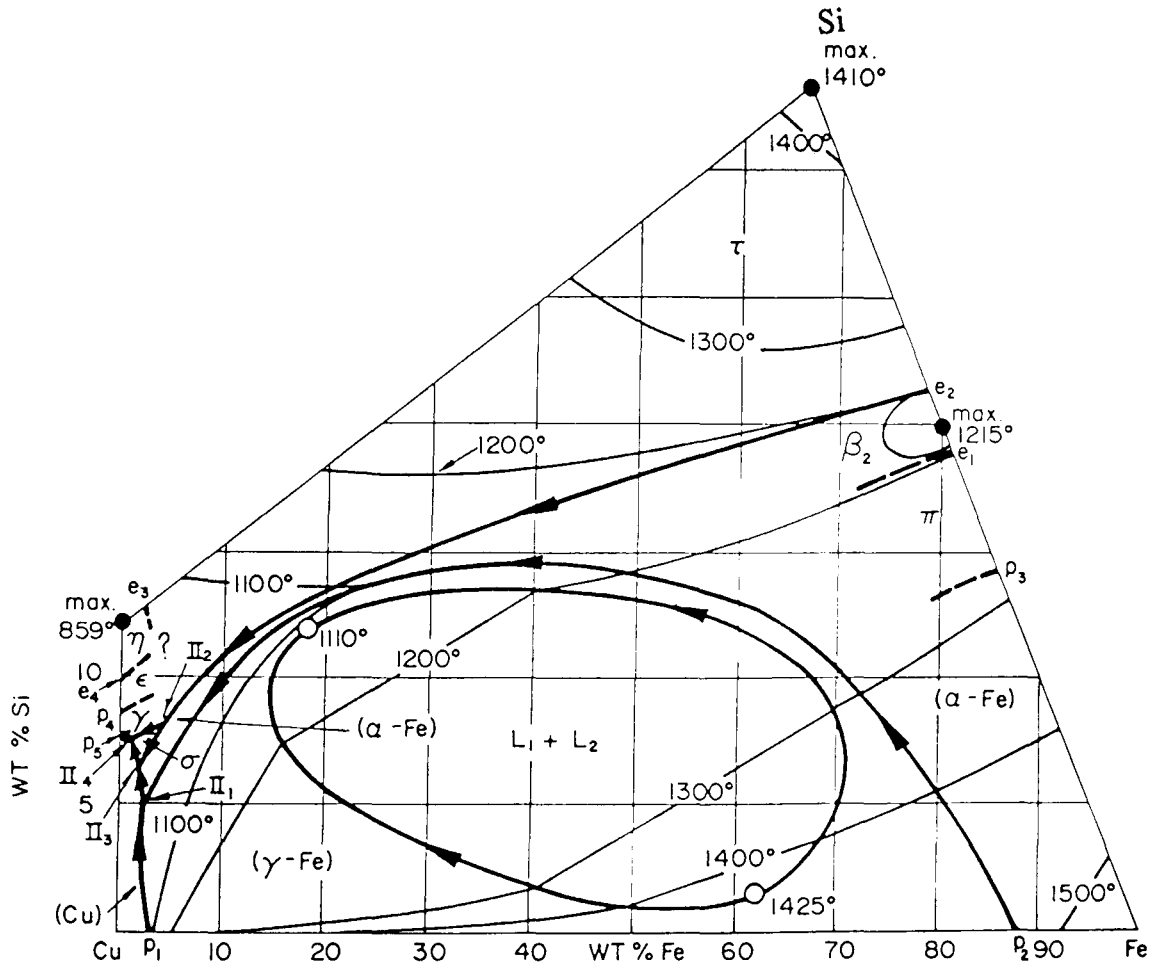

Fig 7.12:- Liquidus Projection of Cu-Fe-Si Ternary System.

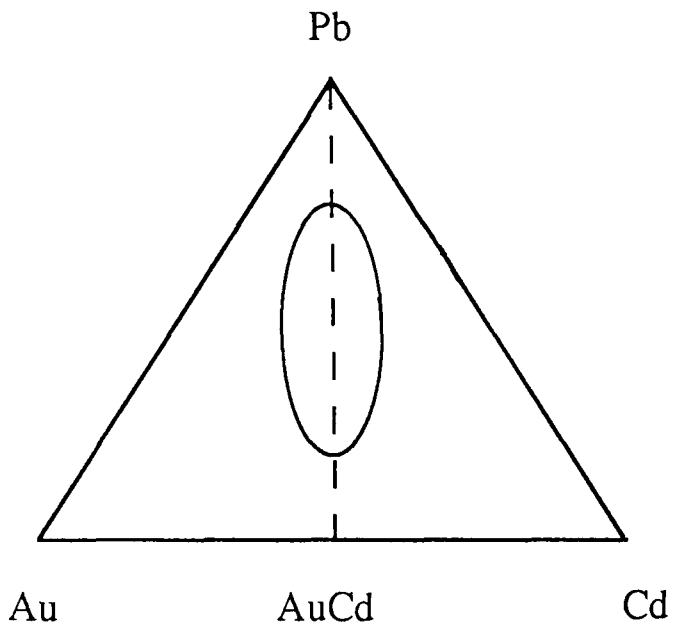

Fig 7.13:- Liquidus Projection of Au-Pb-Cd Ternary System.

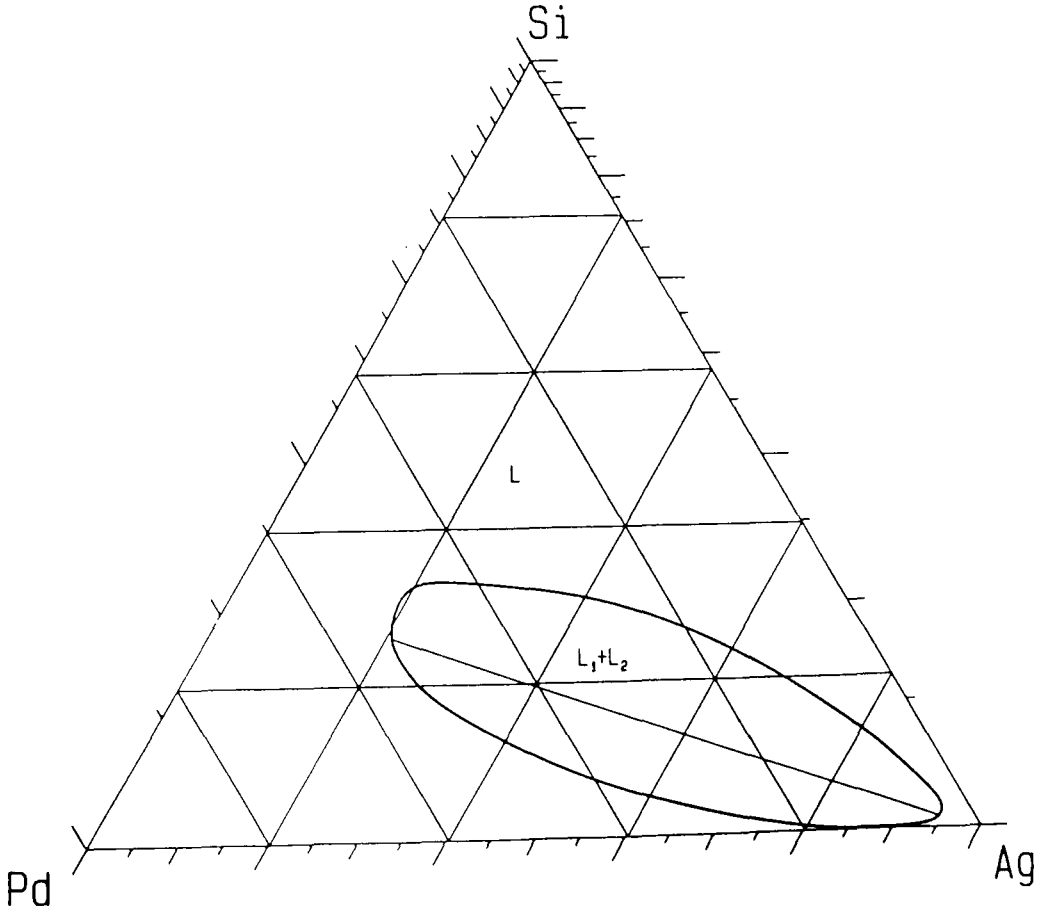

Fig 7.14:- Liquidus Projection of Pd-Si-Ag Ternary System.

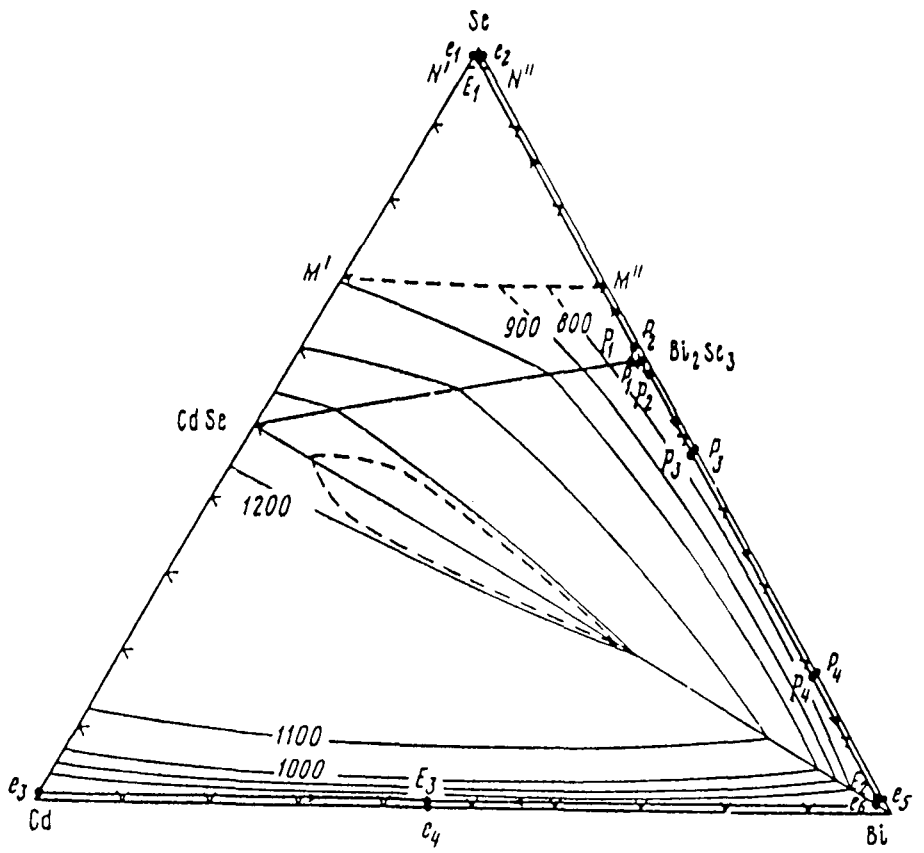

Fig 7.15:- Liquidus Projection of Cd-Bi-Se Ternary System.

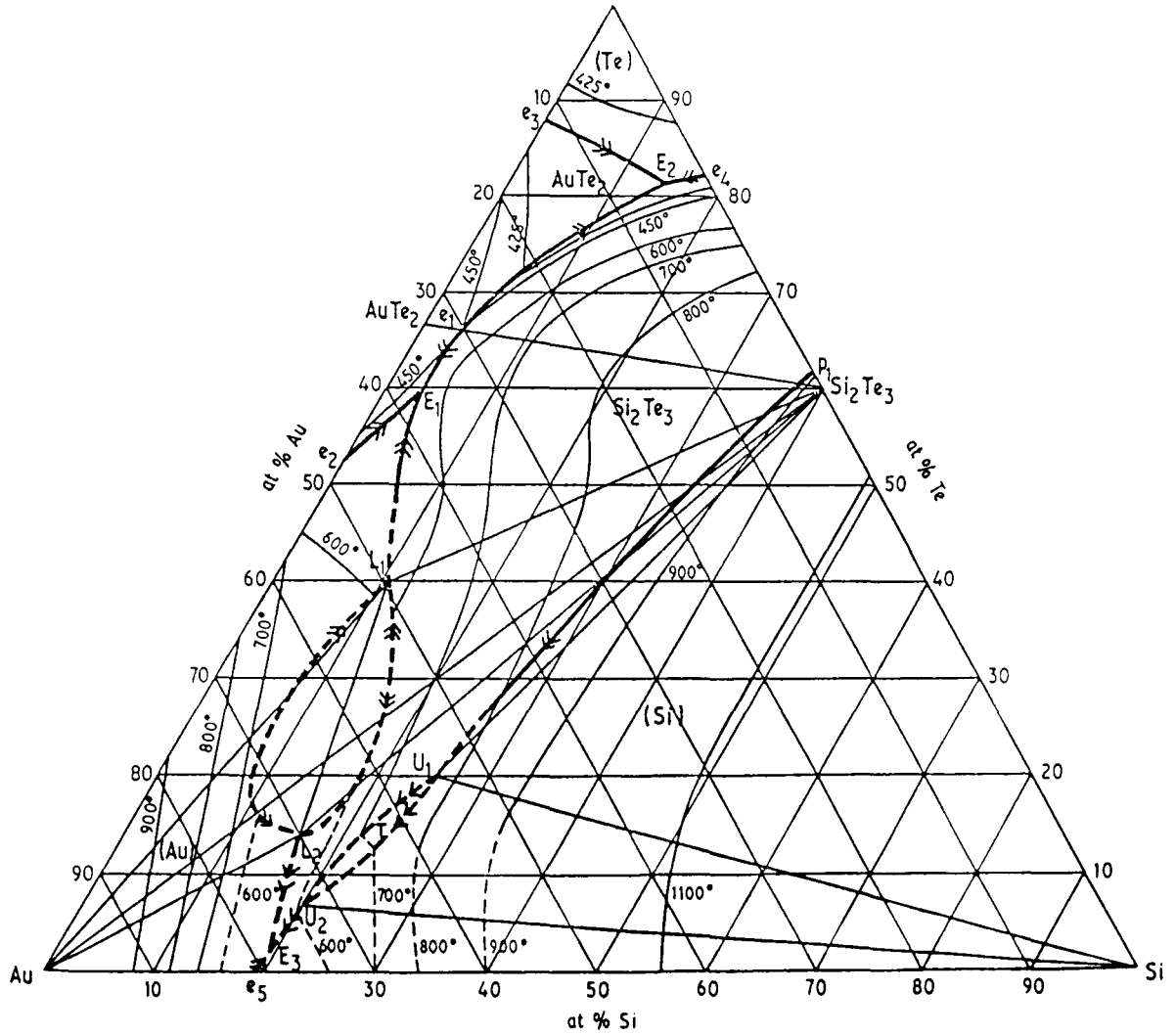

Fig 7.16:- Liquidus Projection of Au-Te-Si Ternary System.

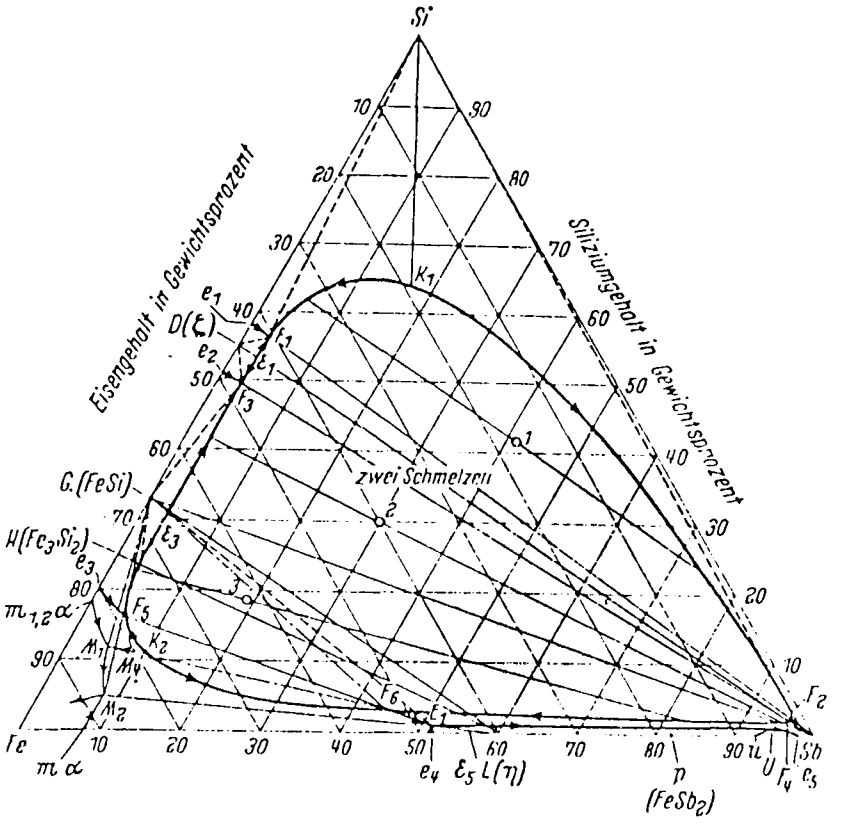

Fig 7.17:- Liquidus Projection of Fe-Sb-Si Ternary System.

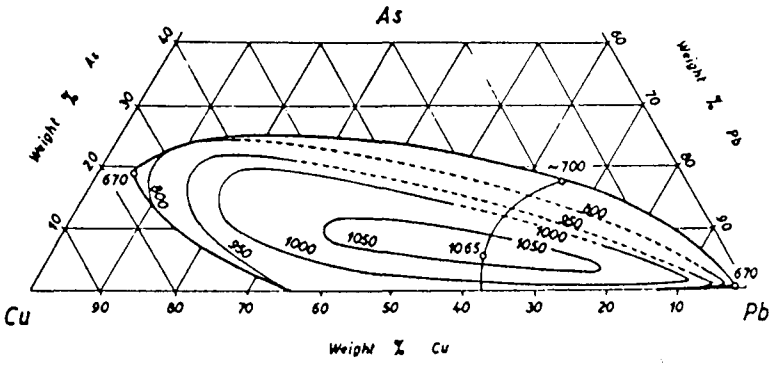

Fig 7.18:- Liquidus Projection of As-Pb-Cu Ternary System.

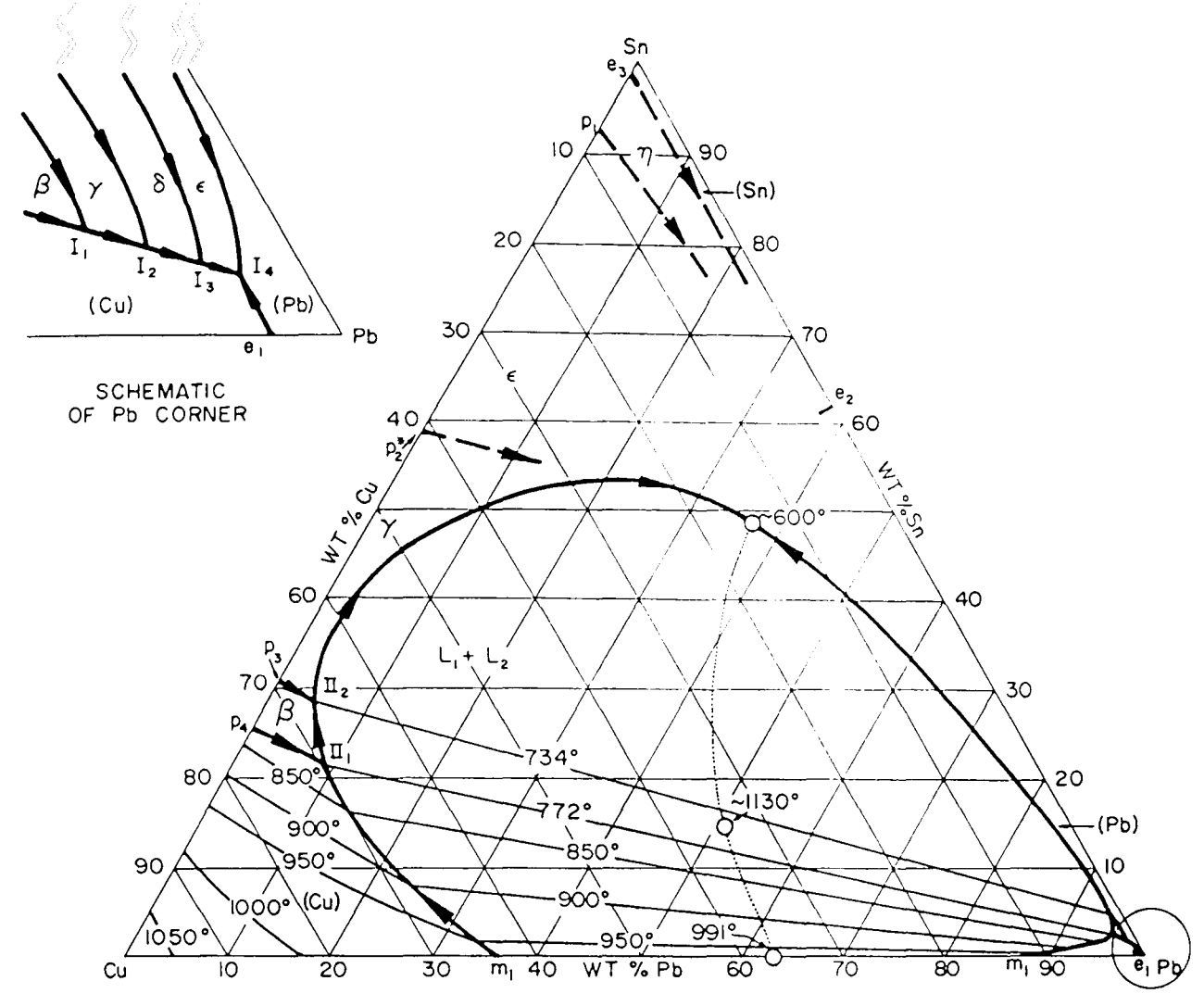

Fig 7.19(a)

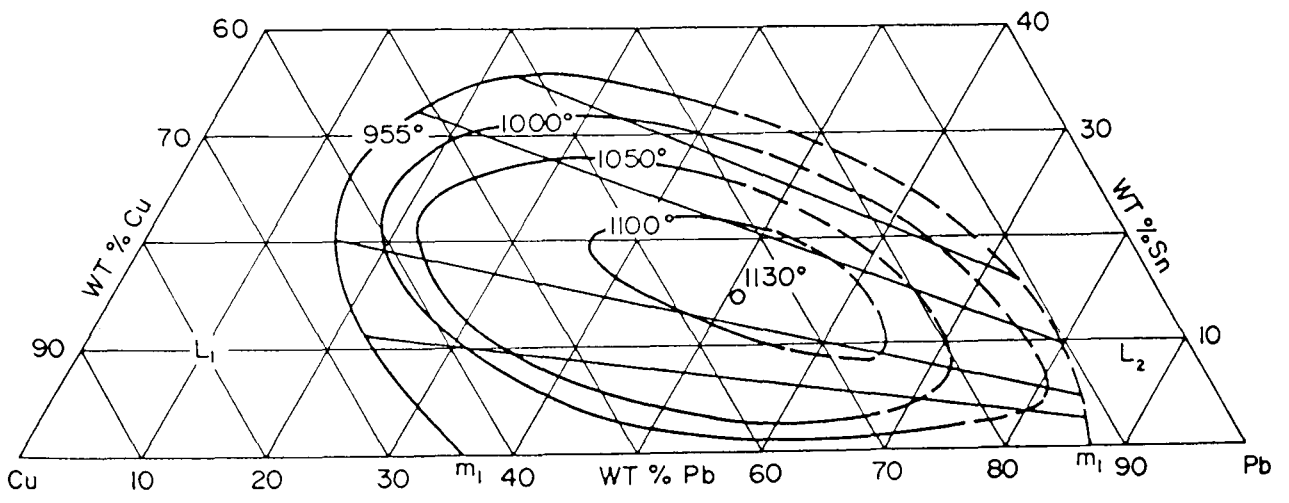

Fig 7.19(b)

Fig 7.19(a,b):- Liquidus Projection of Cu-Pb-Sn Ternary System.

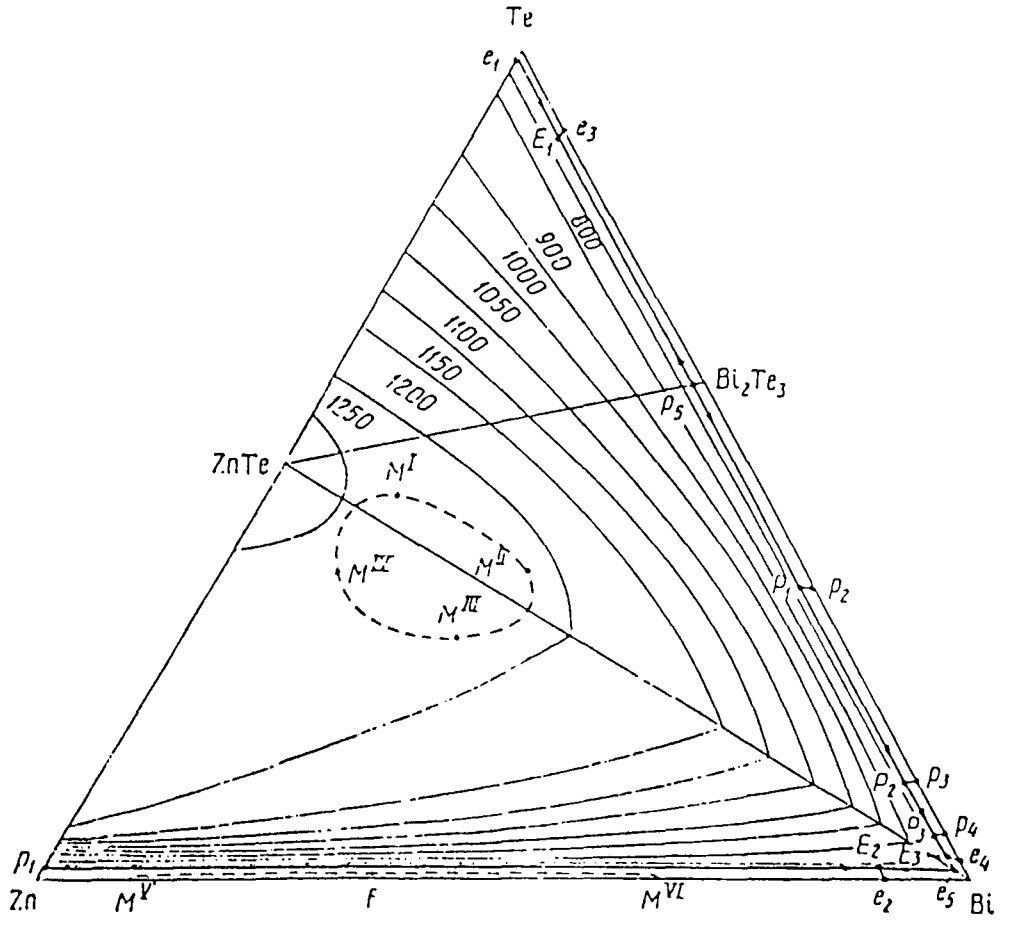

Fig 7.20:- Liquidus Projection of Zn-Bi-Te Ternary System.

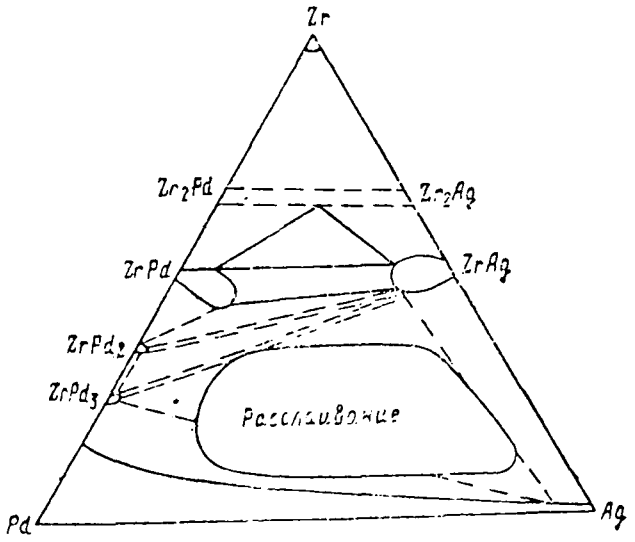

Fig 7.21:- Liquidus Projection of Pd-Zr-Ag Ternary System.

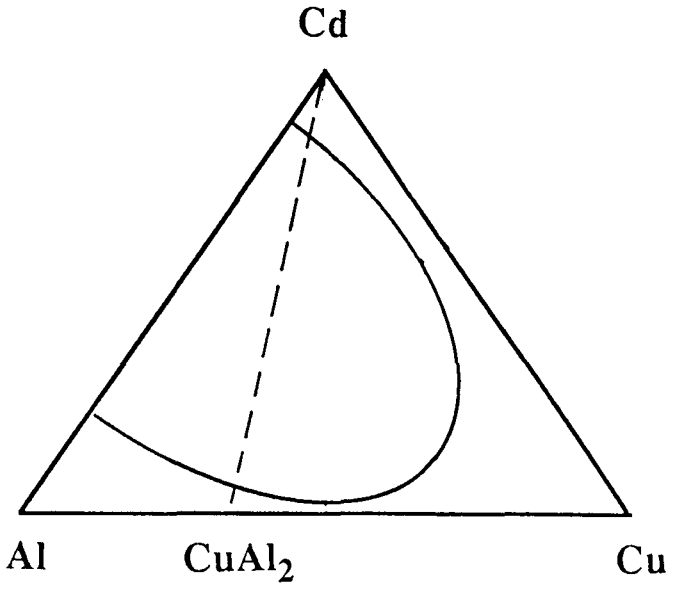

Fig 7.22:- Liquidus Projection of Cu-Cd-Al Ternary System.

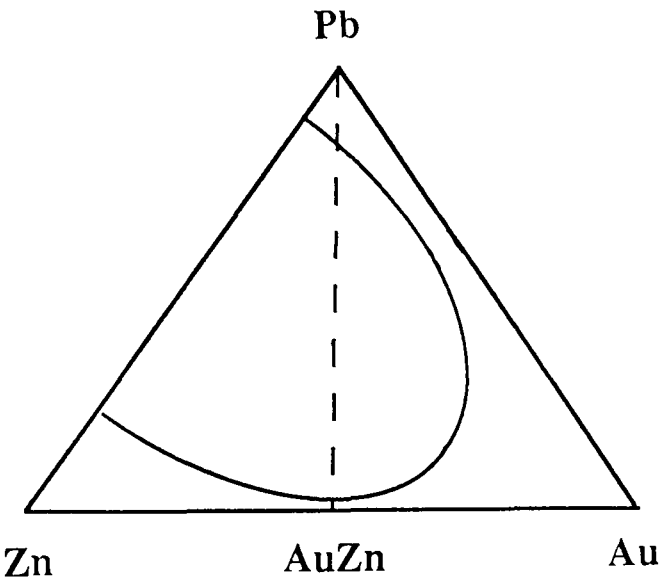

Fig 7.23:- Liquidus Projection of Au-Pb-Zn Ternary System.

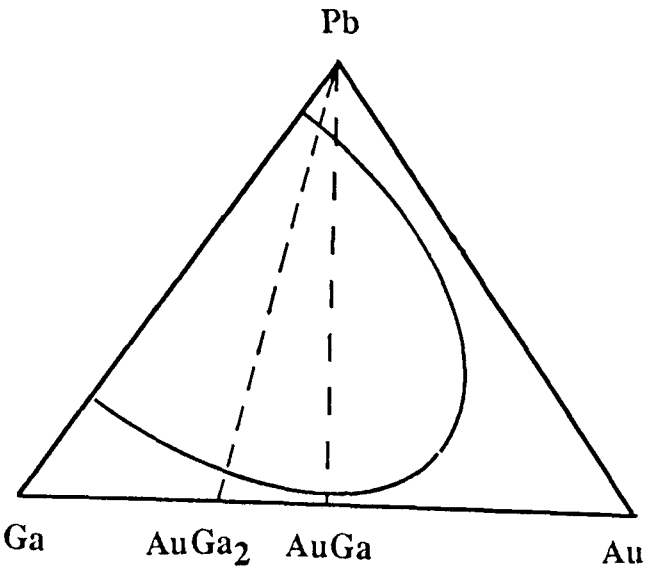

Fig 7.24:- Liquidus Projection of Au-Pb-Ga Ternary System.

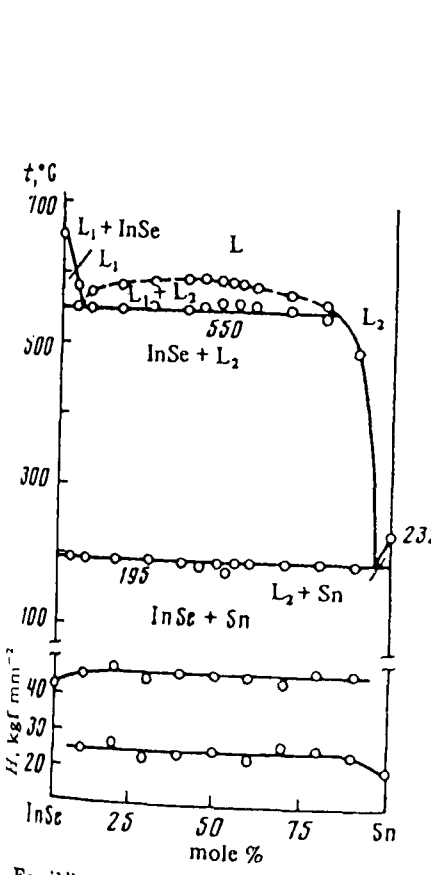

Equilibrium diagram of the InSe–Sn system.

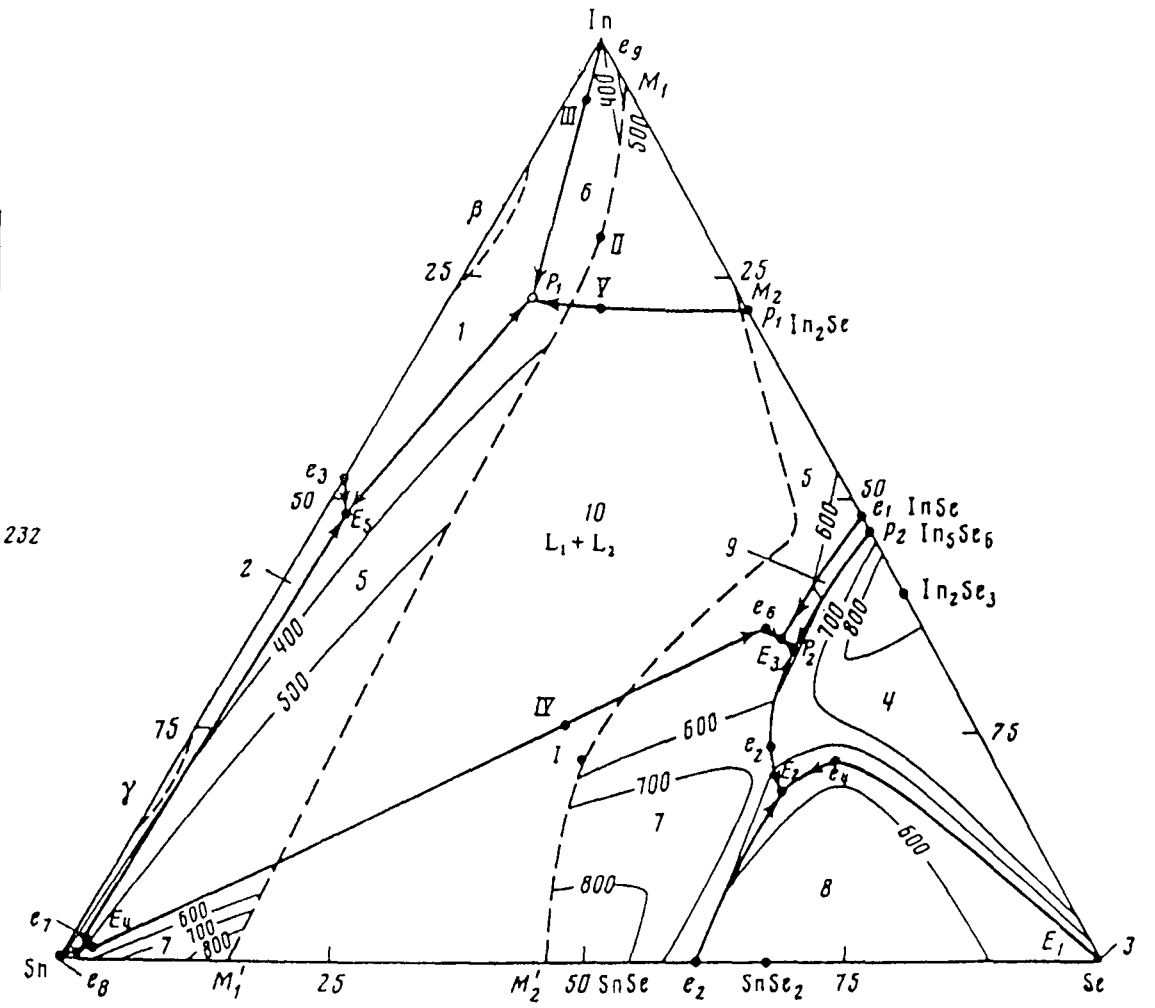

Fig 7.25:- Liquidus Projection of In-Sn-Se Ternary System.

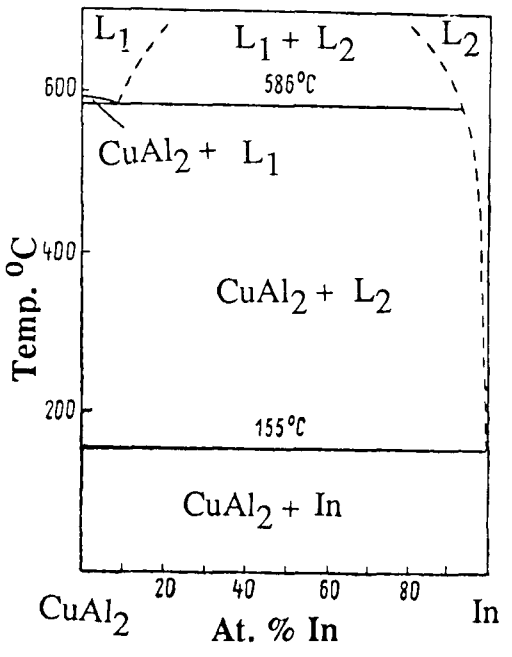

Fig 7.26:- The $CuAl_2$-In Section in the Cu-In-Al Ternary System Showing Liquid Immiscibility.

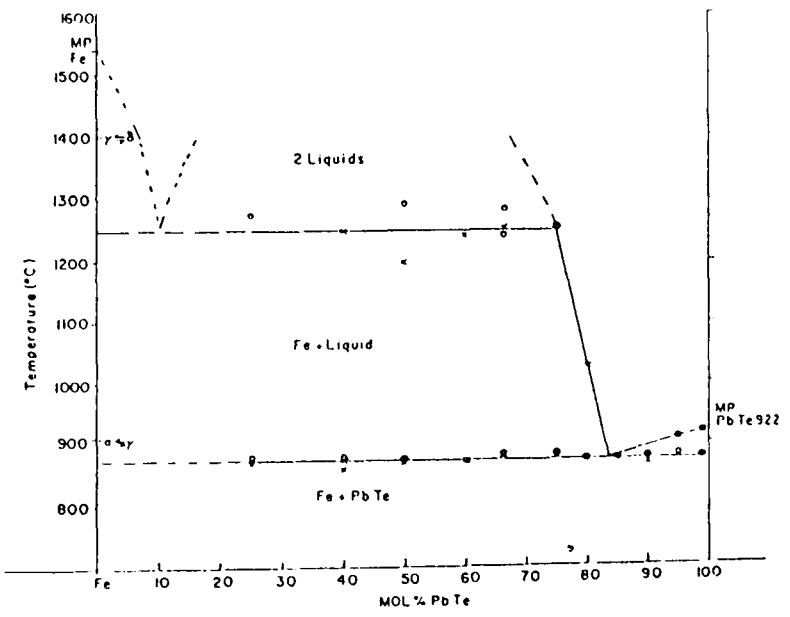

Fig 7.27:- The PbTe-Fe Section in the Pb-Fe-Te Ternary System Showing Liquid Immiscibility.

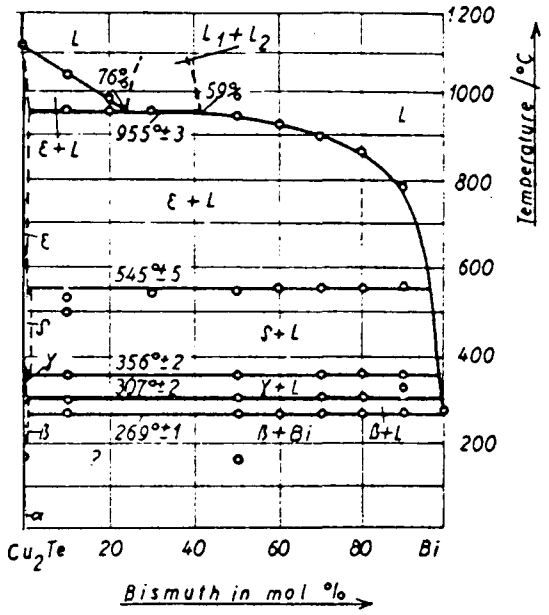

Fig 7.28:- The Cu_2Te-Bi Section in the Cu-Bi-Te Ternary System Showing Liquid Immiscibility.

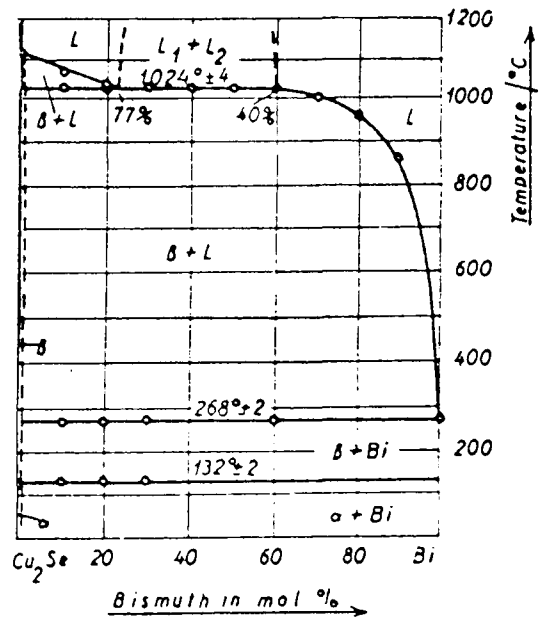

Fig 7.29:- The Cu_2Se-Bi Section in the Cu-Bi-Se Ternary System Showing Liquid Immiscibility.

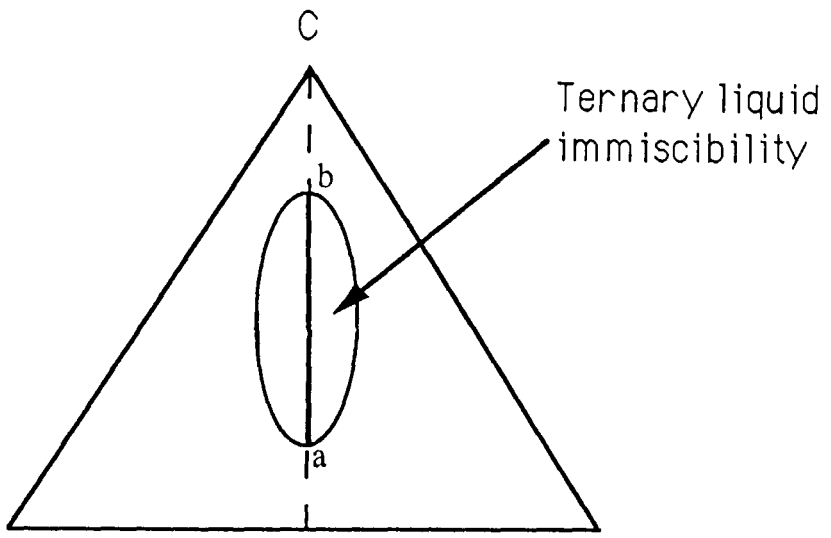

Fig 7.30:- The Ternary System A, B and C Showing the Direction of the Tie-Line.

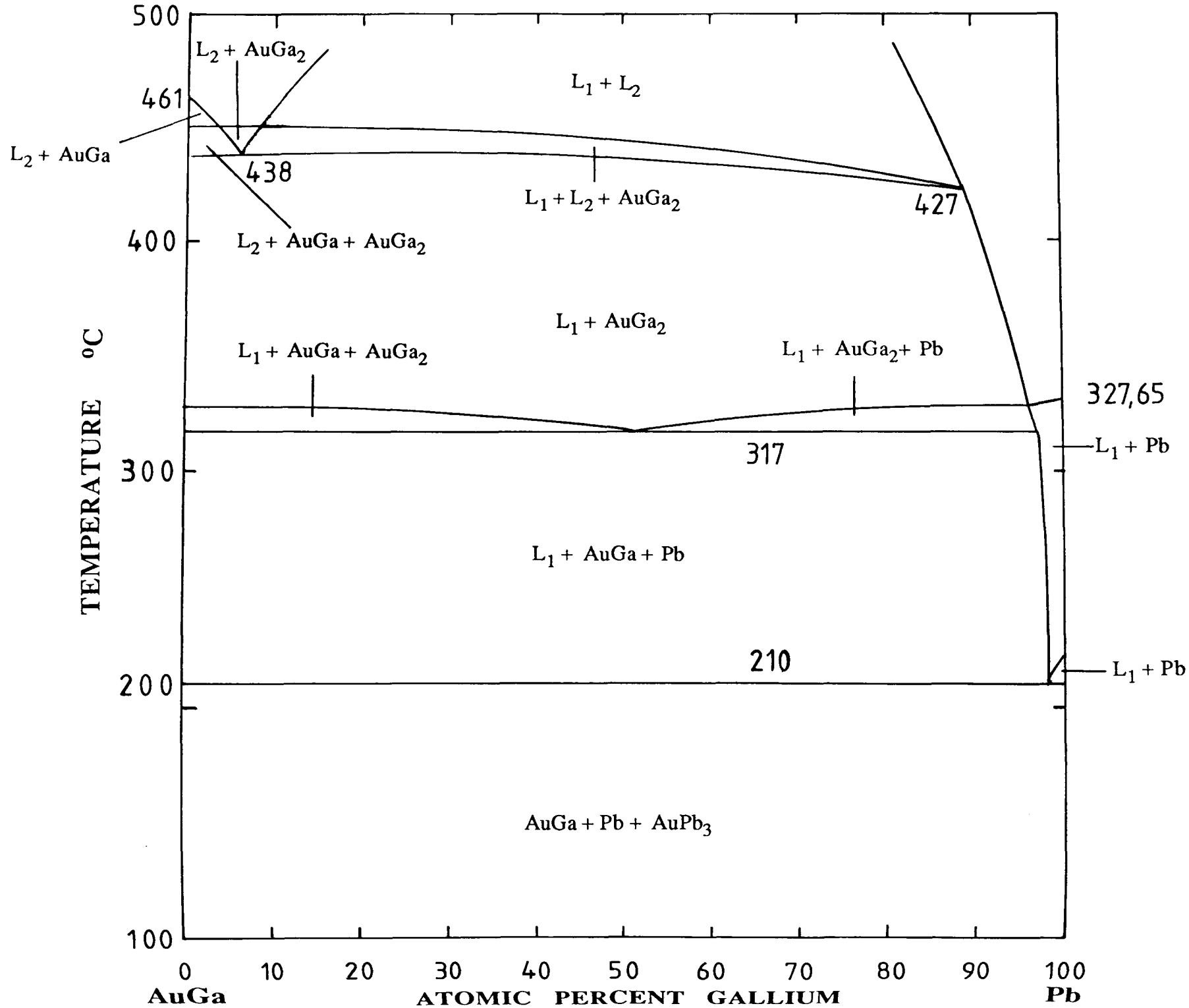

Fig 7.31(a):- AuGa-Pb Section
[See Fig 6.19]

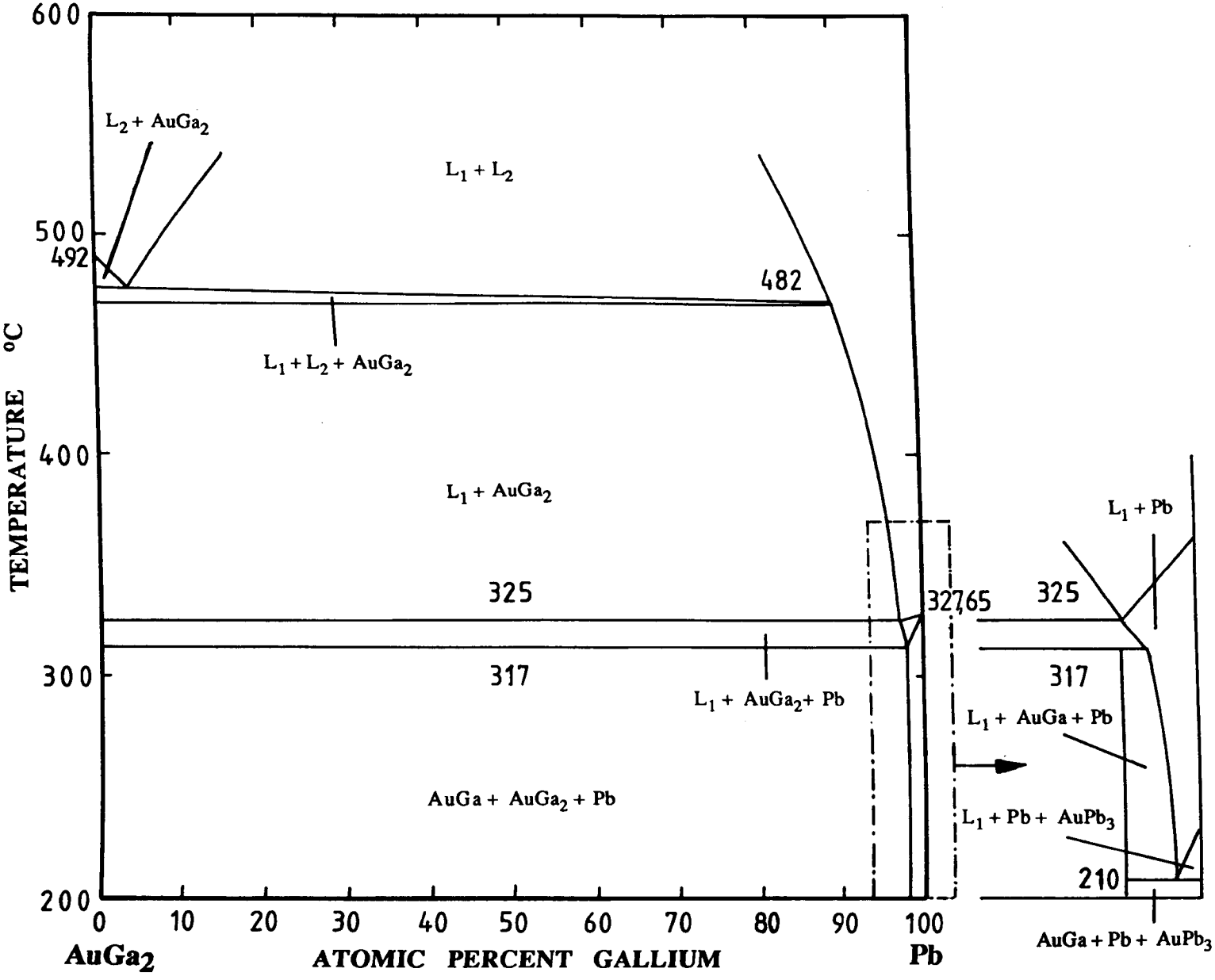

Fig 7.31(b):- $AuGa_2$-Pb Section
[See Fig 6.21]

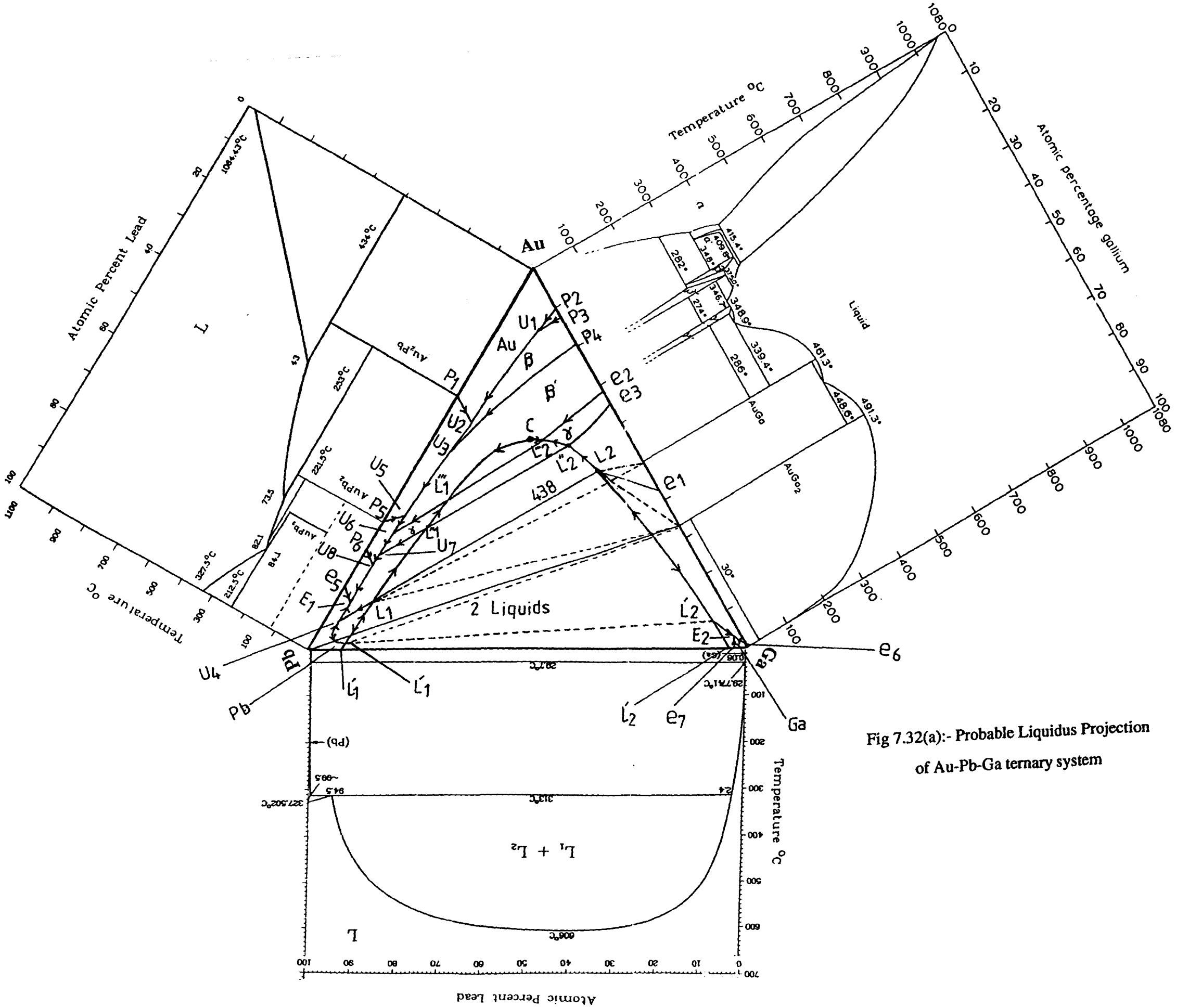

Fig 7.32(a):- Probable Liquidus Projection of Au-Pb-Ga ternary system

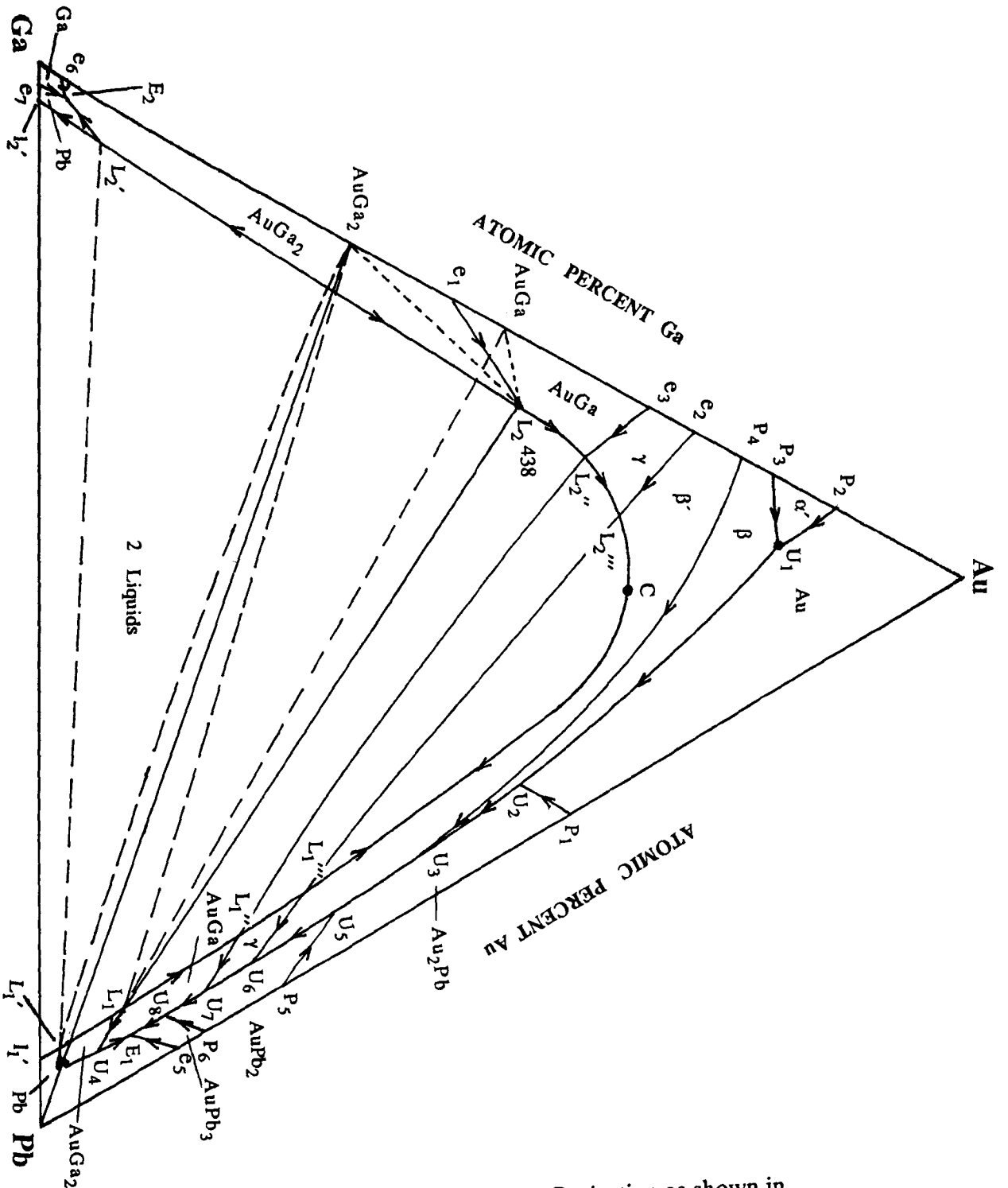

Fig 7.32(b):- Enlarged Liquidus Projection as shown in Fig 7.32(a)

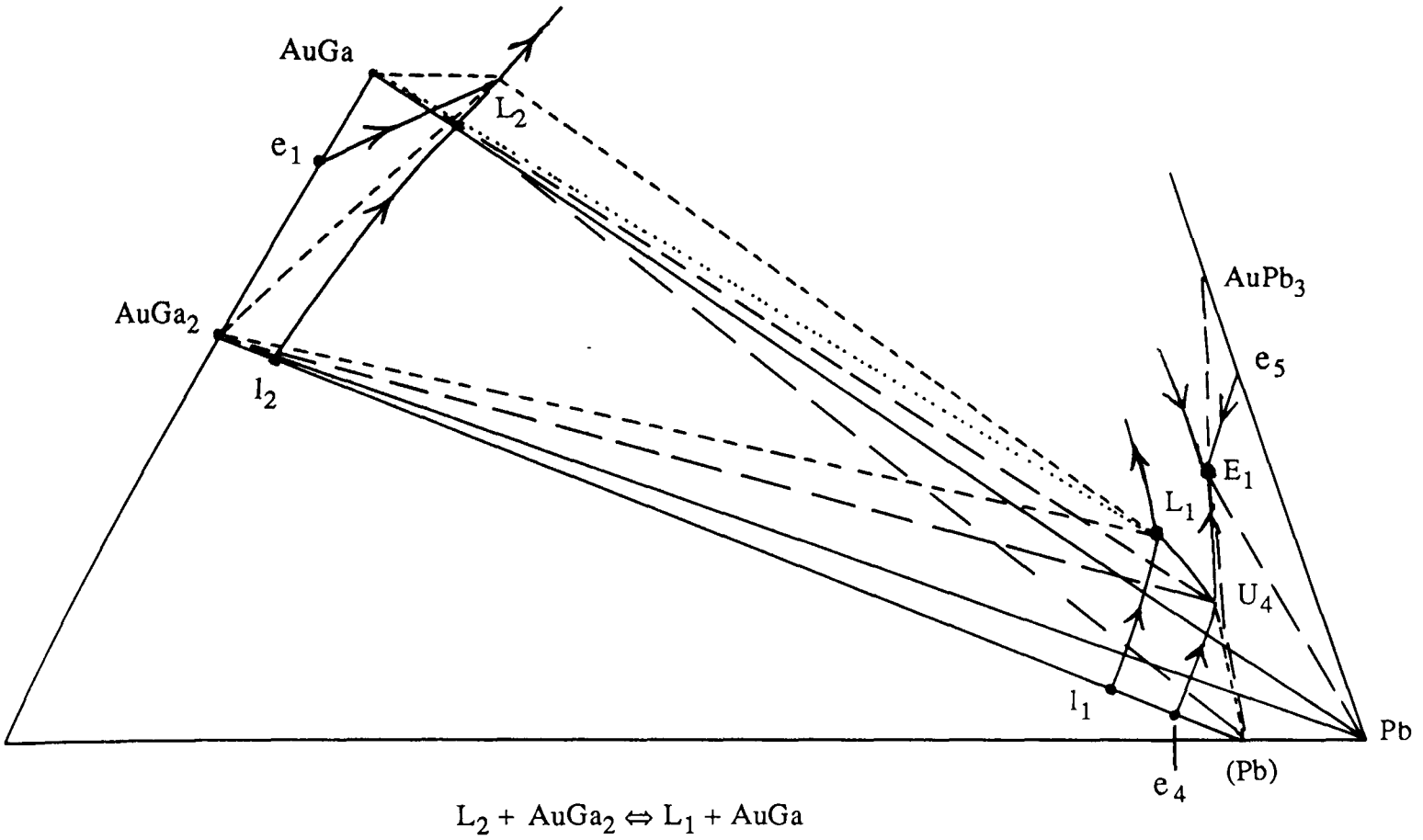

$L_2 + AuGa_2 \Leftrightarrow L_1 + AuGa$

Fig 7.33(a)

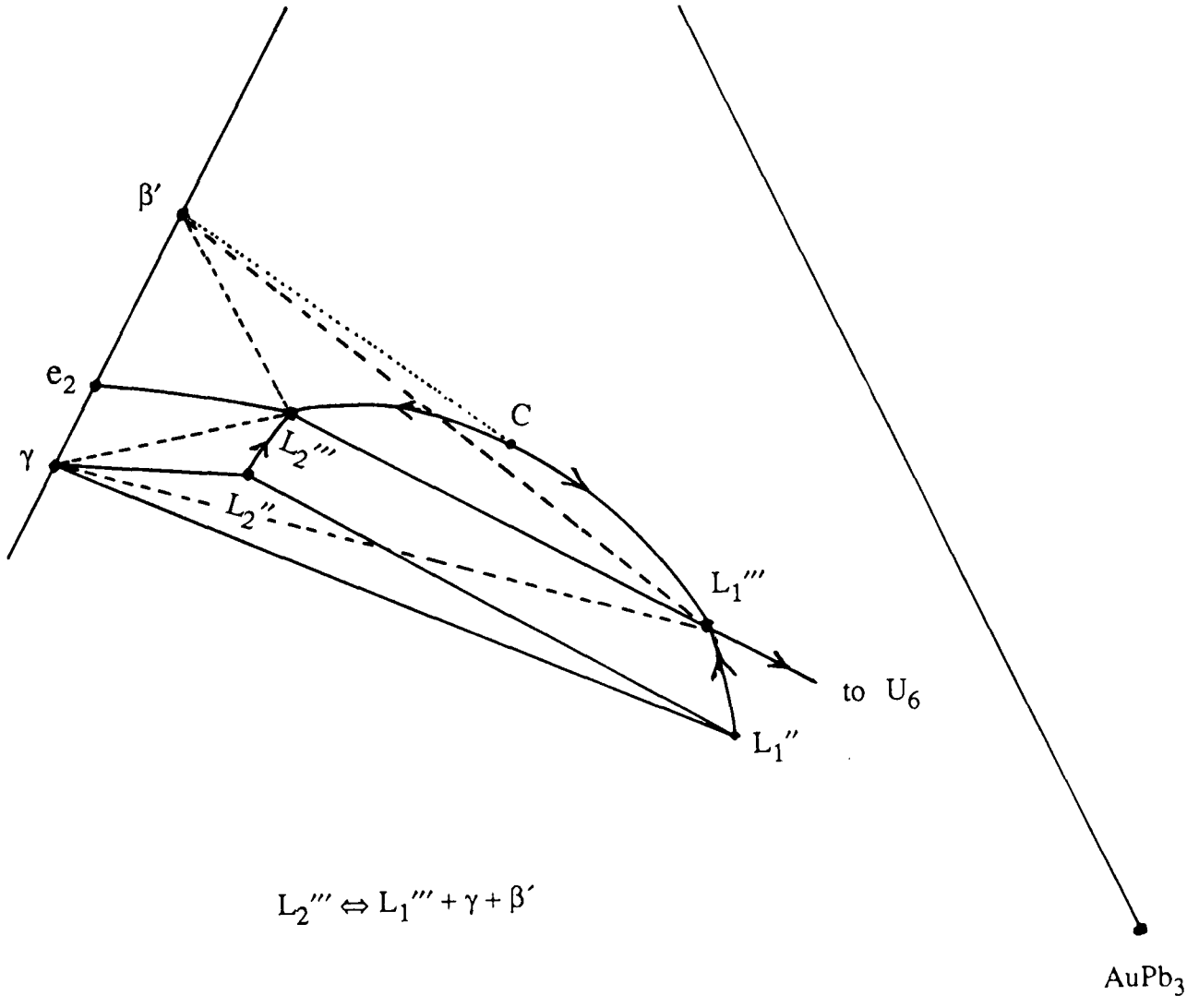

$L_2''' \Leftrightarrow L_1''' + \gamma + \beta'$

Fig 7.33(b)

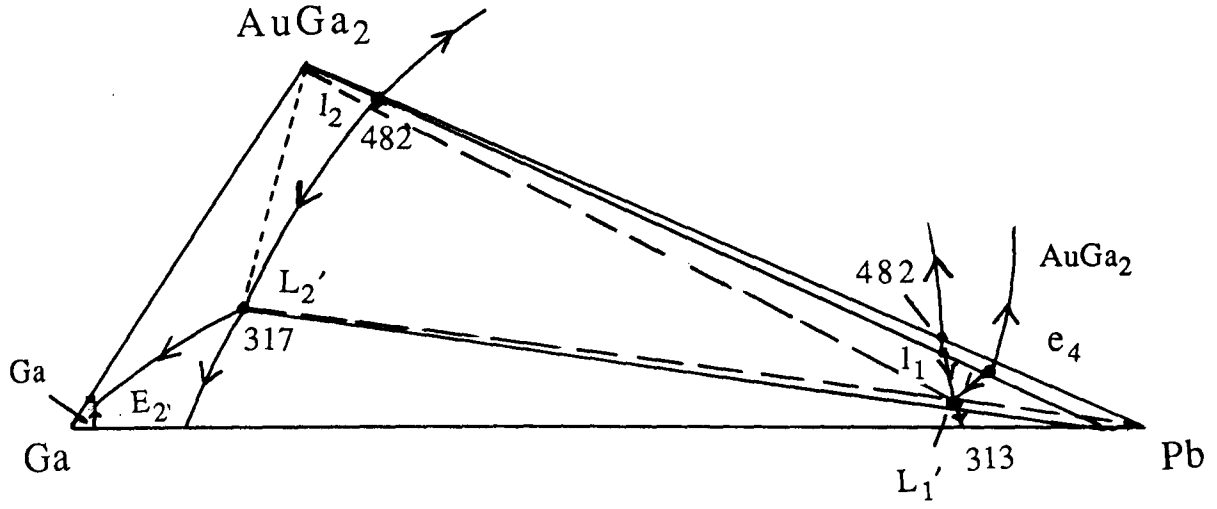

$L_1' + AuGa_2 \Leftrightarrow L_2' + (Pb)$

[Here $AuGa_2$, l_2, l_1, e_4 and (Pb) are all in straight line]

Fig 7.33(c)

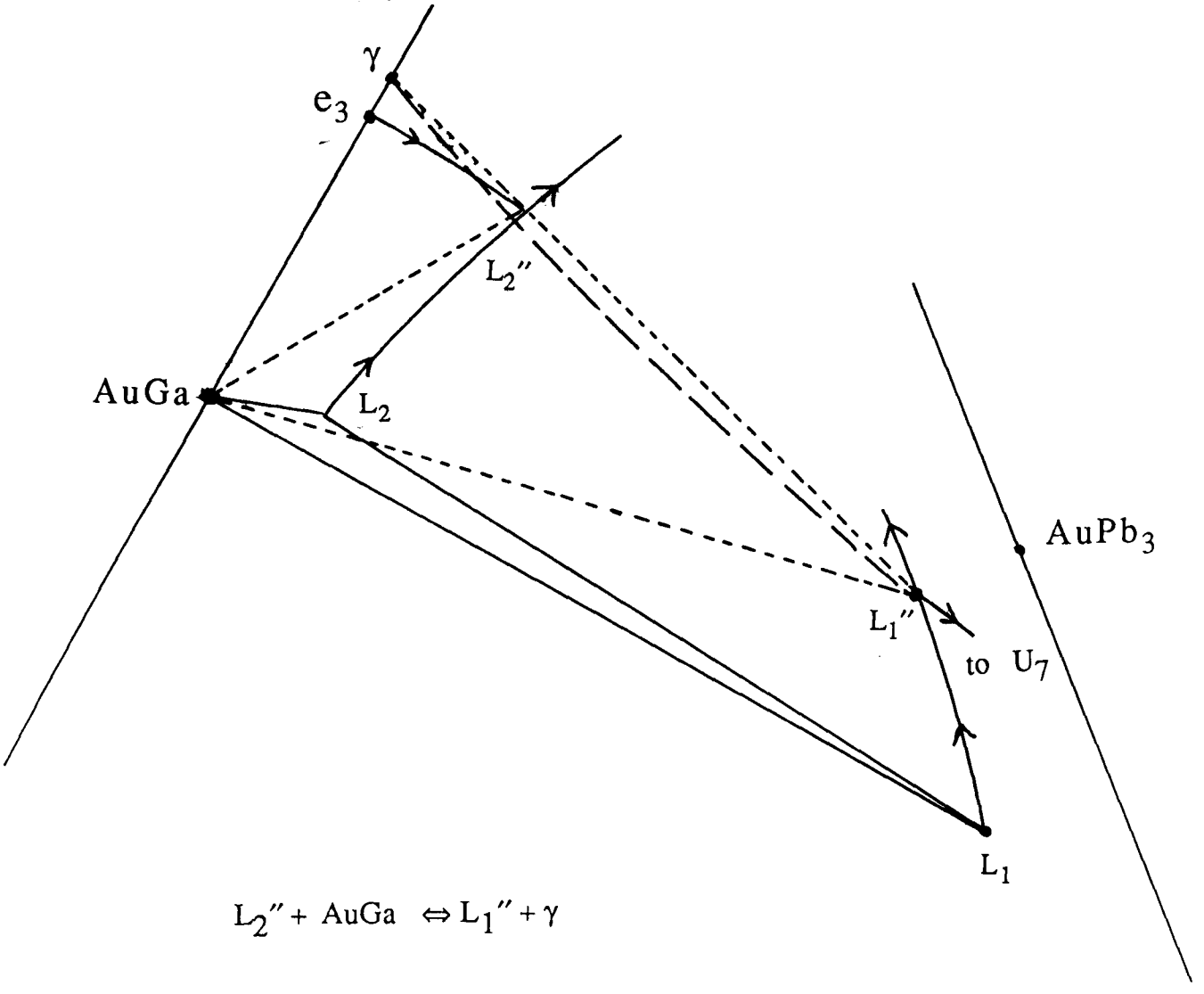

$L_2'' + AuGa \Leftrightarrow L_1'' + \gamma$

Fig 7.33(d)

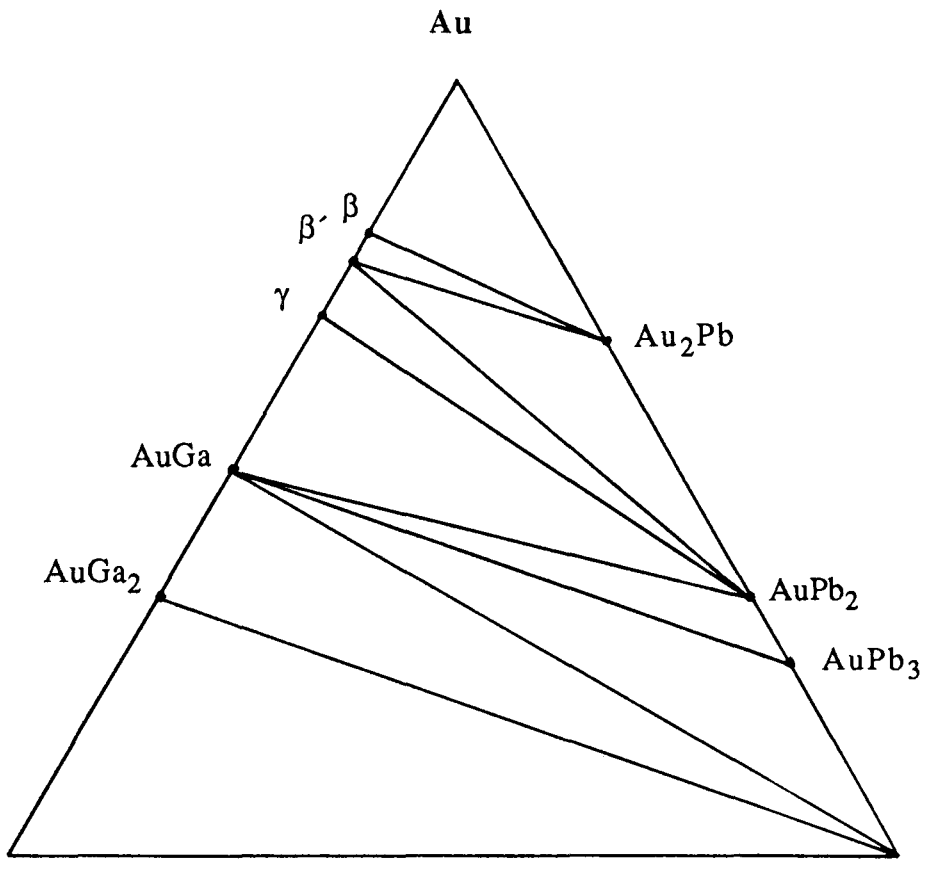

Fig 7.33(e):- Triangulation of Au-Pb-Ga ternary system

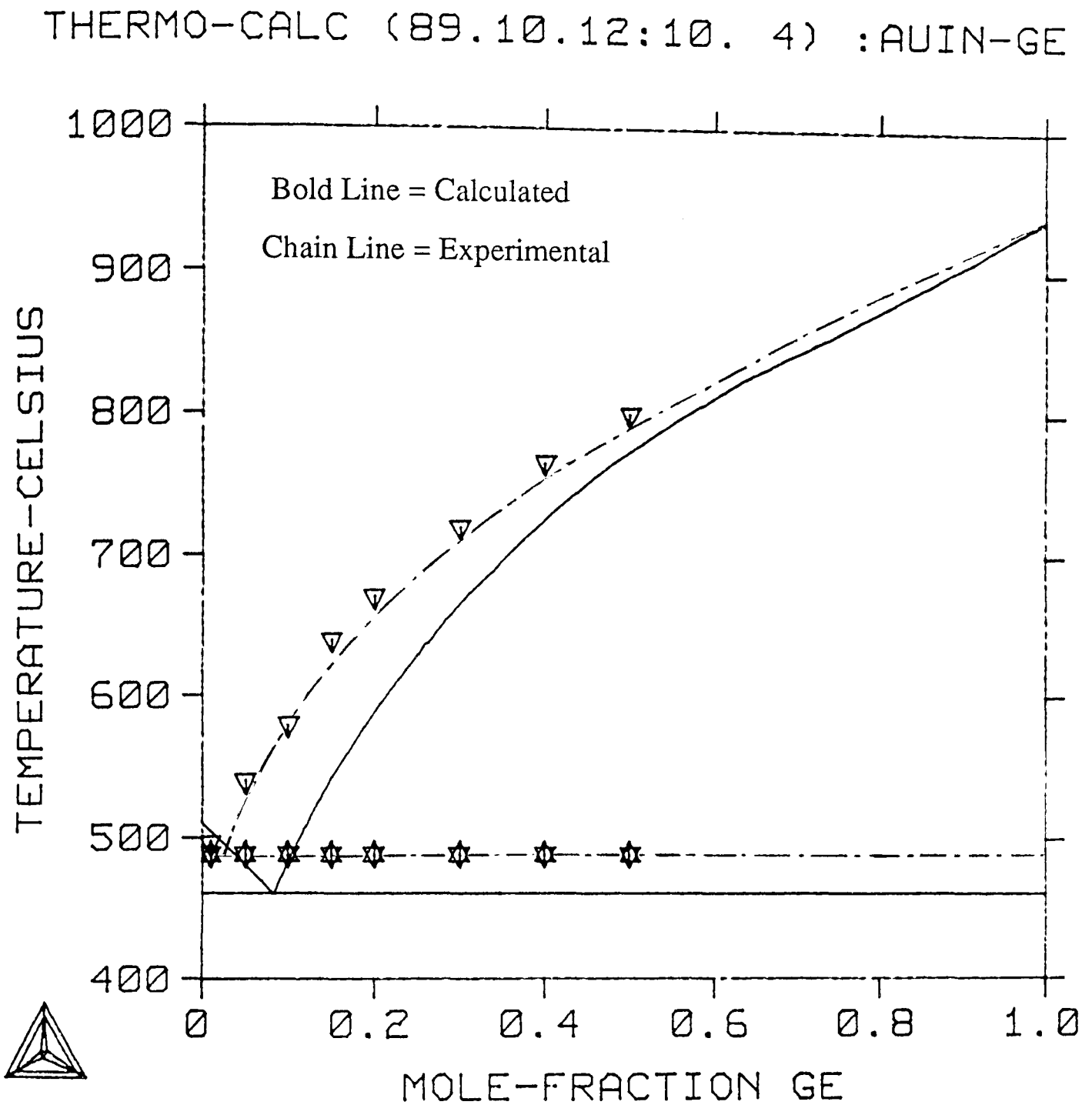

Calculated Eutectic Temperature = 460°C

Experimental Eutectic Temperature = 488°C

Calculated Eutectic Composition = 4.0 at.% Ge

Experimental Eutectic Composition = 2.0 at.% Ge

Fig 7.34:- Comparison between the calculated and experimental AuIn-Ge Section.

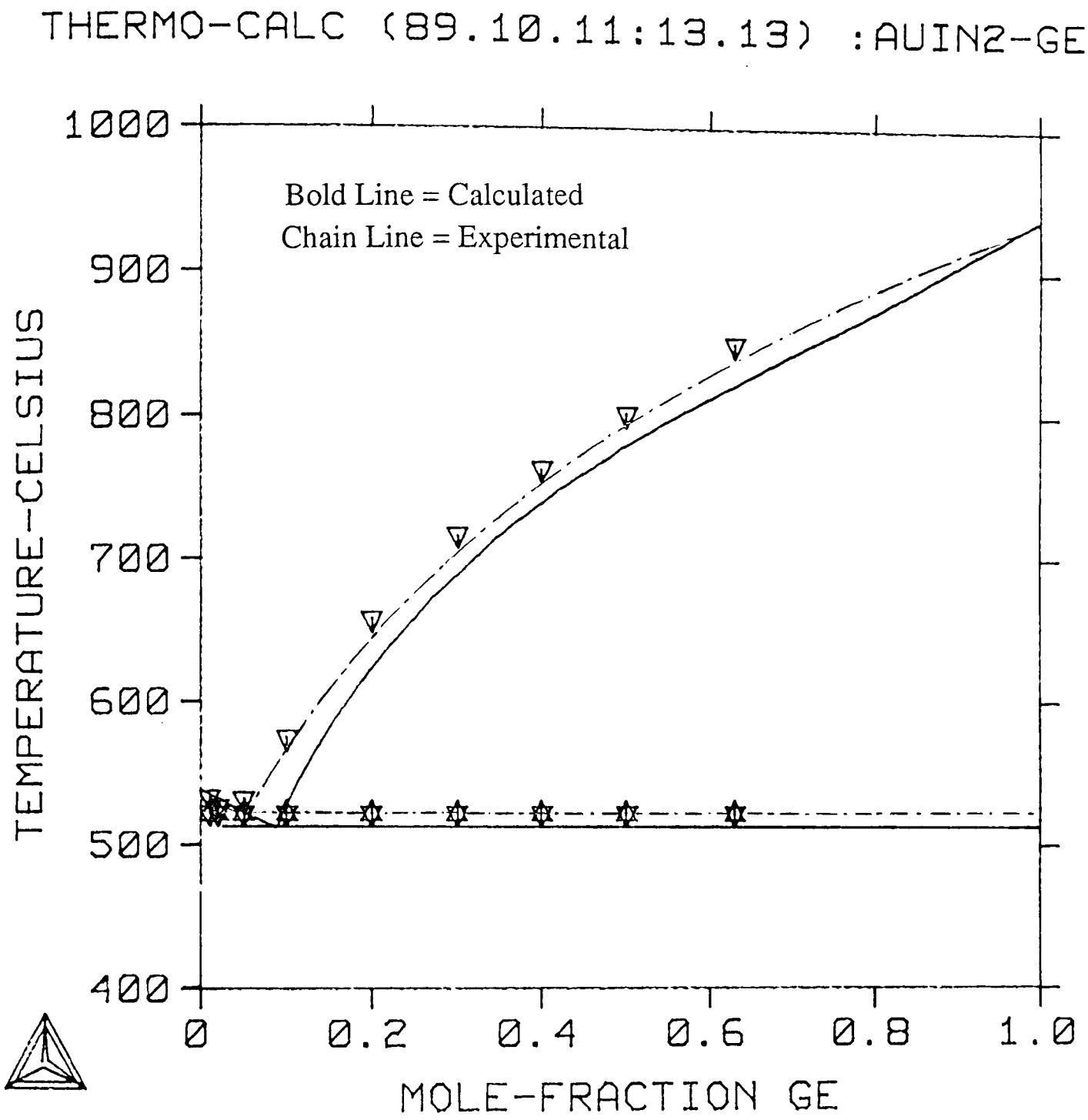

Calculated Eutectic Temperature = 513°C

Experimental Eutectic Temperature = 522°C

Calculated Eutectic Composition = 8.5 at.% Ge

Experimental Eutectic Composition = 4.1 at.% Ge

Fig 7.35:- Comparison between the calculated and experimental $AuIn_2$-Ge Section.

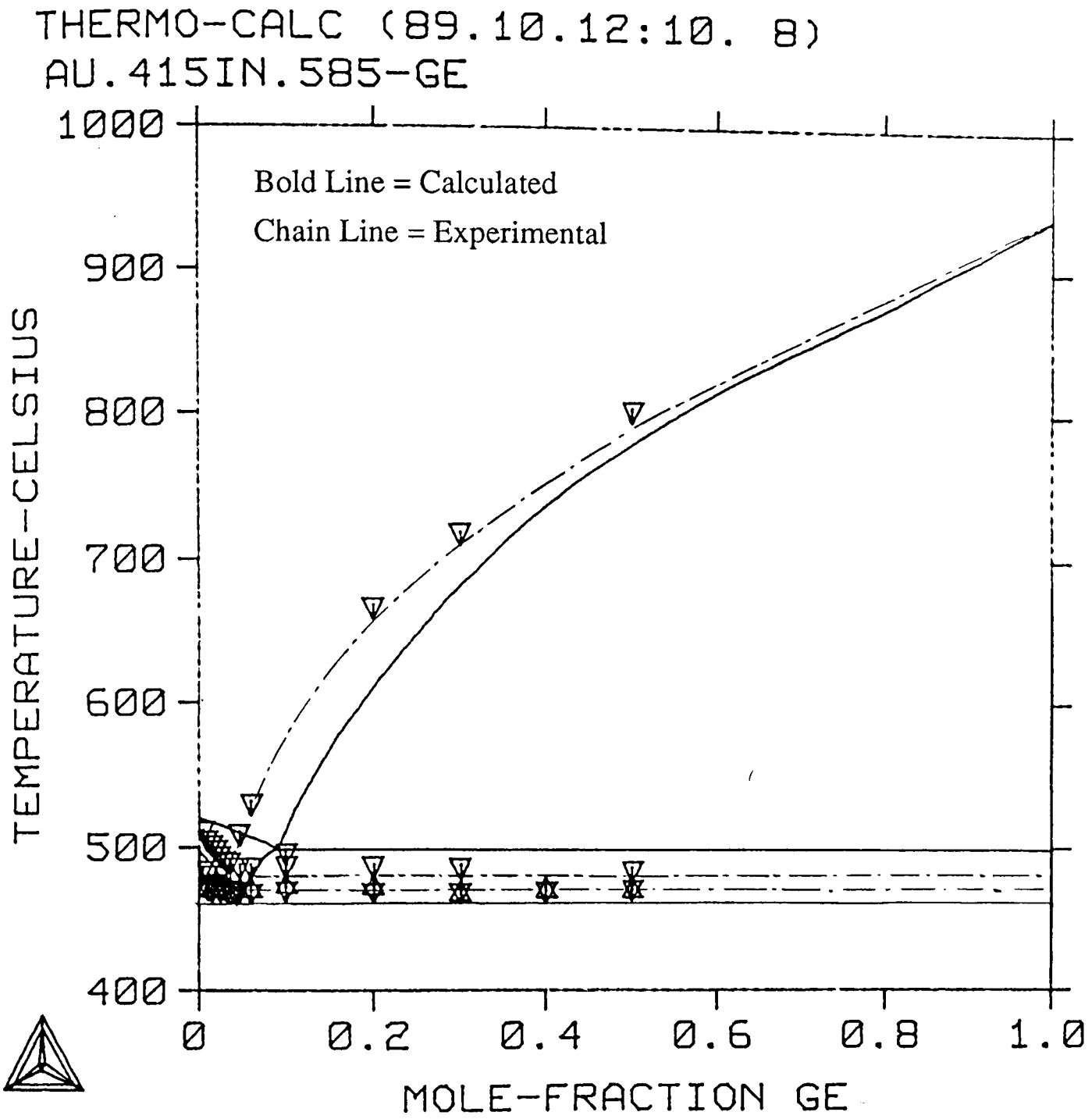

Calculated Ternary Eutectic Temperature = 460^{O}C

Experimental Ternary Eutectic Temperature = 471^{O}C

Calculated Temperature for Monovariant Curve = 498^{O}C

Experimental Temperature for Monovariant Curve = 488^{O}C

Calculated Composition of Monovariant Point = 8.9 at.% Ge

Experimental Composition of Monovariant Point = 4.0 at.% Ge

Calculated Tie-Line between Ternary Eutectic and $AuIn_2$ is at 4.34 at.% Ge at 460^{O}C

Experimental Tie-Line between Ternary Eutectic and $AuIn_2$ is at 2.75 at.% Ge at 471^{O}C

Fig 7.36:- Comparison between the calculated and experimental $Au_{41.5}In_{58.5}$ to Ge Isopleth.

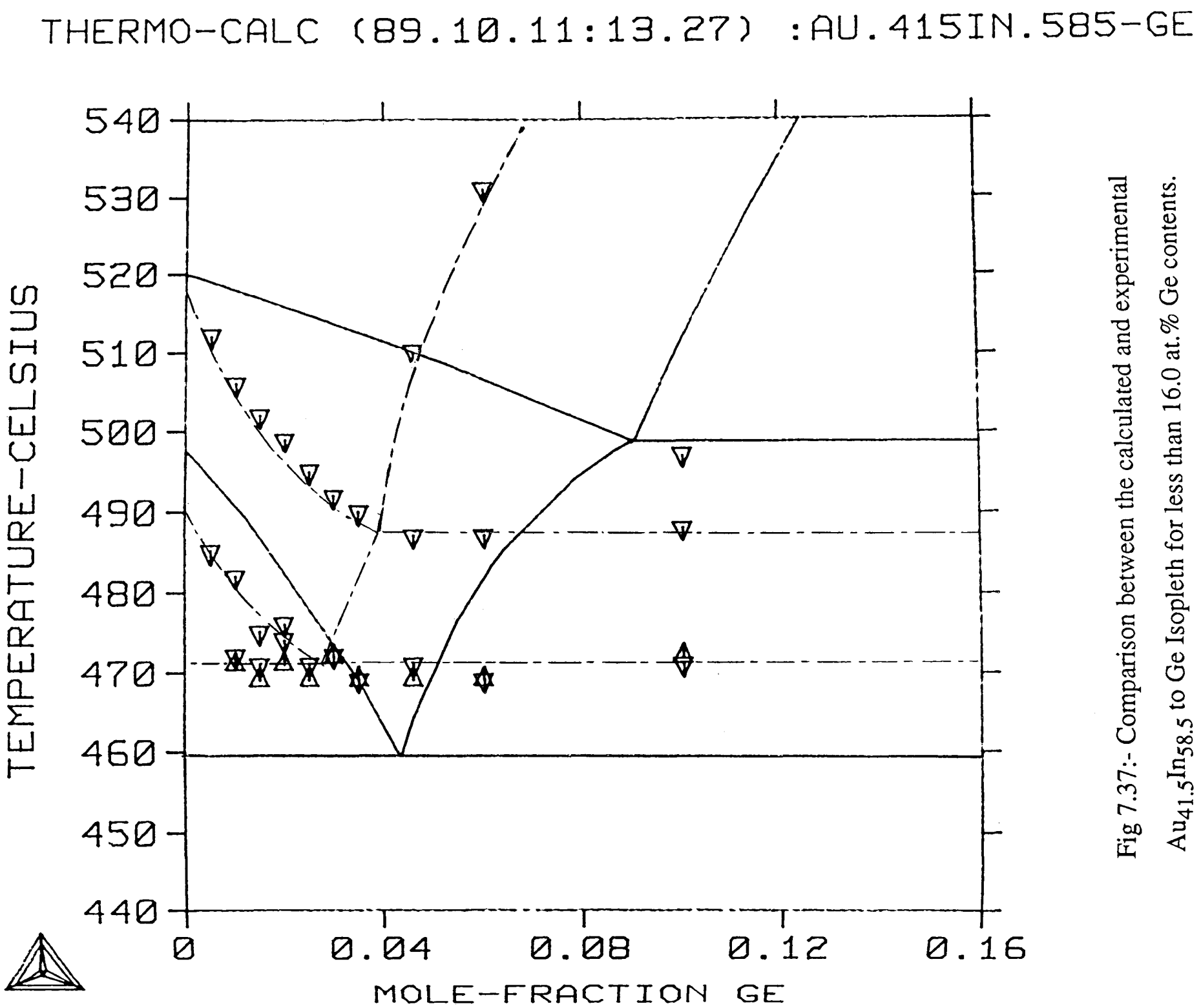

Fig 7.37:- Comparison between the calculated and experimental $Au_{41.5}In_{58.5}$ to Ge Isopleth for less than 16.0 at.% Ge contents.

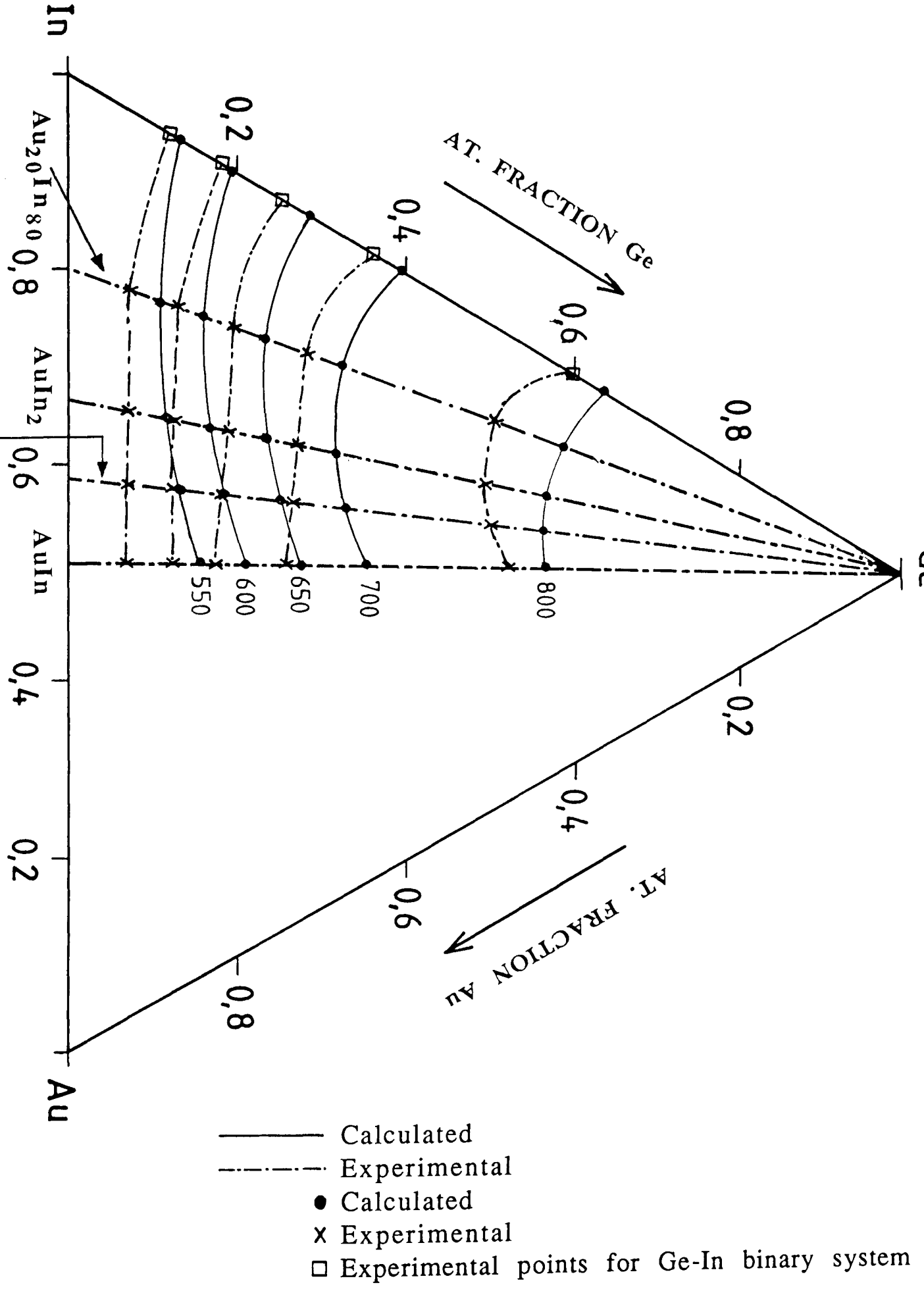

Fig 7.38:- Comparison between the calculated and experimental isotherms on the liquidus surface of the sub-ternary system Ge-In-AuIn.

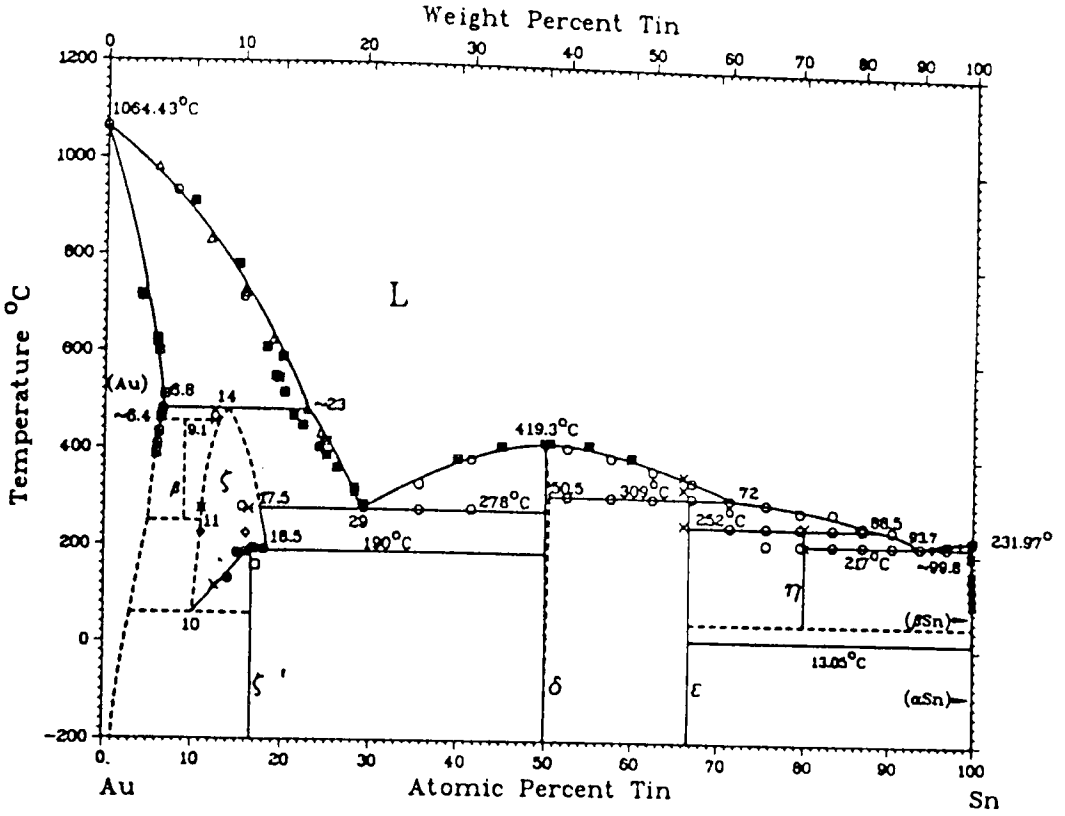

Fig 7.39:- The Au-Sn binary phase diagram (132).

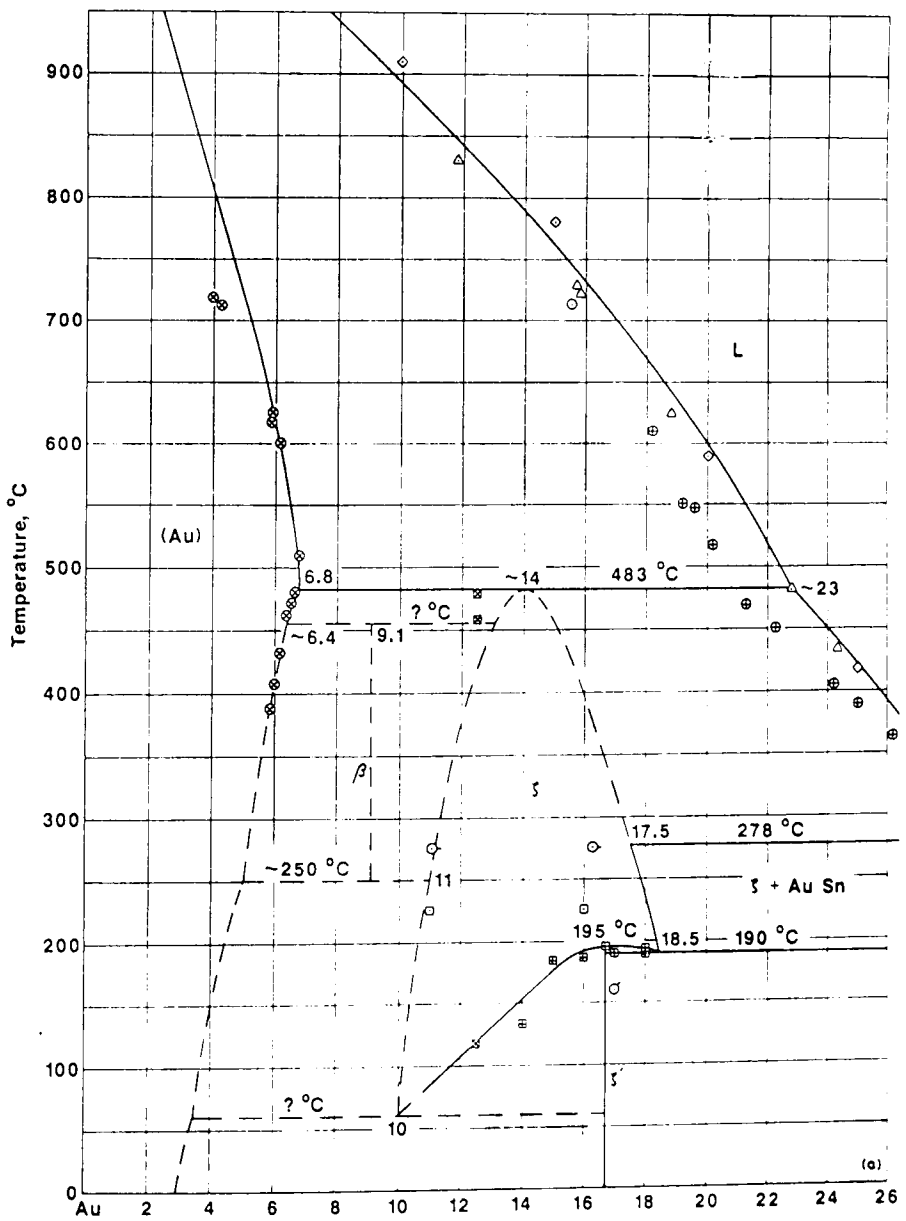

Fig 7.40:- The enlarged Au-rich portion of the Au-Sn binary phase diagram.

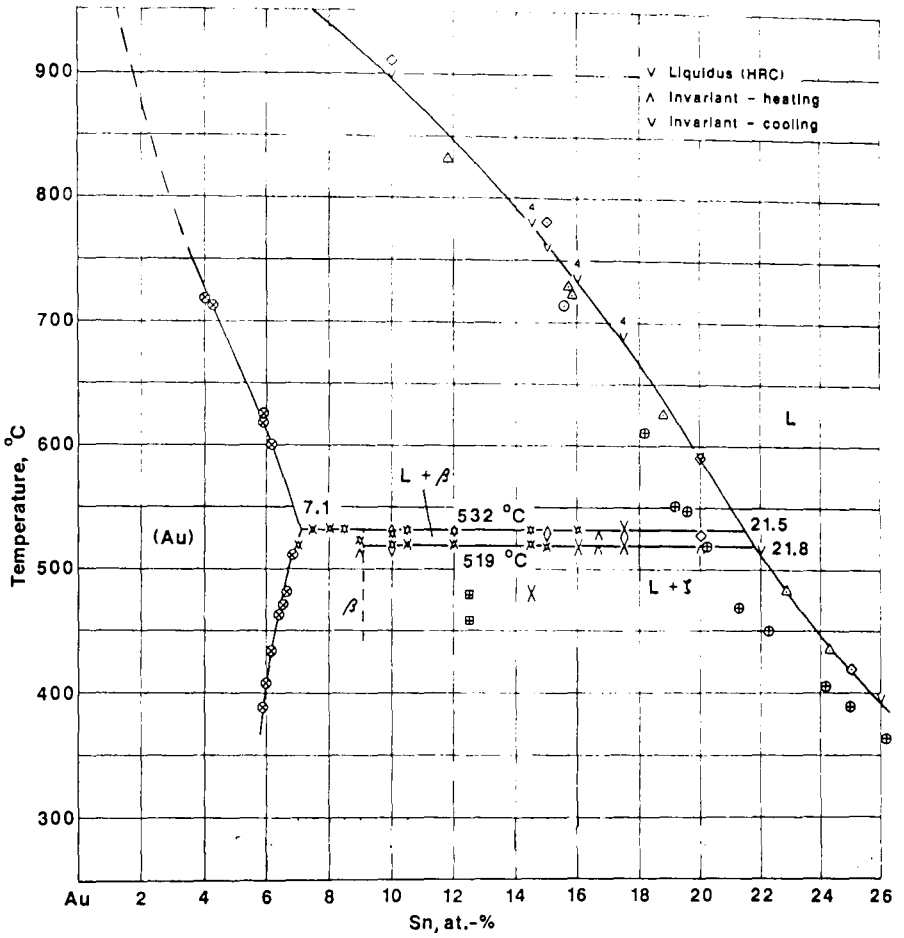

Fig 7.41:- The Au-rich portion of the Au-Sn binary phase diagram investigated by Legendre, Prince and co-worker for > 400°C.

TABLES

TABLE 1:- Summary of the AuX-Ge Pseudobinary Systems.

Section	Eutectic Composition (at.% Ge)	Eutectic Temperature (^{o}C)	Solubility of Ge in AuX	Phase Diagrams, Figures	Appendix
AuIn-Ge	2.0	488	< 1 at.% Ge	6.1	2
$AuIn_2$-Ge	4.1	522	< 1 at.% Ge	6.2	3
AuGa-Ge	5.5	446	< 1 at.% Ge	6.3	4
$AuGa_2$-Ge	5.0	476	< 1 at.% Ge	6.4	5
AuZn-Ge	12.2	673	1.3 at.% Ge	6.5	6
AuCd-Ge	10.0	555	1.3 at.% Ge	6.6	7

TABLE 2

ALLOY COPOMPOSITION OF Au-Sn (at.% Sn)	PHASE/PHASES FORMED AFTER ALLOYS			
	Equilibrated at 300°C for 4464 hrs (≅ 6 Months)	Equilibrated at 300°C for 12864 hrs (≅ 18 Months)	Equilibrated at 220°C for 13488 hrs (≅ 19 Months)	Equilibrated at 220°C for 17000 hrs (≅24 Months)
7.5	Non-Equilibrium Structure	Two Phase Mixture of Au + β	Two Phase Mixture of Au + β	Two Phase Mixture of Au + β
10.5	Non-Equilibrium Structure	Two Phase Mixture of Au + ζ	———	———
12.0	Non-Equilibrium Structure	Single Phase ζ	Single Phase ζ	Single Phase ζ
14.5	Non-Equilibrium Structure	Single Phase ζ	Single Phase ζ	Single Phase ζ
16.0	Non-Equilibrium Structure	Single Phase ζ	ζ Phase + Small Amount of AuSn	ζ Phase + Small Amount of AuSn
17.5	———	———	Two Phase Mixture of ζ + AuSn	Two Phase Mixture of ζ + AuSn
20.0	———	———	Two Phase Mixture of ζ + AuSn	Two Phase Mixture of ζ + AuSn

TABLE 3:- The Microhardness of single phase congruent melting compounds

Congruent Melting Compounds	*Microhardness (H_v)*	*Weight Used*
AuIn	222	20 g
$AuIn_2$	78	20 g
AuGa	116	100 g
$AuGa_2$	74	100 g
AuZn	137	20 g

TABLE 4:- Reaction Scheme of:

(i) $AuIn_2$-AuIn-Ge Partial Ternary System

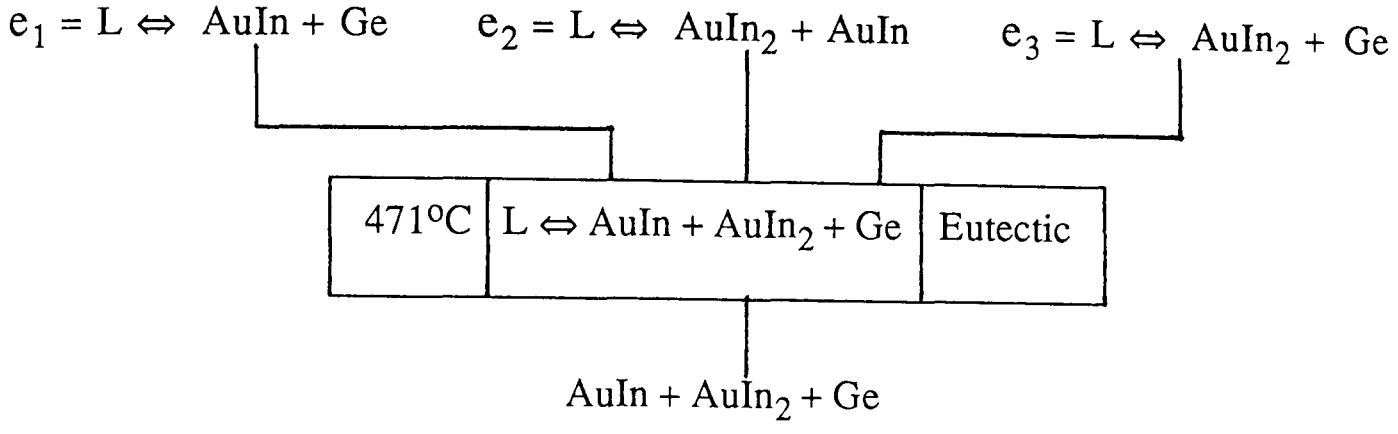

(ii) $AuIn_2$-In-Ge Partial Ternary System

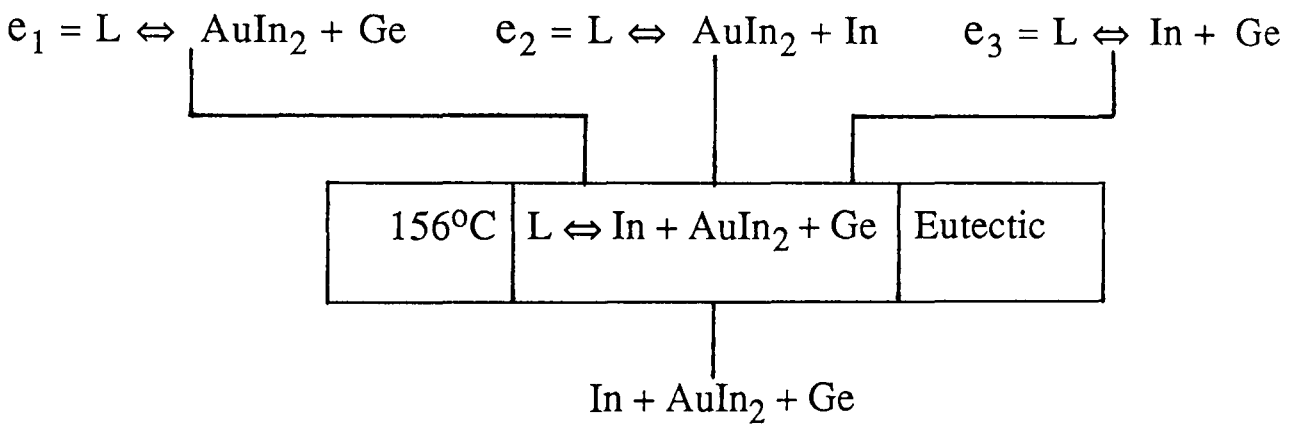

(iii) $AuGa_2$-AuGa-Ge Partial Ternary System

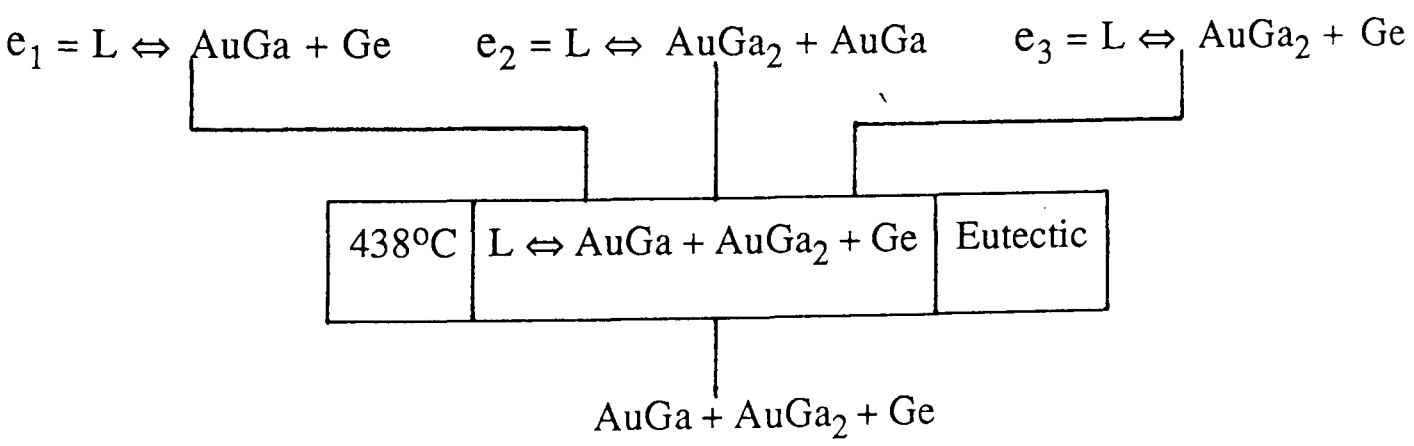

TABLE 5:- SYSTEMS SHOWING TRUE LIQUID IMMISCIBILITY.

[For Rule 1 Based on Atomic Size and Melting point].

No	SYSTEMS	REF.	FIG No.	TYPE OF IMMISC-IBILITY	CONSTITU-ENTS ELEMENTS	GOLDSCHM-IT ATOMIC RADII °A	DISTANCE OF CLOSEST APPROACH °A	MELT-ING POINT K
1	CuTi-Ag CuTi→Ag	106	7.4	Case I	Cu	1.28	2.55	1358.02
					Ti	1.47	2.89	1943.00
					Ag	1.44	2.89	1235.08
2	PdTi-Ag PdTi→Ag	107	7.5	Case I	Pd	1.37	2.75	1828.5
					Ti	1.47	2.89	1943.00
					Ag	1.44	2.89	1235.08
3	Cu_3Sb-Bi CuSb→Bi	108	7.6	Case I	Cu	1.28	2.56	1358.02
					Sb	1.61	2.90;3.36	903.90
					Bi	1.82	3.11;3.47	544.52
4*	Mg_3Sb_2-Al MgSb→Al	109	7.7	Case I	Mg	1.60	3.19;3.20	923.00
					Sb	1.61	2.90;3.36	903.90
					Al	1.43	2.86	933.60
5	AuSn-Pb AuSn→Pb	65	7.8	Case I	Au	1.44	2.88	1337.58
					Sn	1.58	3.18;2.80;3.02	505.12
					Pb	1.75	3.499	600.65
6	AuIn-Pb AuIn→Pb	101	7.9	Case I	Au	1.44	2.88	1337.58
					In	1.57	3.37;3.24	429.78
					Pb	1.75	3.499	600.65
7	AuSn-Bi AuSn→Bi	50	7.10	Case I	Au	1.44	2.88	1337.58
					Sn	1.58	3.18;2.80;3.02	505.12
					Bi	1.82	3.11;3.47	544.52

No	SYSTEMS	REF.	FIG No.	TYPE OF IMMISC-IBILITY	CONSTITU-ENTS ELEMENTS	GOLDSCHM-IT ATOMIC RADII ^{0}A	DISTANCE OF CLOSEST APPROACH ^{0}A	MELT-ING POINT K
8	$CuAl_2$-Sn	110	7.11	Case I	Cu	1.28	2.56	1358.02
	CuAl→Sn				Al	1.43	2.86	933.60
					Sn	1.57	3.18;2.80;3.02	505.12
9	FeSi-Cu	111	7.12	Case I	Fe	1.28;1.26	2.48;2.58	1811.00
	FeSi→Cu				Si	1.17	2.35	1687.00
					Cu	1.28	2.56	1358.02
10	AuCd-Pb	Pres-	7.13	Case I	Au	1.44	2.88	1337.58
	AuCd→Pb	ent			Cd	1.52	2.97;3.29	594.26
		Work			Pb	1.75	3.499	600.65
11	PdSi-Ag	112	7.14	Case I	Pd	1.37	2.75	1828.5
	$PdSi_2$-Ag				Si	1.17	2.35	1687.00
	PdSi→Ag				Ag	1.44	2.89	1235.08
12	CdSe-Bi	113	7.15	Case II	Cd	1.52	2.97;3.29	594.26
	CdSe→Bi				Se	1.60	2.32	494.00
					Bi	1.82	3.11;3.47	544.52
13	AuSi→Te	101	7.16	Case I	Au	1.44	2.88	1337.58
					Si	1.17	2.35	1687.00
					Te	1.4;1.7	2.86;3.46	722.72
14	$FeSi_2$-Sb	114	7.17	Case I	Fe	1.28;1.26	2.48;2.58	1811.00
	FeSi→Sb				Si	1.17	2.35	1687.00
					Sb	1.61	2.90;3.36	903.90

No	SYSTEMS	REF.	FIG No.	TYPE OF IMMISC-IBILITY	CONSTITU-ENTS ELEMENTS	GOLDSCHM-IT ATOMIC RADII ^{o}A	DISTANCE OF CLOSEST APPROACH ^{o}A	MELT-ING POINT K
15	Cu_3As-Pb CuAs→Pb	115	7.18	Case III	Cu	1.28	2.55	1358.02
					As	1.28	2.556	1358.02
					Pb	1.75	3.499	600.65
16	CuSn→Pb	116	7.19	Case III	Cu	1.28	2.55	1358.02
					Sn	1.57	3.18;2.80;3.02	505.12
					Pb	1.75	3.499	600.65
17	ZnTe-Bi ZnTe→Bi	117	7.20	Case III	Zn	1.37	2.66;2.91	692.73
					Te	1.4;1.7	2.86;3.46	722.72
					Bi	1.82	3.11;3.47	544.52
18*	PdZr-Ag PdZr→Ag	107	7.21	Case I	Pd	1.37	2.75	1828.5
					Zr	1.6;1.61	3.12;3.16;3.22	2127.86
					Ag	1.44	2.89	1235.08

* Systems showed disagreement due to Atomic Size.

TABLE 6:- SYSTEMS SHOWING LIQUID IMMISCIBILITY (Case IV). [For RULE 1 Based on Atomic Size and Melting Points].

No	SYSTEMS	REF.	FIG No.	CONSTITU-ENTS ELEMENTS	GOLDSCHM-IT ATOMIC RADII ^{o}A	DISTANCE OF CLOSEST APPROACH ^{o}A	MELTING POINTS K
1	$CuAl_2$-Cd	118	7.22	Cu	1.28	2.556	1358.02
	CuAl→Cd			Al	1.43	2.862	933.60
				Cd	1.52	2.979;3.29	594.26
2	AuZn-Pb	Pres-	7.23	Au	1.44	2.88	1337.58
	AuZn→Pb	ent		Zn	1.37	2.66;2.91	692.65
		Work		Pb	1.75	3.499	600.65
3*	AuGa-Pb	Pres-	7.24	Au	1.44	2.88	1337.58
	$AuGa_2$-Pb	ent		Ga	1.35	2.43;2.79	302.92
	AuGa→Pb	Work		Pb	1.75	3.499	600.65
4	InSe-Sn		7.25	In	1.57	3.24;3.37	429.78
	InSe→Sn			Se	1.60	2.32	494.0
				Sn	1.58	2.80;3.02	505.12
5	$CuAl_2$-In	121	7.26	Cu	1.28	2.556	1358.02
	CuAl→In			Al	1.43	2.862	933.60
				In	1.57	3.24;3.37	429.78
6**	PbTe-Fe	122	7.27	Pb	1.75	3.499	600.65
	PbTe→Fe			Te	1.43;1.7	2.86;3.46	722.72
				Fe	1.27	2.48;2.58	1811.56
7	Cu_2Te-Bi	123	7.28	Cu	1.28	2.556	1358.02
	CuTe→Bi			Te	1.43;1.7	2.86;3.46	722.72
				Bi	1.82	3.11;3.47	544.52
8	Cu_2Se-Bi	123	7.29	Cu	1.28	2.556	1358.02
	CuSe→Bi			Se	1.60	2.32	494.0
				Bi	1.82	3.11;3.47	544.52

* System showed disagreement due to Melting Point.

** System showed disagreement due to Atomic Size.

TABLE 7:- SYSTEMS SHOWING LIQUID MISCIBILITY.

[For RULE 1 Based on Atomic Size and Melting Point].

No	SYSTEMS	TYPE OF MISCIBILITY	CONSTITUENTS ELEMENTS	GOLDSCHMIT ATOMIC RADII ^{0}A	DISTANCE OF CLOSEST APPROAH ^{0}A	MELTING POINT K
1*	AuIn→Ge	Case I	Au	1.44	2.88	1337.58
	$AuIn_2$→Ge		In	1.57	3.37;3.24	429.78
			Ge	1.39	2.44	1211.50
2*	AuGa→Ge	Case I	Au	1.44	2.88	1337.58
	$AuGa_2$→Ge		Ga	1.35	2.43;2.79	302.92
			Ge	1.39	2.44	1211.50
3*	AuZn→Ge	Case I	Au	1.44	2.88	1337.58
			Zn	1.37	2.66;2.91	692.73
			Ge	1.39	2.44	1211.50
4*	AuCd→Ge	Case I	Au	1.44	2.88	1337.5
			Cd	1.52	2.97;3.29	594.26
			Ge	1.39	2.44	1211.50
5*	$AgTe_2$→Sb	Case I	Ag	1.44	2.89	1235.08
			Te	1.47;1.7	2.86;3.46	722.72
			Sb	1.61	2.90;3.36	903.90
6	PbTe→Au	Case I	Pb	1.75	3.499	600.65
			Te	1.47;1.7	2.86;3.46	722.72
			Au	1.44	2.88	1337.58
7	GaSb→Bi	Case II; Bi-Ga	Ga	1.35	2.43;2.79	302.92
		is an immiscible	Sb	1.61	2.90;3.36	903.90
		Binary System	Bi	1.81	3.11;3.47	544.52
8	InTe→Sb	Case II; In-Te	In	1.57	3.37;3.24	429.78
		is an immiscible	Te	1.47;1.7	2.86;3.46	722.72
		Binary System	Sb	1.61	2.90;3.36	903.90
9*	Cu_2Se→As	Case II; Cu-Se	Cu	1.28	2.55	1358.02
		is an immiscible	Se	1.60	2.32;3.46	494.00
		Binary System	As	1.25	2.51;3.15	1080.00
10*	Cu_2Te→As	Case II; Cu-Te	Cu	1.28	2.55	1358.02
		is an immiscible	Te	1.47;1.7	2.86;3.46	722.72
		Binary System	As	1.25	2.51;3.15	1080.00

No	SYSTEMS	TYPE OF MISCIBILITY	CONSTITUENTS ELEMENTS	GOLDSCHMIT ATOMIC RADII ^{0}A	DISTANCE OF CLOSEST APPROAH ^{0}A	MELTING POINT K
11*	$Cu_2Se \rightarrow Sb$	Case II; Cu-Se	Cu	1.28	2.55	1358.02
		is an immiscible	Se	1.60	2.32;3.46	494.00
		Binary System	Sb	1.61	2.90;3.36	903.90
12*	$Cu_2Te \rightarrow Sb$	Case II; Cu-Te	Cu	1.28	2.55	1358.02
		is an immiscible	Te	1.47;1.7	2.86;3.46	722.72
		Binary System	Sb	1.61	2.90;3.36	903.90
13†	$InTe \rightarrow Bi$	Case II; In-Te	In	1.57	3.37;3.24	429.78
		is an immiscible	Te	1.47;1.7	2.86;3.46	722.72
		Binary System	Bi	1.81	3.11;3.47	544.52
14	$CdTe \rightarrow Ge$	Case I	Cd	1.52	2.97;3.29	594.26
			Te	1.47;1.7	2.86;3.46	722.72
			Ge	1.39	2.44	1211.50
15	$In_2Se_3 \rightarrow$ Ge	Case I	In	1.57	3.37;3.24	429.78
			Se	1.60	2.32;3.46	494.00
			Ge	1.39	2.44	1211.50
16	$CdTe \rightarrow Co$	Case I	Cd	1.52	2.97;3.29	594.26
			Te	1.47;1.7	2.86;3.46	722.72
			Co	1.25	2.49;2.51	1768.00
17	$CdTe \rightarrow Mn$	Case I	Cd	1.52	2.97;3.29	594.26
			Te	1.47;1.7	2.86;3.46	722.72
			Mn	1.30	2.24;2.37;2.73	1517.01
18	$GaAs \rightarrow Ge$	Case I	Ga	1.35	2.43;2.79	302.92
			As	1.25	2.51;3.15	1080.00
			Ge	1.39	2.44	1211.50
19*	$AuIn \rightarrow Sb$	Case I	Au	1.44	2.88	1337.58
			In	1.57	3.37;3.24	429.78
			Sb	1.61	2.90;3.36	903.90
20*	$Mg_2Si \rightarrow Al$	Case I	Mg	1.60	3.19;3.20	923.00
			Si	1.17	2.35	1687.00
			Al	1.43	2.86	933.60
21	$CdTe \rightarrow Sn$	Case I	Cd	1.52	2.97;3.29	594.26
			Te	1.47;1.7	2.86;3.46	722.72
			Sn	1.58	3.18;2.80;3.02	505.12
22	$CoZr \rightarrow Nb$	Case I	Co	1.25	2.49;2.51	1768.00
			Zr	1.60	3.17	2127.86
			Nb	1.47	2.859	2750.00

No	SYSTEMS	TYPE OF MISCIBILITY	CONSTITUENTS ELEMENTS	GOLDSCHMIT ATOMIC RADII ^{0}A	DISTANCE OF CLOSEST APPROAH ^{0}A	MELTING POINT K
23	CdSb→Ag	Case I	Cd	1.52	2.97;3.29	594.26
			Sb	1.61	2.90;3.36	903.90
			Ag	1.44	2.89	1235.08
24	CdSb→Au	Case I	Cd	1.52	2.97;3.29	594.26
			Sb	1.61	2.90;3.36	903.90
			Au	1.44	2.88	1337.58
25	CdSb→Cu	Case I	Cd	1.52	2.97;3.29	594.26
			Sb	1.61	2.90;3.36	903.90
			Cu	1.28	2.55	1358.02
26	NiSb→Co	Case I	Ni	1.25	2.49	1728.00
			Sb	1.61	2.90;3.36	903.90
			Co	1.25	2.49;2.51	1768.00
27†	Ni_2Si→Cu	Case I	Ni	1.25	2.49	1728.00
			Si	1.17	2.35	1687.00
			Cu	1.28	2.55	1358.02
28	NiSb→Fe	Case I	Ni	1.25	2.49	1728.00
			Sb	1.61	2.90;3.36	903.90
			Fe	1.28;1.26	2.48;2.58	1811.00
29	Ni_3Sn_2→ Fe	Case II; Fe-Si is an immiscible Binary System	Ni	1.25	2.49	1728.00
			Sn	1.58	3.18;2.80;3.02	505.12
			Fe	1.28;1.26	2.48;2.58	1811.00
30	PbAl→Cu	Case II; Al-Pb is an immiscible Binary System	Pb	1.75	3.499	600.65
			Al	1.43	2.86	933.60
			Cu	1.28	2.55	1358.02
31†	GaAs→Sn	Case I	Ga	1.35	2.43;2.79	302.92
			As	1.25	2.51;3.15	1080.00
			Sn	1.58	3.18;2.80;3.02	505.12
32†	GaAs→Cd	Case I	Ga	1.35	2.43;2.79	302.92
			As	1.25	2.51;3.15	1080.00
			Cd	1.52	2.97;3.29	594.26
33	$AuAl_2$→Si	Case I	Au	1.44	2.88	1337.58
			Al	1.43	2.86	933.60
			Si	1.17	2.35	1687.00
34*	AuSn→Ge	Case I	Au	1.44	2.88	1337.58
			Sn	1.58	3.18;2.80;3.02	505.12
			Ge	1.39	2.44	1211.50

No	SYSTEMS	TYPE OF MISCIBILITY	CONSTITUENTS ELEMENTS	GOLDSCHMIT ATOMIC RADII ^{0}A	DISTANCE OF CLOSEST APPROAH ^{0}A	MELTING POINT K
35*	GaAs→Zn	Case I	Ga	1.35	2.43;2.79	302.92
			As	1.25	2.51;3.15	1080.00
			Zn	1.37	2.66;2.91	692.73
36	Bi_2Mg_3→ Cu	Case I	Bi	1.81	3.11;3.47	544.52
			Mg	1.60	3.19;3.20	923.00
			Cu	1.28	2.55	1358.02

Note:- The systems from no. 1 to 4 were investigated in present work.

Total number of systems examined = 36

The number of systems that agreed with the Rule = 36

The number of systems that disagreed with the Rule = nil

* The systems that showed agreement due to both Atomic Size and Melting Point conditions = 13

† The systems showed that agreement due to Melting Point condition = 5

All other systems showed agreement due to Atomic Size condition = 18

TABLE 8:- SYSTEMS SHOWING TRUE LIQUID IMMISCIBILITY.

[For RULE 2 Based on Solubility Parameters and Electronegativities].

No	SYSTEMS	REF.	FIG No.	TYPE OF IMMISC-IBILITY	CONSTITU-ENTS ELEMENTS	SOLUBILITY PARAMETER $(J/cm^3)^{1/2}$	ELECTRON-EGATIVITY (e.V)
1	CuTi-Ag CuTi→Ag	106	7.4	Case I	Cu Ti Ag	219 192 168	1.9 1.6 1.9
2	PdTi-Ag PdTi→Ag	107	7.5	Case I	Pd Ti Ag	209 192 168	2.2 1.6 1.9
3	Cu_3Sb-Bi CuSb→Bi	108	7.6	Case I	Cu Sb Bi	219 121 98	1.9 1.9 1.8
4	Mg_3Sb_2-Al MgSb→Al	109	7.7	Case I	Mg Sb Al	102 121 176	1.2 1.9 1.5
5	AuSn-Pb AuSn→Pb	65	7.8	Case I	Au Sn Pb	190 133 96	3.1 1.7 1.8
6	AuIn-Pb AuIn→Pb	101	7.9	Case I	Au In Pb	190 123 96	3.1 1.4 1.8
7	AuSn-Bi AuSn→Bi	50	7.10	Case I	Au Sn Bi	190 133 98	3.1 1.7 1.8
8	$CuAl_2$-Sn CuAl→Sn	110	7.11	Case I	Cu Al Sn	219 176 133	1.9 1.5 1.7
9	FeSi-Cu FeSi→Cu	111	7.12	Case I	Fe Si Cu	207 180 219	1.8 1.8 1.9
10*	AuCd-Pb AuCd→Pb	Present Work	7.13	Case I	Au Cd Pb	190 92 96	3.1 1.7 1.8

No	SYSTEMS	REF.	FIG No	TYPE OF IMMISC-IBILITY	CONSTITU-ENTS ELEMENTS	SOLUBILITY PARAMETER $(J/cm^3)^{1/2}$	ELECTRON-EGATIVITY (e.V)
11	PdSi-Ag	112	7.14	Case I	Pd	209	2.2
	$PdSi_2$-Ag				Si	180	1.8
	PdSi→Ag				Ag	168	1.9
12	CdSe-Bi	113	7.15	Case II	Cd	92	1.7
	CdSe→Bi				Se	70	2.4
					Bi	98	1.8
13	AuSi→Te	101	7.16	Case I	Au	190	3.1
					Si	180	1.8
					Te	74	2.1
14	$FeSi_2$-Sb	114	7.17	Case I	Fe	207	1.8
	FeSi→Sb				Si	180	1.8
					Sb	121	1.9
15	Cu_3As-Pb	115	7.18	Case III	Cu	219	1.9
	CuAs→Pb				As	135	2.0
					Pb	96	1.8
16	CuSn→Pb	116	7.19	Case III	Cu	219	1.9
					Sn	133	1.7
					Pb	96	1.8
17*	ZnTe-Bi	117	7.20	Case III	Zn	108	1.2
	ZnTe→Bi				Te	74	2.1
					Bi	98	1.8
18	PdZr-Ag	107	7.21	Case I	Pd	209	2.2
	PdZr→Ag				Zr	192	1.6
					Ag	168	1.9

* Systems showed disagreement due to Solubility parameter.

TABLE 9:- SYSTEMS SHOWING LIQUID IMMISCIBILITY (Case IV). [For RULE 2 Based on Solubility Parameters and Electronegativities].

No	SYSTEMS	REF.	FIG No.	CONSTITU-ENTS ELEMENTS	SOLUBILITY PARAMETER $(J/cm^3)^{1/2}$	ELECTRON-EGATIVITY (e.V)
1	$CuAl_2$-Cd	118	7.22	Cu	219	1.9
	CuAl→Cd			Al	176	1.5
				Cd	92	1.7
2	AuZn-Pb	Pres-	7.23	Au	190	3.1
	AuZn→Pb	ent		Zn	108	1.2
		Work		Pb	96	1.8
3	AuGa-Pb	Pres-	7.24	Au	190	3.1
	$AuGa_2$-Pb	ent		Ga	151	1.4
	AuGa→Pb	Work		Pb	96	1.8
4	InSe-Sn		7.25	In	123	1.4
	InSe→Sn			Se	70	2.4
				Sn	133	1.7
5	$CuAl_2$-In	121	7.26	Cu	219	1.9
	CuAl→In			Al	176	1.5
				In	123	1.4
6	PbTe-Fe	122	7.27	Pb	96	1.8
	PbTe→Fe			Te	74	2.1
				Fe	207	1.8
7*	Cu_2Te-Bi	123	7.28	Cu	219	1.9
	CuTe→Bi			Te	74	2.1
				Bi	98	1.8
8*	Cu_2Se-Bi	123	7.29	Cu	219	1.9
	CuSe→Bi			Se	70	2.4
				Bi	98	1.8

* Systems showed disagreement due to Solubility parameter.

TABLE 10:- SYSTEMS SHOWING LIQUID MISCIBILITY.

[For RULE 2 Based on Solubility Parameters and Electronegativities].

No	SYSTEMS	TYPE OF MISCIBILITY	CONSTITUENTS ELEMENTS	SOLUBILITY PARAMETER $(J/cm^3)^{1/2}$	ELECTRONEGATIVITY (e.V)
1*	AuIn→Ge $AuIn_2$→Ge	Case I	Au In Ge	190 123 155	3.1 1.4 1.7
2*	AuGa→Ge $AuGa_2$→Ge	Case I	Au Ga Ge	190 151 155	3.1 1.4 1.7
3*	AuZn→Ge	Case I	Au Zn Ge	190 108 155	3.1 1.2 1.7
4*	AuCd→Ge	Case I	Au Cd Ge	190 92 155	3.1 1.7 1.7
5*	$AgTe_2$→Sb	Case I	Ag Te Sb	168 74 121	1.9 2.1 1.9
6**	PbTe→Au	Case I	Pb Te Au	96 74 190	1.8 2.1 3.1
7♥♥	GaSb→Bi	Case II; Bi-Ga is an immiscible Binary System	Ga Sb Bi	151 121 98	1.4 1.9 1.8
8*	InTe→Sb	Case II; In-Te is an immiscible Binary System	In Te Sb	123 74 121	1.4 2.1 1.9
9*	Cu_2Se→As	Case II; Cu-Se is an immiscible Binary System	Cu Se As	219 70 135	1.9 2.4 2.0
10*	Cu_2Te→As	Case II; Cu-Te is an immiscible Binary System	Cu Te As	219 74 135	1.9 2.1 2.0

No	SYSTEMS	TYPE OF MISCIBILITY	CONSTITUENTS ELEMENTS	SOLUBILITY PARAMETER $(J/cm^3)^{1/2}$	ELECTRONEGATIVITY (e.V)
11*	$Cu_2Se \rightarrow Sb$	Case II; Cu-Se is an immiscible Binary System	Cu	219	1.9
			Se	70	2.4
			Sb	121	1.9
12*	$Cu_2Te \rightarrow Sb$	Case II; Cu-Te is an immiscible Binary System	Cu	219	1.9
			Te	74	2.1
			Sb	121	1.9
13*	InTe→Bi	Case II; In-Te is an immiscible Binary System	In	123	1.4
			Te	74	2.1
			Bi	98	1.8
14♥	CdTe→Ge	Case I	Cd	92	1.7
			Te	74	2.1
			Ge	155	1.7
15♥♥	$In_2Se_3 \rightarrow$ Ge	Case I	In	123	1.4
			Se	70	2.4
			Ge	155	1.7
16**	CdTe→Co	Case I	Cd	92	1.7
			Te	74	2.1
			Co	258	1.8
17**	CdTe→Mn	Case I	Cd	92	1.7
			Te	74	2.1
			Mn	194	1.5
18♥	GaAs→Ge	Case I	Ga	151	1.4
			As	135	2.0
			Ge	155	1.7
19♥	AuIn→Sb	Case I	Au	190	3.1
			In	123	1.4
			Sb	121	1.9
20*	$Mg_2Si \rightarrow Al$	Case I	Mg	102	1.2
			Si	180	1.8
			Al	176	1.5
21*	CdTe→Sn	Case I	Cd	92	1.7
			Te	74	2.1
			Sn	133	1.7

No	SYSTEMS	TYPE OF MISCIBILITY	CONSTITUENTS ELEMENTS	SOLUBILITY PARAMETER $(J/cm^3)^{1/2}$	ELECTRONEGATIVITY (e.V)
22*	CoZr→Nb	Case I	Co	245	1.8
			Zr	192	1.6
			Nb	239	1.8
23♥	CdSb→Ag	Case I	Cd	92	1.7
			Sb	121	1.9
			Ag	168	1.9
24**	CdSb→Au	Case I	Cd	92	1.7
			Sb	121	1.9
			Au	190	3.1
25♥	CdSb→Cu	Case I	Cd	92	1.7
			Sb	121	1.9
			Cu	219	1.9
26*	NiSb→Co	Case I	Ni	254	1.8
			Sb	121	1.9
			Co	245	1.8
27*	Ni_2Si→Cu	Case I	Ni	254	1.8
			Si	180	1.8
			Cu	219	1.9
28*	NiSb→Fe	Case I	Ni	254	1.8
			Sb	121	1.9
			Fe	207	1.8
29*	Ni_3Sn_2→ Fe	Case II; Fe-Si is an immiscible Binary System	Ni	254	1.8
			Sn	133	1.7
			Fe	207	1.8
30**	PbAl→Cu	Case II; Al-Pb is an immiscible Binary System	Pb	96	1.8
			Al	176	1.5
			Cu	219	1.9
31♥	GaAs→Sn	Case I	Ga	151	1.4
			As	135	2.0
			Sn	133	1.7
32♥♥	GaAs→Cd	Case I	Ga	151	1.4
			As	135	2.0
			Cd	92	1.7
33*	$AuAl_2$→Si	Case I	Au	190	3.1
			Al	176	1.5
			Si	180	1.8

No	SYSTEMS	TYPE OF MISCIBILITY	CONSTITUENTS ELEMENTS	SOLUBILITY PARAMETER $(J/cm^3)^{1/2}$	ELECTRONEGATIVITY (e.V)
34*	AuSn→Ge	Case I	Au	190	3.1
			Sn	133	1.7
			Ge	155	1.7
35**	GaAs→Zn	Case I	Ga	151	1.4
			As	135	2.0
			Zn	108	1.2
36**	Bi_2Mg_3→ Cu	Case I	Bi	98	1.8
			Mg	102	1.2
			Cu	219	1.9

Note:- The systems from no. 1 to 4 were investigated in present work.

Total number of systems examined = 36

The number of systems that agreed with the Rule = 27

The number of systems that disagreed with the Rule = 9

* The systems that showed agreement due to Solubility Parameter condition = 21

** The systems that showed agreement due to Electronegativity condition = 7

♥ The systems that showed slight disagreement (i.e on borderline) = 6

♥♥ The systems that showed marked disagreement = 3

TABLE 11:- The Solid Solubility of Ge In AuX Congruent Melting Compound.

Congruent Melting Compounds	Closest Distance Of Approach ^{O}A	Max. Solubility of Ge in AuX	Size Factor
$AuIn_2$	5.72	< 1 at.%	57%
$AuGa_2$	5.25	< 1 at.%	53%
AuZn	2.77	1.3 at.%	13%
AuCd	2.89	1.3 at.%	15%

TABLE 12:- Reaction Scheme of Au-Pb-Ga Ternary System

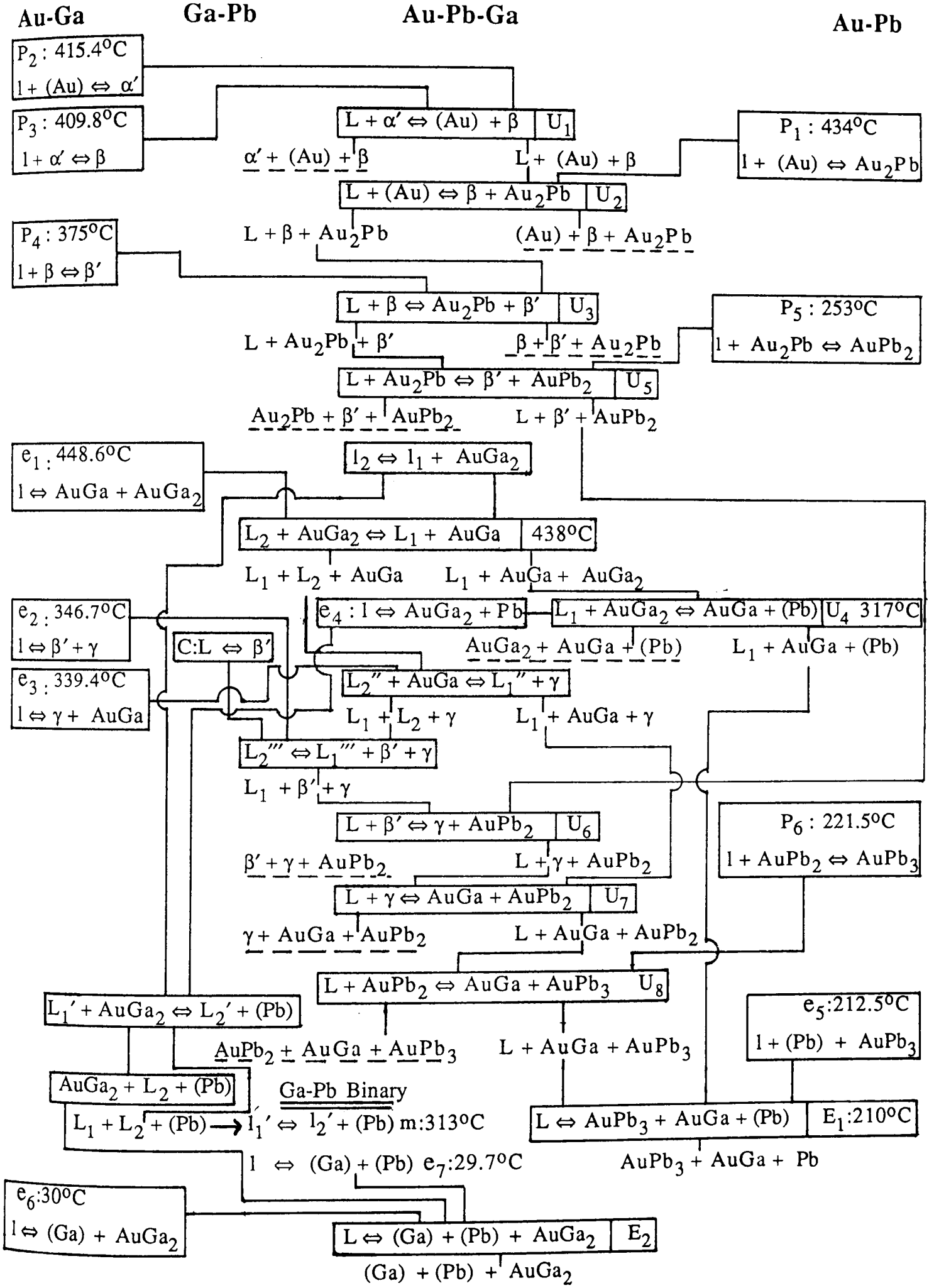

APPENDIX

APPENDIX 1

Etchant Used For:

(1) Au-Ge-X Ternary Alloys:

50 ml of Nitric Acid (1.40).

30 ml of Hydrofluoric Acid (40%).

30 ml of Glacial Acetic Acid.

0.6 ml of Bromine.

To distinguish the Ge phase from the AuX phase.

(2) Au-Sn Binary Alloys:

Very dilute solution of Iodine in KI

APPENDIX 2:- Arrest temperatures (^oC) in the AuIn-Ge pseudobinary section obtained using STA.

COMPOSITION	SOLIDUS		LIQUIDUS
At. % Ge	Heating	Cooling	Cooling
1.0	489.7	486.7	497.54
2.0	488.20	487.83	489.00
5.0	485.00	488.21	531.5
10.0	489.23	488.13	587.00
15.0	486.31	488.63	627.53
20.0	486.12	488.73	668.54
25.0	490.19	484.00	699.40
30.0	485.95	487.34	719.00
40.0	489.27	487.41	762.00
50.0	488.00	488.00	808.32

APPENDIX 3:- Arrest temperatures (^oC) in the $AuIn_2$-Ge pseudobinary section obtained using STA.

COMPOSITION	SOLIDUS		LIQUIDUS
At. % Ge	Heating	Cooling	Cooling
1.0	522.12	522.19	531.80
2.0	521.24	522.79	528.25
4.0	523.23	522.40	522.28
5.5	522.27	522.79	531.0
10.0	520.34	522.27	582.58
15.0	522.27	522.48	582.58
20.0	522.34	522.27	655.95
30.0	520.54	522.02	769.36
40.0	519.32	522.18	769.36
50.0	524.43	522.13	801.73
60.0	525.48	522.1	841.21

APPENDIX 4:- Arrest temperatures (°C) of $Au_{41.5}In_{58.5}$-Ge isopleth obtained using STA.

COMPOSITION At. % Ge	COOLING	HEATING
0.5	512.12;485.2	-----
1.0	506.17;481.09;472.71	471.14
1.5	502.13;475.44;471.23	469.02
2.0	498.97;476.43;473.92	470.27
2.5	495.18;471.01	469.29
3.0	492.00;472.30	472.38
3.5	490.08;471.31	469.43
4.5	508.80	-----
6.0	531.41;487.01;469.34	-----
10.0	597.37;488.12;470.23	472.40
20.0	667.79;487.92;470.27	471.33
30.0	718.97;487.10;467.19	470.51
40.0	761.39;484.89;469.23	472.31
50.0	803.00;485.31;469.21	472.32

APPENDIX 5:- Arrest temperatures (°C) of $Au_{20}In_{80}$-Ge isopleth obtained using STA.

COMPOSITION At. % Ge	COOLIING	HEATING
0.5	490.08	-----
1.0	495.13;490.34;156.02	155.92
1.5	497.18;491.02;156.31	155.73
2.0	493.35;156.1	156.51
3.0	489.03;156.3	156.41
6.0	527.48;489.71;156.34	156.32
15.0	619.19;489.21;156.31	156.13
25.0	682.68;489.17;156.29	156.17

APPENDIX 6:- Arrest temperatures (^{o}C) in the AuGa-Ge pseudobinary section obtained using STA.

COMPOSITION	SOLIDUS		LIQUIDUS
At. % Ge	Heating	Cooling	Cooling
1.0	445.21	444.07	452.01
2.0	441.37	446.38	450.13
5.0	_____ ONE	ARREST	_____
6.0	_____ ONE	ARREST	_____
7.5	448.03	444.81	512.31
10.0	446.21	446.42	555.39
15.0	448.43	446.21	613.14
20.0	446.01	448.13	649.05
30.0	449.06	448.77	712.87
40.0	445.19	449.41	760.01
50.0	448.23	448.37	794.79
60.0	446.31	445.93	832.21

APPENDIX 7:- Arrest temperatures (^{o}C) in the $AuGa_2$-Ge pseudobinary section obtained using STA.

COMPOSITION	SOLIDUS		LIQUIDUS
At. % Ge	Heating	Cooling	Cooling
1.0	474.07	473.89	487.31
2.0	489.38	472.68	483.38
4.0	_____ ONE	ARREST	_____
6.0	_____ ONE	ARREST	_____
7.5	472.13	474.48	521.18
10.0	475.88	475.16	549.29
15.0	476.18	475.69	598.78
20.0	472.72	476.18	646.37
30.0	476.91	477.08	711.08
40.0	479.46	479.23	764.98
50.0	475.35	476.96	809.31
60.0	477.12	476.39	841.21

APPENDIX 8:- Arrest temperatures (°C) of $Au_{40}Ga_{60}$-Ge isopleth obtained using STA.

COMPOSITION At. % Ge	COOLING	HEATING
1.0	470.02;445.97;439.92	438.03
1.6	470.03;444.78;438.34	439.14
2.1	469.68;442.10;437.1	439.02
2.7	467.10;452.91;437.21	439.31
3.2	467.00;461.11;437.24	439.21
3.5	468.00;463.26;438.03	438.34
4.0	470.01;466.89;439.89	439.26
4.5	497.08;462.69;439.67	436.15
7.0	534.13;466.26;437.68	438.41
10.6	576.19;465.91;438.01	439.13;465.08
15.6	628.33;461.16;436.31	437.02;460.35
25.0	688.18;456.24;436.21	438.28;460.16
35.0	738.02;454.38;433.33	436.91;456.86

APPENDIX 9:- Arrest temperatures (°C) in the AuZn-Ge pseudobinary section obtained using STA.

COMPOSITION	SOLIDUS		LIQUIDUS
At. % Ge	Heating	Cooling	Cooling
0.5(for solvus curve)	603.20;708.00	606.00	754.24
1.0(for solvus curve)	658.08;691.08	691.5;656.98	754.04
1.5	675.3	670.89	746.30
2.0	672.00	672.00	744.31
5.0	674.01	671.39	720.16
10.0	673.13	673.29	685.27
15.0	672.61	671.60	689.00
20.0	637.35	672.47	718.21
30.0	677.28	673.22	758.35
40.0	672.00	670.16	788.92
50	671.35	669.17	814.48
60	670.20	673.00	847.00

APPENDIX 10:- Arrest temperatures (^{o}C) in the AuCd-Ge pseudobinary section obtained using STA.

COMPOSITION	SOLIDUS		LIQUIDUS
At. % Ge	Heating	Cooling	Cooling
1.0(for solvus curve)	539.15;589.68	538.68	601.09
1.5	555.47	556.27	619.44
2.5	552.39	555.56	605.16
5.0	558.25	556.29	585.27
12.5	556.28	553.79	603.03
15.0	554.21	559.19	639.03
20.0	556.38	555.04	674.18
30.0	555.43	555.48	736.64
40	548.31	556.63	768.81
50	548.98	548.09	809.21

APPENDIX 11:- Arrest temperatures (^{o}C) of AuGa-Pb section obtained using STA.

COMPOSITION	COOLING	HEATING
At. % Pb		
2.0	450;317;202	-------
5.0	430;311;212	319
15.0	436;316;183	317
25.0	443;313;177;	317
40.0	439;309;204;	224;322
50.0	435;310;202	211;321
60.0	439;318;189	211306
70.0	427;313;186	214;309
80.0	431;318;195	209;319
90.0	427;322;190	221;326
95.0	327;198	326
97.0	307;194	326

APPENDIX 12:- Arrest temperatures (^{o}C) of $AuGa_2$-Pb section obtained using STA.

COMPOSITION At. % Pb	COOLING	HEATING
3.0	480;325;317	318;326
10.0	481;325;317	315;325
20.0	482;324;317	316;323
30.0	483;424;316	318;324
40.0	481;325;317	318;325
50.0	481;324;316	318;325
60.0	481;325;317	316;325
70	482;325;316	318;325
80.0	481;326;316	316;325
90.0	480;325;315	315;326
97.0	324;317	316;324

APPENDIX 13:- Arrest temperatures (^{o}C) of AuZn-Pb section obtained using STA.

COMPOSITION At. % Pb	COOLING	HEATING
5.0	772;752;210	213
10.0	753;281;210	213
20.0	752;280;211	213
30.0	752;260;211	212
40.0	750;282;211	217
50.0	750;296;210	213
60.0	748;299;215	216
70.0	732;300;213	214
80.0	730;307;209	211
85.0	712;207	211
90.0	634;323;208	211
95.0	222;212	214

APPENDIX 14:- Arrest temperatures (°C) of AuCd-Pb section obtained using STA.

COMPOSITION At. % Pb	COOLING	HEATING
40.0	595;261;244;192	192;246;296
50.0	592;274;245;188	190;245;274
70.0	584;560;283;242	245;284
80	296;244	245;295
90	426;325;207	325
95	326;179	325

APPENDIX (15)

When the thesis preparation was completed, one more system was found. This was the ternary system Ag-Zn-Pb which showed liquid immiscibility of the type as shown in Fig 7.1(a), (case IV). The direction of the tie-lines were from AgZn to Pb. The liquidus projection of this system is shown in Figure below. This system agreed with both of the rules described in this thesis.

[Reference: T. R. A. Davey, Trans. A.I.M.M.E., 1954, 200, 838].

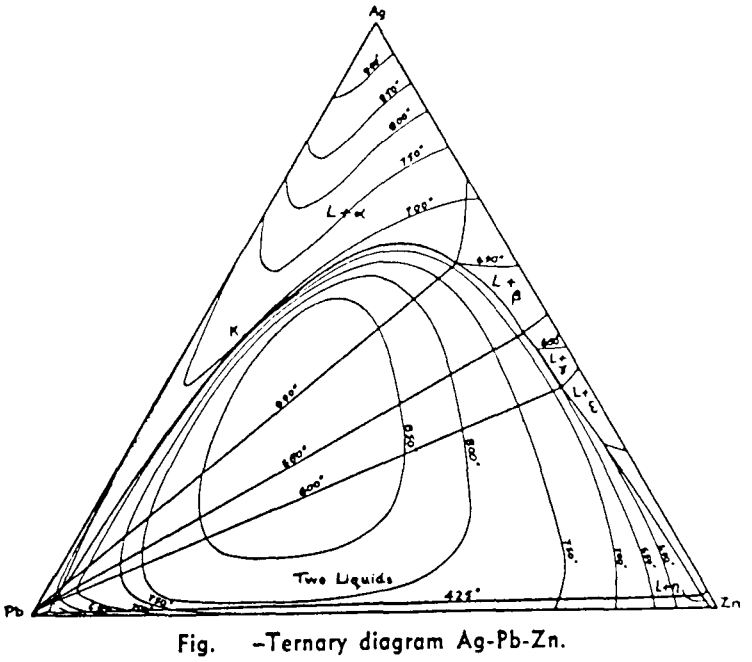

Fig. –Ternary diagram Ag-Pb-Zn.